Giant unilamellar vesicles : an efficient membrane biophysical tool and its application in drug delivery studies

Lopez Mora, N.F.

Giant unilamellar vesicles:

An efficient membrane biophysical tool and its application in drug delivery studies

NESTOR FABIAN LOPEZ MORA

Giant unilamellar vesicles:

An efficient membrane biophysical tool and its application in drug delivery studies

Proefschrift

ter verkrijging van

de graad van Doctor aan de Universiteit Leiden,

op gezag van Rector Magnificus prof.mr. C.J.J.M. Stolker,

volgens besluit van het College voor Promoties

te verdedigen op donderdag 7 juli 2016

klokke 11.15 uur

door

Nestor Fabian Lopez Mora

geboren te Mexico D. F., Mexico, 1978

Promotiecomissie

Promotor: Prof. dr. A. Kros Faculty of Science, LIC

Thesis Comissie:

Prof. dr. J. Brouwer (VZ), Faculty of Science, LIC

Prof. dr. M.H.M. Noteborn (secretaris), Faculty of Science, LIC

Prof. dr. N.A.J.M. Sommerdijk, Eindhoven University of Technology

Prof. dr. P. Booth, King's College London

Dr. R. Kieltyka, Faculty of Science, LIC

ISBN: 978-94-6332-039-9

Dedicated to my family:

my parents Javier and Raquel,

my sister Minerva and my brother Leonardo.

Table of Contents

Chapter I

Introduction

The plasma cellular membrane together with the cytoskeleton defines the shape of the cell.[1] The cellular membrane is an essential component in all cells that defines the boundaries between the cytoplasm and the external environment. The cellular membrane consists of a complex mixture of lipids, proteins and carbohydrates that control and regulate the transport of ions and molecules across the membrane to perform complex biological cellular functions. Due to the complexity of cellular membranes, there is great interest in generating simplified membrane models to enable the study of membrane function.[2] The use of supported bilayers,[3-8] nanodiscs[9-16] and liposomes[17, 18] are some of the platforms that have been used as biophysical models.

Giant unilamellar vesicles (GUVs) with sizes between 5-100 µm, have been proposed as a biophysical platform because they are readily observable by optical microscopy and the size and membrane curvature are similar to cells.[19, 20] GUVs are assemblies of natural or synthetic lipids composed of a single lipid bilayer separating the aqueous interior compartment from the exterior (**Figure 1**). GUVs have been used as a biophysical model system in studies of lipid organization,[21] membrane-peptide,[22] and membrane-protein interactions.[23]

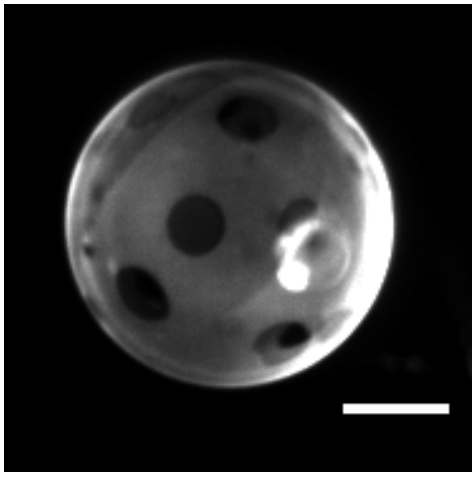

Figure 1. Confocal image of Giant Unilamellar Vesicle (GUV) composed of DPhPC/DPPC/Cholesterol (2/2/1). The lipid membrane shows phase separation (L_o and L_d phases). Black spots are cholesterol rich domains which prefer the L_o phase. The scale bar is 20 µm.

The morphology, production and size distribution of the GUVs depends on the selected formation method and growth conditions. Traditional methods for the preparation of GUVs are gentle hydration and electroformation.[24, 25] However, the growth of GUVs under physiologically relevant conditions (>300 mOsm/kg) has been challenging for those methods. As an alternative, the formation of GUVs by emulsion methods has been proposed for the preparation of GUVs at relevant salt conditions, but the presence of remaining solvent in the lipid bilayer of the final GUVs and its effect on the biophysical properties of the membrane are still under discussion.[26, 27]

Recently the preparation of GUVs assisted by agarose gel films has enabled the production of GUVs at physiological conditions.[28] Moreover, the use of agarose gel films allow the reconstitution of membrane proteins in the lipid bilayer of GUVs. The agarose film produces successfully GUVs with several lipid compositions, however the agarose gel dissolves during the rehydration of the lipids resulting in traces of agarose contaminating the lipid membrane of the GUVs. Furthermore, a detailed study of agarose-GUVs showed that a fraction of GUVs contains encapsulated agarose in the inner volume of the vesicles and the residual agarose across the membrane affects the mechanical properties of the lipid membrane in electrodeformation studies.[29] In the same study, Lira et. al. proposed a thermal post-treatment of agarose-GUVs to release the encapsulated agarose and recover the vesicle responses to electro deformation. Alternatively, films of crosslinked polyacrylamide (PAA) and synthetic gels of poly(vinyl alcohol) (PVA) have been employed for the preparation of GUVs.[28, 30] Whilst PAA and PVA polymers are not detected in the lipid bilayer of the GUVs formed through this approach, they afford minimal ability to control the characteristics of the GUVs in terms of the yield, morphology and size distribution.

This thesis presents a hydrogel-based method for the preparation of GUVs at physiological conditions, without contamination of the lipid membrane of GUVs from the hydrogel matrix. **Chapter II** presents the method used for the preparation of GUVs at physiological conditions, based on the use of a chemically crosslinked Dextran hydrogel film (DexPEG). The maleimide-functionalized Dextran is chemically crosslinked by a dithiolated polyethylene glycol (PEG) and ligated to the glass substrate to avoid dissolution of the polymeric network during the formation of GUVs. GUVs with several lipid compositions were prepared in PBS and HEPES buffers to validate the general applicability of the method. **Chapter III** describes how the physical chemical properties of the hydrogel network affect GUV formation. Here, the effect

of the hydrogel precursor composition and structure on GUV formation is systematically studied by modifying the degree of substitution of maleimide in the dextran polymer backbone as well as the architecture of the PEG crosslinker. The resulting GUVs for each combination of precursors were characterized in terms of the yield and size distribution by flow cytometry. In addition, GUV formation in real time experiments was imaged to obtain better understanding of the formation process of GUVs in DexPEG hydrogels.

Next in this thesis, the production of GUVs by this method is applied to cases where high ionic strength conditions are a prerequisite for biophysical studies in the GUV membrane model. **Chapter IV** discusses the use of GUVs as biophysical membrane models for the imaging of red to blue light upconversion, driven by triplet-triplet annihilation. Here, GUVs growth in the presence of high concentrations of sodium sulphite (300 mM), included in the buffer as an oxygen scavenger, allowed the imaging of light upconversion within the lipid membrane of GUVs.

Chapter V describes the transport of ions across the lipid membrane of GUVs through membrane incorporation of a synthetic transmembrane chloride transporter. Giant vesicles with the anion transporter located in the lipid bilayer were formed in a solution of a chloride-sensitive fluorophore and $NaNO_3$ (225 mM). The external addition of NaCl triggers the transport of chloride and the exchange with nitrate through the lipid membrane of GUVs. The quenching of the encapsulated fluorophore in the GUVs allowed the visualization of ion transport and the evaluation of the activity of the chloride transporter. The potential use of this synthetic transporter is limited by the lipophilicity of the molecule which difficult the deliverability of the transporter. Therefore in **Chapter VI** this delivery problem was solved by targeted membrane fusion. Membrane fusion is triggered by two complementary coiled-coil forming peptides K_4 [$(KIAALKE)_4$] and E_4 [$(EIAALEK)_4$], which are located in different membranes. The formation of a dimeric coiled-coil by these peptides brings the two opposing membranes into close proximity, thereby inducing efficient membrane fusion and the targeted delivery of the synthetic transporter. Large unilamellar vesicles (LUVs) were used as drug delivery system with the transporter pre-incorporated in the lipid membrane and with the insertion of the complementary peptide amphiphiles on the membrane, the lipophilic transporter was delivered to the membrane of GUVs by targeted membrane fusion. GUVs as a biophysical model in relevant physiological conditions, validated that the transporter is efficiently transferred and active in the membrane of GUVs after membrane fusion. Next, the

same methodology was successfully applied for the delivery of the transporter to live cells by membrane fusion.

The formation of GUVs on DexPEG substrates at physiological ionic strength conditions allowed monitoring the membrane fusion process by fluorescence microscopy. Membrane fusion between GUVs and Large Unilamellar Vesicles (LUVs) driven by the complementary K_4 and E_4 coiled-coil peptide amphiphiles was further studied in the Chapter **VII**. Membrane fusion was assayed by lipid and content mixing between GUVs and LUVs. The visualization of the fusion process in GUVs gave new insights about the incorporation of the lysine rich lipopeptide K_4 [$(KIAALKE)_4$] on the lipid membrane of GUVs. Fluorescence correlation spectroscopy (FCS) experiments in GUVs supported the aggregation of lipopeptide in the membrane of GUVs founded by fluorescence microscopy. The use of a co-surfactant (Tween 20) improved the incorporation of this peptide amphiphile and the membrane fusion between GUVs and LUVs.

Finally in the Chapter **VIII**, new research lines are proposed and supported by preliminary experiments. This chapter shows that there is plenty of room for further applications of the GUV biophysical model and the study of membrane - molecule interactions at physiologically relevant ionic strength conditions. Moreover, the possibility of forming multi-compartmentalized GUVs by the DexPEG method; opens a novel window of future applications in the “bottom – up” approach of creating an artificial cell in the field of Synthetic Biology.

The use of GUVs as a biophysical model is leading to a better understanding of membrane related processes because they are easily produced, readily observable by microscopy techniques, and their similarity with cellular membranes. Thus, fluorescence-based methods and the synthesis of new fluorescent indicators together with the use of GUVs at relevant ionic strength conditions are a powerful tool for studying membrane fusion, viral infection, signalling and drug targeting in the coming years.

References

1. Tsai, F.C., Stuhrmann, B. & Koenderink, G.H. Encapsulation of Active Cytoskeletal Protein Networks in Cell-Sized Liposomes. *Langmuir* **27**, 10061-10071 (2011).
2. Pomorski, T.G., Nylander, T. & Cardenas, M. Model cell membranes: Discerning lipid and protein contributions in shaping the cell. *Adv Colloid Interfac* **205**, 207-220 (2014).
3. Chiantia, S., Kahya, N. & Schwille, P. Raft domain reorganization driven by short- and long-chain ceramide: A combined AFM and FCS study. *Langmuir* **23**, 7659-7665 (2007).
4. Visco, I., Chiantia, S. & Schwille, P. Asymmetric Supported Lipid Bilayer Formation via Methyl-beta-Cyclodextrin Mediated Lipid Exchange: Influence of Asymmetry on Lipid Dynamics and Phase Behavior. *Langmuir* **30**, 7475-7484 (2014).
5. Plochberger, B. et al. Cholesterol SlOWS down the Lateral Mobility of an Oxidized Phospholipid in a Supported Lipid Bilayer. *Langmuir* **26**, 17322-17329 (2010).
6. Simonsen, A.C. & Bagatolli, L.A. Structure of spin-coated lipid films and domain formation in supported membranes formed by hydration. *Langmuir* **20**, 9720-9728 (2004).
7. Tanaka, M. & Sackmann, E. Polymer-supported membranes as models of the cell surface. *Nature* **437**, 656-663 (2005).
8. Hirst, D.J. et al. Effect of acyl chain structure and bilayer phase state on binding and penetration of a supported lipid bilayer by HPA3. *Eur Biophys J Biophy* **40**, 503-514 (2011).
9. Bayburt, T.H. & Sligar, S.G. Self-assembly of single integral membrane proteins into soluble nanoscale phospholipid bilayers. *Protein Sci* **12**, 2476-2481 (2003).
10. Stepien, P., Polit, A. & Wisniewska-Becker, A. Comparative EPR studies on lipid bilayer properties in nanodiscs and liposomes. *Bba-Biomembranes* **1848**, 60-66 (2015).
11. Matsuzaki, N., Handa, T. & Nakano, M. Kinetic and Thermodynamic Analysis of Cholesterol Transfer between Phospholipid Vesicles and Nanodiscs. *J Phys Chem B* **119**, 9764-9771 (2015).
12. Han, L. et al. Protein-Glycolipid Interactions Studied in Vitro Using ESI-MS and Nanodiscs: Insights into the Mechanisms and Energetics of Binding. *Anal Chem* **87**, 4888-4896 (2015).
13. Kucharska, I., Edrington, T.C., Liang, B.Y. & Tamm, L.K. Optimizing nanodiscs and bicelles for solution NMR studies of two beta-barrel membrane proteins. *J Biomol Nmr* **61**, 261-274 (2015).
14. Akkaladevi, N. et al. Following Natures Lead: On the Construction of Membrane-Inserted Toxins in Lipid Bilayer Nanodiscs. *J Membrane Biol* **248**, 595-607 (2015).
15. Wang, X.M., Mu, Z.J., Li, Y., Bi, Y.C. & Wang, Y.J. Smaller Nanodiscs are Suitable for Studying Protein Lipid Interactions by Solution NMR. *Protein J* **34**, 205-211 (2015).
16. Bayburt, T.H. & Sligar, S.G. Membrane protein assembly into Nanodiscs. *Febs Lett* **584**, 1721-1727 (2010).
17. Aurora, T.S., Li, W., Cummins, H.Z. & Haines, T.H. Preparation and Characterization of Monodisperse Unilamellar Phospholipid-Vesicles with Selected Diameters of from 300 to 600 Nm. *Biochim Biophys Acta* **820**, 250-258 (1985).
18. Lasic, D.D. Liposomes: from physics to applications. *Amsterdam: Elsevier.* (1993).

19. Walde, P., Cosentino, K., Engel, H. & Stano, P. Giant Vesicles: Preparations and Applications. *ChemBioChem* **11**, 848-865 (2010).
20. Morales-Penningston, N.F. et al. GUV preparation and imaging: Minimizing artifacts. *Biochimica Et Biophysica Acta-Biomembranes* **1798**, 1324-1332 (2010).
21. Lipowsky, R. The morphology of lipid membranes. *Current opinion in structural biology* **5**, 531-540 (1995).
22. Koller, D. & Lohner, K. The role of spontaneous lipid curvature in the interaction of interfacially active peptides with membranes. *Bba-Biomembranes* **1838**, 2250-2259 (2014).
23. Kahya, N. Protein-protein and protein-lipid interactions in domain-assembly: Lessons from giant unilamellar vesicles. *Bba-Biomembranes* **1798**, 1392-1398 (2010).
24. Reeves, J.P. & Dowben, R.M. Formation and properties of thin-walled phospholipid vesicles. *Journal of Cellular Physiology* **73**, 49-60 (1969).
25. Angelova, M.I. & Dimitrov, D.S. Liposome Electroformation. *Faraday Discuss.* **81**, 303-+ (1986).
26. Hansen, J.S. et al. Formation of Giant Protein Vesicles by a Lipid Cosolvent Method. *ChemBioChem* **12**, 2856-2862.
27. Nishimura, K., Suzuki, H., Toyota, T. & Yomo, T. Size control of giant unilamellar vesicles prepared from inverted emulsion droplets. *Journal of Colloid and Interface Science* **376**, 119-125 (2012).
28. Horger, K.S., Estes, D.J., Capone, R. & Mayer, M. Films of Agarose Enable Rapid Formation of Giant Liposomes in Solutions of Physiologic Ionic Strength. *Journal of the American Chemical Society* **131**, 1810-1819 (2009).
29. Lira, R.B., Dimova, R. & Rieke, K.A. Giant Unilamellar Vesicles Formed by Hybrid Films of Agarose and Lipids Display Altered Mechanical Properties. *Biophysical Journal* **107**, 1609-1619 (2014).
30. Weinberger, A. et al. Gel-Assisted Formation of Giant Unilamellar Vesicles. *Biophysical Journal* **105**, 154-164 (2013).

Chapter II

Preparation of size tunable giant vesicles from crosslinked dextran(ethylene glycol) hydrogels

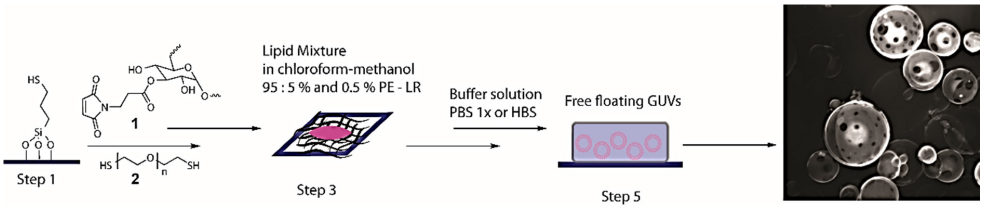

This work is published: Nestor Lopez Mora, Jesper S. Hansen, Yue Gao, Andrew A. Ronald, Roxanne Kieltyka, Noah Malmstadt, and Alexander Kros, *Chem. Commun*. **2014**, 50, 1953-1955.

Abstract

We present a novel chemically crosslinked dextran-poly(ethylene glycol) hydrogel substrate for the preparation of dense vesicle suspensions under physiological ionic strength. These vesicles can be easily diluted for individual study. Modulating the degree of crosslinking within the hydrogel network results in tuning of the vesicle size distribution.

Introduction

The growth of high-quality giant (1-100 µm diameter) unilamellar lipid vesicles (GUVs) under physiologically relevant conditions (>300 mOsm/kg) is generally difficult using most common GUV fabrication methods.[1] For this aim, the most widely used methods are gentle hydration and electroformation.[2, 3] Gentle hydration involves the deposition of a lipid on a glass substrate and swelling of the lipid lamella into vesicles by rehydration in aqueous solutions. To adapt this method to grow vesicles at moderate ionic strength (200 mOsm/kg), it is necessary to include negatively charged lipids and heat the lipids above their phase transition temperatures.[4] Most often, the vesicle yield of this method is variable and occasionally low. However, the addition of non-electrolytic monosaccharides in the dry lipid film promotes lamellar lipid repulsion to increase vesicle yield.[5] Electroformation can provide higher yields and more homogeneous GUVs through the application of an electric field during GUV growth. However, to grow GUVs under high ionic strength conditions, high field frequencies and longer hydration times are required with the main drawback that lipid hydrolysis and peroxidation can occur.[6, 7]

More recently, hydrogel forming polymer substrates have been employed for the preparation of GUVs in order to reach physiological ionic strength conditions. These substrates include agarose gels,[8] polyacrylamide[8] and thin films of poly(vinyl alcohol).[9] While these methods have allowed GUV formation at moderate ionic strengths (~200-280 mOsm/kg), they afford minimal ability to control the characteristics of the GUV in terms of morphology and size distribution.

Here, we form GUVs on a covalently crosslinked hydrogel substrate. We demonstrate that control over crosslink density can alter the size distribution of the GUVs formed. We use dextran polymers crosslinked by poly(ethylene glycol) (PEG) chains using Michael addition to simultaneously prepare the hydrogel (Dex-PEG) and anchor it to a glass surface. Our hypothesis is that an anchored covalent hydrogel cannot be dissolved during the GUV formation process to potentially contaminate the lipid bilayer, which may be a concern with non-covalently crosslinked hydrogels.[8] Moreover, covalent hydrogel matrices enable the possibility for control over GUV size distributions through modulation of crosslinker density and thus, network topology.

Results and Discussion

Dextran (MW= 70 kDa) was modified with N-maleoyl-β-alanine following a previously described protocol to provide polymer **1** to be used for Michael addition with reactive thiols on the PEG polymer and the glass surface.[10-13] The degree of substitution (DS) on the polymer was controlled by the molar ratio of N-maleoyl-β-alanine relative to Dextran and subsequently validated by ^{1}H-NMR. Concurrently, microscope slides were prepared for anchoring of the chemically crosslinked hydrogel directly to the glass surface. A reactive thiol moiety was introduced on the glass slide surface with 3-mercaptopropyl trimethoxysilane. The thiol coated microscope slides were crosslinked to the hydrogel by drop-casting the dextran solution (2 wt %) and PEG dithiol **2** at various molar ratios at 40 °C (**Figure 1**, step 2) until a homogeneous hydrogel film was formed. Following the formation of the hydrogel, the desired lipid mixture was deposited on the hydrogel surface and the solvents were evaporated in a vacuum oven for 30 minutes at 35 °C or at room temperature under a gentle stream of nitrogen gas to prevent lipid oxidation (**Figure 1**, step 3). In a final step, the hydrogel and lipid film on the glass slide were rehydrated in aqueous buffer solutions for 1-2 hours to form free-floating vesicles (**Figure 1**, step 5). In all cases, hydration of the lipid film was performed above the T_m of all the lipids used. To validate the widespread applicability of the Dex-PEG chemically crosslinked network for GUV growth, several buffers, lipid compositions, and crosslinking ratios were tested.

First, the effect of physiological ionic strength conditions on vesicle growth was examined. Hence, two buffers used ubiquitously in biological cell studies were examined for vesicle growth: phosphate buffered saline (PBS) and HEPES potassium chloride saline buffer (HBS). The osmolality of these buffers were experimentally determined by measuring the freezing point depression for both PBS (310 mOsm/kg) and HBS (320 mOsm/kg). In general, qualitative differences were noted between both buffers; HEPES buffer produced slightly greater yields and larger sized vesicles (see *Experimental Section*). However, in both of these buffers high yields of free floating vesicles were easily obtained.

The capacity of the Dex-PEG network to support vesicle growth using a variety of lipid compositions was then explored. Binary mixtures of lipids containing both anionic and neutral lipids and ternary mixtures incorporated cholesterol were examined. The lipid compositions A – H (see details in **Table 1** *Experimental Section*) were designed to examine the effect of three different parameters on vesicle formation; cholesterol (CH) content, negatively charged lipid content (POPG and DOPS), and liquid ordered lipid phases (DPPC). Free floating GUVs using

lipid mixtures (**Figure 1**. A, B and, F up to 25% CH provided a good yield of GUVs with a spherical morphology in PBS and HBS buffers.

This result is in contrast to previous reports where gentle hydration methods showed exclusive formation of tubular morphologies and liposome networks connected by tubes using POPC/CH with 5–30% CH in HEPES.[14] Using the Dex-PEG system, we found numerous spherical GUVs alongside such morphologies.

Another parameter that was explored was the effect of increasing the anionic lipid content in GUV formation. Previously, it was found that lipid mixtures containing more than 10-20% anionic lipids were difficult to grow by gentle hydration methods.[15] Hence, we selected lipid mixtures ranging from 10-50% in POPG (**Figure 1**. C and D). Using our method, we were able to obtain high yields of spherical vesicles under high ionic strength conditions.

Moreover, we examined mixtures with DOPS (10%); a lipid that is known to decrease vesicle yields at high ionic strength conditions. Consistent with this notion we also observed high yields of spherical GUVs with 10% DOPS (**Figure 1** E). Finally, lipid mixtures known to undergo phase separation through phase coexistence of liquid ordered (L_o) and liquid disordered (L_d) phases were tested.[16] We found using the Dex-PEG system, that phase-separated GUVs consisting of 30-50% DPPC can be easily grown at 50 °C (**Figure 2**). Moreover, we can prepare such kinetically trapped GUVs by the Dex-PEG method without the use of additional additives under high ionic strength conditions. Overall, all lipid compositions using the additive free Dex-PEG method to grow GUVs under high ionic strength conditions yielded high quantities of free floating vesicles. A Gaussian size distribution centered between 10-15 μm was found after 1 hour of GUV preparation for all lipid compositions when using an equimolar ratio between the dextran polymer and the crosslinker (see *Experimental Section*). This result suggests a relationship between the method of vesicle growth and size.

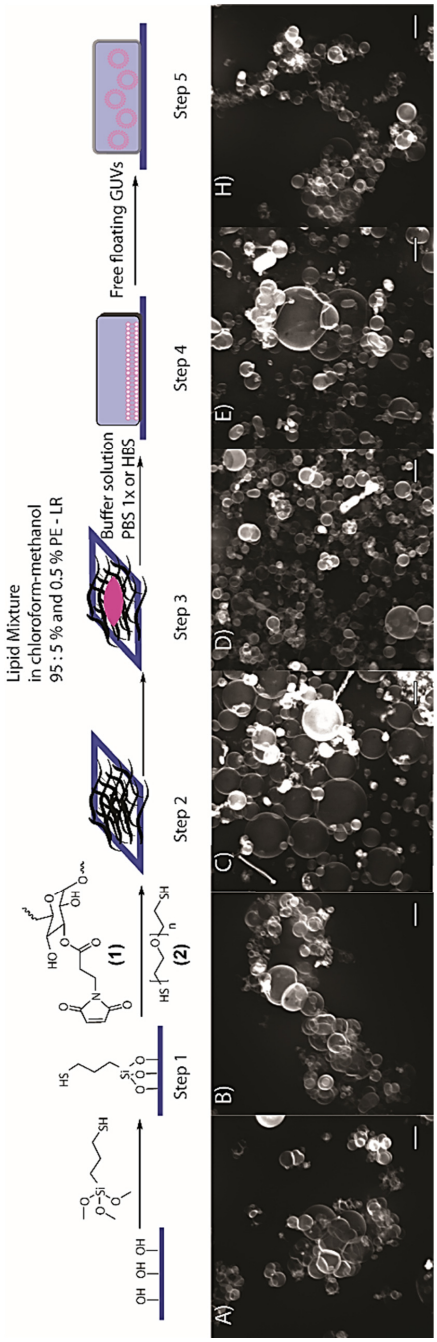

Figure 1. On top GUVs preparation method and on the bottom of the image Z-projections images with high yields of free floating GUVs for various lipid compositions (details for those lipid mixtures are presented in the *Experimental Section*). The scale bars are 10 µm.

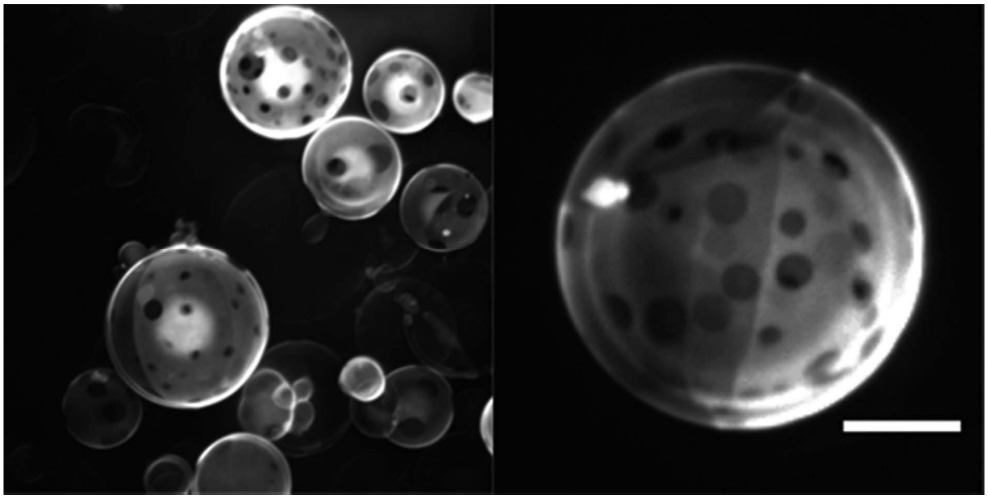

Figure 2. Z-projections of phase separated GUVs with the lipid composition 40% DPhPC / 40% DPPC / 20% CH (mol %) in PBS at physiological ionic strength. The scale bars are 10 µm.

Excitingly, a correlation between crosslink density and vesicle size distribution was observed (**Figure 3**). On average, a population of a hundred GUVs was sized for each experiment. Decreasing the molar ratio of PEG to 75 and 50 % mol with respect to dextran polymer resulted in a concomitant increase in the vesicle size distribution in a single step. Current methods used to gain control over vesicle size require a minimum of two-steps to achieve similar results whereas vesicle size can be tuned within the Dex-PEG system through modifying the composition of the chemical network in a single step.[17] The success of the Dex-PEG method in enabling growth of GUVs based on various lipid compositions under high ionic strength arises from several pertinent chemical features and materials properties.

Based on our data we hypothesize that the driving force for generating free floating GUVs is due to the high swelling behavior of the hydrogel upon hydration. Specifically the water content differs within the hydrogel from 2% in the dry state to 90% in the wet state. The ability for the Dex-PEG hydrogel to imbibe a high percentage of an aqueous solution on the order of less than 1 hour, most likely contributes to interlamellar repulsion that generates the necessary forces to facilitate efficient growth of giant vesicles under physiological ionic strength. In addition, the starting water content of the film plays an important role; vesicles are not formed

without a pre-hydrated film. Moreover, chemical ligation to the glass surface is essential due to the rapid growth of the hydrogel layer on the glass surface upon exposure to buffer. Earlier experiments showed that unligated hydrogels resulted in simultaneous detachment from the glass substrate during vesicle formation. To examine whether hydrogel components were dissociated from the surface or incorporated in vesicles, we synthesized a fluorescently labeled dextran polymer with 1 and 2.5 mol % of methoxycoumarin-3-carboxylic acid (Dex-PEG-C) to be tracked by two-photon fluorescence microscopy. Analysis of free floating GUVs produced from Dex-PEG-C showed no fluorescence either in the membrane or inside the formed GUVs at room temperature (see *Experimental Section*).

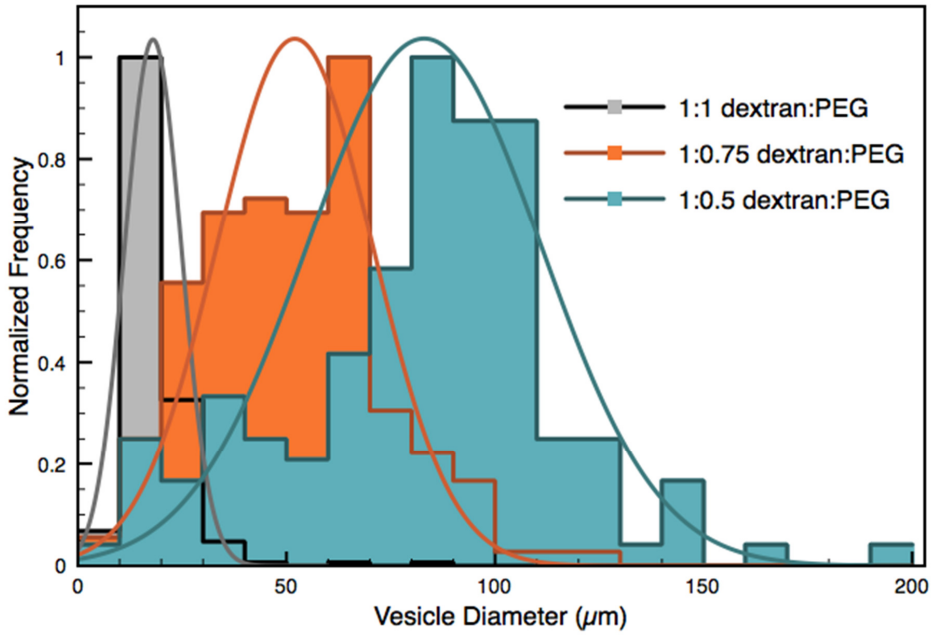

Figure 3. Tuneability of GUVs size distribution (50 % DOPC / 25% DOPE / 25% CH) as a function of crosslink density of PEG relative to dextran in PBS. Average diameters were found to be 18 ± 8 µm (N=215) for 1:1 ratio of dextran-PEG, 52 ± 22 µm (N=171) for a 1:0.75 dextran-PEG and 83 ± 33 µm for a 1: 0.5 dextran:PEG (N=139).

Conclusion

In conclusion, we present a widely applicable method that facilitates the additive-free growth of GUVs under physiological ionic strength conditions based on a variety of lipid compositions. The high swelling capacity of the Dex-PEG promotes the formation of high yields of spherical, free-floating GUVs. Additionally, this method enables the growth of GUVs possessing phase separated domains under physiological conditions. Finally, modulating the crosslink density of the Dex-PEG network provides a handle to tune vesicle size. This Dex-PEG hydrogel system is a powerful method that can be exploited to grow vesicles for applications such as membrane interactions, drug delivery, molecular recognition, lipid raft organization, and membrane fusion studies.[18-21]

Experimental Section

Materials and methods

Cholesterol (CH), 1,2-dioleoyl-*sn*-glycero-3-phosphocholine (DOPC), 1,2-dioleoyl-*sn*-glycero-3-phosphoethanolamine (DOPE), 1-palmitoyl-2-oleoyl-*sn*-glycero-3-phosphocholine (POPC), 1-palmitoyl-2-oleoyl-*sn*-glycero-3-phospho-(1'-rac-glycerol) (sodium salt) (POPG), 1,2-dioleoyl-*sn*-glycero-3-phosphoethanolamine-*N*-[methoxy(polyethylene glycol) - 2000] (ammonium salt) (PEG2000-PE), 1,2-dioleoyl-*sn*-glycero-3-phosphoethanolamine-*N*-(lissamine rhodamine B sulfonyl) (ammonium salt) (PE-LR) were purchased from Avanti Polar Lipids. 1,2-dipalmitoyl-*sn*-glycero-3-phosphocholine (DPPC), 4-nitrophenyl disulfide, 4-(dimethylamino) pyridine (DMAP), 1500 and 3400 Da poly (ethylene glycol) dithiol (PEGDT), 7-methoxycoumarin-3-carboxylic acid, and 4-(2-Hydroxyethyl)piperazine-1-ethanesulfonic acid, *N*-(2-Hydroxyethyl) piperazine-*N*′-(2-ethanesulfonic acid) (HEPES) were purchased from Aldrich. Maleic anhydride, *N*,*N*'-Diisopropylcarbodiimide (DIC), *p*-toluene sulfonic acid monohydrate (PTSA) and maleimide were purchased from Fluka. Dextran (M_n = 2 000, 70 000 and, 150 000, Pharmacia Fine Chemicals, Sweden) was dried in the vacuum oven for several days before use. *N*-Maleoyl-*β*-alanine was synthesized according to a reported procedure.[22] 4-(Dimethylamino) pyridinium 4-toluenesulfonate (DPTS) was synthesized from DMAP and PTSA.[23] Dextran Maleimide (Dex-Mal) was synthesized by esterification of the hydroxyl group of the dextran with *N*-Maleoyl-*β*-alanine.[11]

Synthesis of Dex-Mal (**1**)

Dex-Mal (molecule **1**) was synthesized by DIC mediated esterification of the hydroxyl groups of dextran with *N*-Maleoyl-*β*-alanine. Briefly, *N*-Maleoyl-*β*-alanine (1 eq.), DPTS (0.15 eq.) and DIC (1.5 eq.) were dissolved in anhydrous DMSO. The mixture was stirred at room temperature for two hours, followed by adding the DMSO solution of Dextran (2.5 eq.). After overnight stirring at room temperature, the formed *N*, *N*'-dialkylurea was removed by filtration and the crude product was obtained by precipitation in cold isopropanol. The precipitate was dissolved in water and extensively dialyzed against Milli-Q water for two days and subsequently lyophilized. ^{1}H NMR (400 MHz, D2O): δ 3.3-4.0 (m, dextran glucopyranosyl ring protons), 4.9 (s, dextran anomeric proton), 6.8 (s, maleimide). The degree of substitution (DS) of Dex-Mal is defined as the number of maleimide groups per 100 glucopyranose residues of dextran, which was calculated from the ^{1}H NMR spectra based on the protons of maleimide

(δ 6.8) and the anomeric proton (δ 4.9). The DS of Dex-PEG was controlled by the molar ratio between dextran and N-Maleoyl-β-alanine.

Synthesis of Dex-Mal-C.

The covalently fluorescent labeled Dex-Mal (Dex-Mal-C) was synthesized by a similar procedure as Dex-Mal. Briefly, 7-methoxycoumarin-3-carboxylic acid (0.025 eq. or 0.05 eq.) was added together with *N*-Maleoyl-*β*-alanine (1 eq.), DPTS (0.15 eq.) and DIC (1.5 eq.) in anhydrous DMSO. Dextran (2.5 eq.) was also dissolved in anhydrous DMSO and added into the previous mixture. After overnight stirring at room temperature, the product was purified by filtration, precipitation and dialysis. All these steps were carried out in dark to prevent the bleaching of coumarin.

Glass slides functionalization

Cleaning and thiol surface modification (silanization) was performed according to a previously reported method.[24] Glass substrates were standard microscope glass slides (Menzel-Gläser) 76 x 26 mm.

Dex-PEG Hydrogel

Maleimide-modified Dextran (**1**) (2 % weight solution) was crosslinked by using PEG (**2**) in three different ratios (1:1, 1:0.75 and, 1:0.5) at room temperature. Typically, **1** (60 mg) (DS=4) was dissolved in water (2.5 g) and 11.11 mg of molecule **2** (1500 Da) in water (0.5 g) were mixed to provide a hydrogel solution in 1:1 molar ratio. The mixture was shaken in a vortex for 1 minute and immediately used for the substrate preparation.

Dex-PEG coated glass slides

A solution of 2% Dex-PEG (600 µL) was added onto the prepared thiol functionalized microscope glass slides. A homogenous polymeric film was formed after 30–45 minutes at 40 °C. The Dex-PEG coated microscope slides were stored for further use.

Lipid Mixtures

Each of the lipid mixtures used was made by mixing 14 mM lipid solutions of the individual various lipids together to obtain the indicated molar ratios and yield a final mixture of a 14 mM lipid solution (see **Table 1**). Additionally 1,2–dioleoyl–*sn*–glycerol–3–phosphoethanolamine–

N-(lissamine rhodamine B sulfonyl) (ammonium salt) (PE-LR) was added to each lipid mixture in 0.5 molar % for the purpose of gathering fluorescence images. All lipid mixtures were stored at -20 °C until they were used.

GUVs formation

The desired lipids (10 μL) were drop-casted, using a micropipette, onto the Dex-PEG coated slides. Subsequently, the deposited lipid layer was dried for 30 minutes in a vacuum oven at 35°C. The GUV growth chamber was made by placing a 15 mm (OD) glass O-Ring on top of the hydrogel and sealed with high vacuum silicon grease. Finally, the lipid film was swelled using the desired immersion media (300 μL). GUVs were growth in two different immersion media: PBS and HEPES Potassium Chloride saline (HBS) buffers. All lipid compositions (see **Table 1**) were tested in PBS and HBS growth buffers. The vesicle diameter is the average of measuring between 50 to 100 different GUVs in PBS buffer. GUVs smaller than 1 μm cannot be resolved due to they are below the resolution limit of optical microscopy. Lipid mixtures (A–I) were prepared in 95 chloroform : 5 methanol % volume at 14 mM. PE-LR was used as fluorescent probe in 0.5 % mol (A–E, H–I) or 0.1 % mol (F, G) concentration. Results for all different tested lipid compositions are presented in **Figures A1, A3, A5, A7, A9, A11, A12, A13,** and **A15**. At the left side results for GUVs growth in PBS and right side in HBS. The compositions of those buffers are shown in **Table 2** (PBS) and **Table 3** (HBS). All images were taken from free floating vesicles after waiting 30 minutes in order to allow them to sink in the bottom of the observation chamber. Imaging of GUVs was made using 20x (top image) and 63x (bottom image) objectives in fluorescence microscopy mode (see **Annex**). Comparing qualitatively the sizes of GUVs in those two different immersion media, the diameter size of GUVs was bigger when the immersion media was HBS than in PBS. Additionally, quantitative size distribution analysis was performed by counting GUVs that were grown in PBS buffer during one hour (**Figures A2, A4, A6, A8, A10** and **A14**).

Osmomolality

Osmomolality was determined from the freezing point depression using an Osmometer Roebling Type 13. The Osmometer was calibrated using 100 mOsm/kg NaCl standard solution.

Overview of lipid compositions and GUVs diameters

Table 1. Lipid compositions tested for GUVs growth on Dex-PEG at physiological ionic strength (>300 mOsm/kg).

	Lipid composition (% mol)	PBS	HBS	Diameter (µm)	Figure
A	90% POPC / 10% CH	√	√	12.62 ± 5.89	A1
B	80% POPC / 20% CH	√	√	9.38 ± 5.04	A3
C	90% POPC / 10% POPG	√	√	12.19 ± 4.75	A5
D	50% POPC / 50% POPG	√	√	14.45 ± 7.51	A7
E	90% POPC / 10% DOPS	√	√	9.80 ± 3.50	A9
F	50% DOPC / 50% DPPC	√	√	N.D.	A11
G	33.3% DOPC / 33.3% DPPC / 33.3% CH	√	√	N.D.	A12
H	50% DOPC / 25% DOPE / 25% CH	√	√	11.62 ± 5.35	A13
I	50% DOPC / 20% DOPE / 5% PEG2000-PE / 25% CH	√	√	N.D.	A15

N.D. represents not determined.

Buffer composition

Table 2. Phosphate buffered saline (PBS) composition in 1 liter water.

Reagent	Final concentration	Mass
NaCl	150 mM	8.77 g
K_2HPO4	15 mM	2.61 g
KH_2PO4	5 mM	0.68 g

Table 3. HEPES buffered saline (HBS) composition in 1 liter water.

Reagent	Final concentration	Mass
KCl	150 mM	11.18 g
HEPES	20 mM	5.2 g

Characterization GUVs

Fluorescence Microscopy of GUVs

A Zeiss axiovert-200 inverted microscope equipped with Chroma TRITC and DAPI BP 445/50 fluorescence filter sets was used. Images were recorded with a black and white CCD camera (AxioCam NRm). GUVs were grown from lipid mixture doped with 0.5 mol % PE-LR on Dex-PEG-C hydrogel film. To examine if there is association between Dex-PEG-C and GUVs, two different experiments were performed on Dex-PEG-C hydrogel film. Firstly, GUVs were grown without any fluorescent probe on the lipid mixture. Imaging of non-fluorescent GUVs was performed using phase contrast at 20 x magnification (**Figure 4A**) and phase contrast at 63 x magnification (**Figure 4B**). For imaging in epifluorescence mode, a DAPI bandpass filter centered at 450 nm was used to determine the fluorescence of free floating GUVs. The result is presented in **Figure 4C** where non- fluorescence due to coumarin was found either in the membrane or inside GUVs.

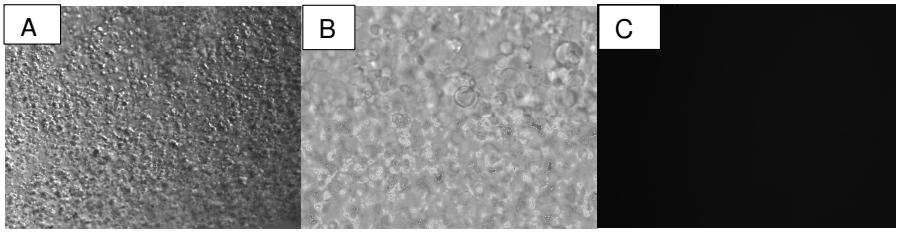

Figure 4. A) Phase contrast microscopy 20 x magnification; **B**) Phase contrast microscopy 63 x magnification and, **C**) Epifluorescence microscopy using a DAPI bandpass filter centered at 450 nm.

A single GUV was imaged in phase contrast microscopy (**Figure 5A**) and in epifluorescence microscopy using a TRITC filter (**Figure 5B**); however when the filter was changed to DAPI bandpass filter there was no membrane fluorescence of this GUV (**Figure 5C**). Even when the lipid mixture penetrates around 15 µm into the hydrogel network (*vide infra*), the association between GUVs and Dex-PEG gel was not detected via fluorescence in the membrane or inside the GUVs. The high swelling efficiency of the hydrogel (90 %) promotes the lipid inter-lamellar repulsion, without doping the lipid lamella with none-electrolytic monosaccharides, producing high yields of GUVs.

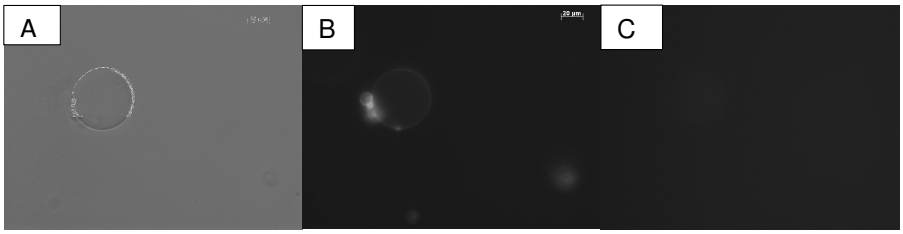

Figure 5. A) Phase contrast microscopy 20 x magnification; **B**) Epifluorescence using a TRITC filter and, **C**) Epifluorescence using a DAPI bandpass filter.

Confocal Imaging of GUVs

A TI-Eclipse inverted microscope (Nikon, Japan) equipped with a 16-bit Cascade II 512 EMCCD camera (Photometrics, USA) was used. Spinning-disc confocal microscopy was performed using a CSUX confocal head (Yokogawa, Japan). Illumination was provided by a 50 mW solid-state laser at 561 nm (Coherent Inc., Germany). Fluorescence was imaged through a bandpass filter centred at 595 nm. Epifluorescence was performed with a 40× objective and confocal microscopy was carried out using a 60× NA1.43 Plan-Apo Nikon oil-immersion objective. Size distribution analysis was made by using Analyze Particles tool in ImageJ software.

Characterization of Dex-PEG substrate

Contact Angle

The characterization of functionalized microscope glass slides before and after silanization was made by drop shape analysis. To measure the contact angle, drop shape analysis was made by using LBADSA plugin in ImageJ software. Results for chemically cleaned and modified surfaces (**Figure 6**) showed an angle of 10 ± 1° before, 67 ± 4° after silanization and 26± 7° for Dex-PEG film.

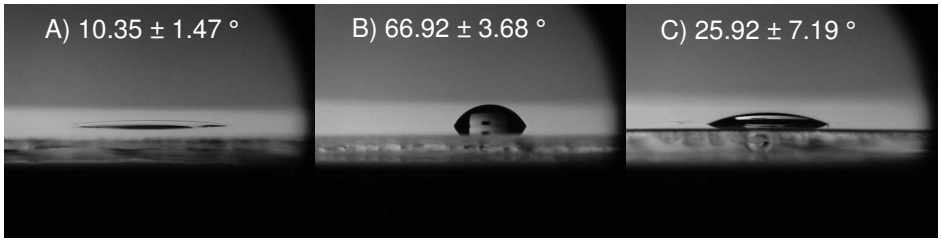

Figure 6. Contact angle measurements for **A**) Microscope glass slide after cleaning, **B**) Microscope glass slide after silanization and, **C**) Microscope glass slide after Dex-PEG hydrogel coating.

Water Uptake

The water uptake of the Dex-PEG hydrogel film was determined by weight increase. Dex-PEG functionalized microscope glass slides were immersed in 1x PBS and the weight was taken every hour. The water uptake content against time is plotted in **Figure 7**. These results indicate that the hydrogel film in the wet state takes up to 90 % PBS buffer during swelling after one hour and then stays constant. The remaining water content in the dry Dex-PEG film was determined by weight lost. We found, after drying the hydrogel film at 110°C overnight, a water content of 1.9±0.14 % in the dry state. This high swelling efficiency produces the forces normal to lipid bilayers that promote the growing of GUVs, without addition of any non-electrolytic monosaccharaides to promote lamellar repulsion.

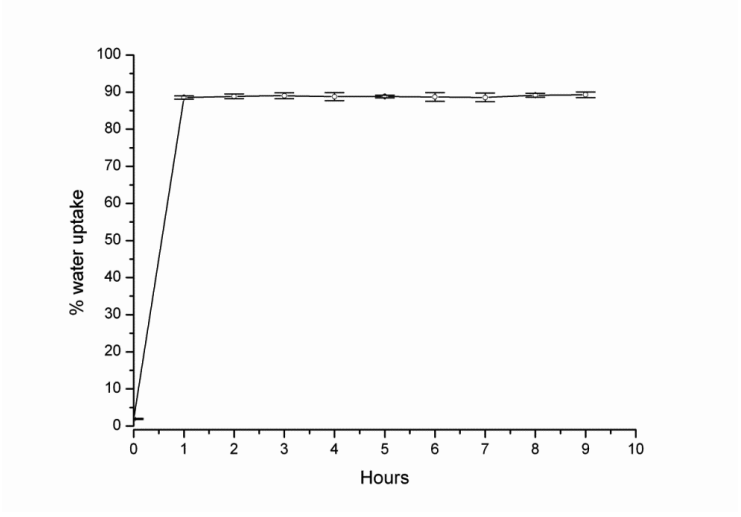

Figure 7. Water uptake in a Dex-PEG hydrogel film after 9 hours of swelling in 1x PBS buffer.

Fluorescence spectroscopy of DexPEG

A FS920 Fluorometer (Edinburgh Instruments) equipped with a DTMS-300X excitation monochrometer and a peltier-controlled thermostatic cell was used. A quartz cuvette with a 1 cm path length was used. The excitation and emission slit widths were 1 nm. Scans were performed with steps of 0.5 nm, with a sampling time of 0.5 s per wavelength. Dex-Mal was fluorescently labeled (1 and 2.5 % mol) with 7-methoxycoumarin-3-carboxylic acid as fluorescent probe to produce Dex-Mal-C (labeling of molecule **1**). On the right side of **Figure 8** the absorption spectra of Dex-Mal-C (2 % weight solution) is presented. The emission spectra of coumarin had a displacement from 402 nm to 410 nm (maximum peak) after labeling (Dex-Mal-C) due to chemical modification.

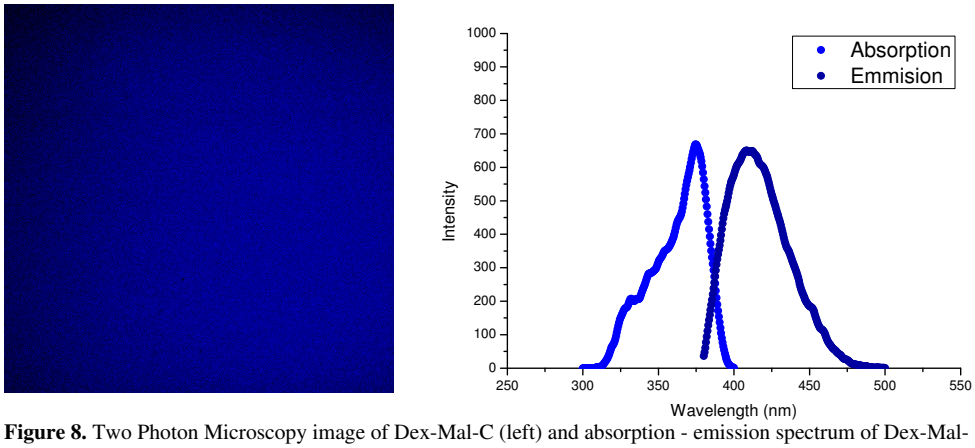

Figure 8. Two Photon Microscopy image of Dex-Mal-C (left) and absorption - emission spectrum of Dex-Mal-C (right) both of them at 2.5 mol % labeling.

Two photon microscopy

A Bio-Rad 2100MP confocal and multi-photon microscope with inverted TE 2000U Nikon microscope was used. Fluorescence was imaged using a 20x Nikon objective (Plan Apo, NA 0.75). Illumination was provided by a 5-W Tsunami laser (Spectra Physics, Mountain View, CA, USA) with a range of 700 – 900 nm. The images were collected using Lasersharp 4.0 software by Biorad. Two Photon microscopy (**Figure 8** left) was used to visualize Dex-PEG-C hydrogel film in a microscope glass slide. The background signal corresponding to none labeled Dex-PEG hydrogel film in a glass slide was subtracted from the signal of Dex-PEG-C

image to remove the noise associated to measurement. Similar results were obtained for Dex-PEG-C (1 % mol) labeling. Two photon confocal microscopy was performed to determine the thickness of the hydrogel film in the microscope glass slide. Sectioning of 1 µm was done from the highest to the lowest fluorescence intensity layer. The resulting images are presented in **Figure 9** after the background has been subtracted from those measurements. Those images correspond from left to right to the highest fluorescence, the middle fluorescence and non-fluorescence images in the confocal sectioning. The estimated thickness of the film is around 26 µm going from the highest to none fluorescence point.

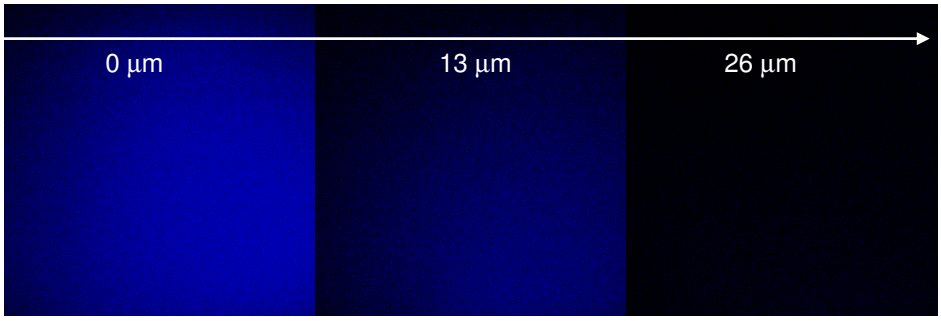

Figure 9. Two photon confocal microscopy images of Dex-PEG-C hydrogel film.

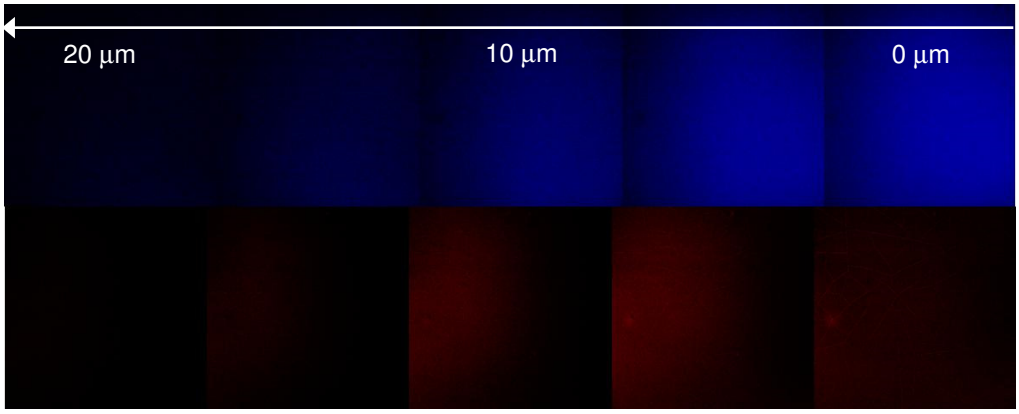

Figure 10. Two Photon Confocal Microscopy of an hybrid film composed of Dex-PEG-C hydrogel and lipid mixture doped with 0.5 mol % PE-LR before immersion in buffer. On top, channel for coumarin and on bottom channel for rhodamine. Each sequence of images corresponds to 5 µm layer sectioning.

Lipid mixture doped with 0.5 % PE-LR was place on top of a Dex-PEG-C hydrogel film and 1 µm sectioning was made following the previously described procedure. The fluorescence signal was detected by using two photon confocal microscopy in two different channels, one for coumarin and another one for rhodamine. These sequence of images is presented in **Figure 10** from highest to lowest intensity layer (right to left). The thickness of the film was measured in 25 µm by doing 1 µm confocal sectioning. The image shows how the doped lipid mixture penetrates the hydrogel network until 15 µm.

References

1. Morales-Penningston, N.F. et al. GUV preparation and imaging: Minimizing artifacts. *Biochimica Et Biophysica Acta-Biomembranes* **1798**, 1324-1332 (2010).
2. Reeves, J.P. & Dowben, R.M. Formation and properties of thin-walled phospholipid vesicles. *Journal of Cellular Physiology* **73**, 49-60 (1969).
3. Angelova, M.I. & Dimitrov, D.S. Liposome Electroformation. *Faraday Discuss.* **81**, 303-+ (1986).
4. Akashi, K., Miyata, H., Itoh, H. & Kinosita Jr, K. Preparation of giant liposomes in physiological conditions and their characterization under an optical microscope. *Biophysical Journal* **71**, 3242-3250 (1996).
5. Tsumoto, K., Matsuo, H., Tomita, M. & Yoshimura, T. Efficient formation of giant liposomes through the gentle hydration of phosphatidylcholine films doped with sugar. *Colloid Surface B* **68**, 98-105 (2009).
6. Pott, T., Bouvrais, H. & Meleard, P. Giant unilamellar vesicle formation under physiologically relevant conditions. *Chemistry and Physics of Lipids* **154**, 115-119 (2008).
7. Montes, L.R., Alonso, A., Goni, F.M. & Bagatolli, L.A. Giant unilamellar vesicles electroformed from native membranes and organic lipid mixtures under physiological conditions. *Biophysical Journal* **93**, 3548-3554 (2007).
8. Horger, K.S., Estes, D.J., Capone, R. & Mayer, M. Films of Agarose Enable Rapid Formation of Giant Liposomes in Solutions of Physiologic Ionic Strength. *Journal of the American Chemical Society* **131**, 1810-1819 (2009).
9. Weinberger, A. et al. Gel-Assisted Formation of Giant Unilamellar Vesicles. *Biophysical Journal* **105**, 154-164 (2013).
10. Peng, K. et al. Dextran based photodegradable hydrogels formed via a Michael addition. *Soft Matter* **7**, 4881-4887 (2011).
11. Peng, K., Tomatsu, I., Korobko, A.V. & Kros, A. Cyclodextrin-dextran based in situ hydrogel formation: a carrier for hydrophobic drugs. *Soft Matter* **6**, 85-87 (2010).
12. Peng, K., Tomatsu, I. & Kros, A. Light controlled protein release from a supramolecular hydrogel. *Chemical Communications* **46**, 4094-4096 (2010).
13. Peng, K. et al. Cyclodextrin/dextran based drug carriers for a controlled release of hydrophobic drugs in zebrafish embryos. *Soft Matter* **6**, 3778-3783 (2010).
14. Nomura, S.-i.M., Mizutani, Y., Kurita, K., Watanabe, A. & Akiyoshi, K. Changes in the morphology of cell-size liposomes in the presence of cholesterol: Formation of neuron-like tubes and liposome networks. *Biochimica et Biophysica Acta (BBA) - Biomembranes* **1669**, 164-169 (2005).
15. Akashi, K., Miyata, H., Itoh, H. & Kinosita, K. Formation of giant liposomes promoted by divalent cations: Critical role of electrostatic repulsion. *Biophysical Journal* **74**, 2973-2982 (1998).
16. Veatch, S.L. & Keller, S.L. Organization in lipid membranes containing cholesterol. *Physical Review Letters* **89** (2002).
17. Nishimura, K., Suzuki, H., Toyota, T. & Yomo, T. Size control of giant unilamellar vesicles prepared from inverted emulsion droplets. *Journal of Colloid and Interface Science* **376**, 119-125 (2012).

18. Zope, H.R.V., F.; Ordas, A.; Voskuhl, J.; Spaink, H.P.; Kros, A. In vitro and In vivo supramolecular biomembrane engineering using a lipidated coiled-coil motif. *Angewandte Chemie-International Edition* **52**, in press (2013).
19. Versluis, F. et al. In Situ Modification of Plain Liposomes with Lipidated Coiled Coil Forming Peptides Induces Membrane Fusion. *J Am Chem Soc* **135**, 8057-8062 (2013).
20. Zheng, T. et al. Controlling the rate of coiled coil driven membrane fusion. *Chemical Communications* **49**, 3649-3651 (2013).
21. Robson Marsden, H., Elbers, N.A., Bomans, P.H.H., Sommerdijk, N.A.J.M. & Kros, A. A reduced SNARE model for membrane fusion. *Angewandte Chemie (International ed. in English)* **48**, 2330-2333 (2009).
22. de Figueiredo, R.M., Oczipka, P., Frohlich, R. & Christmann, M. Synthesis of 4-maleimidobutyric acid and related maleimides. *Synthesis-Stuttgart*, 1316-1318 (2008).
23. Moore, J.S. & Stupp, S.I. Room-Temperature Polyesterification. *Macromolecules* **23**, 65-70 (1990).
24. Cras, J.J., Rowe-Taitt, C.A., Nivens, D.A. & Ligler, F.S. Comparison of chemical cleaning methods of glass in preparation for silanization. *Biosensors and Bioelectronics* **14**, 683-688 (1999).

Annex

Chapter II

Microscopy imaging and size distribution for lipid mixtures presented in Table 1.

*Lipid mixture **A** (90 % POPC / 10 % CH)*

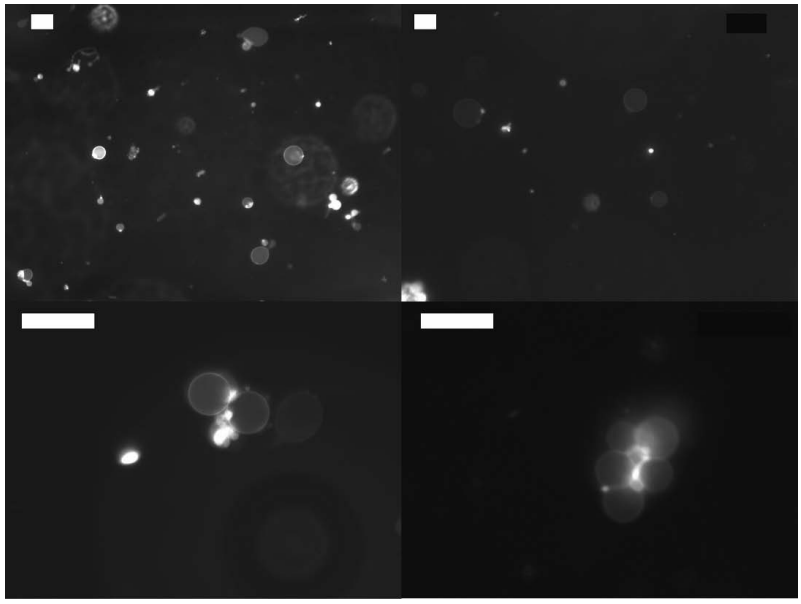

Figure A1. Free floating GUVs formed from POPC/CH (90:10 % mol) in PBS left column and HBS right column. On top 20x magnification and, bottom 63x magnification. The scale bars are 50 μm.

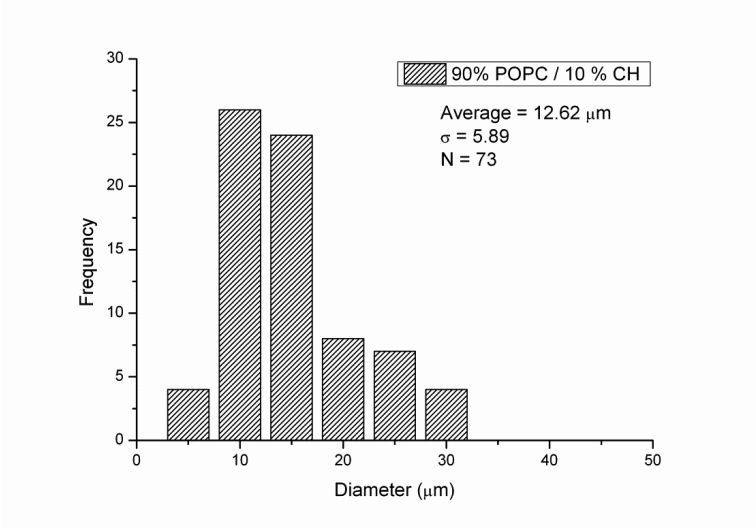

Figure A2. Size distribution of GUVs with lipid composition **A** (90% POPC / 10% CH) in PBS.

*Lipid mixture **B** (80 % POPC / 20 % CH)*

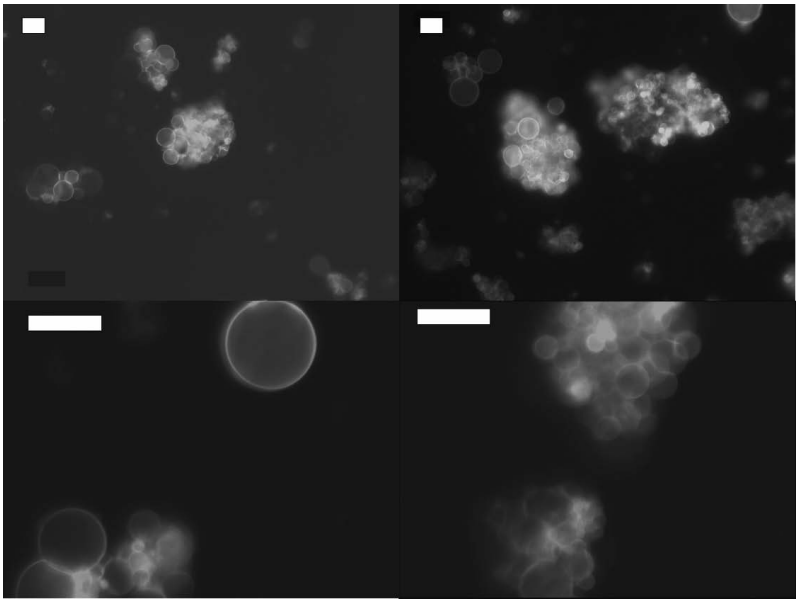

Figure A3. Free floating GUVs formed from POPC/CH (80:20 % mol) in PBS left column and HBS right column. On top 20x magnification and, bottom 63x magnification. The scale bars are 50 μm.

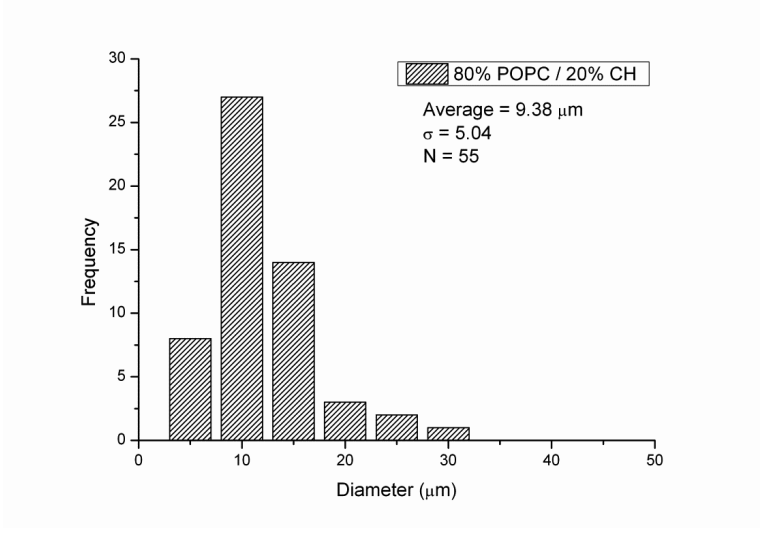

Figure A4. Size distribution of GUVs with lipid composition **B** (80% POPC / 20% CH) in PBS.

*Lipid mixture **C** (90 % POPC / 10 % POPG)*

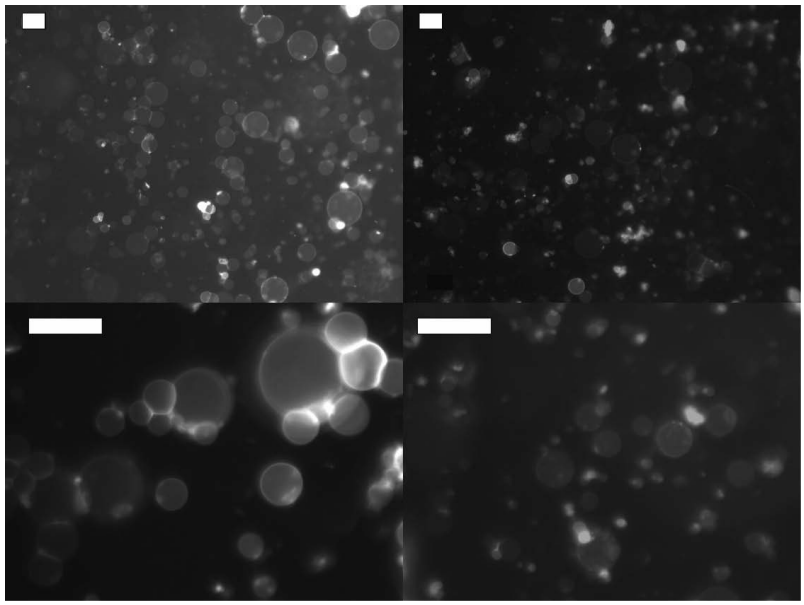

Figure A5. Free floating GUVs formed from POPC/POPG (90:10 % mol) in PBS left column and HBS right column. On top 20x magnification and, bottom 63x magnification. The scale bars are 50 μm.

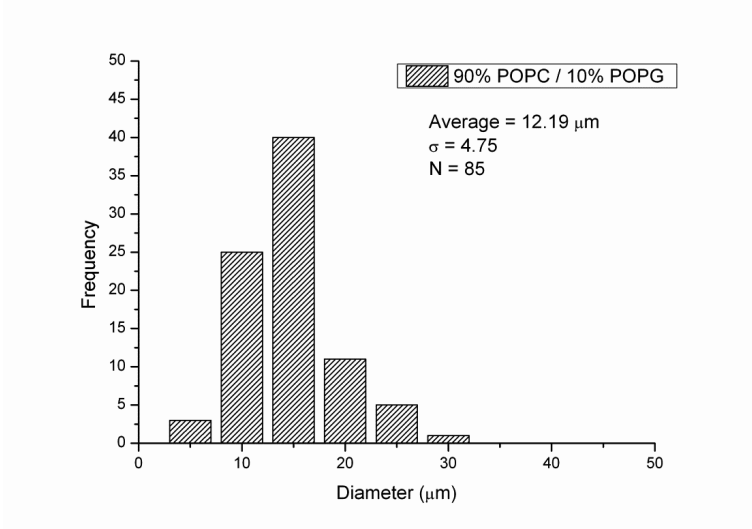

Figure A6. Size distribution of GUVs with lipid composition C (90% POPC / 10% POPG) in PBS.

*Lipid mixture **D** (50 % POPC / 50 % POPG*

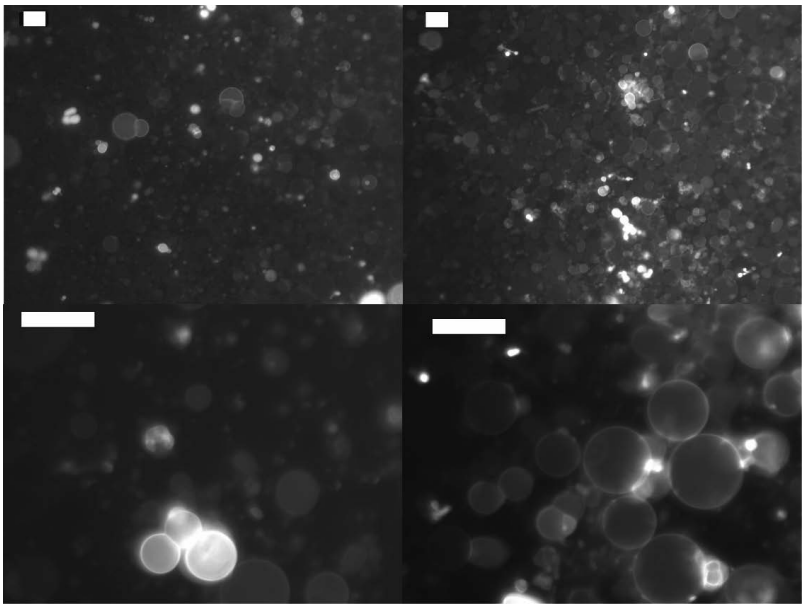

Figure A7. Free floating GUVs formed from POPC/POPG (50:50 %mol) in PBS left column and HBS right column. On top 20x magnification and, bottom 63x magnification. The scale bars are 50 µm.

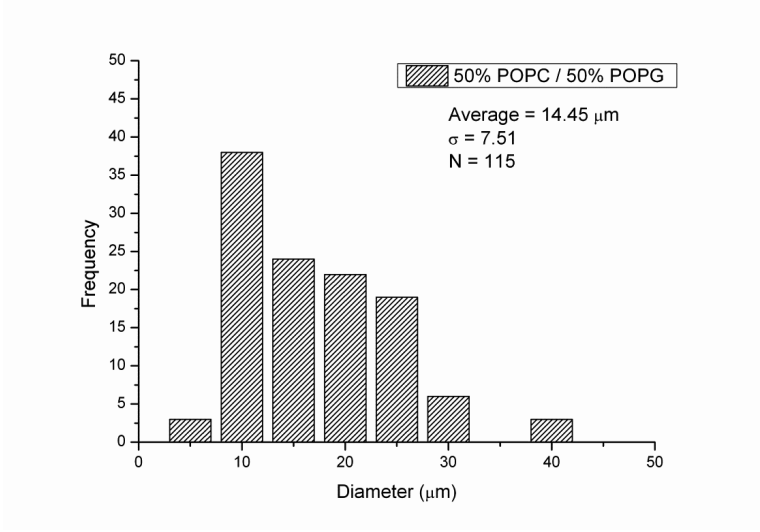

Figure A8. Size distribution of GUVs with lipid composition **D** (50% POPC / 50% POPG) in PBS.

*Lipid mixture **E** (90 % POPC / 10 % DOPS*

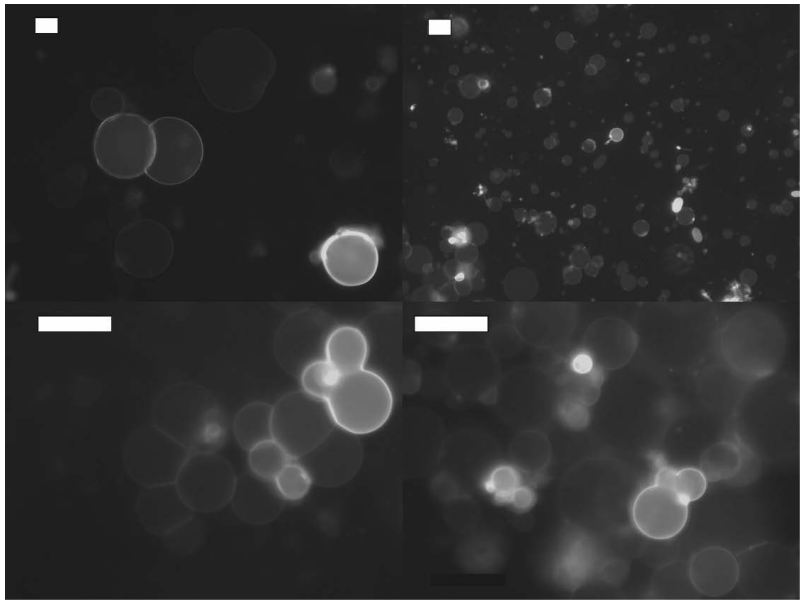

Figure A9. Free floating GUVs formed from POPC/DOPS (90:10 % mol) in PBS left column and HBS right column. On top 20x magnification and, bottom 63x magnification. The scale bars are 50 µm.

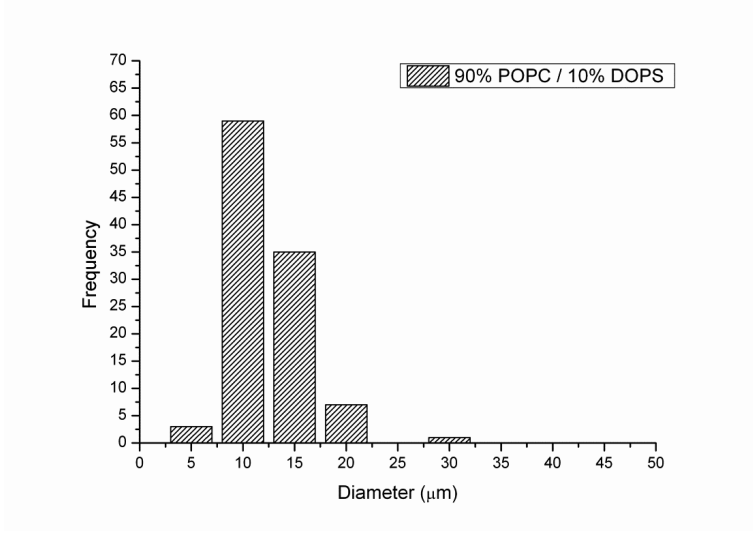

Figure A10. Size distribution of GUVs with lipid composition **E** (90% POPC / 10% DOPS) in PBS.

*Lipid mixture **F** (50 % DOPC / 50 % DPPC)*

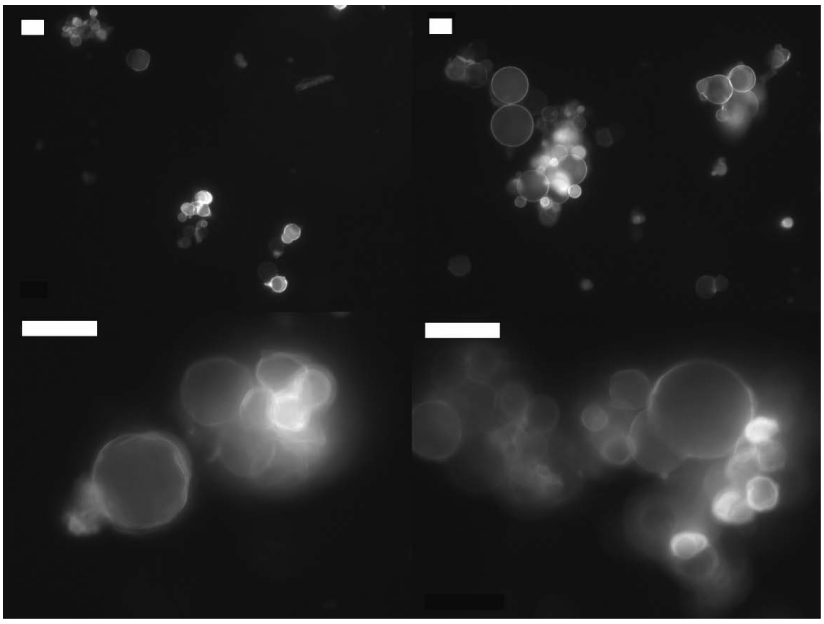

Figure A11. Free floating GUVs formed from DOPC/DPPC (50:50 % mol) in PBS left column and HBS right column. On top 20x magnification and, bottom 63x magnification. The scale bars are 50 µm.

*Lipid mixture **G** (33.3 % DOPC / 33.3 % DPPC / 33.3)*

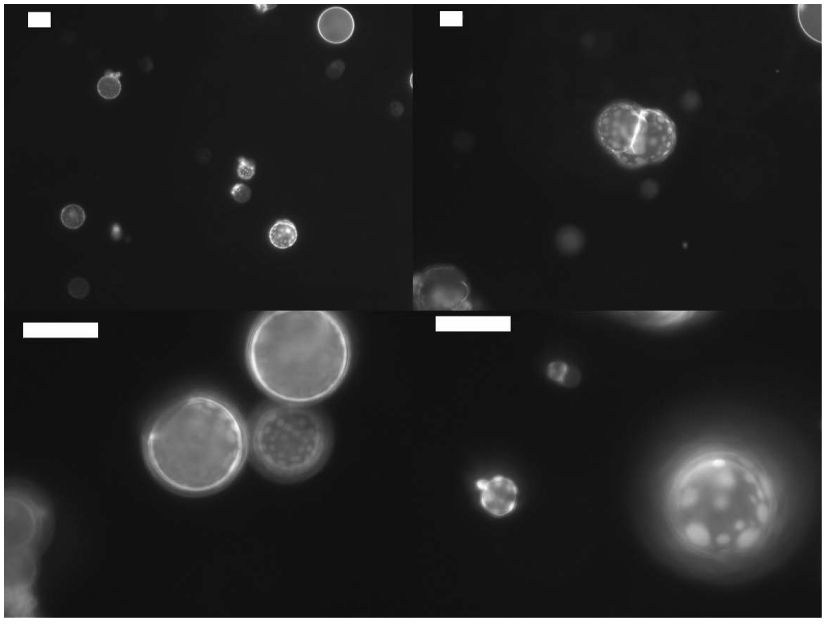

Figure A12. Free floating GUVs formed from DOPC/DPPC/CH (33.3:33.3:33.3 % mol) in PBS left column and HBS right column. On top 20x magnification and, bottom 63x magnification. The scale bars are 50 µm.

*Lipid mixture **H** (50 % DOPC / 25 % DOPE / 25 % CH)*

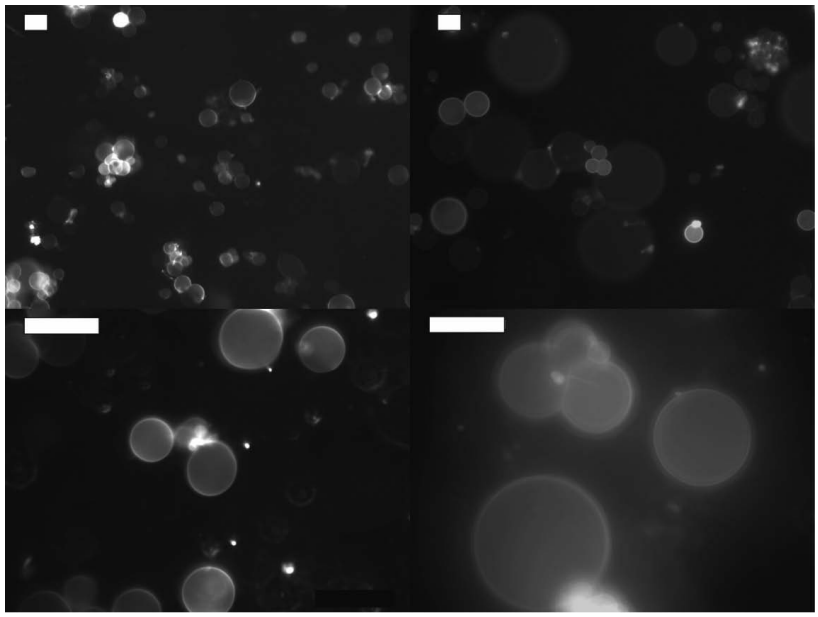

Figure A13. Free floating GUVs formed from DOPC/DOPE/CH (50 : 25 : 25 % mol) in PBS (left column) and HBS (right column). On top 20x magnification and, bottom 63x magnification. The scale bars are 50 µm.

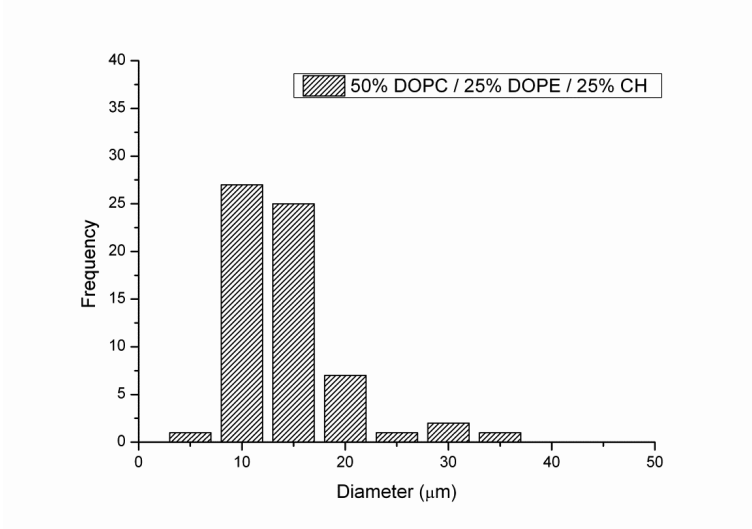

Figure A14. Size distribution of GUVs with lipid composition **H** (50% DOPC / 25% DOPE / 25% CH) in PBS.

*Lipid mixture **I** (50 % DOPC / 20 % DOPE / 5 % PEG2000-PE / 25 % CH)*

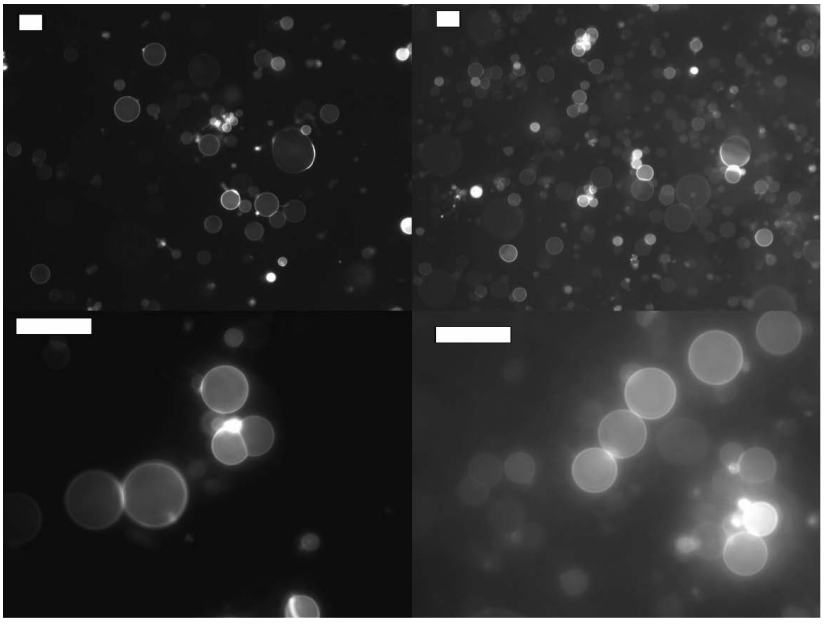

Figure A15. Free floating GUVs formed from DOPC / DOPE / PEG2000-PE / CH (50:20:5:25 % mol) in PBS left column and HBS right column. On top 20x magnification and, bottom 63x magnification. The scale bars are 50 µm.

Chapter III

The effect of crosslink density on hydrogel-assisted giant unilamellar vesicle growth

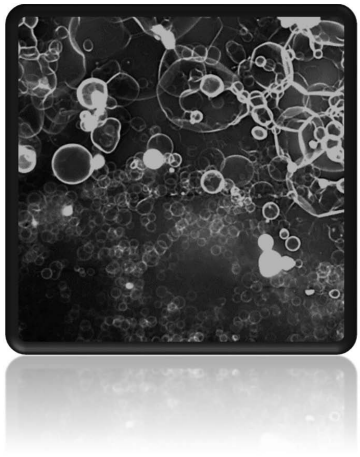

Manuscript in preparation: Nestor Lopez Mora, Yue Gao, M. Gertrude Gutierrez, Justin Peruzzi, Ivan Bakker, Ruud J.R.W. Peters, Bianka Siewert, Sylvestre Bonnet, Roxanne E. Kieltyka, Jan C. M. van Hest, Noah Malmstadt and Alexander Kros

Abstract.

Giant Unilamellar Vesicles (GUVs) are becoming popular membrane model systems for use in biophysical studies. The quality, size and yield of GUVs depend on the preparation method. In this study hydrogels consisting of dextran polymers crosslinked by poly(ethylene glycol) (DexPEG) were used as hydrophilic frameworks for the preparation of vesicle suspensions at physiological ionic strength conditions. A comparative study was performed using hydrogels with varied mechanical and morphological properties to evaluate their performance for GUV production. The efficiency of GUV production was quantified by flow cytometry with the size distribution being estimated by the Coulter Principle. We find that hydrogels of lower mechanical strength and increased swellability promote the production of GUVs, while their resulting size is determined by the surface roughness of the hydrogel film.

Introduction

The cellular membrane defines the boundary between the cytoplasm and the cell exterior regulating important intra- and intercellular processes in the biological milieu.[1] Therefore, the necessity of minimal cell models that allow *in vitro* studies, thereby simplifying these investigations, becomes highly relevant.[2] Giant Unilamellar Vesicles (GUVs) are exploited *in vitro* as a biomembrane model because of their membrane curvature and similarity in size to cells, being readily observable by optical microscopy.[3, 4] The GUV model has been used in the study of biomembrane properties,[5-8] membrane-protein[9-13] and membrane-peptide interactions,[14] channel formation in membranes[15, 16] or transmembrane transport of ions.[17, 18] Thus, the efficient formation of high quality GUVs under relevant physiological conditions is highly desirable.

The use of hydrogels as substrates for GUV growth is attractive due their potential to circumvent the disadvantages encountered in traditionally used methods such as natural swelling[19] and electroformation.[20] Covalent hydrogels are insoluble crosslinked polymer networks consisting of hydrophilic precursors that swell rapidly upon the addition of water creating a three dimensional network structure.[21] Most often, such networks have been applied in the areas of controlled drug delivery[22-24] and tissue engineering,[25, 26] but rarely in the growth of cell-sized vesicles (GUVs). Only recently, it has been shown that the use of hydrogel films enables the formation of GUVs at relevant physiological conditions. Horger et. al.[27] have proposed the use of physical gel substrates based on non-crosslinked agarose for the preparation of GUVs at near physiological conditions. The hydrogel produces GUVs successfully with several lipid compositions. However, traces of the agarose hydrogel substrate in the vesicle inner volume and the lipid membrane affect their mechanical properties. To tackle these drawbacks Lira *et al.*[28] used a thermal post-treatment of agarose-GUVs to release the encapsulated agarose and recover the GUV responses in electrodeformation studies. Alternatively films of hydrogels based on poly(vinyl alcohol)[29] and crosslinked polyacrylamide[27] have also been employed for the preparation of GUVs. While these polymers are not detected in the lipid bilayer of GUVs, they afford minimal control over the production and size.[30] We recently presented a facile method to form GUVs under physiological ionic strength conditions using a neutral, chemically crosslinked hydrogel substrate (DexPEG) consisting of a dextran polymer cross-linked by polyethylene glycol (PEG).[31] Maleimide-thiol

coupling chemistry was used to simultaneously crosslink the polymer chains and to anchor the forming gel to a glass surface. Chemically anchoring the hydrogel to the glass surface prevents its detachment during the rapid swelling of the DexPEG hydrogel film upon immersion of the glass slides in water. The use of the biocompatible DexPEG polymer that rapidly imbibes water from the dry state enables the formation of GUVs upon rehydration of a lipid film using physiologically relevant buffers.

Herein, we examine the effect of modulating hydrogel physicochemical properties on GUV production by controlling the crosslink density. We synthesised various DexPEG hydrogels by reacting a dextran polymer containing a controlled number of maleimide moieities and polyethyleneglycol (PEG) polymers with varied architecture, molecular weight and number of thiol functionalities (**Scheme 1** and **Table 1**). The production of GUVs on the various DexPEG hydrogel substrates was compared with respect to GUV size and yield by flow cytometry using the same lipid composition, ionic strength and growth times. The GUV formation process during hydrogel swelling was followed by imaging vesicle growth in time to better understand the effect of the various DexPEG substrates.

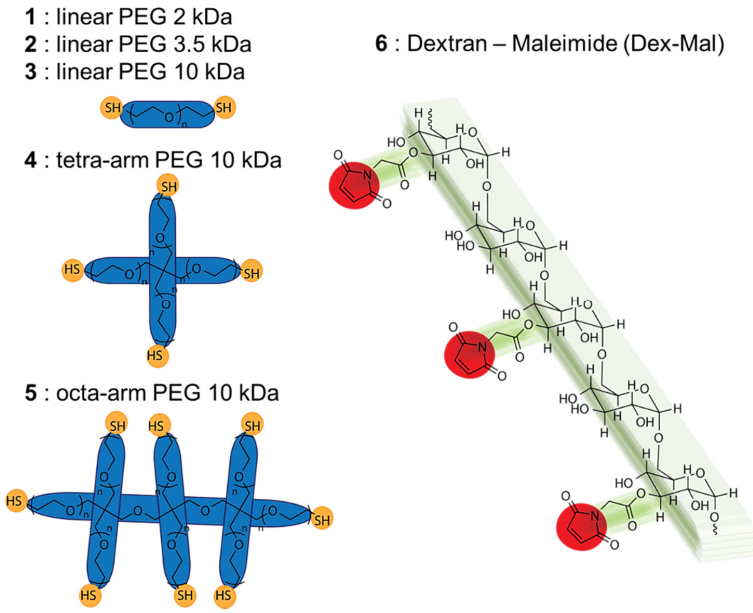

Scheme 1. Chemical structures of the precursors in the DexPEG hydrogel.

Table 1. Combinations of precursors for the formation of DexPEG hydrogels used in this study.

PEG crosslinker	Dex-Mal (**6**) DS=2	Dex-Mal (**6**) DS=4	Dex-Mal (**6**) DS=6	Dex-Mal (**6**) DS=9	Dex-Mal (**6**) DS=12
PEG (**1**)	✓	✓	✓	✓	✓
PEG (**2**)	✓	✓	✓	n.p.	✓
PEG (**3**)	n.p.	✓	n.p.	n.p.	n.p.
PEG (**4**)	✓	✓	✓	n.p.	✓
PEG (**5**)	✓	✓	✓	n.p.	✓

n.p. Not prepared

Results and Discussion

The degree of substitution (DS) and the architecture of the polymer crosslinker were systematically varied to modulate the physicochemical properties of the hydrogel materials (**Scheme 1**). Esterification of the dextran polymer with various equivalents of *N*-Maleoyl-*β*-alanine at room temperature resulted in functionalized polymers with a varying degree of substitution. The DS of the maleimide modified dextran (Dex-Mal), defined as the number of maleimide groups per 100 glucopyranose residues of dextran, was characterized by ^{1}H NMR. A proportional increase in the DS with the number of equivalents of *N*-Maleoyl-*β*-alanine added was observed up to DS=6. For DS>6, the addition of smaller quantities of *N*-Maleoyl-*β*-alanine resulted in greater changes in DS values (**Figure 7**, *Experimental Section*). Successful reaction of *N*-Maleoyl-*β*-alanine with the dextran polymer was confirmed by IR spectroscopy through the growth of the band 1700 (C=O), 1650 and 700 (vinyl) cm-1 increasing sharply with substitution degree (**Figure 8**, *Experimental Section*). In order to form hydrogels, thiolated linear (molecules **1**, **2** and **3**), tetra-arm or octa-arm PEGs (molecules **4** and **5**) were mixed to the various Dex-Mal polymers at a 1:1 molar ratio (maleimide:thiol) resulting in crosslinking of polymers via Michael addition. The polymer mixture (DexPEG) was drop-casted on thiolated glass slides as previously described.[31] The quality of the hydrogel film formed on the glass surface varied with DS by visual inspection. DexPEG polymers with a DS from 2 to 4 produced clear and homogeneous films on the glass surface regardless of the

architecture of the PEG crosslinker used, whereas higher DS dextran polymers resulted in inhomogeneous hydrogel films.

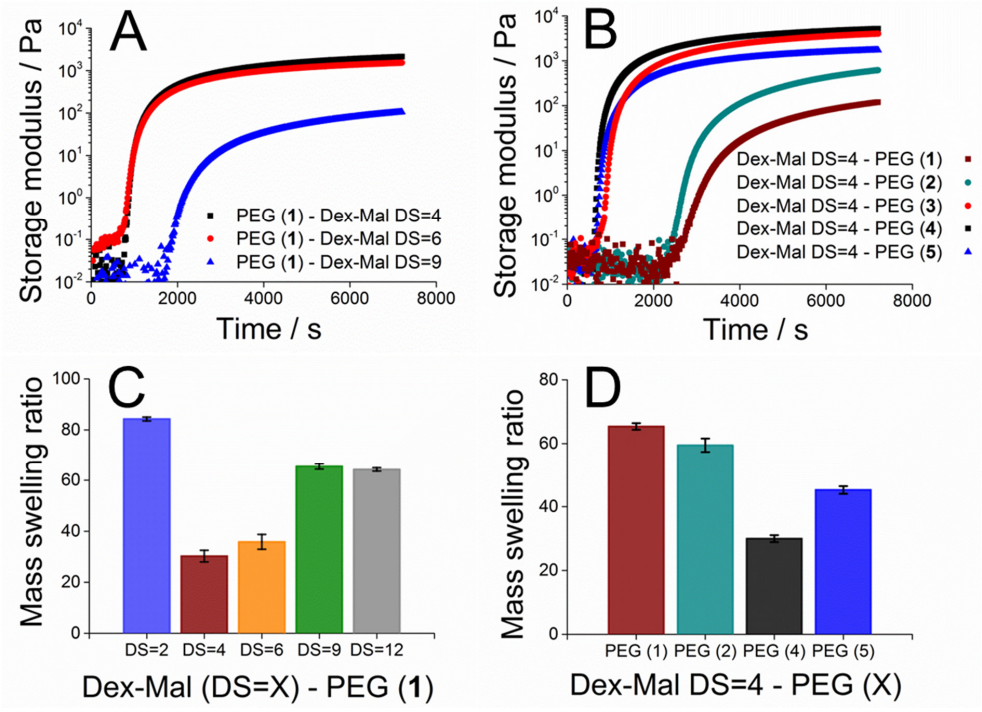

Figure 1. Mechanical and equilibrium swelling data of various DexPEG hydrogels with varied DS of the maleimide units in the dextran backbone and crosslinker (molecules **1**–**5**). *Top:* Oscillatory time sweeps for DexPEG hydrogels: **A**) **1** (1.2 wt %) and **6** (3.5 wt %) with DS = 4, 6 and 9. **B**) Molecules **1**–**5** and **6** with a DS = 4. *Bottom:* Equilibrium mass swelling ratio for DexPEG hydrogels with **C**) **1** and **6** DS = 2, 4, 6, 9 and 12. **D**) Molecules **1**– **5** and **6** (DS = 4).

Oscillatory rheology time sweeps were performed to provide insight into the gelation time and mechanical properties of the various DexPEG hydrogels. Their mechanical strength was examined as a function of the DS in Dextran (**6**) and the molecular weight, the number of thiols, and architecture of the crosslinker precursor (**1**, **2**, **3**, **4** and **5**). DexPEG combinations with higher DS in **6** produced weaker network structures with slower gelation rate (**Figure 1A**),

while higher molecular weight of the crosslinker precursor resulted in faster gelation and stronger networks (**Figure 1B**). Loose network structures were formed with linear based gels architecture (**1**, **2**) and interestingly, tetra-arm PEG (**4**) produced higher storage modulus than the octa-arm PEG (**5**) architecture which contains two times more thiol reactive groups. This phenomenon has been previously reported for hydrogel networks bearing substantial amounts of intramolecular loops or unreacted groups in the polymer network.[26]

The swelling properties of DexPEG hydrogels were examined to better understand the rehydration of the dried hydrogel films during the GUV formation. We studied the equilibrium mass swelling ratio of DexPEG hydrogels in glass vials excluding lipids. The equilibrium mass swelling ratio is defined as *Ws*/*Wd*, where *Ws* is the swollen weight of the gel after equilibration in buffer and *Wd* is the dry weight of the lyophilized gel. The swelling ratio decreases when the DS in Dex-Mal (**6**) increases, but for higher DS this trend is reversed (**Figure 1C**). This increase in the swelling ratio data revealed that those DexPEG combinations consist of a loose network structure. The opposite was observed with increasing the number of thiols in the PEG crosslinker, resulting in decreased swelling (**Figure 1D**). Consistent with mechanical measurements, the DexPEG hydrogel containing octa-arm PEG displayed a higher swelling ratio as compared to hydrogels crosslinked with tetra-arm PEG. This result is most likely due to the restricted accessibility of thiol groups on the octa-arm PEG to react efficiently with maleimides on the dextran polymer (Dex-Mal, molecule **6 Scheme 1**). Thus, the presence of more reactive groups on the same polymer chain increase the probability of reacting on the same polymer chain, producing more defective, looser and sweallable polymeric networks.

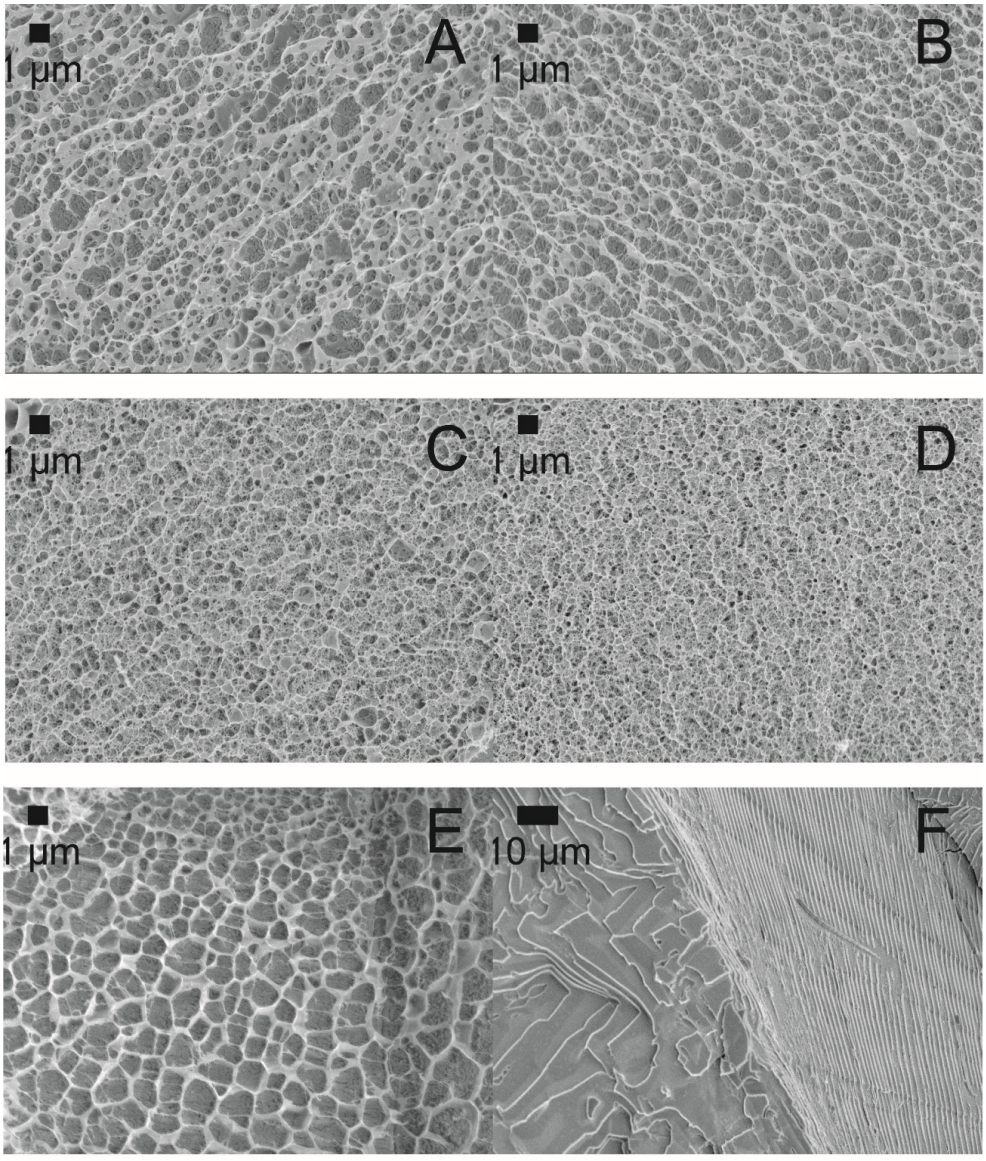

Figure 2. Cryo-SEM of DexPEG hydrogels with different DS and PEG crosslinker. **A**) **6** DS=4 and crosslinker **1**; **B**) **6** DS=4 and crosslinker **2**; **C**) **6** DS=4 and crosslinker **4**; **D**) **6** DS=4 and crosslinker **5**, **E**) **6** DS=6 and crosslinker **2**, **F**) **6** DS=12 and crosslinker **2**. The effect of the crosslinker in the morphology of hydrogels can be observed in Figures 2A and 2B for DexPEG hydrogel containing linear PEG (**1, 2**), Figure 2C for DexPEG hydrogel containing tetra-arm PEG (**4**) and Figure 2D for DexPEG hydrogel containing octa-arm PEG (**5**).

Next, we examined the morphology of selected DexPEG hydrogels in the swollen state by cryo-scanning electron microscopy (cryo-SEM), see **Figure 2**. We observed that hydrogels composed of **6** with a DS>6 lacked the ability to form a three dimensional network structure (i.e. **Figure 2F**). In contrast, hydrogels with a DS<6 produced a continuous honeycomb-like network structure in the swollen state, but with different pore size. For example, the DexPEG hydrogel with DS=6 (**Figure 2E**) forms a porous network morphology with pore sizes greater (~1 μm) whereas a hydrogel with DS=4 (**Figure 2B**) displays pore sizes around 200 nm in size. This finding is in contrast to photocrosslinked dextran-methacrylate hydrogels containing the same dextran backbone, where the pore size decreased when the degree of substitution increased.[32] A possible explanation may be due to the decreased solubility of Dex-Mal (**6**) in water when the degree of substitution is increased, while the solubility of methacrylate functionalized dextran is not significantly affected by the DS. Additionally, increasing the number of thiol groups in the PEG crosslinker yielded DexPEG hydrogels with a highly porous honeycomb-like structure.

We found previously that DexPEG hydrogels with a decreased crosslink density present the ability to growth GUVs with larger mean diameter.[31] The morphology of those hydrogels was also examined by cryo-SEM as a function of the maleimide/thiol ratio (**Figure 9**, *Experimental Section*). Overall, these results show that decreasing the PEG crosslinker concentration leads to formation of an inhomogeneous network structure due to the formation of fewer crosslinks. These observations are in good agreement with the mechanical data (**Figure 10**, *Experimental Section*) that point to the formation of a weak and loose network structure consistent with the crosslink density.

The correlation between hydrogel crosslink density and its effect on GUV yield was quantified by fluorescence-activated cell sorting (FACS) experiments. Stock solutions of the lipid mixtures POPC : Cholesterol (80 : 20 mol%) and POPC : Cholesterol : PEG2000-PE (75 : 20 : 5 mol%) were deposited on the DexPEG hydrogel coated microscope slides with varied DS and crosslinkers. Both lipid compositions also contained 0.7 % mol of 1,2-dioleoyl-*sn*-glycero-3-phosphoethanolamine-*N*-(7-nitro-2-1,3-benzoxadiazol-4-yl) (ammonium salt) (DOPE-NBD) to allow fluorescence detection of the formed GUVs. Subsequently, the solvent was evaporated under a gentle stream of nitrogen and in a vacuum oven overnight. Finally, the lipid-coated hydrogel films were hydrated in phosphate-buffered saline (PBS) and the resulting free-floating GUVs were collected and characterized by FACS. PEGylated and non-PEGylated

GUVs were formed on all hydrogels and detected in both fluorescence and side scattering channels, producing typical populations of GUVs (**Figures 11** and **12**, Experimental Section). The use of PEGylated lipids in the lipid composition of GUVs decreased the aggregation of GUVs, resulting in an increased frequency of single events (i.e. a more precise counting of single GUVs) for all DexPEG combinations (**Figure 3**). Firstly, increasing the DS in Dex-Mal resulted in a higher GUV yield (**Figure 3A**). These observations were in good agreement with the swelling ratio studies confirming that this is the main parameter in GUV formation. In contrast, increasing the number of thiol groups of PEG crosslinkers decreased the yield of GUVs (**Figure 3B**). Only hydrogels synthesized with the octa-arm PEG (**5**) did not follow this trend also in line with swelling data. The effect of the degree of substitution and crosslinker density on GUVs production is in good agreement with the oscillatory rheology, equilibrium mass swelling ratio, and SEM imaging of the various DexPEG substrates. Moreover, these results inidicate that the main driving force for efficient GUV production is the high swellability of the dextran hydrogel network during the rehydration of the lipid-coated hydrogel films.

The size distribution of the produced GUVs was estimated using the Coulter Principle in a Quanta SC FACS instrument based on electrical impedance.[33, 34] The Electric Volume (*EV*) parameter is proportional to the electrical impedance and does not depend on the laser wavelength, geometry or refractive index of the sample, overcoming limitations of forward and side scattering monotonic measurements for the determination of particle size by flow cytometry.[35] We transformed the *EV* parameter measured to GUV diameter (μm) (See **equation 1** and **2** in *Experimental Section*). Validation of this method was made with microsphere standards with nominal sizes of 10 μm and 20 μm (**Figure 13**, *Experimental Section*). These measurements yielded a size distribution profile for a large set of PEGylated GUVs. The advantage of this method is the possibility to count large populations of GUVs, as compared to microscopy-based methods which can only consider smaller population sizes due to the small focal volume.

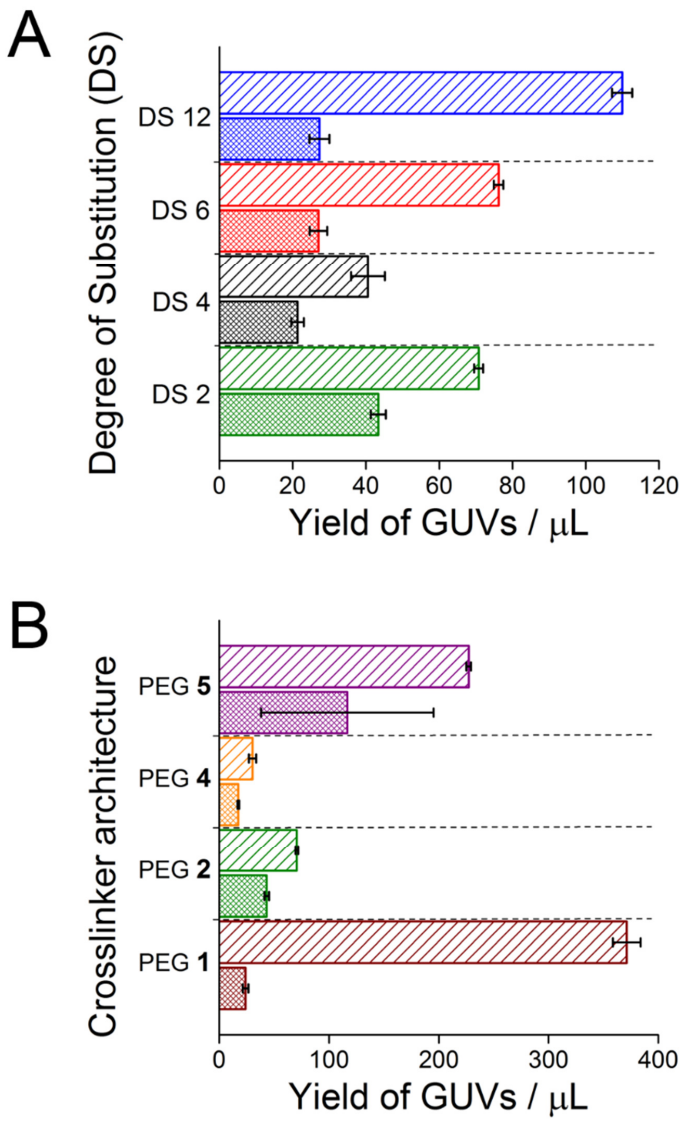

Figure 3. Yield of fluorescently labelled GUVs produced on the various DexPEG substrates as determined by FACS. Cross-hatched bars represent GUVs with the lipid composition POPC : Cholesterol (80 : 20 mol%) and line patterned bars represent PEGylated GUVs with the lipid composition POPC : Cholesterol : PEG2000-PE (75 : 20 : 5 mol%). **A**) Effect of the DS on the production of GUVs for DexPEG hydrogel films with linear crosslinker **2** and **6** DS from 2 – 12. **B**) Effect of the functionality of the PEG crosslinker on the production of GUVs for DexPEG hydrogel films with **6** DS=2 and linear PEG (**1**), linear PEG (**2**), tetra-arm PEG (**4**) and octa-arm PEG (**5**) crosslinkers.

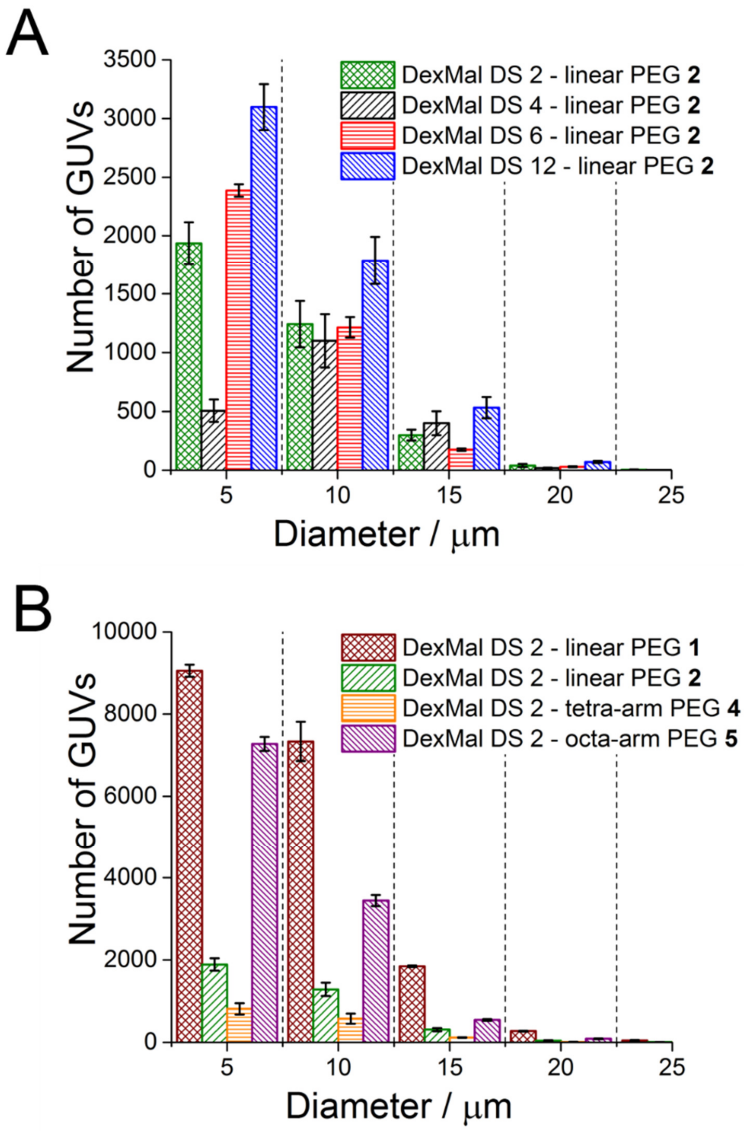

Figure 4. Determination of the size distribution by the Coulter principle for GUV populations with the lipid composition POPC:Cholesterol:PEG2000-PE (75 : 20 : 5 mol%) produced on various DexPEG substrates. **A**) Effect of the DS on the size of GUVs for DexPEG hydrogel films with linear crosslinker **2** and **6** with DS from 2–12. **B**) Effect of the functionality of the PEG crosslinker on the size of GUVs for DexPEG hydrogel films with **6** DS=2 and linear PEG (**1**), linear PEG (**2**), tetra-arm PEG (**4**) and octa-arm PEG (**5**) crosslinkers.

In **Figure 4**, the effect of the DS and the crosslinker functionality of the hydrogels on the GUV size distribution are presented. All tested DexPEG hydrogel substrates, independent of the DS or crosslinker functionality, produced GUVs populations with sizes ranging between 5 µm and 20 µm in diameter. DexPEG hydrogels designed with multi-arm PEG crosslinkers **4** and **5** produced GUVs with a similar size distribution as compared to linear PEG crosslinker **1** and **2** based hydrogels, but with lower yields. These size distributions are in line with those previously reported by optical microscopy using a lipid composition of POPC : Cholesterol (80 : 20 mol%) on DexPEG substrates with equimolar ratio of precursors (diameter = 10 ± 5 µm, N = 55 GUVs).[31] Moreover, we previously found that by decreasing the crosslink density by reducing the molar ratio of PEG (**1**) crosslinker respect to Dex-Mal (**6** DS=4) the GUVs size distribution could be tuned. In this work, we further explore the potential to tune GUV size by increasing the crosslink density through the use of multi-arm PEG crosslinkers **4** and **5**. No significant differences in the GUVs size distribution were observed, however lower yields due to the decreased swelling of these networks were observed (**Figure 4B**). Collectively, these data together with oscillatory rheology and cryo-SEM imaging of those hydrogels (*vide supra*) indicate that the formation of inhomogeneous and loose networks by decreasing the crosslink density leads to wider and larger size distributions of GUVs, while the formation of homogeneous and compact networks with small pore sizes does not affect significantly the size distribution the GUVs.

The GUV formation and growth from DexPEG hydrogels was studied by differential interference contrast (DIC) microscopy. Lipids (POPC : Cholesterol, 80 : 20 mol%) were spread on DexPEG hydrogels composed of linear PEG (**1**) and tetra-arm PEG (**4**) crosslinkers and observed before and during swelling. The hydrogel was swollen with 200 mM sucrose in PBS (pH 7.4) and images were taken every second for 10 minutes. The initial GUV diameter was a few microns and became larger due to coalescence from crowding. Most likely, the GUVs take on the size of the pores of the honeycomb network of DexPEG upon exposure to the buffer. These GUV coalescence events are quantified as a function of time in **Figure 5A**. Upon GUV coalescence, the average size of GUVs increases while the number of GUVs decreases. Variation in the initial GUV sizes was observed as a function of the varying surface roughness within the hydrogel of the DexPEG with linear PEG (**1**) and tetra-arm PEG (**4**). Meticulous inspection of hybrid lipid/DexPEG hydrogel film showed rougher surfaces and smoother surfaces consistent with the quality of the drop-casted gel. On rougher surfaces (**Figure 5B**) GUVs coalesced less and maintained a smaller size (~5 µm diameter), while in

smoother surfaces (**Figure 5C**), the formed GUVs were larger (~14 μm diameter). Therefore thickness and roughness of the DexPEG hydrogel film should be considered for controlling polydispersity in the final size distribution of GUVs.

Overall, the physical data obtained by oscillatory rheology, equilibrium swelling and cryo-SEM show that the number of thiols and polymer architecture strongly affect the effective crosslinking density of hydrogel network formed via maleimide-thiol addition. Examining the physicochemical properties of the various combinations of the DexPEG hydrogels revealed that a lower mechanical strength and an increased swelling ratio of the network favour GUV growth, whereas an increased crosslink density negatively impacts the lipid self-assembly process. GUVs swell from the surface of the hydrogel matrix (DexPEG) as depicted in **Figure 6**. Here, the growth of fluorescent labelled GUVs is shown using a confocal microscopy imaging reconstruction. The orthogonal reconstruction of the confocal image allows the imaging of the budding of vesicles during the first minutes of lipid hydration on the hydrogel scaffold.

Finally, we investigated the interaction of lipids with a dry DexPEG film. The gel to liquid-crystalline phase transition of DOPC lipids in the presence and absence of DexPEG film was determined by differential scanning calorimetry (DSC). A single sharp endothermic transition (T_m) was found for pure DOPC at -6 °C, meaning that the water/lipid ratio was ~3.[36] The T_m for DOPC on a DexPEG film shifted to -18 °C and was broadened (**Figure 14A**, *Experimental Section*), indicative of lipid-DexPEG interaction. For comparison we also determined the T_m of DOPC in the presence of only PEG gel (2 wt% of tetra-arm PEG (**4**), crosslinked with 0.05 vol% H_2O_2, *Experimental Section*). Surprisingly, the T_m of DOPC was now fully depressed (**Figure 14B**, *Experimental Section*). This finding shows that DOPC interacts more strongly with PEG as compared to dextran. Moreover, the growth of GUVs on films of PEG (**4**) gel was not observed. Therefore lipid-hydrogel interactions should be considered when designing new hydrogels for GUV formation and studies understanding these interactions are required.

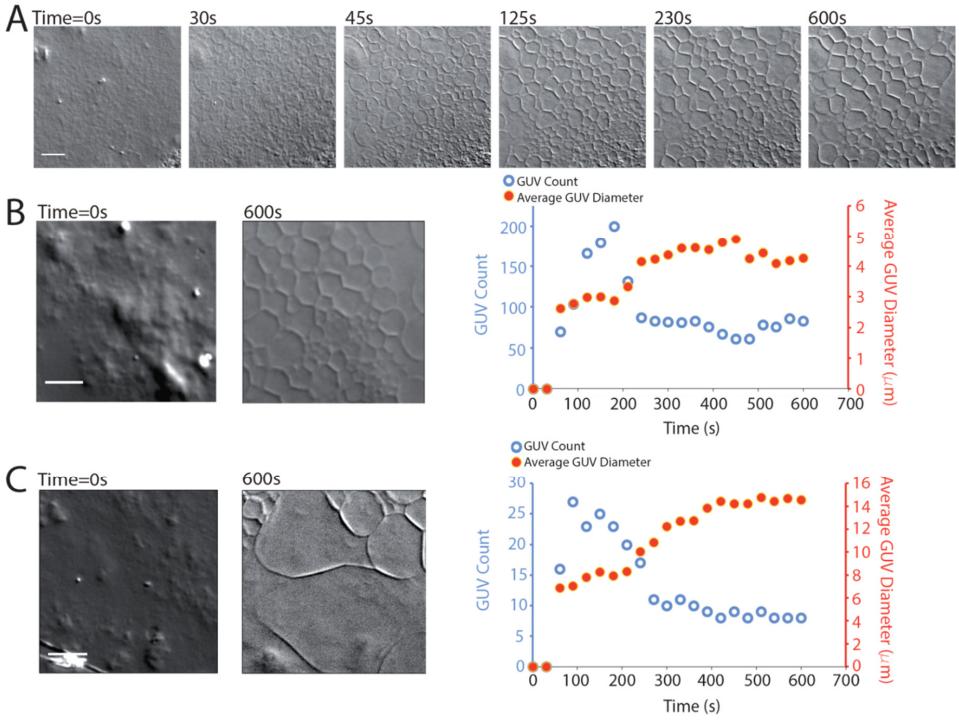

Figure 5. GUV swelling observed on the DexPEG surface. **A**) DIC time lapse series of micrographs of POPC : Cholesterol (80 : 20 mol%) on DexPEG hydrogel with DS=2 and tetra-arm PEG (**4**) crosslinker. The scale bars are 10 μm. The first image shows dried lipid film on top of the hydrogel. The subsequent images are indicated according to time of swelling. GUVs form off of the DexPEG hydrogel network and coalesce to form larger GUVs. **B**) Left micrographs show areas of rough DexPEG with lipid before hydration (Time=0s) and after hydration (600s). The right plot shows how GUV number and average size changes with time. **C**) Micrographs are examples of areas of smooth DexPEG with lipid and associated kinetics of swelling plot is on the right. As coalescence occurs, GUV size increases and count decreases. Smooth DexPEG areas form larger GUVs as compared with rougher areas.

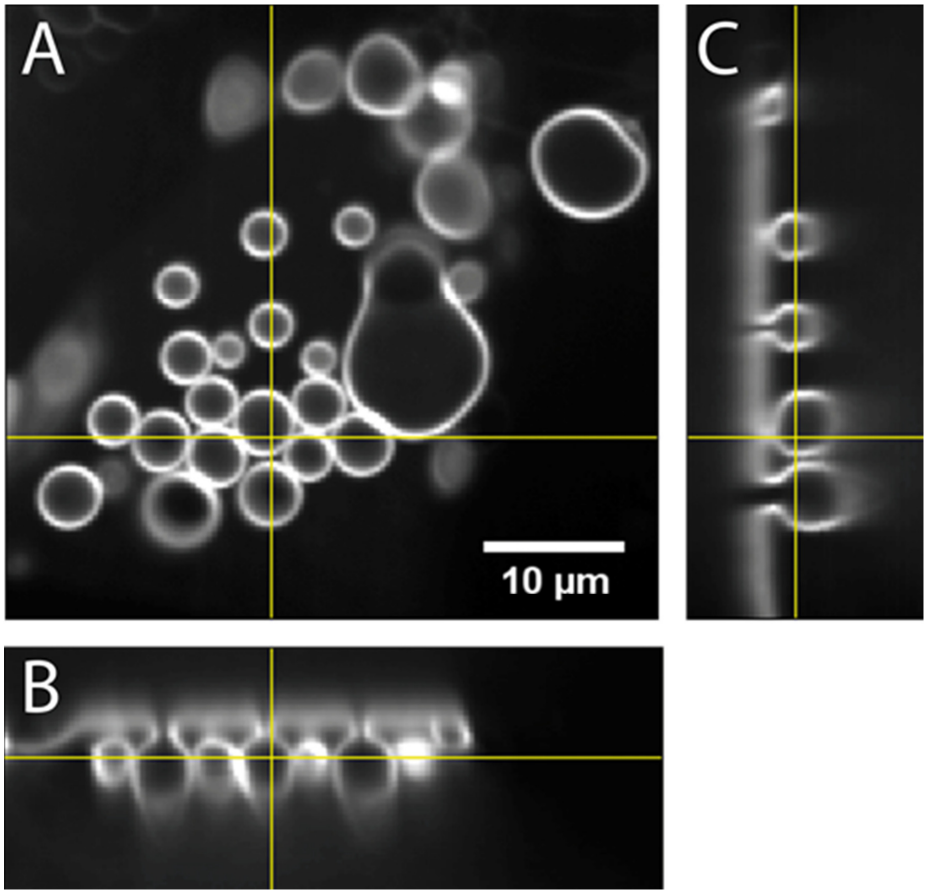

Figure 6. Confocal images GUVs formed from a DexPEG surface. **A**) A single confocal slice of an image stack of GUVs swollen on DexPEG. Lipid composition is POPC : Cholesterol (80 : 20 mol%) fluorescently labelled with ATTO-488-DPPE (0.4 mol%). The yellow lines indicate the orthogonal slices in B and C. **B**) Horizontal orthogonal slice of GUVs in A reconstructed from confocal image stack. **C**) Vertical orthogonal slice of GUVs in A. B and C show GUVs that are not yet fully formed closed spheres. Rather, they are still attached by budding necks to the surface of the lipid film.

Conclusion

In conclusion, we designed a very facile and efficient method for GUV preparation. The effect of increased crosslinking on the dextran hydrogel by poly(ethylene glycol) on the yield, size distribution and formation of GUVs revealed that the physicochemical properties of DexPEG hydrogels strongly influence the production of GUVs in PBS. The most optimal hydrogel scaffolds for GUV growth exhibit the highest swelling capacities. Furthermore, we observed that the final size distribution of the GUVs is not affected by the honeycomb architecture of the DexPEG substrate but rather by the homogeneity of the network and surface roughness of the film. We envisage that controlling the roughness of the DexPEG film might provide a way to produce monodisperse GUVs populations. Finally, hybrid lipid/DexPEG films facilitate the budding and coalescence of vesicles to produce high yields of GUVs under high ionic strength. The efficient formation of GUVs at physiological salt concentrations has the potential to increase the applicability of GUVs as a biophysical model in the study of membrane interactions at similar conditions than those required in *in vivo* systems.

Experimental Section

Materials and methods

1-palmitoyl-2-oleoyl-*sn*-glycero-3-phosphocholine (POPC), 1,2-dioleoyl-*sn*-glycero-3-phosphoethanolamine-*N*-[methoxy(polyethylene glycol)-2000] (ammonium salt) (PEG2000-PE) and 1,2-dioleoyl-*sn*-glycero-3-phosphoethanolamine-*N*-(7-nitro-2-1,3-benzoxadiazol-4-yl) (ammonium salt) (18:1 NBD-PE) were purchased from Avanti Polar Lipids. Dextran from Leuconostoc (M_n = 70 000, dried in vacuum oven for several days before use), Cholesterol (CH), *β*-Alanine, 4-(dimethylamino) pyridine (DMAP), Magnesium Sulfate ($MgSO_4$), 3400 Da poly (ethylene glycol) dithiol, *N*,*N*'-Diisopropylcarbodiimide (DIC), Acetic Acid, Ethyl Acetate, Toluene, Dimethyl Sulfoxide (DMSO) and 2-propanol were purchased from Sigma-Aldrich. Maleic Anhydride and *p*-Toluene Sulfonic Acid Monohydrate (PTSA) were purchased from Fluka. 2000 Da poly (ethylene glycol) dithiol was purchased from Iris Technologies GmbH. 4 arms poly (ethylene glycol) thiol (pentaerythritol core) and 8 arms poly (ethylene glycol) thiol (tripentaerythritol core) were purchased from JenKem Technology, USA. NIST Traceable Latex Particles Standards nominal sizes 10 µm and 20 µm were purchased from Beckman Coulter. The salt of pyridinium 4-(Dimethylamino) pyridinium 4-toluenesulfonate (DPTS) was prepared from DMAP and PTSA in equimolar quantities.[37]

*Synthesis and characterization of N-Maleoyl-β-alanine and Dex-Mal (**6**) with different degree of substitution.*

N-Maleoyl-*β*-alanine was prepared in a large scale synthesis following the previously reported procedure for obtaining maleimido alkanoic acids.[38] Maleic anhydride (9.95 g) and *β*-Alanine (9.18 g) were added to 75 mL acetic acid. The mixture was refluxed at 170 °C for 90 minutes. Then the solution was cooled to room temperature. The acetic acid was evaporated in vacuum. The residual acetic acid was removed by forming an azeotrope with toluene and evaporation under vacuum. The crude was extracted three times in ethyl acetate and the organic layer was dried with $MgSO_4$. The crude was recrystallized in ethyl acetate at 4 °C overnight.

The compound was sublimed using a cold finger to increase the purity. The final yield is 31.6 %. The compound was characterized with ^{1}H-NMR (400MHz, $CDCl_3$): δ = 6.7 (s, -C**H**=C**H**-), δ = 3.8 (HOOC-C**H**$_2$-CH$_2$), δ =2.7 (-CH$_2$-C**H**$_2$-N).

Dex-Mal (**6**) was synthesized by DIC mediated esterification of the hydroxyl groups of dextran with *N*-Maleoyl-*β*-alanine. For instance to obtain a substitution degree of 4, Dextran (0.62 g), *N*-Maleoyl-*β*-alanine (0.42 g) and DPTS (0.15 g) were dissolved in anhydrous DMSO (25 mL). The mixture was stirred at room temperature for two hours, followed by the addition of DIC (0.48 mL). After overnight stirring (19 hours) at room temperature, the formed *N*, *N*'-dialkylurea was removed by filtration and the crude product was obtained by precipitation in cold isopropanol. The precipitate was dissolved in water and extensively dialyzed against Milli-Q water for two days and subsequently lyophilized. ^{1}H NMR (400 MHz, D_2O): δ 3.3-4.0 (m, dextran glucopyranosyl ring protons), 4.9 (s, dextran anomeric proton), 6.8 (s, maleimide). ^{13}C NMR (400MHz, D_2O): δ=134.5, 97.7, 73.4, 71.4, 69.5, 65.5.

The degree of substitution (DS) of Dex-Mal is defined as the number of maleimide groups per 100 glucopyranose residues of dextran, which was calculated from the ^{1}H NMR spectra based on the protons of maleimide (δ 6.8) and the anomeric proton (δ 4.9). The DS of Dex-Mal was controlled by the molar ratio between Dextran and N-Maleoyl-β-alanine as it is showed in the **Figure 7**. The incorporation of *N*-Maleoyl-*β*-alanine in the Dextran backbone was confirmed by the presence of an ester FT-IR band at 1700 cm^{-1} (**Figure 8**). This band increases with the increase in the degree of substitution on the Dextran, while the broad hydroxyl group band between 3000 - 3700 cm^{-1} does not show a significant decrease, indicating the presence of hydroxyl free groups.

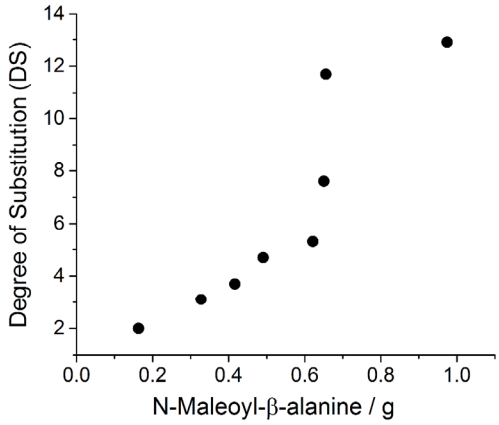

Figure 7. Degree of substitution (DS) as a function of the mass of *N*-Maleoyl-*β*-alanine added in the reaction to produce Dex-Mal (**6**). The degree of substitution (DS) of the product **6** is determined from the ^{1}H NMR.

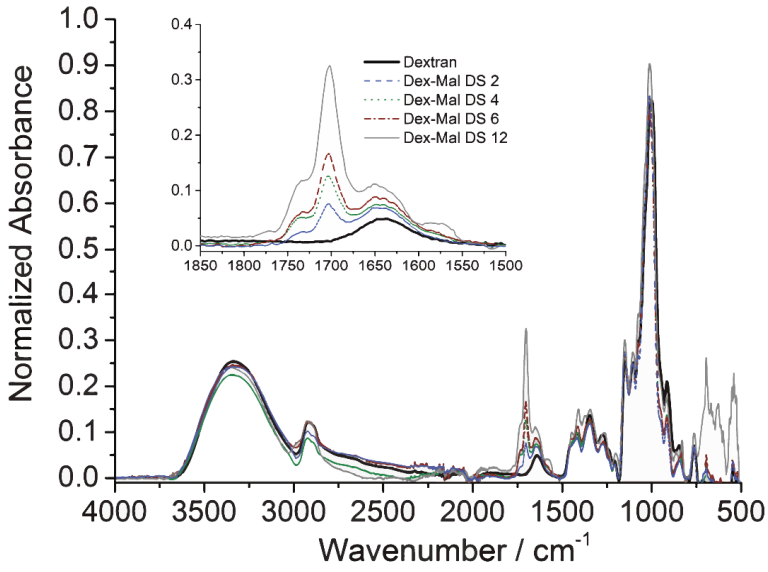

Figure 8. FT-IR spectra of Dextran and Dex-Mal (**6**) with degree of substitution (DS) 2, 4, 6, 12. The inset image shows the increase of the ester band (1700 cm^{-1}) corresponding to the bond between Dextran and *N*-Maleoyl-*β*-alanine.

DexPEG and PEG Hydrogel substrates preparation

DexPEG coated glass substrates. Dex-Mal (2 wt% solution, DS = 2, 4, 6 and 12) was crosslinked using **1**, **2**, **4** and **5** in equimolar ratios at room temperature to form several DexPEG hydrogels. For instance, Dex-Mal (**6**, DS= 4, 60 mg) was dissolved in water (2.5 g) and 11.11 mg of **1** (2000 Da) in water (0.5 g) were reacted to provide a DexPEG hydrogel solution. The mixture was shaken in a vortex for 1 minute and immediately used for the preparation of glass substrates. DexPEG solution (600 µL) was drop casted onto previously thiol functionalized microscope glass slides. A homogenous polymeric film was formed after evaporating water during 30 – 45 minutes at 40 °C. The DexPEG coated microscope slides were stored for further use.

PEG hydrogel coated glass substrates. Commercial 4-thiol armed PEG was crosslinked with hydrogen peroxide (H_2O_2) by forming disulfide tetramers. 4 armed- poly (ethylene glycol) thiol (pentaerythritol core) (**4**, 2 wt% solution) was dissolved in 100 µL water and mixed with 10 µL H_2O_2 (50 wt% in water). The mixture was shaken in a vortex for 1 minute and immediately used for the substrate preparation. Drop casting of the solution on thiol functionalized microscope slides resulted in the formation of an inhomogeneous hydrogel film after 5 minutes. The PEG coated microscope slides were stored for further use.

Formation of GUVs

Giant Unilamellar Vesicles (GUVs) were grown in various Dex-PEG hydrogel coated microscope glass slide substrates. A lipid solution (10 µL) with the lipid composition POPC and Cholesterol (80:20 molar ratio, 14 mM) and DOPE-NBD (0.7 mol%) or POPC / Cholesterol / PEG 2000 - PE (75 : 20 : 5 molar ratio, 14 mM) and DOPE-NBD (0.7 mol%) was deposited on a hydrogel coated glass slide, then the lipid solution was dried by evaporating the chloroform under a gentle stream of nitrogen and placed in a vacuum oven overnight. A liquid chamber was made by placing a 15 mm (OD) glass O-Ring on top of the hydrogel, which was sealed with high vacuum silicon grease. The lipid film was hydrated by adding 400 µL of PBS and the GUVs were growth overnight at room temperature.

Confocal and DIC Imaging.

Spinning-disc confocal microscopy was performed on a TI-Eclipse inverted microscope (Nikon, Japan) equipped with a 16-bit Cascade II 512 EMCCD camera (Photometrics, USA) and a CSUX confocal head (Yokogawa, Japan). Illumination was provided by a 50 mW solid-state laser at 561 nm (Coherent Inc., Germany) and the objective used was a 60× NA1.43 Plan-Apo Nikon oil-immersion objective. DIC imaging was performed on an Axio Observer (Zeiss, Germany) equipped with a Hamamatsu CMOS camera (Hamamatsu, Japan). Illumination was provided by a halogen lamp 12V 100W using a differential interference contrast prism with polarizer (Zeiss, Germany) and the objective used was a 20x NA0.8 Plan-Apo Zeiss objective.

Cryo-Scanning Electron Microscopy (cryo-SEM).

The morphologies of the hydrogels in the swollen states were observed in a JEOL 6330 Cryo Field Emission Scanning Electron Microscope from the General Instrumentation Facility at Radboud University (Nijmegen, The Netherlands). 5 μL of Dex-PEG hydrogel was taken and injected into a hollow cylindrical sample holder and immediately flash frozen in liquid nitrogen. The sample was then inserted in the cold-stage of the SEM cryo-preparation chamber and cleaved to make a horizontal fracture plane. The water was sublimated during 15 minutes and the fracture plane was coated with a thin gold-palladium layer and subsequently the sample is transferred into the SEM chamber, where it remained frozen during the imaging.

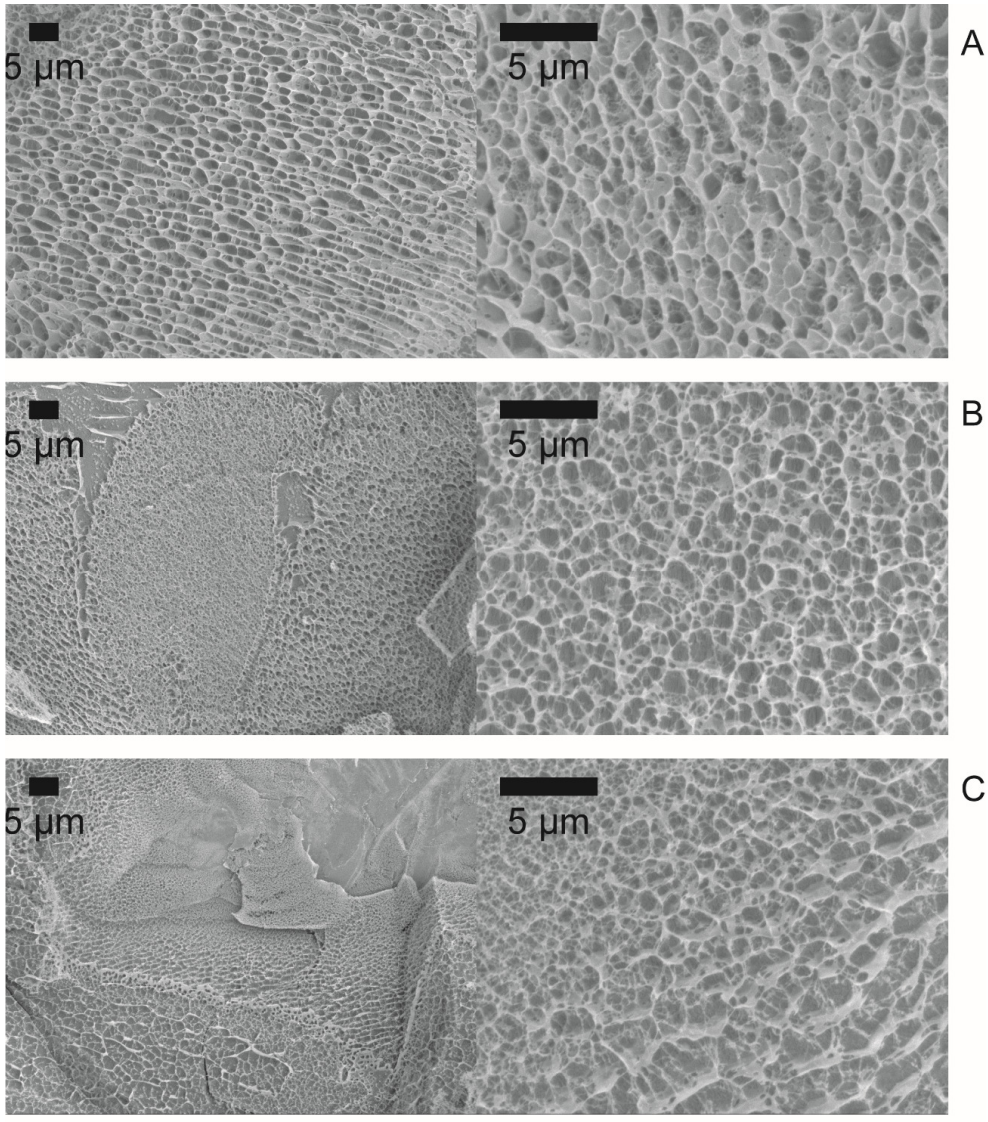

Figure 9. Cryo-SEM of DexPEG hydrogels with different molar ratio between precursors. **A**) Dex-Mal (DS 4) – PEG (**1**) crosslinker (1:1 molar ratio). **B**) Dex-Mal (DS 4) – PEG (**1**) crosslinker (1:0.75 molar ratio). **C**) Dex-Mal (DS 4) – PEG (**1**) crosslinker (1:0.5 molar ratio).

Oscillatory Rheology.

Oscillatory time sweeps were performed on a Hybrid Rheometer (DHR-2) from TA Instruments using a plate – plate geometry. The precursors Dex-Mal (**6**) with various DS and thiolated PEG solutions (molecules **1** – **5**) were loaded on the lower plate and the upper plate (25 mm diameter) was immediately lowered to a gap distance of 0.5 mm for all experiments. Oscillatory time sweeps were performed on the various forming hydrogel materials following the storage (G') and loss (G") moduli with respect to time at 1% strain and 0.1 – 100 rad/s angular frequency.

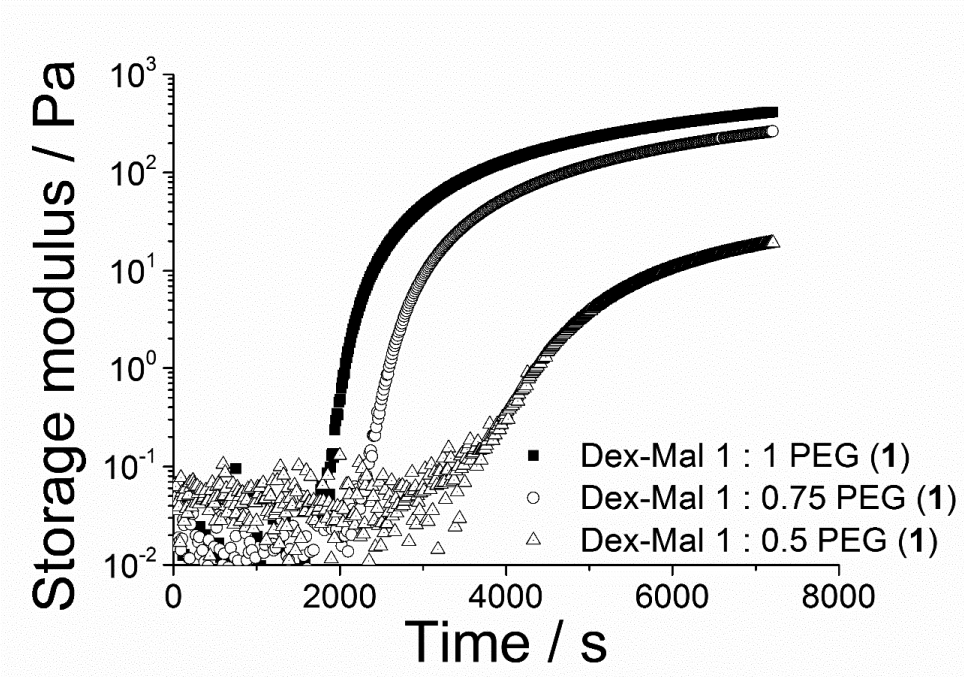

Figure 10. Mechanical characterization of DexPEG hydrogels with increasing PEG cross-linker using oscillatory rheology time sweeps. The trace in squares represents 1:1 molar ratio Dex-Mal (DS 4) – PEG (**1**). The trace in circles represents 1:0.75 molar ratio Dex-Mal (DS 4) – PEG (**1**). The trace in triangles represents 1:0.5 molar ratio Dex-Mal (DS 4) – PEG (**1**).

Flow Cytometry.

A Beckman Coulter Quanta instrument was used to analyze the yield and the size distribution of several GUV batches. In contrast to common fluorescence flow cytometers, which only depend on optical parameters, i.e. light scattering and fluorescence, the employed Beckman Coulter system additionally utilizes the electrical impedance, also known as Coulter Principle.[33, 39] Briefly, particles pass through the orifice of a saline-filled cell. A constant (DC) current is applied across this aperture with an electrical circuit. Whenever the nonconductive GUVs pass through this orifice a voltage pulse will be generated.[35] The amplitude thereof is theoretically proportional to the volume of the particles, and expressed as electric volume (*EV*). Based on the principle an accurate size measurement can be guaranteed, as the *EV* is in contrast to the forward scatter (*FSC*) monotonic.[35] In addition and simultaneously, each particle is irradiated by a 488 nm laser beam, leading to the possibility of detecting the side scatter (*SSC*), and therewith the density of the investigated particles, as well as light emission, thus fluorescence (available filters: 525 BP (*FL1*), 575 BP (*FL2*), 670 LP (*FL3*)).

Labelling of the lipid membrane of GUVs with DOPE-NBD ($\lambda_{max,\ abs}$ = 460 nm, $\lambda_{max,\ em}$ = 535 nm) allowed a clear distinction between sample and background or noise signals. A suspension of freshly prepared GUVs (500 µL) was gently mixed, transferred to a 24 well plate and placed in the auto sampler of the Beckman Coulter Quanta instrument. Before injecting the suspension (50 µL), the 24 well plate was orbitally shaken to avoid biases due to the settlement of GUVs and prevent the damage of the GUVs by harsh suspending through a syringe. The *EV*, *SSC* and *FL-1* signals of each GUV suspension were measured as a technical triplicate (see representative counter maps in **Figures 11** and **12**). As detection limit $1x10^5$ events was set. The raw data was exported as listmode files and processed with FlowJo. Only GUVs with a diameter >4 µm were considered in our analysis and all events showing a fluorescence signal were gated and defined as GUV population. The electronic volume values (*EV)* were exported to excel, transformed via **Eq. 1** into the electronic radius (*Er*), and thereafter standardized over **Eq. 2** utilizing fluorescent labeled standard beads (NIST traceable latex particle, indicated as STD in Eq. 2 with a nominal diameter of 10 µm. The ratio ($10\ \mu m/\mathrm{ER_{STD}}$) between the known diameter (10 µm) and the measured *Er* for the standard

(ER_{STD}) was used to transform the non-specified electronic volume of GUVs to the diameter in µm.

$$Er = \sqrt[3]{\frac{3}{4\pi}EV} \qquad \textbf{(Eq. 1)}$$

$$d_{GUV} = \frac{Er_{GUV}}{Er_{STD}} \cdot d_{STD} \qquad \textbf{(Eq. 2)}$$

The scale was verified with standard particles of 20 µm (see **Figure 13**), and the accuracy tested. The size of all the measured GUVs was categorized into five different groups for clarity, and the yield was expressed as GUVs per µL.

Access to FlowJo was kindly provided by Sander van Kasteren from the bio-organic synthesis group, Leiden University.

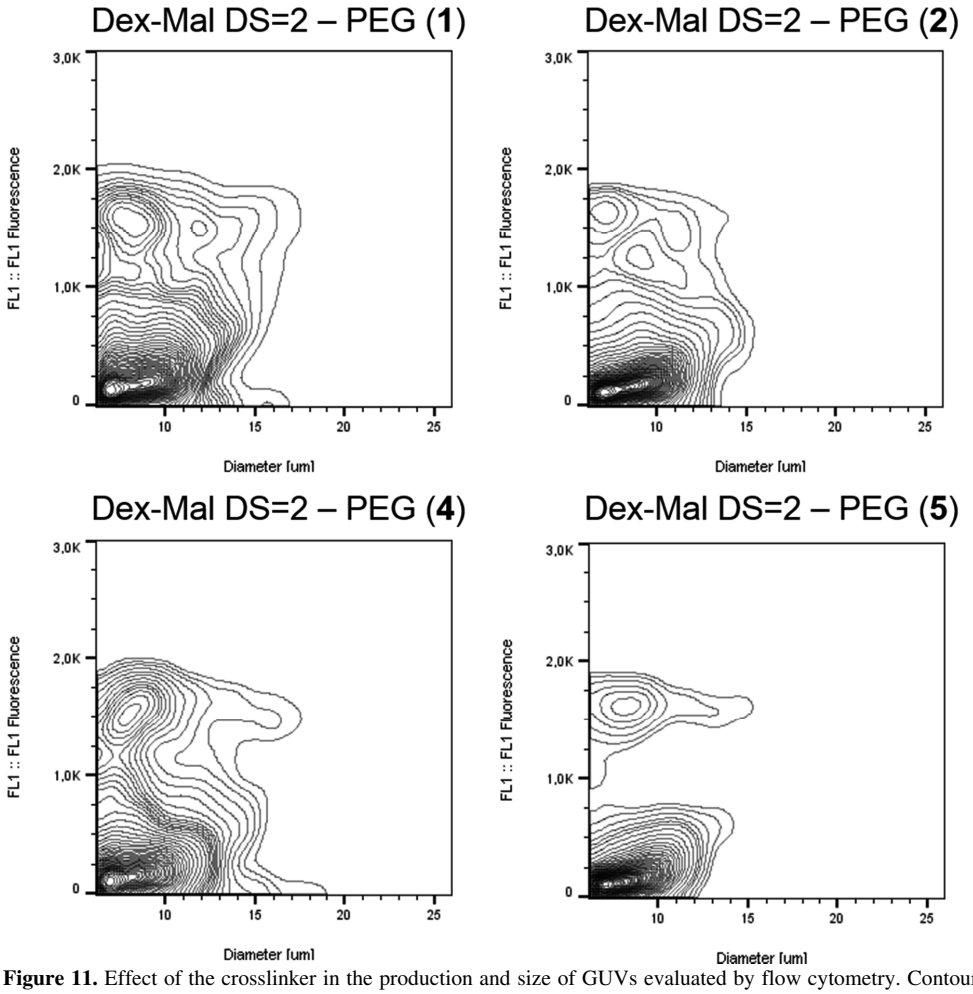

Figure 11. Effect of the crosslinker in the production and size of GUVs evaluated by flow cytometry. Contour maps of the relative frequency of GUVs populations with the lipid composition POPC/Cholesterol/PEG 2000-PE (75:20:5 molar ratio, 14 mM) fluorescently labeled with DOPE-NBD (0.7 mol%) and prepared in DexPEG hydrogel substrates with DS = 2 and PEG crosslinkers **1**, **2**, **4** and **5**.

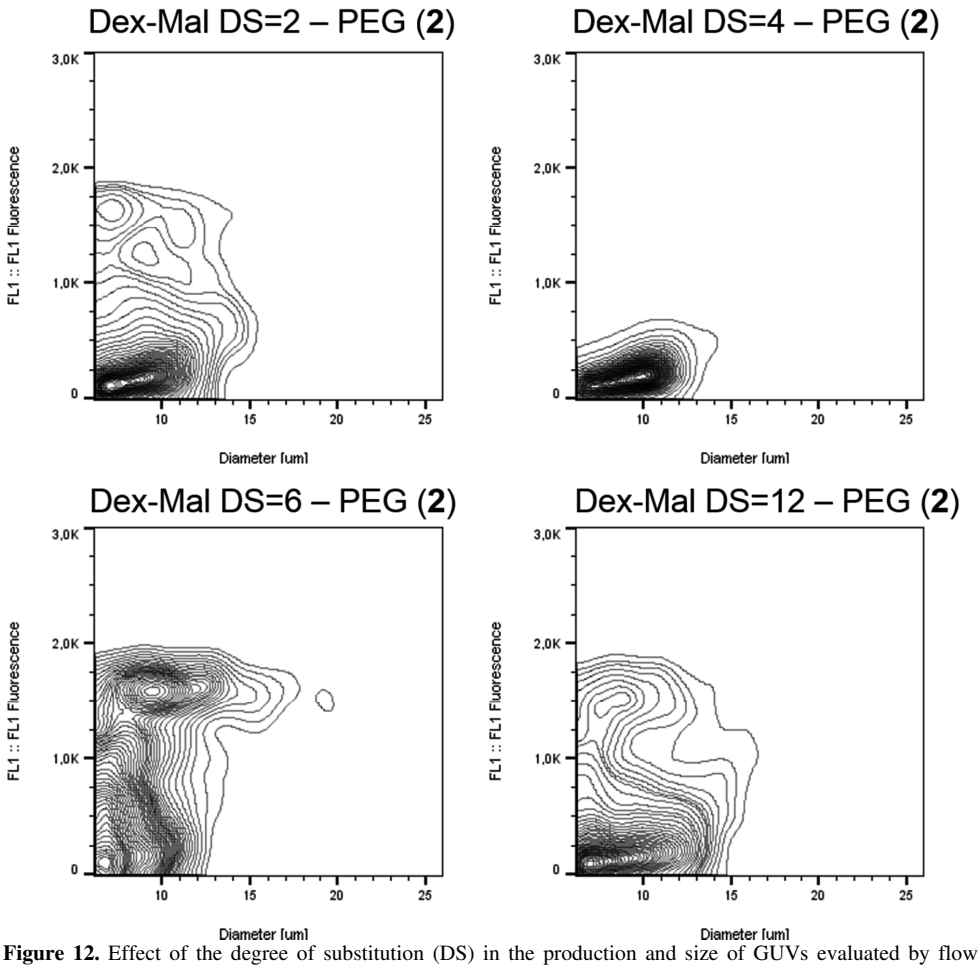

Figure 12. Effect of the degree of substitution (DS) in the production and size of GUVs evaluated by flow cytometry. Contour maps of the relative frequency of GUVs populations with the lipid composition POPC/Cholesterol/PEG 2000-PE (75:20:5 molar ratio, 14 mM) fluorescently labeled with DOPE-NBD (0.7 mol%) and prepared in DexPEG hydrogel substrates with DS = 2, 4, 6, 12 and PEG crosslinker **2**.

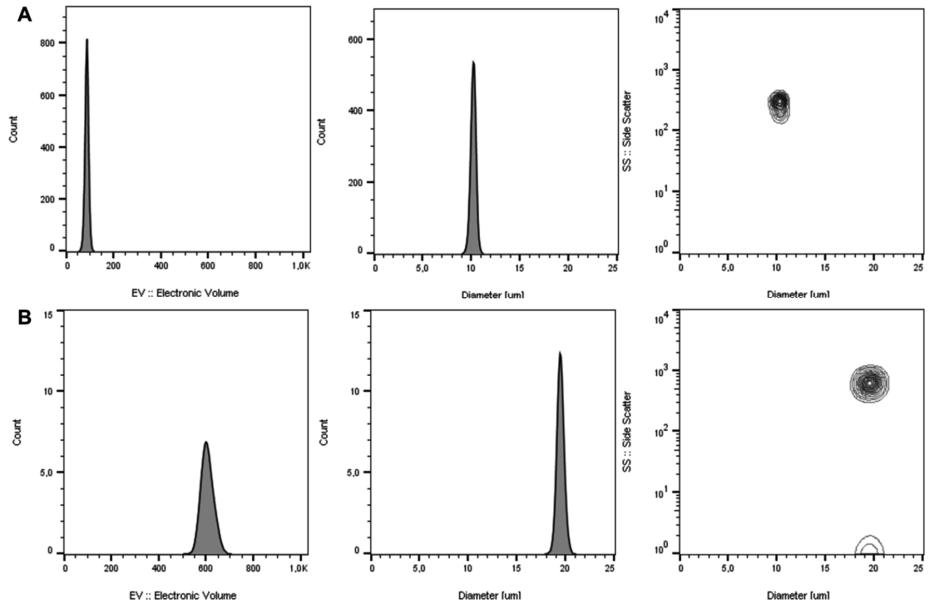

Figure 13. Verification of the diameter with NIST Traceable Latex Particles Standards. **A**) Histogram and contour map for latex particles with standard nominal of size 10 µm and **B**) Histogram and contour map for latex particle with standard nominal of size 20 µm.

Differential Scanning Calorimetry (DSC).

Temperature scans were performed in a Discovery DSC from TA instruments. The samples were scanned from -50 to 50 °C at a heating rate of 10 °C/min. The heat scans were performed and recorded two times. No difference was observed between the first and the second heating run. DSC traces for the first heating run are presented in **Figure 14**. The baseline was subtracted and the heat flow signal was normalized for all samples. A well-defined melting transition (T_m) was detected for pure DOPC lipid at -6 °C (black trace). This value is in good agreement with the value reported for hydrated DOPC (*ca* 3 H_2O).[36] Figure **Figure 14A** shows the DSC traces for both dry DexPEG hydrogel film (gray trace) and dry hybrid DOPC – DexPEG hydrogel film (blue trace). Thermal analysis indicates slight interaction between DOPC and DexPEG by the displacement of DOPC T_m to -12 °C and PEG T_m from 45 °C to 42 °C. In **Figure 14B** the strong interaction of DOPC lipid with PEG hydrogel is detected by 1 °C displacement of PEG T_m and the depression of the DOPC melting transition.

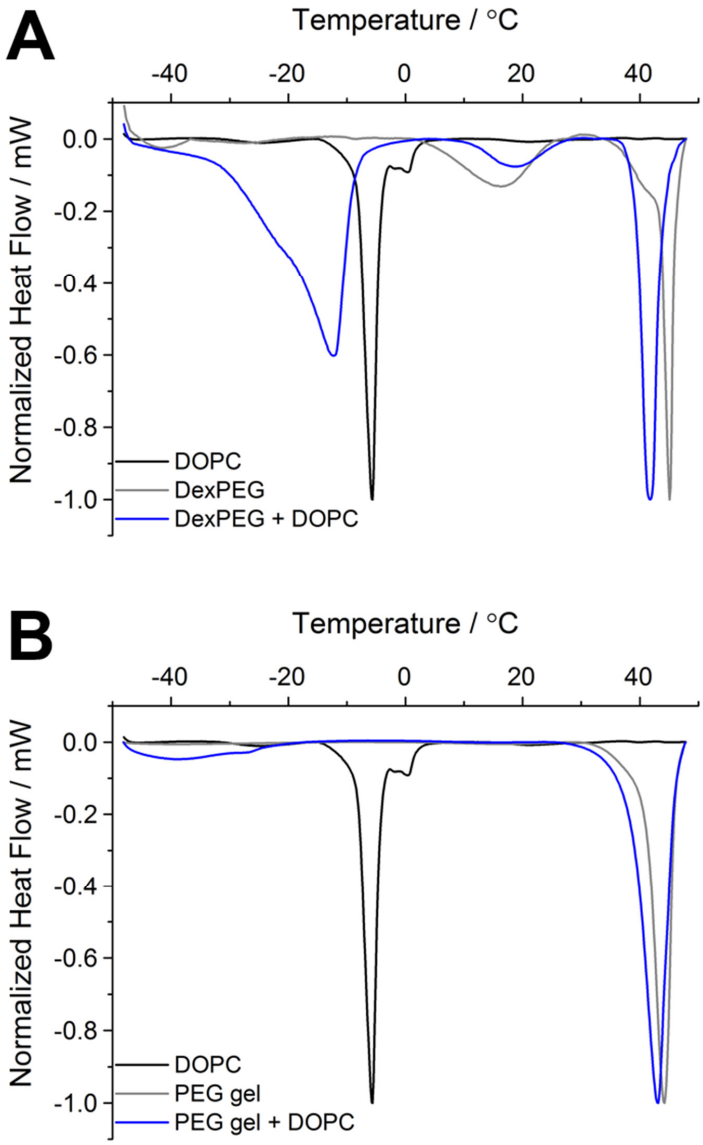

Figure 14. Thermal analysis of DexPEG and PEG hydrogels. **A**) Normalized Thermograms of DexPEG, DOPC and DexPEG - DOPC. **B**) Normalized Thermograms of PEG gel, DOPC and PEG gel - DOPC. The base line was subtracted for all the traces.

References

1. Fenz, S.F. & Sengupta, K. Giant vesicles as cell models. *Integr Biol-Uk* **4**, 982-995 (2012).
2. Tsai, F.C., Stuhrmann, B. & Koenderink, G.H. Encapsulation of Active Cytoskeletal Protein Networks in Cell-Sized Liposomes. *Langmuir* **27**, 10061-10071 (2011).
3. Menger, F.M. & Keiper, J.S. Chemistry and physics of plant vesicles as biomembrane models. *Curr Opin Chem Biol* **2**, 726-732 (1998).
4. Walde, P., Cosentino, K., Engel, H. & Stano, P. Giant Vesicles: Preparations and Applications. *Chembiochem* **11**, 848-865 (2010).
5. Lipowsky, R. The Morphology of Lipid-Membranes. *Curr Opin Struc Biol* **5**, 531-540 (1995).
6. Pautot, S., Frisken, B.J. & Weitz, D.A. Engineering asymmetric vesicles. *P Natl Acad Sci USA* **100**, 10718-10721 (2003).
7. Needham, D. & Evans, E. Structure and Mechanical-Properties of Giant Lipid (Dmpc) Vesicle Bilayers from 20-Degrees-C Below to 10-Degrees-C above the Liquid-Crystal Crystalline Phase-Transition at 24-Degrees-C. *Biochemistry-Us* **27**, 8261-8269 (1988).
8. Kato, A. et al. Phase Separation on a Phospholipid Membrane Inducing a Characteristic Localization of DNA Accompanied by Its Structural Transition. *J Phys Chem Lett* **1**, 3391-3395 (2010).
9. Hansen, J.S., Thompson, J.R., Helix-Nielsen, C. & Malmstadt, N. Lipid Directed Intrinsic Membrane Protein Segregation. *Journal of the American Chemical Society* **135**, 17294-17297 (2013).
10. Gutierrez, M.G. & Malmstadt, N. Human Serotonin Receptor 5-HT1A Preferentially Segregates to the Liquid Disordered Phase in Synthetic Lipid Bilayers. *Journal of the American Chemical Society* **136**, 13530-13533 (2014).
11. Horger, K.S. et al. Hydrogel-assisted functional reconstitution of human P-glycoprotein (ABCB1) in giant liposomes. *Bba-Biomembranes* **1848**, 643-653 (2015).
12. Motta, I. et al. Formation of Giant Unilamellar Proteo-Liposomes by Osmotic Shock. *Langmuir* **31**, 7091-7099 (2015).
13. Kahya, N. Protein-protein and protein-lipid interactions in domain-assembly: Lessons from giant unilamellar vesicles. *Bba-Biomembranes* **1798**, 1392-1398 (2010).
14. Koller, D. & Lohner, K. The role of spontaneous lipid curvature in the interaction of interfacially active peptides with membranes. *Bba-Biomembranes* **1838**, 2250-2259 (2014).
15. Tamba, Y. & Yamazaki, M. Magainin 2-Induced Pore Formation in the Lipid Membranes Depends on Its Concentration in the Membrane Interface. *J Phys Chem B* **113**, 4846-4852 (2009).
16. Tamba, Y., Ariyama, H., Levadny, V. & Yamazaki, M. Kinetic Pathway of Antimicrobial Peptide Magainin 2-Induced Pore Formation in Lipid Membranes. *J Phys Chem B* **114**, 12018-12026 (2010).
17. Akashi, K., Miyata, H., Itoh, H. & Kinosita, K. Preparation of giant liposomes in physiological conditions and their characterization under an optical microscope. *Biophysical Journal* **71**, 3242-3250 (1996).

18. Valkenier, H., Mora, N.L., Kros, A. & Davis, A.P. Visualization and Quantification of Transmembrane Ion Transport into Giant Unilamellar Vesicles. *Angew Chem Int Edit* **54**, 2137-2141 (2015).
19. Reeves, J.P. & Dowben, R.M. Formation and properties of thin-walled phospholipid vesicles. *Journal of Cellular Physiology* **73**, 49-60 (1969).
20. Angelova, M.I. & Dimitrov, D.S. Liposome Electroformation. *Faraday Discuss.* **81**, 303-+ (1986).
21. Chen, J., Park, H. & Park, K. Synthesis of superporous hydrogels: Hydrogels with fast swelling and superabsorbent properties. *J Biomed Mater Res* **44**, 53-62 (1999).
22. Shalaby, W.S.W., Blevins, W.E. & Park, K. Use of Ultrasound Imaging and Fluoroscopic Imaging to Study Gastric Retention of Enzyme-Digestible Hydrogels. *Biomaterials* **13**, 289-296 (1992).
23. Peppas, N.A., Hilt, J.Z., Khademhosseini, A. & Langer, R. Hydrogels in biology and medicine: From molecular principles to bionanotechnology. *Adv Mater* **18**, 1345-1360 (2006).
24. Henise, J., Hearn, B.R., Ashley, G.W. & Santi, D.V. Biodegradable Tetra-PEG Hydrogels as Carriers for a Releasable Drug Delivery System. *Bioconjugate Chem* **26**, 270-278 (2015).
25. Kim, T.G., Shin, H. & Lim, D.W. Biomimetic Scaffolds for Tissue Engineering. *Adv Funct Mater* **22**, 2446-2468 (2012).
26. Daniele, M.A., Adams, A.A., Naciri, J., North, S.H. & Ligler, F.S. Interpenetrating networks based on gelatin methacrylamide and PEG formed using concurrent thiol click chemistries for hydrogel tissue engineering scaffolds. *Biomaterials* **35**, 1845-1856 (2014).
27. Horger, K.S., Estes, D.J., Capone, R. & Mayer, M. Films of Agarose Enable Rapid Formation of Giant Liposomes in Solutions of Physiologic Ionic Strength. *Journal of the American Chemical Society* **131**, 1810-1819 (2009).
28. Lira, R.B., Dimova, R. & Rieke, K.A. Giant Unilamellar Vesicles Formed by Hybrid Films of Agarose and Lipids Display Altered Mechanical Properties. *Biophysical Journal* **107**, 1609-1619 (2014).
29. Weinberger, A. et al. Gel-Assisted Formation of Giant Unilamellar Vesicles. *Biophysical Journal* **105**, 154-164 (2013).
30. Garten, M. et al. Methyl-branched lipids promote the membrane adsorption of alpha-synuclein by enhancing shallow lipid-packing defects. *Phys Chem Chem Phys* **17**, 15589-15597 (2015).
31. Mora, N.L. et al. Preparation of size tunable giant vesicles from cross-linked dextran(ethylene glycol) hydrogels. *Chem Commun* **50**, 1953-1955 (2014).
32. Kim, S.H. & Chu, C.C. Synthesis and characterization of dextran-methacrylate hydrogels and structural study by SEM. *J Biomed Mater Res* **49**, 517-527 (2000).
33. Coulter, W.H. High speed automatic blood cell counter and cell analyzer. *Proc. Natl. Electron. Conf.*, 1034–1040 (1956).
34. Rodriguez-Trujillo, R. et al. Label-free protein detection using a microfluidic Coulter-counter device. *Sensor Actuat B-Chem* **190**, 922-927 (2014).
35. Shapiro, H.M. Practical Flow Cytometry. (Wiley, 2005).
36. Ulrich, A.S., Sami, M. & Watts, A. Hydration of Dopc Bilayers by Differential Scanning Calorimetry. *Bba-Biomembranes* **1191**, 225-230 (1994).

37. Moore, J.S. & Stupp, S.I. Room-Temperature Polyesterification. *Macromolecules* **23**, 65-70 (1990).
38. de Figueiredo, R.M., Oczipka, P., Frohlich, R. & Christmann, M. Synthesis of 4-maleimidobutyric acid and related maleimides. *Synthesis-Stuttgart*, 1316-1318 (2008).
39. R, C.W.H.a.H.W. *Google Patents* (1971).

Chapter IV

Triplet-triplet annihilation upconversion in the lipid bilayer of giant unilamellar vesicles

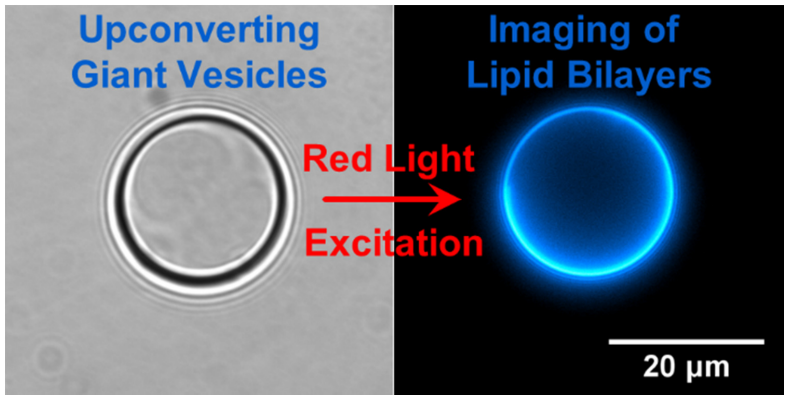

This work is published: Néstor López Mora,* Sven H.C. Askes,* Rolf Harkes, Roman I. Koning, Bram Koster, Thomas Schmidt, Alexander Kros, Sylvestre Bonnet, *Chem. Commun.* **2015**, *51*, 9137-9140.

* Both authors contributed equally.

Abstract.

Red-to-blue triplet-triplet annihilation upconversion was obtained in giant unilamellar vesicles. The upconverted light was homogeneously distributed across the membrane and could be utilized for the imaging of individual giant vesicles in three dimensions. These results show the great potential of TTA-UC for imaging applications under anoxic conditions.

Introduction

Upconversion luminescence (bio)imaging offers great advantages over conventional imaging. The absence of auto-fluorescence results in high contrast images, while photons of low energy, i.e. within the phototherapeutic window (600-1000 nm), afford higher tissue penetration and negligible irradiation damage. For these reasons lanthanoid-based upconverting nanoparticles (UCNPs), for example, have attracted much interest.[1, 2] However, UCNPs suffer from several disadvantages, such as the need for high excitation power, the low absorption cross section of lanthanoid ions, and low upconversion efficiency in aqueous solution (typically ≤0.5%).[2] In contrast, triplet-triplet annihilation upconversion (TTA-UC) requires low excitation power (<100 $mW.cm^{-2}$), employs sensitizers having high extinction coefficients in the phototherapeutic window, and has achieved upconversion quantum yields up to 14% in aqueous solution.[2, 3]

In TTA-UC, low-energy photons are converted into higher-energy photons by means of a photophysical mechanism involving a couple of molecular dyes called the sensitizer and annihilator (see **Figure 5** in *Experimental Section* for a qualitative Jablonski diagram).[4-8] The sensitizer absorbs the low-energy light, undergoes intersystem crossing (ISC) to a triplet state, and transfers its energy to the annihilator molecule by triplet–triplet energy transfer. Further collision of two triplet annihilator molecules leads to triplet–triplet annihilation (TTA), whereby one annihilator molecule is promoted to the excited singlet state, whereas the other one falls back to the ground state. The singlet annihilator returns to the ground state by emission of a high-energy photon, thus realizing upconversion. Most molecular dyes used in TTA-UC are highly lipophilic and require supramolecular strategies to be used in aqueous solution.[9-14] For example, sub-micrometer sized TTA-UC particles have been proposed for *in vitro* or *in vivo* imaging.[2, 11, 12] We now demonstrate that TTA-UC can also be used for the imaging of lipid membranes.

Giant Unilamellar Vesicles (GUVs) are classical tools in fluorescence imaging, as their large size (1–100 µm diameter) allows for direct observation of individual vesicles by optical microscopy techniques.[15] GUVs have for example been used for visualizing lipid rafts, membrane fusion, or ion transport.[16] In this study we functionalized PEGylated GUVs with palladium tetraphenyltetrabenzoporphyrin (**1**) as photosensitizer and perylene (**2**) as the annihilator (**Figure 1a**), and studied red-to-blue TTA-UC in the membrane of the vesicles by optical microscopy. The aim of the study was to investigate the dye distributions across the

membrane, the homogeneity of upconverted emission in the lipid bilayer, and the upconversion stability under imaging conditions. The growth of high-quality giant vesicles with a well-defined shape in physiologically relevant conditions, i.e., at high ionic strengths, was until recently considered as a challenge, but a new method was recently developed by some of us that is compatible with such conditions (up to 320 mOsm.kg^{-1}).[17]

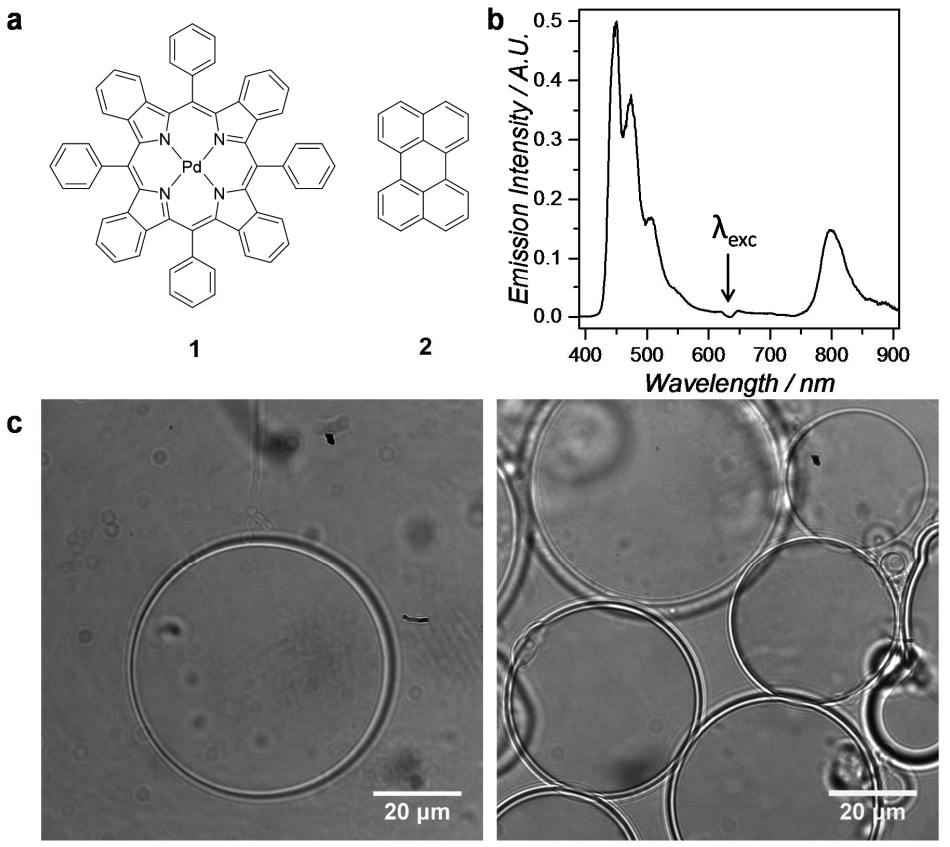

Figure 1. a) Chemical structures of palladium tetraphenyltetrabenzoporphyrin (**1**) and perylene (**2**). **b**) Emission spectra of DOPC upconverting GUVs with 30 mW 630 nm excitation (0.24 W.cm^{-2} intensity) at 298 K in sulfite-supplemented (0.3 M) PBS buffer under air. **c**) Bright field micrographs of DOPC (left) and DMPC (right) upconverting giant vesicles at 298 K.

Upconverting giant vesicles GUV **12** were thus prepared from a lipid mixture of 95 mol % phospholipid (either 1,2-dimyristoyl-sn-glycero-3-phosphocholine, i.e. DMPC, or 1,2-dioleoyl-sn-glycero-3-phosphocholine, i.e. DOPC), 4 mol % sodium N-(carbonyl-

methoxypolyethylene glycol-2000)-1,2-distearoyl-sn-glycero-3-phosphoethanolamine (DSPE-MPEG-2000), 0.5 mol % compound **2**, and 0.02 mol % compound **1**. The complete procedure is described in the *Experimental Section*. Briefly, the dye-containing lipid mixture in chloroform was deposited on a chemically cross-linked dextran–poly(ethylene glycol) hydrogel substrate, dried to form a lipid film, and then the film was re-hydrated with phosphate buffered saline (PBS) supplemented with 0.3 M sodium sulfite (Na_2SO_3) and 0.2 M sucrose at 293 – 308 K. Transferring the solution onto a microscopy slide allowed for bright field imaging on a custom-build microscope based on an inverted microscopy setup. The images (**Figure 1c**) confirmed that for both lipid compositions (DMPC or DOPC) free-floating single vesicles were obtained, together with clusters of smaller vesicles. The images also show that the self-assembled vesicles were giant (diameter 1-100 μm), unilamellar, and spherical. The fact that almost identical procedures can be employed for preparing GUVs from lipids having a marked difference in their gel-to-liquid transition temperature (T_m = -17.3 °C and 23.9 °C for pure DOPC and DMPC, respectively)[18], demonstrates the flexibility of the GUV preparation method. For comparison, much smaller LUVs (samples LUV**12**) with an average diameter of *ca*. 150 nm were prepared from the same lipid mixture but using a standard hydration-extrusion protocol (*Experimental Section*, **Figure 6**).

Sodium sulfite was added in the buffer as an oxygen-scavenging agent. Since the triplet states involved in TTA-UC are readily quenched by molecular oxygen, it is common practice to deoxygenate samples before measuring upconverted emission. With LUVs de-oxygenation can be achieved by, for example, bubbling the solution with argon or N_2. In the case of GUVs imaging however, bubbling an inert gas through the solution would at least impair visualization of single GUVs during a long time period of time due to convection, or even lead to damaging of the giant vesicles, so that supplementing the buffer with an oxygen scavenger is highly preferred. In a preliminary experiment, upconversion emission spectra of LUV**12** samples deoxygenated by either argon bubbling for 30 minutes or by adding 0.3 M sodium sulfite to the buffer, were compared (see **Figure 8** and *Experimental Section* for details). When irradiated at 630 nm the emission spectrum of such LUVs at 298 K shows at 800 nm the phosphorescence band of **1**, and between 450 and 600 nm the blue singlet emission from **2** (**Figure 8**). The spectra from both deoxygenation methods were found to be very similar. It was thus concluded that Na_2SO_3 does not interfere with the photophysical processes at the origin of upconversion, and that sulfite might be used for scavenging dioxygen in a GUV-containing sample as well.

Indeed, even though addition of Na_2SO_3 significantly increased the ionic strength of the buffer (from 278 ± 1 mOsm.kg^{-1} for PBS buffer to 884 ± 11 mOsm·kg^{-1} when supplemented with 0.3 M sodium sulfite), as explained above sodium sulfite did not prevent the assembly of DMPC or DOPC GUV**12** using the hydrogel method. No differences in vesicle yield and morphology were observed in presence or absence of sodium sulfite in the buffer. This result demonstrates that the dextran–poly(ethylene glycol) hydrogel substrate is able to produce GUVs at high ionic strength, which is a significant advantage over alternative GUV preparation methods such as electroformation or gentle hydration, which often fail in such conditions. When irradiated at 630 nm under air, the emission spectrum of the DMPC or DOPC GUV**12** samples prepared in a sulfite-supplemented buffer was identical to the emission spectrum of the corresponding LUV**12** samples (**Figure 1b** and **Figure 8**), showing that the dyes **1** and **2** were indeed incorporated in the lipid bilayer.

GUV**12** samples were then visualized by emission microscopy at 298 K (**Figure 2** and *Experimental Section*). When the vesicles were illuminated with violet light (405 nm), i.e. by direct excitation of perylene (**2**), fluorescence was clearly detected at the membrane (**Figure 2b**). To visualize upconversion, a 630 nm continuous wave PDT laser was coupled into the microscope and set at a power of a few milliwatts, resulting in the focal spot in an intensity of ~300 W.cm^{-2}. All wavelengths other than 450 – 575 nm were strictly blocked by a combination of notch and short-pass filters (**Figure 7**, *Experimental Section*). High-quality images were obtained that were superimposable to the bright field images and to the fluorescence images recorded under white and violet light irradiation, respectively (**Figure 2a-c**). Control samples were prepared in which the porphyrin sensitizer **1** was omitted from the formulation (**GUV2**). Images recorded in identical conditions were black, i.e., no blue emission was observed (**Figure 14**). GUV**12** samples prepared in absence of sulfite oxygen scavenger and observed under air did not give any observable emission either (**Figure 15**). Altogether, these observations prove that the blue images recorded under 630 nm irradiation of GUV**12** samples supplemented with sulfite comes from the TTA upconversion process and are not the result of sensitizer emission (at 800 nm) or of two-photon absorption. Overall, all data conclude that both dyes **1** and **2** co-localize in the membrane and result in TTA upconversion. At this scale of observation the upconverted emission is homogeneous across the membrane and no phase separation of the lipids or dyes was observed.

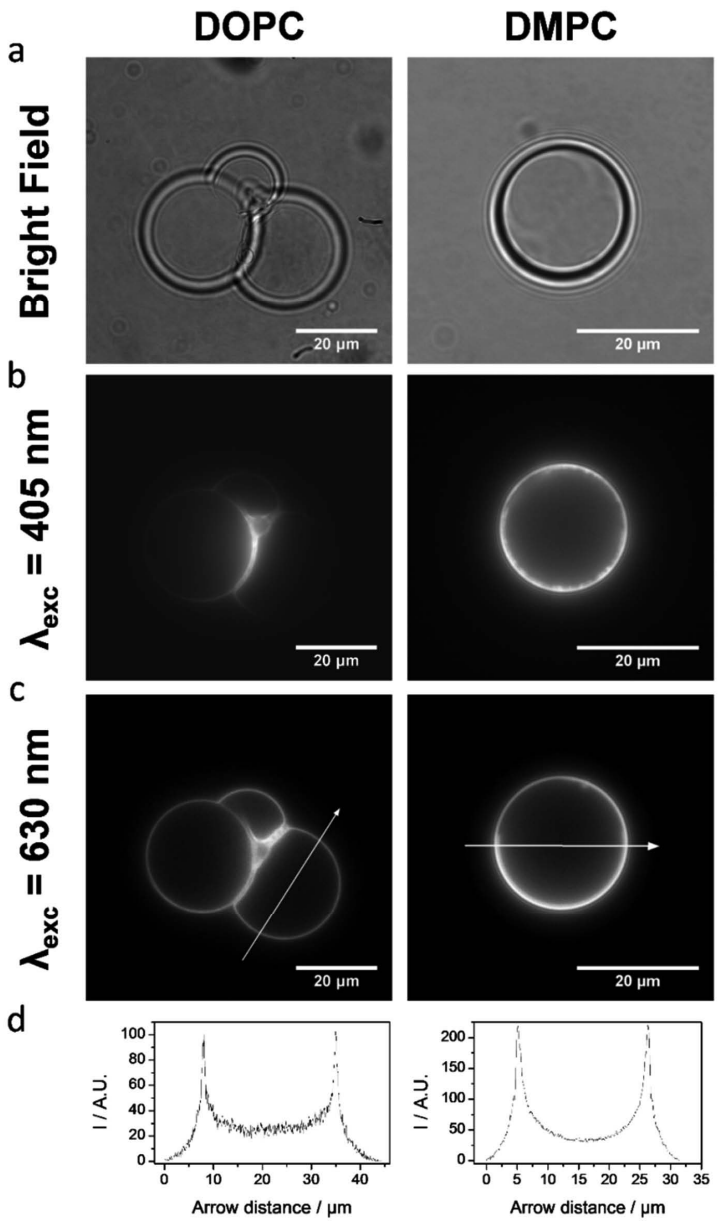

Figure 2. Imaging of DOPC (left) and DMPC (right) upconverting giant vesicles (GUV**12**) with **a**) bright field, **b**) 405 nm excitation and 450-500 nm detection, and **c**) 630 nm excitation and 450-575 nm detection. **d**) Upconversion intensity profile plot following the arrows in the images directly above (c). At 630 nm: laser spot size diameter 39 µm, power 3.8 mW, intensity 320 W.cm^{-2}. At 405 nm: laser spot size diameter 22 µm (power 1 mW, intensity 60 W.cm^{-2}) for DOPC image or 39 µm (power 1 mW, intensity 300 W.cm^{-2}) for DMPC image. Images were acquired at 298 K in sulfite-supplemented (0.3 M) PBS buffer.

Under the red-light irradiation conditions initially used in the microscopy setup (630 nm at an intensity of 320 W.cm^{-2}), substantial bleaching of the upconverted emission of GUV**12** samples was observed even in presence of 0.3 M of sulfite. A plot of the averaged normalized pixel values as a function of red irradiation time shows that the upconverted emission is halved after less than 3 seconds (**Figure 3**). When the light intensity was lowered 60 times (i.e., down to 5.2 W.cm^{-2}) clear upconversion images could still be recorded. In such conditions the bleaching rate was significantly lower (**Figure 3**), and the time necessary for halving the upconverted emission intensity of a pixel increased to approximately 15 seconds. The upconversion luminescence of LUV**-12** in a spectroscopy setup could be observed for less than 8 mW.cm^{-2}, with linear power dependency above 60 mW.cm^{-2} (**Figure 10**). Overall, these findings show that high power is not a requirement for the upconversion imaging of GUV**-12**.

In optimized conditions, we realized that the upconverted emission was intense enough to be utilized for reconstructing in 3D the membrane of the giant vesicles. Z-stack upconversion image acquisition was indeed performed on both DMPC and DOPC GUV**12** samples. The illumination intensity was deliberately chosen to be high (320 W.cm^{-2}) to make sure that z-stack image acquisition was short (200 ms exposure time per slice, *ca*. 45 slices per stack, total acquisition time < 10 s). In such conditions, the slight lateral motion of the GUVs did not significantly affect the imaging process. From these stacks, 3D reconstructions were made (e.g. **Figure 4**), of which a video was compiled. This reconstruction demonstrates that the TTA-upconverted emission can be utilized for the three-dimensional reconstruction of an object that is 10 to 30 μm in size.

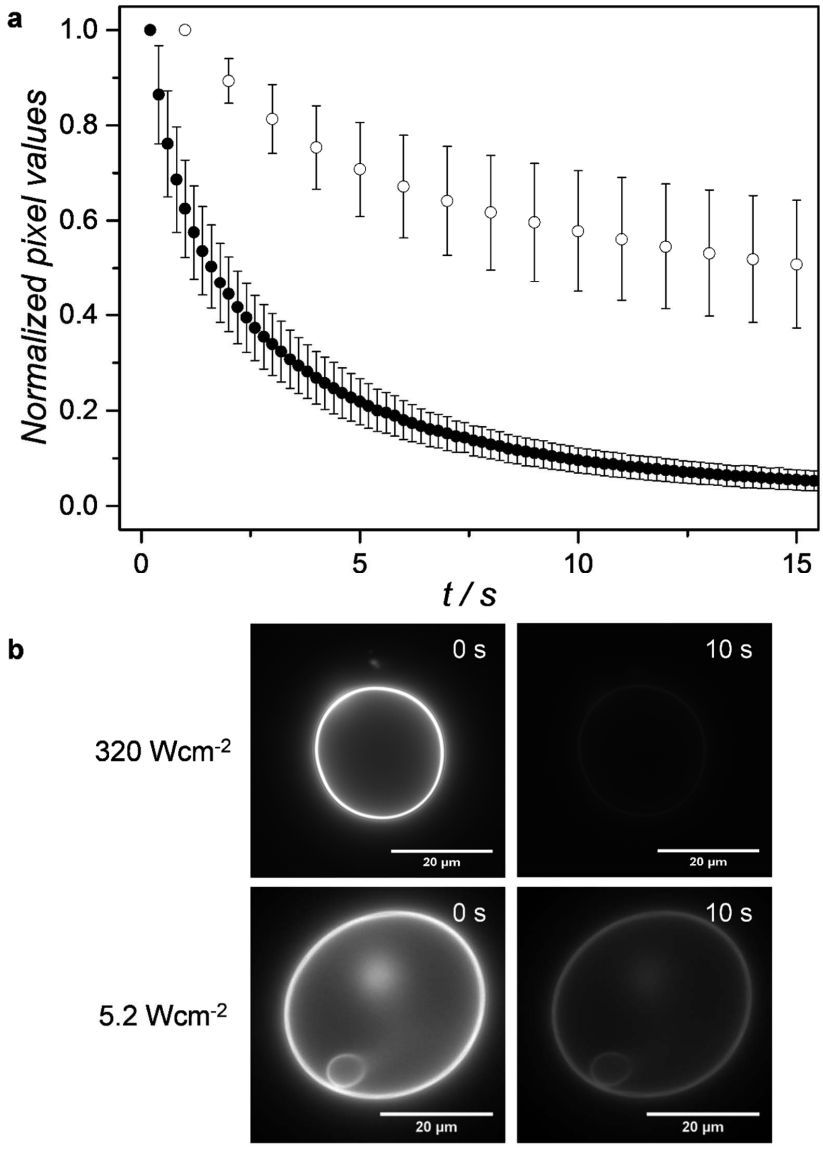

Figure 3. a) Averaged normalized pixel values as a function of red irradiation time during upconversion imaging of GUV**12** samples in sulfite-supplemented PBS buffer (0.3 M). Conditions: 630 nm excitation at 320 W.cm^{-2} (black filled circles) or 5.2 W.cm^{-2} (empty circles), detection in the 450–575 nm region, T=298 K. Snapshots were taken with an exposure time of 0.2 s (320 W.cm^{-2}) or 1.0 s (5.2 W.cm^{-2}). Error bars represent standard deviation based on six individual measurements. **b**) Upconversion emission microscopy images of GUV**12** samples at t = 0 s (left) and at t = 10 s (right) at an illumination intensity of 320 W.cm^{-2} (top) and 5.2 W.cm^{-2} (bottom). Excitation at 630 nm, detection at 450–575 nm.

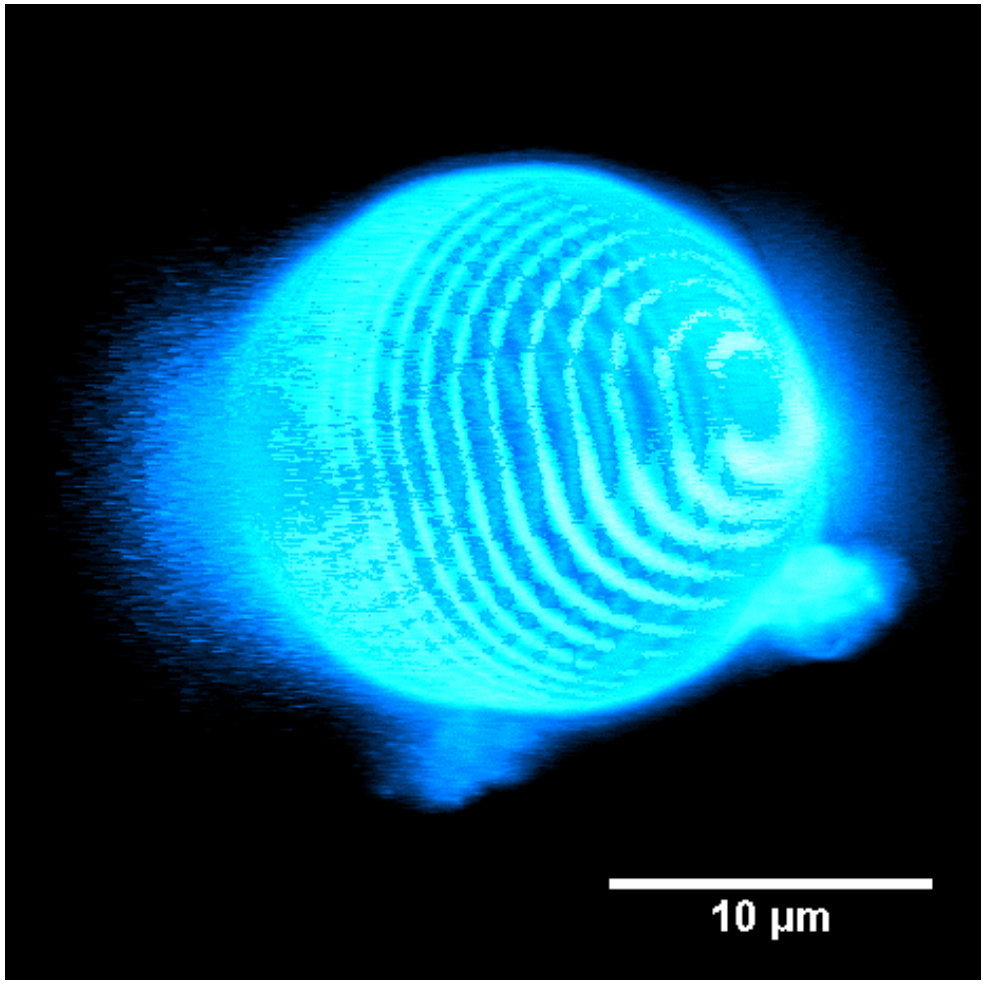

Figure 4. 3D reconstructed image of a DMPC GUV**12** sample, rotated counter-clockwise by 50° about the y-axis. Each z-slice was imaged at 298 K with 630 nm excitation (320 $W.cm^{-2}$) and detection in the 450-575 nm region. The z-distance between slices was 1.0 µm. Video exhibits a 360° rotational view of this image and of four other individual DMPC and DOPC GUV**12**.

Conclusion

In conclusion, DOPC and DMPC giant vesicles capable of upconverting red light to blue light by means of triplet-triplet annihilation were prepared by lipid film hydration on a hydrogel substrate at high ionic strengths. The preparation method is facile and does not involve any specific equipment. Sodium sulphite added as an oxygen scavenger to the vesicle samples allows for observing upconversion even under air. According to optical microscopy, the upconverted emission allows for recording high quality images showing that upconversion is homogeneously realized across the lipid bilayer. The quality and stability of the upconverted images enabled the 3D reconstruction of upconverting GUVs. These results show the great potential of TTA upconversion for imaging applications under anoxic conditions, and open a route towards cell membrane imaging with upconverted light.

Experimental Section

Materials and methods

Palladium tetraphenyltetrabenzoporphyrin (**1**) was purchased from Frontier Scientific, Inc. (Logan, Utah, USA). Perylene (**2**) was purchased from Sigma-Aldrich Chemie BV (Zwijndrecht, The Netherlands). Sodium N-(carbonyl-methoxypolyethylene glycol-2000)-1,2-distearoyl-sn-glycero-3-phosphoethanolamine (DSPE-MPEG-2000), 1,2-dioleoyl-sn-glycero-3-phosphocholine (DOPC), and 1,2-dimyristoyl-sn-glycero-3-phosphocholine (DMPC) were purchased from Lipoid GmbH (Ludwigshafen, Germany) and stored at -18 °C. Dulbecco's phosphate buffered saline (PBS) was purchased from Sigma Aldrich and had a formulation of 8 $g.L^{-1}$ NaCl, 0.2 $g.L^{-1}$ KCl, 0.2 $g.L^{-1}$ KH_2PO_4, and 1.15 $g.L^{-1}$ K_2HPO_4 with a pH of 7.1 – 7.5. All other chemicals were purchased from major chemical suppliers and used as received. Images and data were processed with Fiji ImageJ, Origin Pro, and Microsoft Excel software.

GUV preparation

All GUVs were prepared by lipid film re-hydration on dextran chemically cross-linked hydrogel substrates by a method described elsewhere.[17] The preparation of GUV**12** is described here as an example. Glass microscopy slides were first incubated with 1:1 vol MeOH : HCl (37%) for 30 min, then with 98 % H_2SO_4 for 30 min, and then thiol-functionalized by incubating them for 1 h in a 2 wt % solution of (3-mercaptopropyl)triethoxysilane in dry toluene under a nitrogen atmosphere, and washing them three times with toluene. Directly after, a homogeneous film of Dex-PEG hydrogel was formed on this surface by drop-casting 600 µL of a 1:1 volume mixture of 2 % wt. maleimide-functionalized dextran, with a substitution degree of 3 maleimide groups per 100 glucopyranose residues of dextran (synthesis and characterization detailed in **Chapter II** and **Chapter III**), in water and 2 % wt. α,ω-PEG dithiol (1500 $g.mol^{-1}$) in water at room temperature. A homogenous hydrogel film was formed after 30 – 45 minutes at 40 °C. Then, 10 µL of lipid mixture stock solution in chloroform, containing 20 mM DMPC or DOPC, 0.8 mM DSPE-PEG-2K, 0.1 mM perylene (**2**), and 5 µM of compound **1**, was deposited on the hydrogel surface. The organic solvent was evaporated for 30 minutes under a gentle stream of air followed by a period of at least 30 minutes in a 30 °C vacuum oven. The lipid film was then hydrated with 400 µL phosphate buffered saline (PBS) supplemented with 0.2 M sucrose, and when wanted 0.3 M sodium sulfite, for 1 - 2 hours at room temperature (ca. 293 K) in case of DOPC GUVs, or at 308 K in case of DMPC GUVs.

This receipt produced a solution containing free-floating vesicles that could be directly pipetted in a fluorescence cuvette for emission spectroscopy (*vide infra*). Alternatively, it was further used for the preparation of a microscopy experiment (*vide infra*).

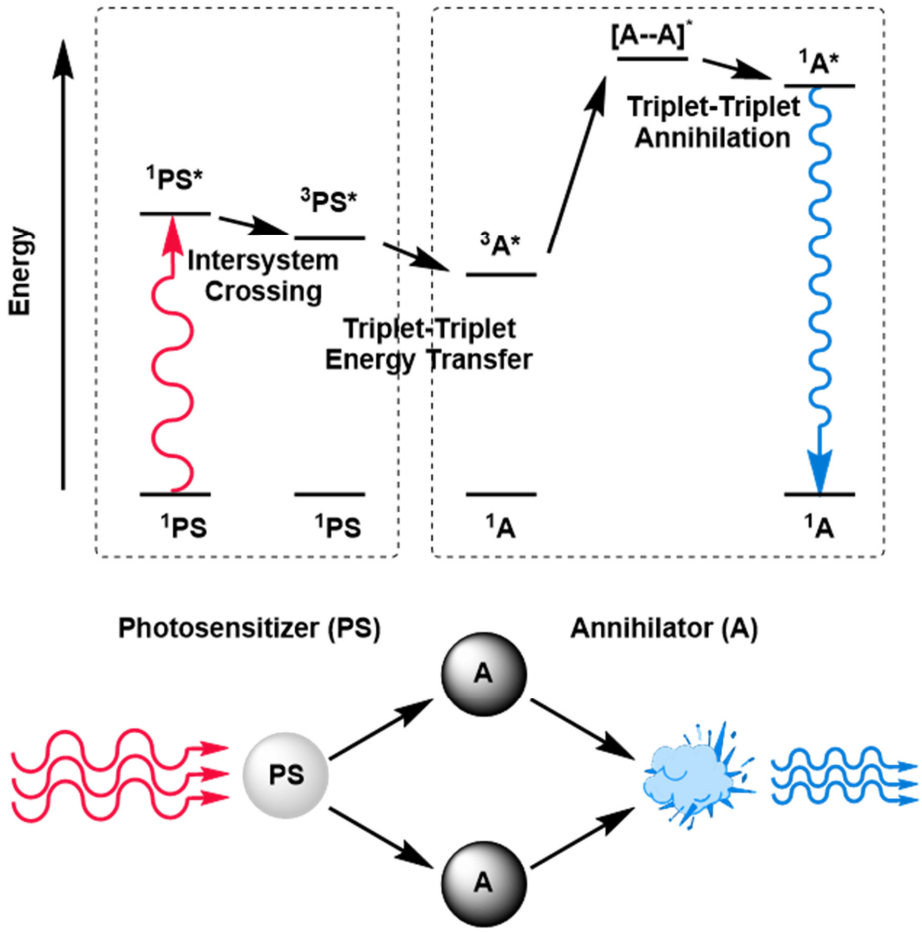

Figure 5. Jablonski diagram of the triplet-triplet annihilation upconversion scheme. Red light is absorbed by the photosensitizer (PS), which undergoes intersystem crossing to a triplet state. This triplet state can be transferred to a ground state annihilator (A) by triplet-triplet energy transfer. Two triplet excited state annihilator molecules can then perform triplet-triplet annihilation, thereby creating one ground state annihilator and one singlet excited state. The latter state returns to the ground state and emits a blue photon. Adapted from Singh-Rachford and Castellano.[4]

Emission spectroscopy on GUVs

For upconversion emission spectroscopy, approximately 700 µL of the above-mentioned solution of free-floating vesicles in buffer was transferred to a semi-micro cuvette and used as such in the setup detailed in **Figure 7**.

Preparation of a microscopy experiment with GUVs

For optical microscopy imaging, 300 µL of the solution containing free-floating vesicles in buffer (*vide supra* GUV preparation) was transferred to an Eppendorf tube containing 700 µL phosphate buffered saline supplemented with 0.3 M sodium sulfite and 0.2 M glucose to allow the sucrose-loaded giant vesicles to sink to the bottom of the tube. After one hour, 200 µL of this GUV suspension was transferred to a visualization microscopy chamber that had previously been coated with bovine serum albumin (BSA). As a result of surface treatment with BSA and of the heavier weight of the sucrose-loaded vesicles, the giant vesicles were immobilized on the glass surface of the chamber, which allowed for imaging with minimal diffusion during image recording. The rest of the chamber was filled with 100 µL PBS supplemented with 0.3 M sodium sulfite and 0.2 M glucose. The vesicles were imaged within 24 hours.

LUV preparation and characterization

Upconverting LUVs, i.e. LUV**12** samples, were prepared as described before as a reference.[14] Aliquots of chloroform stock solutions containing the liposome constituents were added together in a flask to obtain a solution with 20 µmol DMPC, 0.8 µmol DSPE-MPEG-2000, 100 nmol perylene (**2**), and 5 nmol of compound **1**. The organic solvent was removed by rotary evaporation and subsequently under high vacuum for at least 30 minutes to create a lipid film. 1.0 mL PBS buffer, optionally supplemented with 0.3 M Na_2SO_3, was added and the lipid film was hydrated by 5 cycles of freezing the flask in liquid nitrogen and thawing in warm water (50 °C). The resulting dispersion was extruded through a Whatman Nuclepore 0.2 µm polycarbonate filter at 40-50 °C at least 11 times using a mini-extruder from Avanti Polar Lipids, Inc. (Alabaster, Alabama, USA). The number of extrusions was always odd to prevent any unextruded material ending up in the final liposome sample. The extrusion filter remained colourless after extrusion, suggesting complete inclusion of the sensitizer and annihilator in the lipid bilayer. Liposomes were stored in the dark at 4 °C and used within 7 days. The liposomes had an average diameter of *ca*. 150 nm and a polydispersity index of 0.1, as determined from

dynamic light scattering measurements with a Malvern Instruments Zetasizer Nano-S machine, operating at a wavelength of 632 nm. Additionally, cryo transmission electron microscopy was performed on DMPC LUV**12** (see **Figure 6**) as described in Bahreman, A.; Limburg, B.; Siegler, M. A.; Koning, R.; Koster, A. J.; Bonnet, S. *Chem-Eur J* **2012**, *18*, 10271–10280.

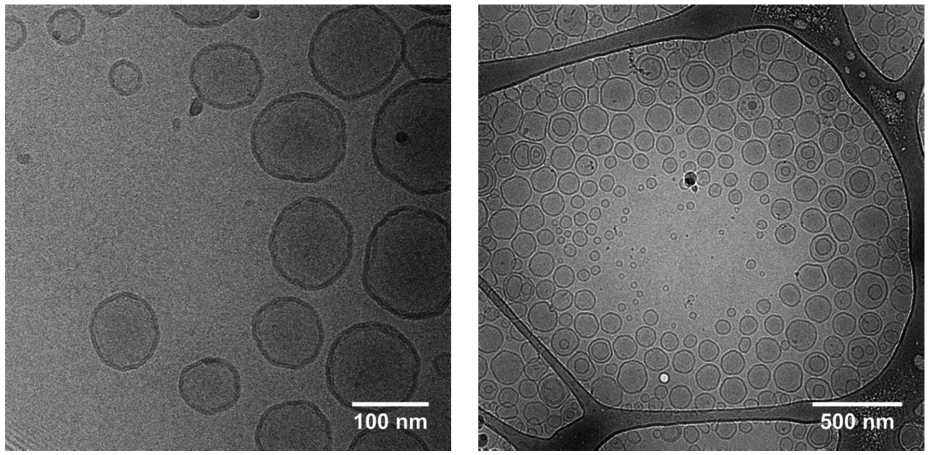

Figure 6. Cryo transmission electron micrographs of DMPC LUV**12**.

Upconversion emission spectroscopy

Upconversion emission spectroscopy was performed in a custom-built setup (**Figure 7**). All optical parts were connected with FC-UVxxx-2 (xxx = 200, 400, 600) optical fibers from Avantes (Apeldoorn, The Netherlands), with a diameter of 200-600 μm, respectively, and that were suitable for the UV-Vis range (200-800 nm). For LUV**12** samples that were deoxygenated by argon bubbling: argon was bubbled through the sample (3.0 mL) with a rate of ~2 bubbles per second for at least 30 minutes in an external ice-cooled pear-shaped flask. After this period, bubbling was stopped while maintaining the argon flow, and the sample was warmed in a water bath of approximately 40 °C for 10 minutes. Then, the sample was transferred by means of cannulation with argon pressure to a 111-OS macro fluorescence cuvette from Hellma in a CUV-UV/VIS-TC temperature-controlled cuvette holder from Avantes, while keeping the sample under a constant flow of argon throughout the measurement. For LUV**12** samples that were deoxygenated by addition of sodium sulfite, 3.0 mL of the sample was simply transferred

to the cuvette and emission spectra were recorded under air. Likewise, GUV**12** samples in sodium sulfite buffer (approximately 700 µL) were transferred to a 104F-QS or 104F-OS semi-micro cuvette from Hellma.

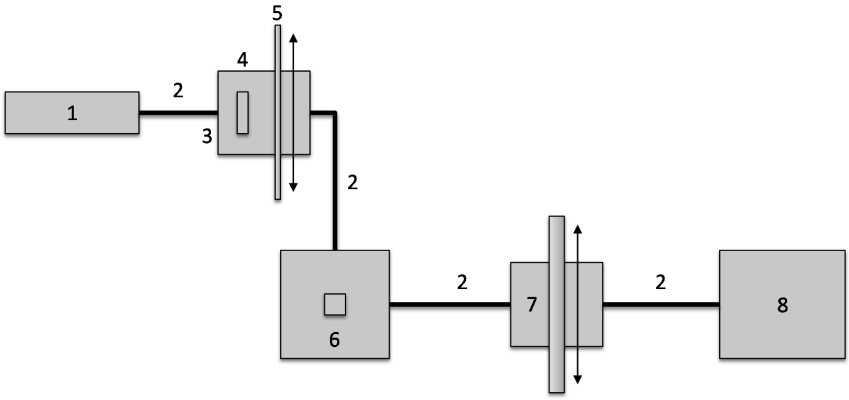

Figure7. Setup used for emission measurements under red light irradiation. Legend: (1) 630 nm laser source, (2) optical fibers, (3) filter holder, (4) 630 nm band pass filter, (5) variable neutral density filter, (6) temperature controlled cuvette holder, (7) variable filter holder, and (8) CCD spectrometer.

The sample in the cuvette holder was allowed to equilibrate at 298 K for 10 minutes. The sample was irradiated from the side with a 30 mW 630 nm laser light beam from a clinical grade Diomed 630 nm PDT laser (4 mm beam, 0.24 $W.cm^{-2}$). The 630 nm light was filtered through an FB630-10, 630 nm band pass filter (Thorlabs, Dachau/Munich, Germany) put between the laser and the sample. The excitation power was controlled using a NDL-25C-4 variable neutral density filter (Thorlabs), and measured using a S310C thermal sensor connected to a PM100USB power meter (Thorlabs). Emission spectra were recorded at a 90° angle with respect to the excitation source using a 2048L StarLine CCD spectrometer from Avantes. To visualize the spectrum from 550 nm to 900 nm, while blocking the red excitation light, a Thorlabs NF-633 notch filter was used in a variable filter holder. To visualize the spectrum from 400 nm to 550 nm, an OD4 575 nm short pass filter (Edmund Optics, York, United Kingdom, part no. 84-709) was used. All spectra were recorded with Avasoft software from Avantes and further processed with Microsoft Office Excel 2010 and Origin Pro software. The emission spectra obtained with the two filters were stitched together at 550 nm to obtain a continuous spectrum from 400 to 900 nm. No correction was needed to seamlessly connect the spectra (**Figure 8**).

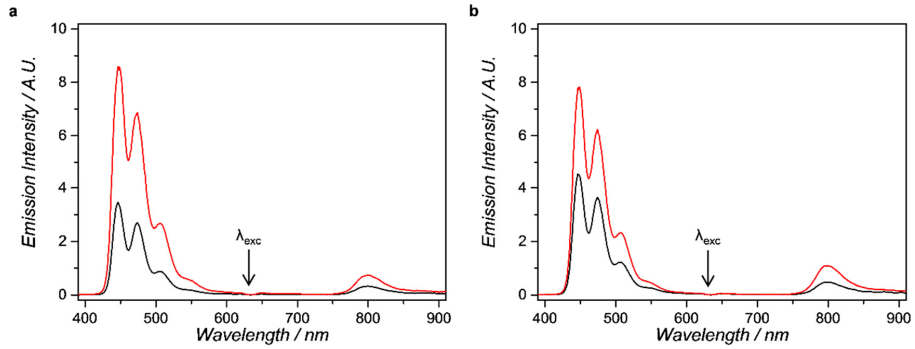

Figure 8. Emission spectra of DOPC (**a**) and DMPC (**b**) LUV**12** samples ([lipid] = 1 mM, [DSPE-PEG-2000] = 0.04 mM, [**2**] = 5 µM, [**1**] = 0.25 µM) under 630 nm excitation at 298 K. The samples were either deoxygenated by bubbling argon for 30 min prior to measurement (black curves) or by addition of sodium sulfite at a concentration of 0.3 M to the buffer (red curves). Irradiation conditions: 3.0 mL sample volume in a macro fluorescence cuvette, with 30 mW 630 nm irradiation power (4 mm beam diameter, intensity 0.24 $W.cm^{-2}$). Bubbling of argon through the sample inevitably results in the formation of small bubbles on the walls of the measurement cuvette, resulting in scattering of light in both the excitation and the detection pathway. These bubbles are absent in the case of deoxygenation using the sodium sulfite oxygen scavenger, which explains why the observed intensities are higher for samples deoxygenated with sulfite.

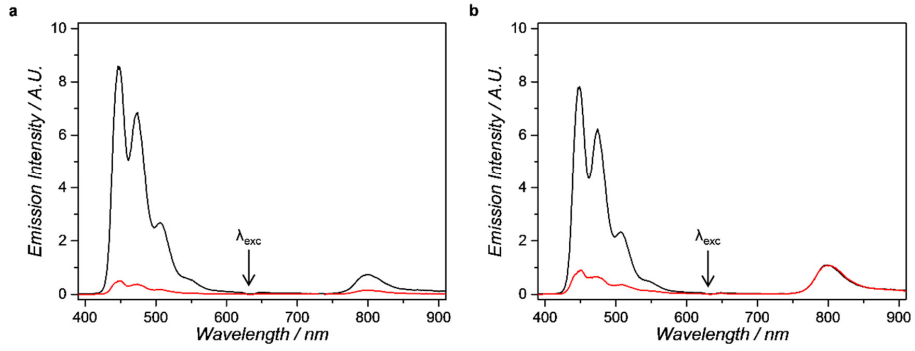

Figure 9. Emission spectra of DOPC (**a**) and DMPC (**b**) LUV**12** (black curves) and GUV**12** (red curves) with 30 mW 630 nm excitation (0.24 $W.cm^2$ intensity) at 298 K. In the case of LUVs, [DMPC] = 1 mM, [DSPE-PEG-2000] = 0.04 mM, [**2**] = 5 µM, [**1**] = 0.25 µM, whereas in the case of GUVs, the lipid concentration was not known, but the components in the membrane were introduced in the same molar ratio as for the LUV samples. In all cases, the buffer was deoxygenated by addition of sodium sulfite (0.3 M) and the spectra were measured under air.

Power dependency measurements

Luminescence emission spectra of DMPC and DOPC liposomes samples LUV**-12** were recorded at various excitation powers from 1 to 40 mW so that the excitation intensity (P) was 8 to 318 mW.cm^{-2} (4 mm laser beam diameter). The samples were placed in a Hellma 101-OS macro fluorescence cuvette (2.25 mL, [lipid] = 1.0 mM) and thermally equilibrated at 298 K before measurement in the same fluorescence setup as described in **Figure 7**. In this case, the spectrum was visualized with only a Thorlabs NF-633 notch filter between the sample and the detector.

The recorded spectra were integrated from 420 to 575 nm to obtain the integrated upconversion luminescence intensity (I_{UC}), which was then plotted in a double logarithmic plot as a function of the excitation intensity (**Figure 10**). The low power ($\leq$ 40 mW.cm^{-2}) and high power ($\geq$ 120 mW.cm^{-2}) regimes were consistently fitted with slopes around 1 and 2, respectively, which shows the typical power dependency of TTA-UC.[1] The intersection of these straight lines represents the intensity threshold (I_{th}) at which the power dependency changes from quadratic to linear. I_{th} was found to be 50 and 59 mW.cm^{-2} for the upconversion in DMPC and DOPC LUV**-12**, respectively. Assuming no difference in power dependency between LUV**-12** and GUV**-12**, these results indicate that all microscopy images with red light excitation (P $\geq$ 5.2 W.cm^{-2}) were acquired in the linear power regime.

Microscopy imaging

Bright field and (upconversion) emission imaging was performed with a customized Zeiss Axiovert S100 TV Inverted Microscope setup (**Figure 11**), fitted with a Zeiss 100x Plan Apochromat 1.4 NA oil objective and an Orca Flash 4.0 V2 sCMOS camera from Hamamatsu, which together produced images with 65 nm pixel size. For direct perylene excitation, a CrystaLaser 50 mW 405 nm Solid State laser was used, combined with a ZT405/514/561rpc dichroic beam splitter (Chroma Technology Corporation) and ZET442/514/568m emission filter (Chroma Technology Corporation) (see **Figure 12** for the transmission spectra of this set). For upconversion emission microscopy, a Diomed clinical grade 630 nm continuous wave PDT laser was used as excitation source. The light was filtered through a FB630-10 630 nm band pass filter (Thorlabs) put between the laser and the Chroma ZT405/532/635rpc dichroic beam splitter. To block everything except upconversion emission, a NF633-25 633 nm notch filter (Thorlabs) and a 575 nm short pass filter (Edmund Optics, part no. #84-709) were placed

between the sample and the camera, resulting in OD >13 at 630 nm and OD>4 around 800 nm (i.e. at the phosphorescence emission of compound **1**). The transmission curves of the filters and dichroic mirror are displayed in **Figure 13**. The output power of the 630 nm laser was typically 3.8 mW (39 µm spot size, 320 W.cm^{-2}) at the sample. The typical camera exposure time was 200 ms, unless otherwise specified.

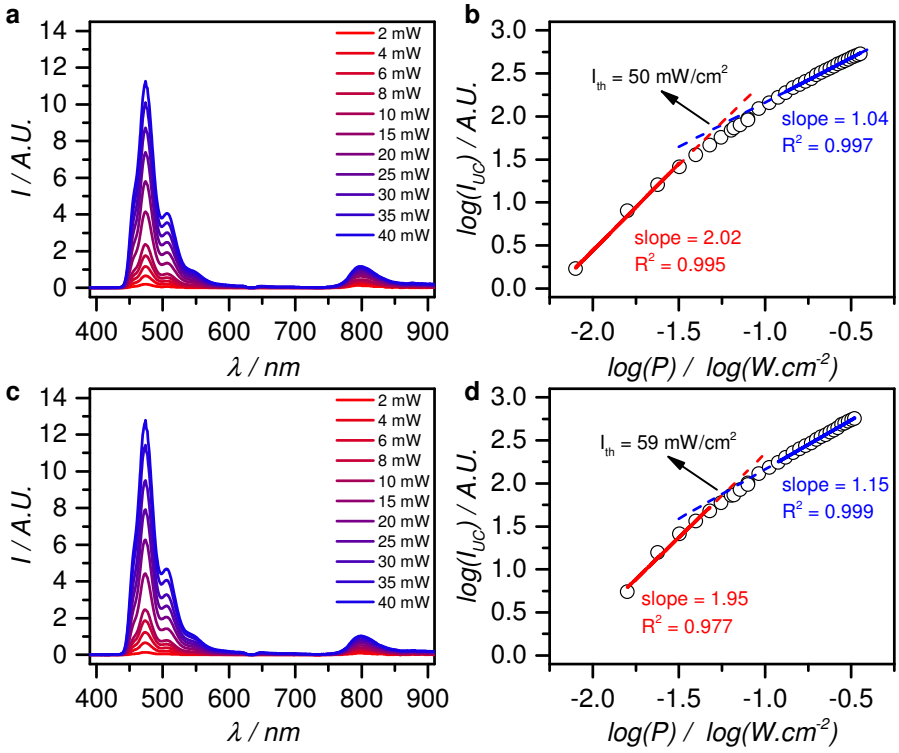

Figure 10. Luminescence emission spectra of DMPC LUV-**12** (**a**) and DOPC LUV-**12** (**c**) at various excitation intensities. Double logarithmic plot of the upconversion luminescence intensity (I_{UC}) of DMPC LUV-**12** (**b**) and DOPC LUV-**12** (**d**), integrated from 420 to 575 nm, as a function of the excitation intensity P (in W.cm^2). The low power regime was fitted with straight lines with slopes 2.02 (R^2 = 0.995) and 1.95 (R^2 = 0.977) for DMPC and DOPC LUV-**12**, respectively (red solid lines), and the high power regime was fitted with straight lines with slopes 1.04 (R^2 = 0.997) and 1.15 for DMPC and DOPC LUV-**12**, respectively (blue solid lines). From the intersection of the extrapolated fits (red and blue dashed lines), the intensity threshold (I_{th}) was found to be 50 mW.cm^{-2} for DMPC LUV-**12** and 59 mW.cm^{-2} for DOPC LUV-12. Irradiation conditions: [lipid] = 1.0 mM, T = 298 K, laser beam diameter 4 mm.

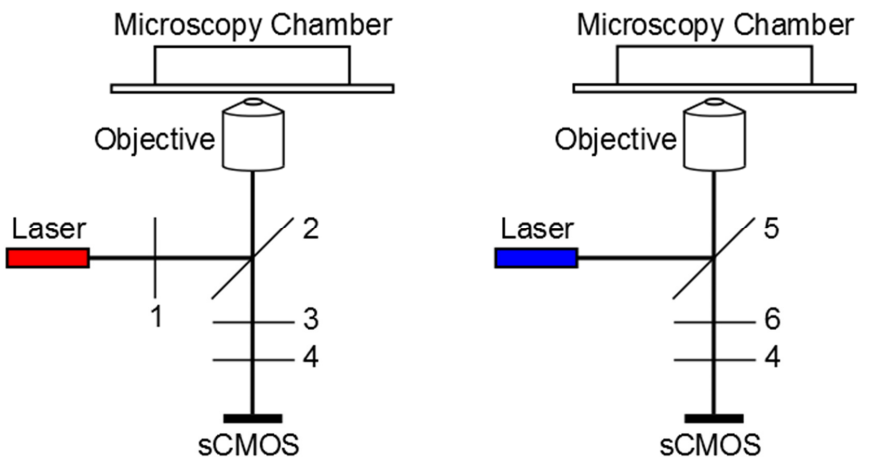

Figure 11. Microscopy setups used for imaging GUVs with 630 nm (left) and 405 nm (right) excitation. Legend: (1) Thorlabs FB630-10 band pass filter, (2) Chroma ZT405/532/635rpc dichroic beam splitter, (3) Edmund Optics 575 nm OD4 short pass filter, 4) Thorlabs NF633-25 notch filter, (5) Chroma ZT405/514/561rpc dichroic beam splitter, (6) Chroma ZET442/514/568 emission filter.

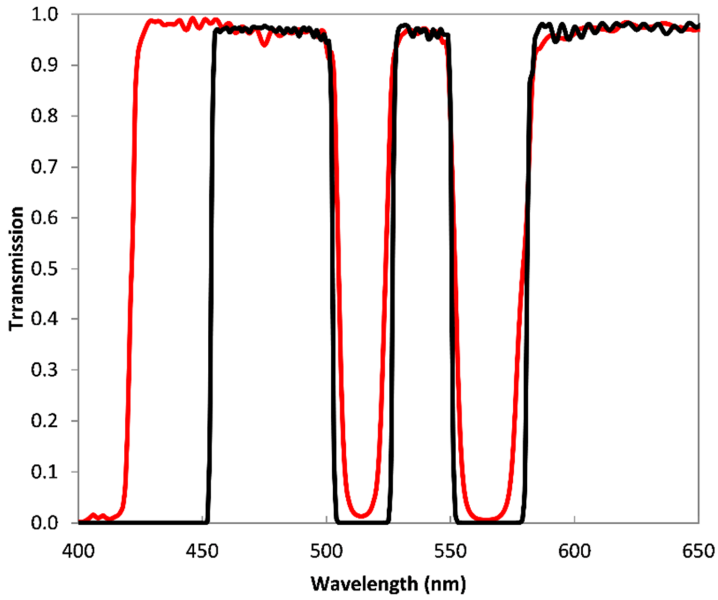

Figure 12. Transmission curves of the filter and dichroic beam splitter that were used for emission microscopy with violet light (405 nm), consisting of a Chroma ZT405/514/561rpc dichroic beam splitter (red) and a Chroma ZET442/514/568m emission filter (black).

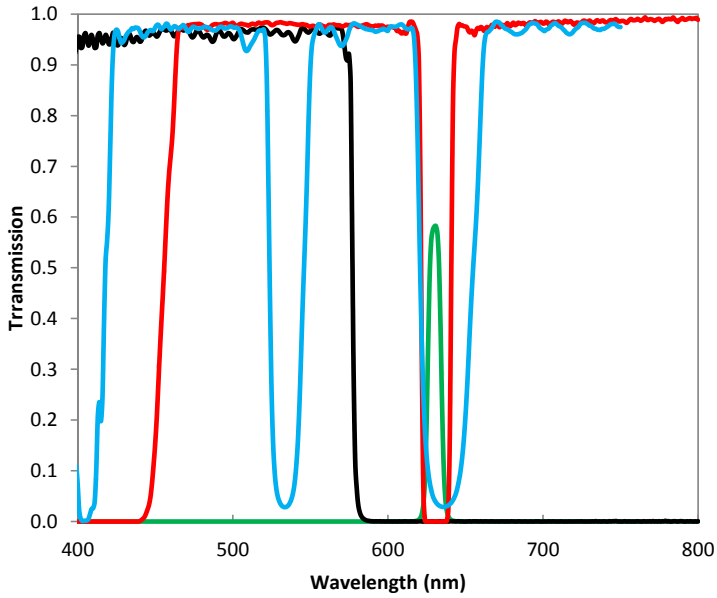

Figure13. Transmission curves of the filters and dichroic beam splitter that were used for emission microscopy with red light (630 nm), consisting of a Thorlabs NF633-25 notch filter (red) and an Edmund Optics 575 nm OD4 short pass filter (black), a Thorlabs FB630-10 band pass filter (green), and a Chroma ZT405/532/635rpc dichroic mirror (blue).

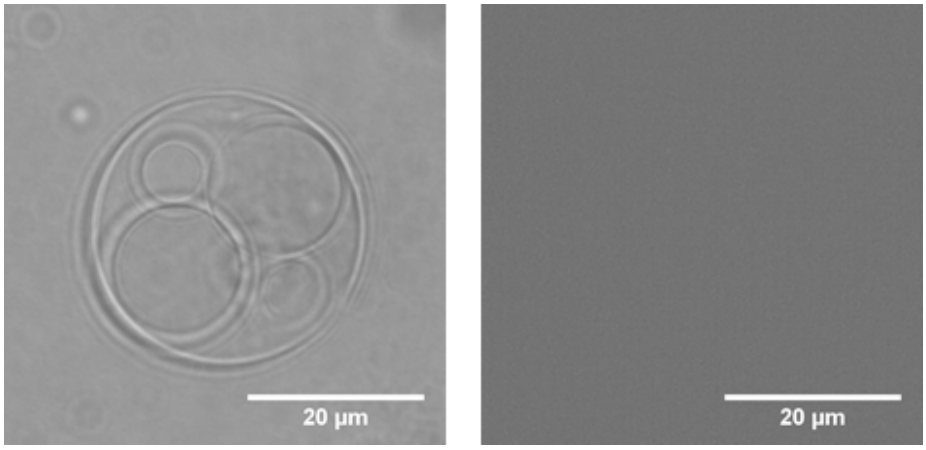

Figure 14. Bright field (left) and upconversion emission (right) photographs of DOPC GUV**2**, i.e. GUVs similar to GUV**12** but deprived of the photosensitizer **1**, in buffer without sodium sulfite and under air atmosphere.

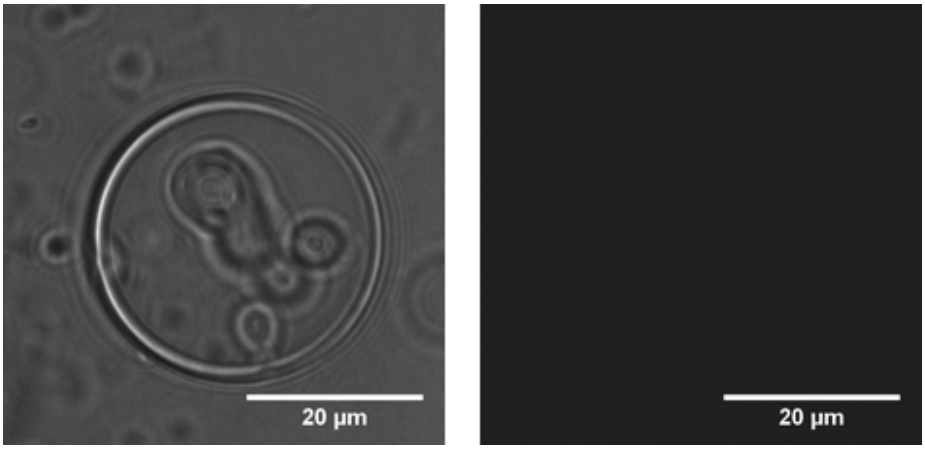

Figure 15. Bright field (left) and upconversion emission (right) photographs of DOPC GUV**12** in air atmosphere in buffer without sodium sulfite.

Determination of bleaching curves

Giant vesicles were first located in bright field mode and were subsequently irradiated for 60 seconds at 630 nm with either 5.2 $W.cm^{-2}$ (62 µW, laser spot size diameter 39 µm) or 320 $W.cm^{-2}$ (3.8 mW, laser spot size diameter 39 µm) illumination intensity while acquiring an image every 1.0 or 0.2 s, respectively. For each image, the pixel values (A.U.) of the brightest half of all the pixels was averaged and normalized to one. Six individual vesicles were measured per time point. The mean and standard deviation are plotted versus time (s) in order to obtain a bleaching curve.

References

1. Zhou, J., Liu, Q., Feng, W., Sun, Y. & Li, F. Upconversion Luminescent Materials: Advances and Applications. *Chem. Rev.* (2014).
2. Liu, Q., Feng, W., Yang, T., Yi, T. & Li, F. Upconversion luminescence imaging of cells and small animals. *Nat. Protocols* **8**, 2033-2044 (2013).
3. Kim, J.-H. & Kim, J.-H. Encapsulated Triplet–Triplet Annihilation-Based Upconversion in the Aqueous Phase for Sub-Band-Gap Semiconductor Photocatalysis. *J. Am. Chem. Soc.* **134**, 17478-17481 (2012).
4. Singh-Rachford, T.N. & Castellano, F.N. Photon upconversion based on sensitized triplet–triplet annihilation. *Coord. Chem. Rev.* **254**, 2560-2573 (2010).
5. Zhao, J., Ji, S. & Guo, H. Triplet-triplet annihilation based upconversion: from triplet sensitizers and triplet acceptors to upconversion quantum yields. *RSC Advances* **1**, 937-950 (2011).
6. Simon, Y.C. & Weder, C. Low-power photon upconversion through triplet-triplet annihilation in polymers. *J. Mater. Chem.* **22**, 20817-20830 (2012).
7. Cheng, Y.Y. et al. Entropically Driven Photochemical Upconversion. *J. Phys. Chem. A* **115**, 1047-1053 (2011).
8. Duan, P., Yanai, N., Nagatomi, H. & Kimizuka, N. Photon Upconversion in Supramolecular Gel Matrices: Spontaneous Accumulation of Light-Harvesting Donor-Acceptor Arrays in Nanofibers and Acquired Air Stability. *J. Am. Chem. Soc.* (2015).
9. Turshatov, A., Busko, D., Baluschev, S., Miteva, T. & Landfester, K. Micellar carrier for triplet–triplet annihilation-assisted photon energy upconversion in a water environment. *New J. Phys.* **13**, 083035 (2011).
10. Penconi, M., Gentili, P.L., Massaro, G., Elisei, F. & Ortica, F. A triplet-triplet annihilation based up-conversion process investigated in homogeneous solutions and oil-in-water microemulsions of surfactant. *Photochem. Photobiol. Sci.* (2013).
11. Liu, Q. et al. A General Strategy for Biocompatible, High-Effective Upconversion Nanocapsules Based on Triplet–Triplet Annihilation. *J. Am. Chem. Soc.* **135**, 5029-5037 (2013).
12. Wohnhaas, C. et al. Triplet–Triplet Annihilation Upconversion Based Nanocapsules for Bioimaging Under Excitation by Red and Deep-Red Light. *Macromol. Biosci.* **13**, 1422–1430 (2013).
13. Tanaka, K. et al. Hypoxic condition-selective upconversion via triplet–triplet annihilation based on POSS-core dendrimer complexes. *Bioorg. Med. Chem.* **21**, 2678-2681 (2013).
14. Askes, S.H.C., Bahreman, A. & Bonnet, S. Activation of a Photodissociative Ruthenium Complex by Triplet–Triplet Annihilation Upconversion in Liposomes. *Angew. Chem., Int. Ed.* **53**, 1029-1033 (2014).
15. Walde, P., Cosentino, K., Engel, H. & Stano, P. Giant Vesicles: Preparations and Applications. *ChemBioChem* **11**, 848-865 (2010).
16. Valkenier, H., López Mora, N., Kros, A. & Davis, A.P. Visualization and Quantification of Transmembrane Ion Transport into Giant Unilamellar Vesicles. *Angew. Chem., Int. Ed.* **54**, 2137-2141 (2015).

17. Lopez Mora, N. et al. Preparation of size tunable giant vesicles from cross-linked dextran(ethylene glycol) hydrogels. *Chem. Commun.* **50**, 1953-1955 (2014).
18. Marsh, D. Handbook of Lipid Bilayers, Edn. 2nd. (Taylor & Francis Group, LLC, Boca Raton, FL, USA; 2013).

Chapter V

Visualisation and quantification of transmembrane ion transport into giant unilamellar vesicles

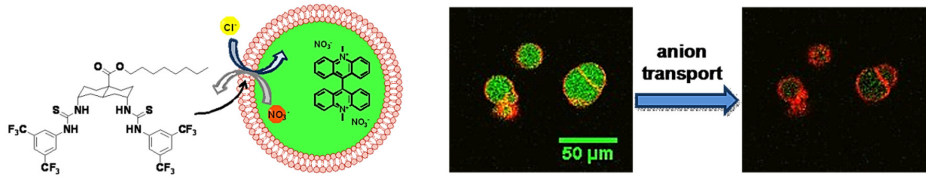

This work is published: Néstor López Mora, Hennie Valkenier, Alexander Kros, and Anthony P. Davis, *Angew. Chem., Int. Ed.,* **2015***, 54,* 2137–2141.

Abstract.

Transmembrane ion transporters (ionophores) are widely investigated as supramolecular agents with potential for biological activity. Tests are usually performed in synthetic membranes, assembled into large unilamellar vesicles (LUVs). However transport must be followed through bulk properties of the vesicle suspension, because LUVs are too small for individual study. Herein we describe an alternative approach whereby ion transport can be revealed and quantified through direct observation. The method employs giant unilamellar vesicles (GUVs), which are 20-60 μm in diameter and readily imaged by light microscopy. This allows characterisation of individual GUVs containing transporter molecules, followed by studies of transport through fluorescence emission from encapsulated indicators. The method provides new levels of certainty and relevance, given that the GUVs are similar in size to living cells. It has been demonstrated using a highly active anion carrier, and should aid the development of compounds for treating channelopathies such as cystic fibrosis.

Introduction

Transmembrane ion transport is a key process in biology. While membranes are intrinsically impermeable to ions, the cell needs to ingest and excrete charged species to sustain metabolism, avoid osmolysis and perform specialist functions. Biological ion transport is mediated by proteins,[1] but it has long been known that small molecules can have similar effects. The naturally-derived ionophore antibiotics act by promoting cation transport across cell membranes,[2] and synthetic analogues can also be effective. More recently it has been shown that anion transport is also achievable by synthetic systems,[3-5] both channels[6-8] and carriers.[9-12] In this case there is particular interest in replacing the activity of defective natural systems, yielding potential therapies for "channelopathies" such as cystic fibrosis (CF). Research on both cation and anion transport is ongoing, attracting a substantial community of bioorganic and supramolecular chemists.[13]

The study of ion transport by small molecules is commonly performed using large unilamellar vesicles (LUVs),[14] spherical assemblies of lipids ~100-200 nm in diameter in which the membrane isolates a small volume of interior aqueous solution. Transport into or out of the vesicles can then be studied by techniques such as fluorescence (using ion-sensitive fluorophores), NMR (using shift reagents to distinguish between interior and exterior), or ion selective electrodes. These methods are easy to implement but have certain disadvantages, especially for quantitative transport studies. Many of the problems relate to their small size, which is less than the wavelength of visible light and hampers imaging by light microscopy.[15] For example, while the standard method of production (extrusion through a microporous filter) allows control over size, a range of diameters are always present in a given sample. Secondly, even though unilamellar vesicles are thermodynamically favoured, the self-assembly of lipids can also produce multilamellar vesicles or other structures. Their presence may be inferred from the bulk behaviour of the suspension, but cannot be observed directly. Thirdly, a typical experiment on the LUV suspension will involve addition of a transporter or substrate, then the observation of a change (e.g. in bulk fluorescence) which reports transport into or out of vesicles. In principle the same change can often be produced by vesicle bursting rather than transport. While circumstances and controls may suggest that bursting is unlikely, doubts may persist. Fourthly, the LUVs are about two orders of magnitude smaller than most cells, which affects their value as cell models. In particular, the LUVs possess much higher surface:volume

ratios which increases their sensitivity to transport processes (see discussion below). Agents that cause major changes in LUVs may thus have limited potential for biological activity.

Herein we report a new method for studying ion transport which circumvents the above problems and allows direct, unambiguous observation of the transport process. Instead of LUVs, the method employs individual giant unilamellar vesicles (GUVs)[16] with diameters of 20-60 µm, similar to many cells and readily observable by microscopy. Fluorescence microscopy of GUVs has been used to study passive diffusion of peptides[17] and organic compounds[18] through membranes, passive diffusion of dyes through pores formed by peptides[19-22] or proteins[23, 24] and to qualitatively study the presence and performance of membrane proteins.[25] However, as far as we know, this is the first report in which the technique has been applied to the transport of inorganic ions. The method has been used to visualise and quantify chloride transport by a powerful anion transporter, and could in principle be applied to many other ion transport processes.

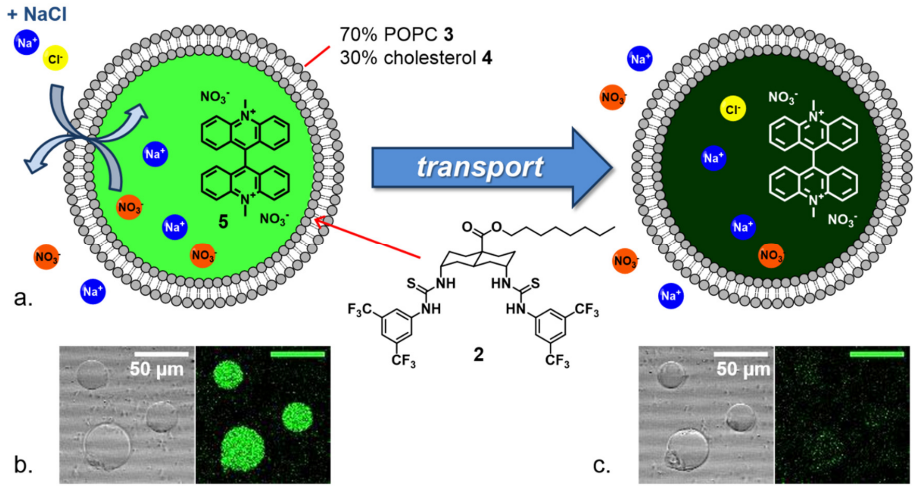

Figure 1. a) Schematic of the transport of chloride by transporter **1** into giant unilamellar vesicles (GUVs). Upon addition of a solution of NaCl, the transporter exchanges exterior chloride for interior nitrate. The chloride that is transported into the GUVs quenches the fluorescence of lucigenin **2** present in the interior of the vesicles. **b,c**) Bright field (left) and confocal fluorescence microscopy images (right) show three giant vesicles with transporter **1** (0.1 mol% of total lipid) preincorporated in the membrane before (b) and after (c) addition of NaCl.

The new method as applied herein is illustrated in **Figure 1**. The transport process is Cl^-/NO_3^- exchange by the bis-(thioureido)decalin **1**, an anion carrier (anionophore) which has recently been prepared by the Bristol group.[26] Giant vesicles are formed in which the transporter is located in the bilayer membrane and the chloride-sensitive fluorophore lucigenin **2** is trapped in the aqueous interior. Both interior and exterior aqueous phases contain $NaNO_3$ (225 mM). When NaCl is added to the exterior solution, the chloride is carried through the membrane by **1** and makes contact with lucigenin, quenching fluorescence.[27-31] Counter-transport of nitrate maintains electroneutrality.

The transfer of this assay to GUVs required a powerful transporter. Absolute transport rates into vesicles depend on the surface area, while the rate of change of substrate concentration depends on the interior volume. For a given vesicle composition, d[substrate]/dt scales with the surface:volume ratio, which decreases linearly with vesicle diameter (see *Experimental Section*). Concentration changes for a 20 μm GUV should therefore be 100 times slower than for a 200 nm LUV, and only the more active transporters are likely to give observable effects. Anionophore **1** features strongly anion-binding thioureido groups preorganised on a trans-decalin scaffold,[32] and a uniformly lipophilic exterior which appears to favour passage through bilayer membranes. It had shown exceptional activity in conventional LUV-based transport experiments[26] and was therefore most likely to succeed in the new test system.

Also needed was a method for preparing GUVs of well-defined size from lipids doped with transporter, at high ionic strength and with a cholesterol rich lipid mixture. The problem was solved using a technique developed by the Leiden group, in which the GUVs are grown on a cross-linked dextran-(polyethylene glycol) hydrogel substrate.[33] Adjusting the density of cross-links allows control of vesicle size between ~20 and ~100 μm. In the present case GUVs were grown from 1-palmitoyl-2-oleoylphosphatidylcholine (POPC) and cholesterol (7:3 ratio), plus a varied amount of transporter **1** (0 mol%, 0.01 mol%, 0.04 mol%, and 0.1 mol% of total lipid), using a hydrogel designed to yield vesicles of 10-40 μm diameter (see *Experimental Section*). The hydrogel with the lipid film containing the transporter was rehydrated with a solution of 225 mM $NaNO_3$, 0.8 mM lucigenin and 200 mM sucrose. The resulting giant vesicles were transferred into a microscopy chamber and the external solution was replaced by perfusion with a solution of 225 mM $NaNO_3$ and 200 mM glucose. This procedure removed the external lucigenin while lowering the density of the medium, causing the GUVs to settle on the viewing surface. The giant vesicles were imaged both in bright-field mode and when

excited with a 488 nm laser in a confocal fluorescence microscope. After 30-60 seconds, 25 µL 1 M NaCl solution was added to the microscopy chamber with a microsyringe, giving rise to an external chloride concentration of ~50 mM. As expected, the intensity of lucigenin emission was observed to decay significantly over a period of ~5 minutes (**Figure 2**). Bright-field images confirmed the presence of intact GUVs after quenching (see **Figure 1b,c** and *Experimental Section*), showing that the apparent disappearance of vesicles was not due to bursting. No fluorescence decay was observed in the absence of transporter (**Figures 2a,e**), and the rate of decay was clearly dependent on the amount of transporter **1** added (**Figures 2b-d, f-h**). The possibility of dye leakage was ruled out by a control experiment in which lucigenin was replaced by carboxyfluorescein. In this case, fluorescence emission from the vesicles underwent negligible change (see **Figure** 7 in *Experimental Section*). Our studies thus provide unambiguous confirmation that bis-thiourea **1** does indeed promote chloride transport across bilayer membranes, while preserving the lipid membrane and GUV integrity.

To obtain more insight into the process, we quantified the fluorescence intensity of the giant vesicles within each frame of the recorded time lapses. We then normalised and averaged the fluorescence intensities of the vesicles within one chamber (and from one NaCl addition experiment) to obtain curves that show the average fluorescence over time (**Figure 3**).

The experiment was performed twice for most concentrations and four times with the GUVs containing 0.01% transporter. **Figure 3** clearly shows how quenching and thus anion transport is fastest when 0.1% transporter is present (red) and how it is only slightly slower when 0.04% transporter is present (blue). When only 0.01% transporter is present (green), the fluorescence intensity has not yet plateaued within 250 seconds and transport is still ongoing. For this reason, the fluorescence intensities of the GUVs with 0.01% transporter were monitored over 20 minutes (see **Figures A1-A11** in *Annex Chapter V* for the full data sets). We also monitored the fluorescence intensity of GUVs over time without adding NaCl to test for photobleaching of lucigenin. As indicated by the black line in **Figure 3** in *Experimental Section* and **Figure A11** in *Annex Chapter V*), no photobleaching was observed in the first 5 minutes and even after 20 minutes of monitoring the bleaching was still below 7%, which is insignificant compared to the loss of fluorescence by quenching caused by transport of chloride.

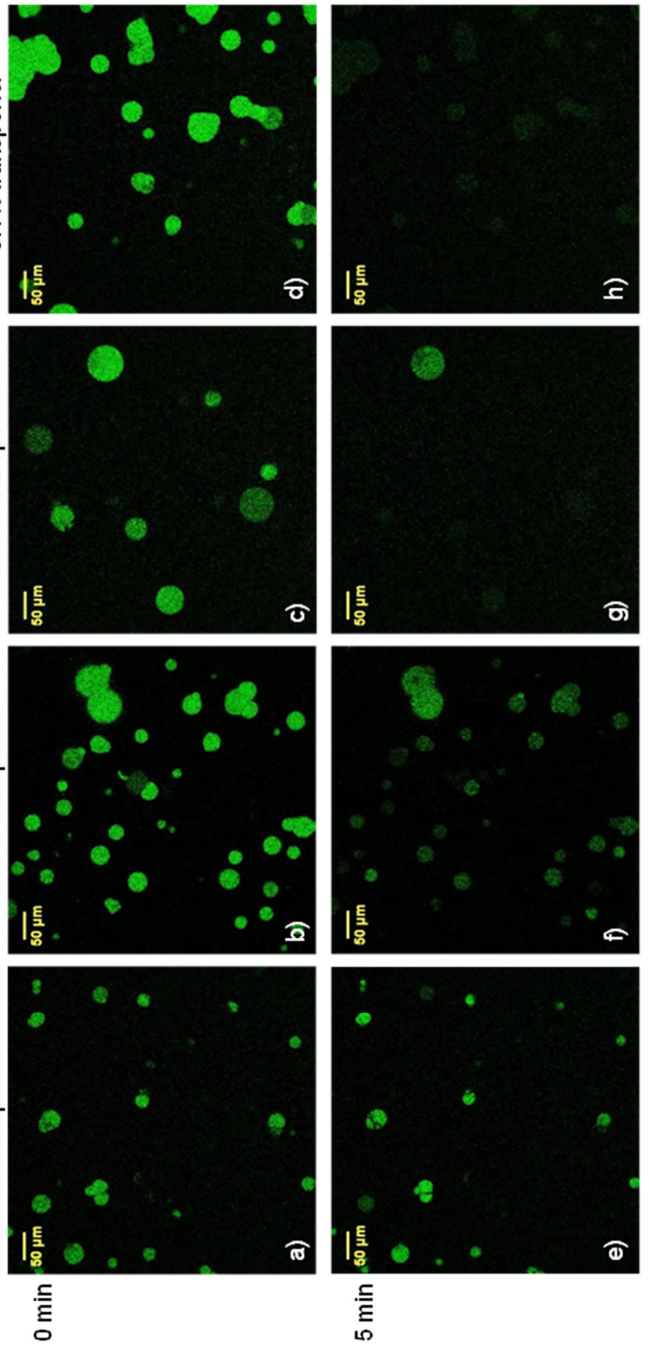

Figure 2. Confocal fluorescence microscopy images of lucigenin-containing GUVs, incorporating varying amounts of transporter **1**, before (a-d) and after addition of NaCl (e-f: images taken ~5 min after the addition of NaCl).

Careful examination of all the fluorescence decay profiles reveals that while most GUVs within one experiment have similarly shaped fluorescence *vs.* time curves (forming a distribution due to the variation in sizes of the vesicles), certain vesicles show distinct behaviour (see full datasets in the *Annex Chapter V*). For instance, the fluorescence of one giant vesicle in **Figure 2g** remains visible where all the others have disappeared into the background (these distinctively slower traces have not been included in the average curves in **Figure 3**). Suspecting that this distinct transport behaviour was due to multilamellarity of certain vesicles, we repeated the experiments employing 0.01% and 0.04% transporter with lissamine rhodamine B-labelled lipid added to the membrane (0.1 mol%) (see **Figure A12** in *Annex Chapter V*). This allowed us to visualise the membranes of the vesicles upon excitation with a 532 nm laser. Multilamellar membranes give higher intensities of rhodamine fluorescence compared to unilamellar membranes.[34] The results of one of these experiments employing 0.01% transporter **1** are presented in **Figure 4**. For typical GUVs the intensity of red fluorescence emitted from the membranes is ~25 units. However, for the vesicles labelled C and D in **Figure 4a** the observed intensity is double this value (~50 units) while the intensities from the membranes of GUVs A and B reach 200-250 and 100-150 units respectively (for details see **Fig. A12**, full datasets in *Annex Chapter V*). In **Figure 4b** we clearly see that the vesicles labelled A-D display a stronger intensity of fluorescence of lucigenin, even after 20 minutes. This is also seen in the normalized fluorescence traces of the individual vesicles as plotted in **Figure 4c**. After 1000 seconds the fluorescence intensity of most vesicles has reached the plateau value of ~20% of the initial fluorescence, while plots from vesicles A-D show much slower decays. As giant vesicles C and D show a rhodamine emission intensity which is double the value of the majority of the vesicles, and both have identical curves, these are likely to have a double lipid bilayer. Vesicles A and B, with even stronger rhodamine emission and slower lucigenin quenching, are likely to have higher orders of multilamellarity. Vesicles A-D are therefore excluded from further quantitative analysis.

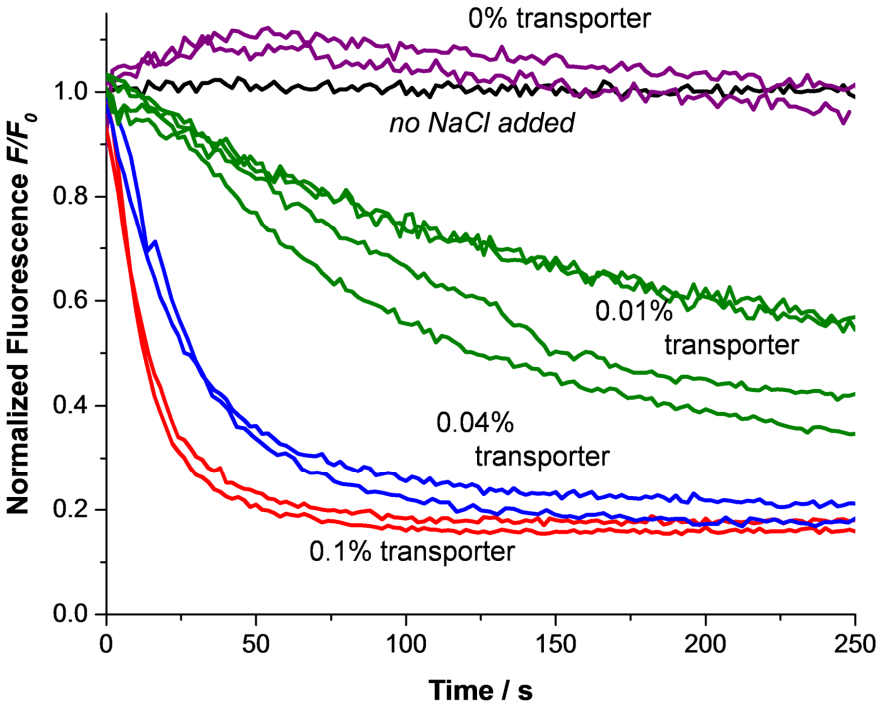

Figure 3. Average traces of the normalised lucigenin emission intensity after addition of 50 mM NaCl to GUVs without transporter (purple), with 0.01% transporter (green), with 0.04% transporter (blue) and with 0.1% transporter present (red) or without NaCl added (black).

Having found a method to distinguish unilamellar and multilamellar giant vesicles, we were able to quantify transport into the unilamellar vesicles. We focused on the slower-transporting GUVs containing 0.01% bis-thiourea **1**, to minimise errors due to the addition of NaCl at the start of the experiment. Relatively slow and careful addition is necessary to avoid disturbing the GUVs in the field of the microscope. The fluorescence decay data were analysed using a protocol previously employed for **1** in LUVs.[26] Values for F_0/F [35] were fitted to a single exponential decay function, which was converted to chloride concentrations by assuming a limiting intravesicular [Cl^-] of 50 mM. This was then used to calculate an initial rate of chloride transport per transporter molecule, taking account of the size of the vesicle. The analysis was performed for 56 GUVs from 6 experiments (all with 0.01% transporter), giving an average initial rate per transporter of 820 ± 260 Cl^- s^{-1}. This value is similar to that obtained from experiments on bulk LUV solutions using the same transporter (850 Cl^- s^{-1}).[26] However,

because the present work was performed on vesicles of known diameters and lamellarities, characterised by microscopy, we believe it is much more reliable. For a full description of the analysis procedure, see the *Experimental Section*.

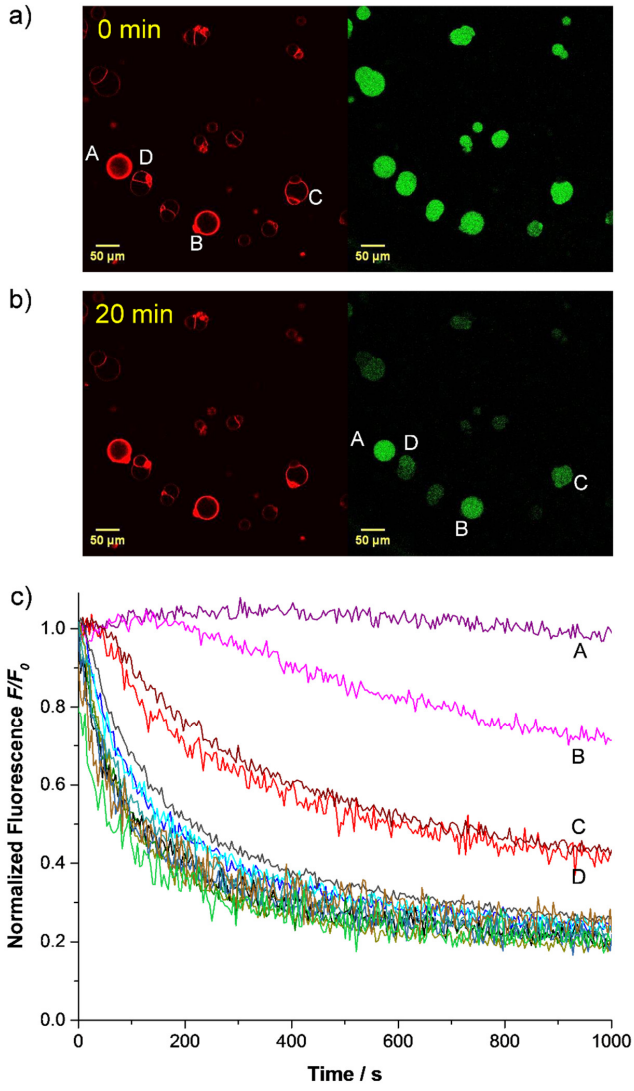

Figure 4. a) Fluorescence microscopy images of GUVs containing lucigenin and incorporating rhodamine-labelled lipid + 0.01% transporter **1**. Left: Illumination at 532 nm visualises the rhodamine in the bilayer. Right: Illumination at 488 nm excites the lucigenin. **b**) As above, 20 min after addition of NaCl. **c**) Traces of the lucigenin fluorescence intensity of individual vesicles over time after addition of 50 mM NaCl. The four vesicles that display stronger rhodamine fluorescence, and their corresponding traces, are labelled A-D.

Conclusion

In conclusion we have devised a new method whereby ion transport by small molecules into individual giant unilamellar vesicles can be observed and quantified. By directly visualising transport into GUVs, the approach offers a high level of certainty and integrity compared to experiments on bulk suspensions of smaller vesicles. Instead of quantifying transport into a population of vesicles with a distribution of sizes, we can now analyse the transport into individual GUVs of which we can verify the lamellarity and measure the size. The method is complementary to studies in LUVs, in that it is better suited to very powerful transporters which can produce measurable effects despite the low surface:volume ratio of GUVs. Indeed, positive results in this test provide clear encouragement that a transporter has potential for biological activity.

In this initial demonstration the method has been used to study chloride/nitrate exchange by an anion carrier. However, it is reasonable to suppose that other types of ion transport could be investigated similarly. A number of fluorescence-based methods have been developed for following transport into LUVs.[14] For example, the pH-sensitive probe 8-hydroxy-1,3,6-pyrenetrisulfonate (HPTS) is used as a general indicator of ion transport, while other dyes have been used to follow transport of specific metal cations. Transfer of these assays to GUVs should be straightforward, while further indicators are readily available[36] and remain to be exploited.

Finally, the success of **1** at mediating Cl^-/NO_3^- exchange in this system, even at the modest loading of 0.01%, further highlights its exceptional activity. This molecule is relatively lipophilic so that dispersion in water and delivery to cell membranes may be challenging. However if the delivery problem can be solved, for example with membrane fusion,[37, 38] the effectiveness of **1** in cell-sized vesicles augurs well for applications in biology and medicine.

Experimental Section

Materials and methods

Cholesterol, 1-palmitoyl-2-oleoyl-sn-glycero-3-phosphocholine (POPC), and bovine serum albumin (BSA) were purchased from Sigma Aldrich. 1,2-Dioleoyl-sn-glycero-3-phosphoethanolamine-N-(lissamine rhodamine B sulfonyl) (ammonium salt) (rhodamine labelled lipid) was purchased from Avanti Polar Lipids and 10,10'-dimethyl-9,9'-biacridinium nitrate (lucigenin, 2) was purchased from Tokyo Chemical Industry UK Ltd. Chloroform was deacidified by passage through a column containing activated basic alumina before the preparation of the lipid solutions. The lucigenin (0.8 mM), $NaNO_3$ (225 mM) and NaCl (1 M) aqueous solutions were prepared with Millipore grade water. Lipid solutions of POPC and cholesterol (70:30 ratio, 14 mM) were prepared in the previously deacidified chloroform and the transporter octyl t-(2,7)-bis(3-(3,5-bis(trifluoromethyl)phenyl)thioureido)-t-8a-decahydronaphthalene-r-4a-carboxylate,[26] (1, 84 μM solution in methanol) was added to this lipid solution at 0.01 mol%, 0.04 mol% and 0.1 mol% (relative to total lipid). Rhodamine labelled lipid was added in 0.1 mol% when membrane imaging was required.

GUVs formation and microscopy chamber preparation

Giant Unilamellar Vesicles (GUVs) were grown in Dex-PEG (1:1 ratio) coated microscope glass slides substrates as described previously.[33] Lipid solution (10 μL) was deposited on a hydrogel coated glass slide, then the lipid solution was dried by evaporating the chloroform under a gentle stream of Nitrogen gas. A liquid chamber was made by placing a 15 mm (OD) glass O-Ring on top of the hydrogel and sealed with high vacuum silicon grease. The lipid film was rehydrated by adding 400 μL of an aqueous solution that contains lucigenin (0.8 mM), $NaNO_3$ (225 mM) and sucrose (200 mM), into each chamber. GUVs were grown during at least 3 hours at room temperature and subsequently the solution with free floating GUVs was transferred into an eppendorf tube containing 600 μL of $NaNO_3$ (225 mM) and glucose (200 mM) aqueous solution. The visualization chamber (μ-Slide 8 well, Ibidi) was pre-treated with an aqueous solution of BSA (1 mg/mL, 500 μL) for one hour. The diluted solution with GUVs was transferred into the microscopy visualization chamber (500 μL per well). The GUVs were left to sediment for at least 30 minutes and the excess of non-encapsulated lucigenin was replaced by the $NaNO_3$ and glucose solution using a peristaltic perfusion pump (Instech P720,

~ 0.4 mL/min, 30 minutes), to produce a clean background for imaging the encapsulated lucigenin dye in the GUVs.

Lucigenin quenching assay

During the imaging of the GUVs in a time lapse experiment, 25 µL 1M NaCl (in NaNO3 and glucose solution) was added to the well after 30-60 seconds with a microsyringe, giving a final NaCl concentration of ~50 mM.

Fluorescence Microscopy of GUVs

All imaging was performed on a Leica TCS SPE confocal microscope system. Illumination was provided by a solid state laser using the 488 nm laser line (15% laser power) for scanning lucigenin's fluorescence and 532 nm laser line (10-15% laser power) for scanning lissamine rhodamine's fluorescence. Confocal microscopy was carried out using a 20× dry objective. The analysis of the images was performed in ImageJ software, by measuring the average intensity of an area corresponding to one GUV for the series of time lapsed confocal image frames.

Osmomolality

The osmolality of a NaNO3 (225 mM) solution was determined from the freezing point depression using an Osmometer Roebling Type 13 (calibrated using 100 mOsm/kg NaCl standard solution) and found to be 378 mOsm/kg (standard PBS buffer was 310 mOsm/kg). Addition of 50 mM NaCl to 225 mM NaNO3 causes the osmolality to increase to 473 mOsm/kg.

Fitting of the fluorescence intensities of individual GUVs

According to the Stern-Volmer relationship:

$$\frac{F_0}{F} = 1 + k_q \tau_0 \, [Q]$$

the fluorescence in absence of quencher (F_0) divided by the fluorescence (F) is proportional to the concentration of quencher [Q], which is chloride in our experiments. In the Stern-Volmer equation k_q is the rate constant of the quenching process and τ_0 is the life time of the emitting state of lucigenin, which are both constants. This allows us to take the reciprocal of our

normalized fluorescence traces (which are F/F_0) to get F_0/F curves, of which the shape directly represents the concentration of chloride in the vesicles over time.

The first 1000 s of the F_0/F curves obtained for individual GUVs (0.01% transporter) are fitted with a single exponential decay function:

$$\frac{F_0}{F} = y - a \cdot e^{-kt} \quad (1)$$

Examples of representative fits are given in **Figure 5**.

We note that the increase of the noise in the curves presented in **Figure 5** is caused by the decrease of fluorescence intensity upon quenching. The error in measuring the fluorescence intensity thus increases over time when transport is occurring.

The value obtained for parameter k is the rate constant for the transmembrane transport process. Since the fits are generally good we can assume that the concentration of chloride inside the GUV [Cl^-] increases from 0 to 50 mM following the exponential decay function given by equation 2:

$$[Cl^-] = 50\ mM(1 - e^{-kt}) \quad (2)$$

The rate constant k is obtained from the fit. Differentiation of equation 2 at t=0 gives the initial rate of chloride transport into the GUVs as 50k in mM s^{-1}. From the measured diameter of the GUVs, the volume and the surface area can be calculated. Subsequently, the initial rate (in mM s^{-1}) can be multiplied by the volume of the GUV (V_{GUV}) and Avogadro's number (N_A) to get the initial rate as number of chloride anions transported into the GUV per second. Dividing this by the calculated number of transporters in the GUVs (two times the surface area A_{GUV}, divided by the surface area per lipid which is assumed to be 46.97 $Å^2$ for POPC/cholesterol 7:3[26, 39] times the ratio of transporter to lipid) gives the initial rate of transport per transporter ($I_{transporter}$) in chloride anions per second (equation 3).

$$I_{transporter} = \frac{50\ mM \cdot k \cdot V_{GUV} \cdot N_A}{\left(\frac{2 \cdot A_{GUV}}{46.97\ Å^2}\right)\left(\frac{transporter}{lipid}\right)} \quad (3)$$

Data on 56 GUVs from 6 experiments were analyzed this way, giving an average initial rate per transporter of 820 ± 260 $Cl^-\ s^{-1}$.

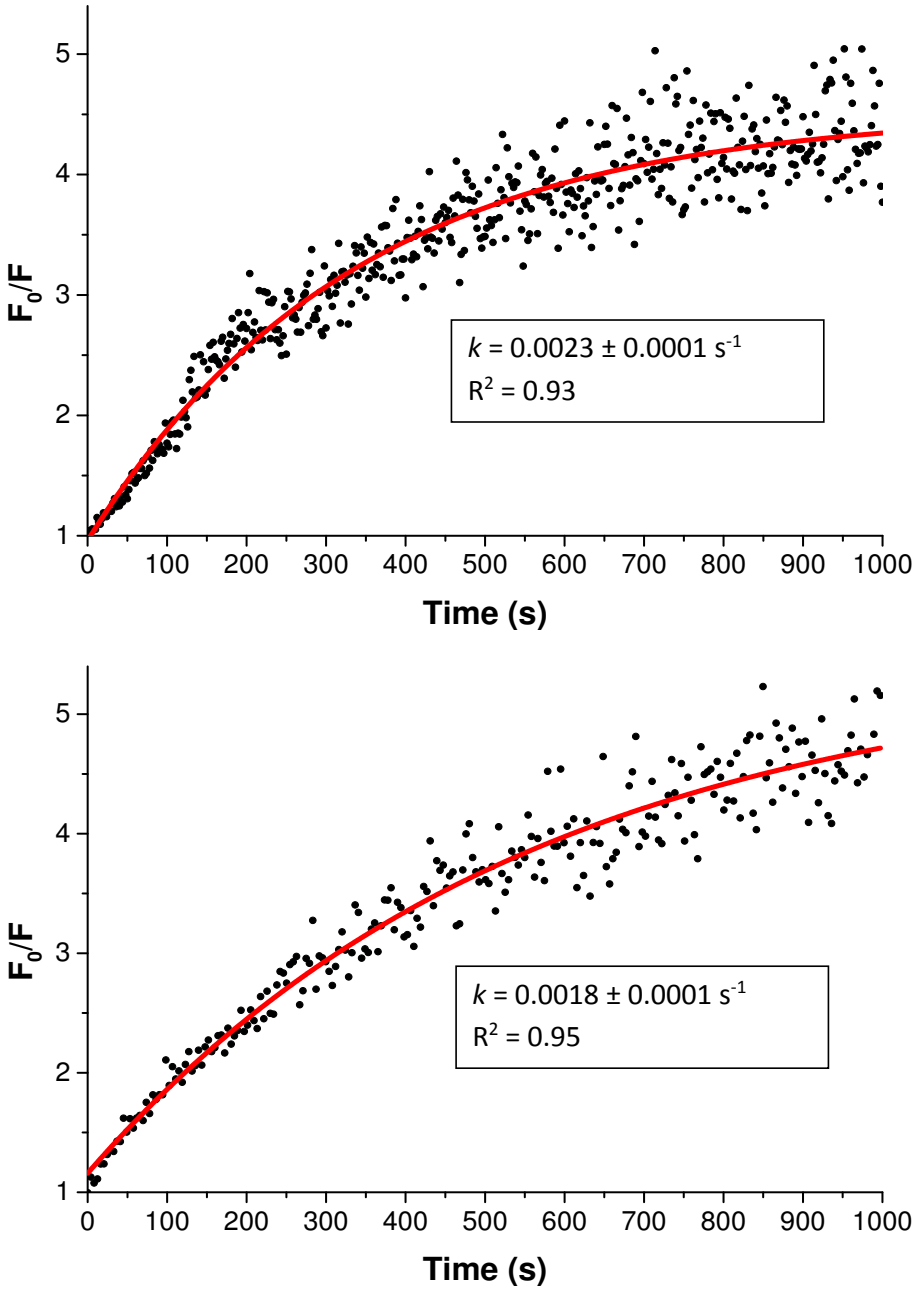

Figure 5. Single exponential fits (red lines) of F_0/F data of individual GUVs (black dots). Note that the noise level of the measured data increases over time. Due to the decreasing fluorescence intensity, the error in measuring the average fluorescence intensity of the area corresponding to a GUV increases.

The half-life of the transport process increases linearly with the diameter of the GUVs

The rate of transport by one transporter molecule is independent of the size of the GUV. However, the first-order rate constant for the transport of chloride into the GUVs (k), as obtained from the fits, depends on the volume of the GUV (V_{GUV}) and on the number of transporters present in the membrane and thus on the surface area (A_{GUV}), according to equation (3). From this it can be shown as follows that, for a given transporter at a given concentration, the half-life ($t_{½}$) is directly proportional to the diameter of the GUVs:

As $I_{transporter}$ is a constant, $\frac{k \cdot V_{GUV}}{A_{GUV}}$ must also be constant, indicating that $k \propto \frac{A_{GUV}}{V_{GUV}}$

For half-life ($t_{½}$) one can therefore write:

$t_{½} = \frac{\ln(2)}{k} \propto \frac{V_{GUV}}{A_{GUV}} \propto \emptyset_{GUV}$ (where $\emptyset_{GUV}$ is the diameter of the GUVs)

Figure 6a gives a plot of the half-lives obtained for the 16 GUVs from one experiment, which show a nearly linear relationship with diameter of the GUVs. The plot in **Figure 6b** shows the half-lives from all the GUVs of six experiments (all with 0.01% transporter). The latter plot shows more deviations from the linear relationship between the half-life and the diameter, but the main trend is still linear, indicating how the size of the GUVs affects the observed rate of quenching of the fluorescence.

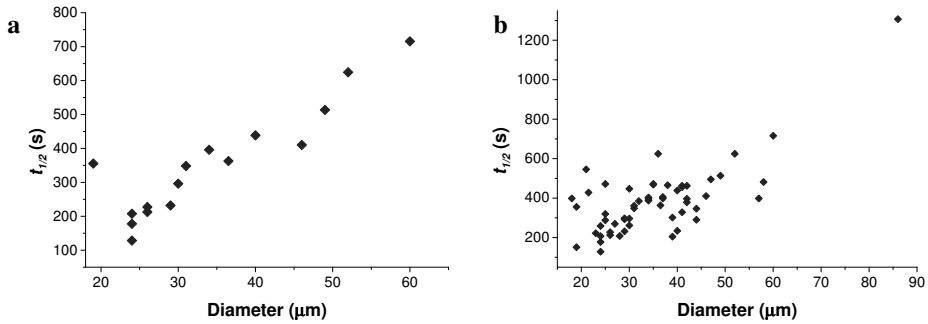

Figure 6. Plot of the half-lives (from single exponential fits, experiments with 0.01% transporter) versus the diameter of 16 individual GUVs from one experiment (**a**) and from 56 GUVs of 6 experiments combined in one graph (**b**).

Test for leaking of a fluorescence dye from the GUVs

To exclude the possibility that the decrease of fluorescence of the GUVs is caused by lucigenin leaking out the GUVs via defects formed by the transport and chloride, we repeated the experiment with carboxyfluorescein as the fluorescent dye.[40] As the fluorescence of carboxyfluorescein is not quenched by chloride, we should be able to distinguish between the dye leaking from the GUVs and transport of chloride into the GUVs.

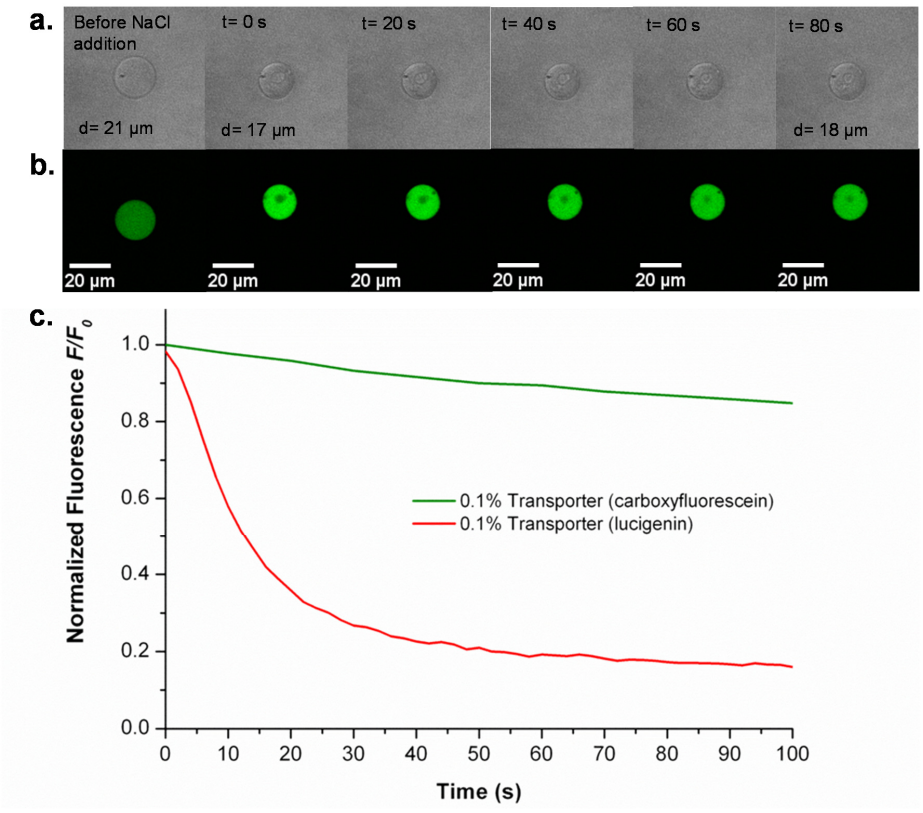

Figure 7. Series of bright-field (**a.**) and fluorescence microscopy images (**b.**) of a GUV made of POPC (70%), cholesterol (30%), and transporter **1** (0.1%) containing carboxyfluorescein (0.1 mM, pH 7) and $NaNO_3$ (225 mM, interior and exterior). The confocal fluorescence imaging is performed with a 488 nm laser at 10% power and a detection filter band between 500-600 nm. Upon the addition of NaCl (25 µL, 1 M) the GUVs shrink producing an increase in the fluorescence, which slightly decreases once the inner content and the exterior reach the equilibrium. **c.** Comparison of the experiments with carboxyfluorescein and lucigenin. The red line corresponds to the average fluorescence of lucigenin with 0.1 % transporter preincorporated in the membrane (see Figure 3 of the main paper). The green line shows the average fluorescence of carboxyfluorescein of 5 individual GUVs with

0.1 % transporter preincorporated in the membrane. The starting time (t = 0 s) corresponds to the addition of 25 µL NaCl (1M).

The results in **Figure 7** show that carboxyfluorescein does not leak from the GUVs. We can therefore conclude that the addition of sodium chloride to the GUVs with transporter does not cause the formation of defects or channels in the membrane. This confirms that the observed quenching of fluorescence of lucigenin is caused by chloride transport into the GUVs.

References

1. Hille, B. Ion Channels of Excitable Membranes. *Sinauer, Sunderland, MA* (2001).
2. Pressman, B.C. Biological Applications of Ionophores. *Annu Rev Biochem* **45**, 501-530 (1976).
3. Davis, A.P., Sheppard, D.N. & Smith, B.D. Development of synthetic membrane transporters for anions. *Chem Soc Rev* **36**, 348-357 (2007).
4. Davis, J.T., Okunola, O. & Quesada, R. Recent advances in the transmembrane transport of anions. *Chem Soc Rev* **39**, 3843-3862 (2010).
5. Busschaert, N. & Gale, P.A. Small-Molecule Lipid-Bilayer Anion Transporters for Biological Applications. *Angew Chem Int Edit* **52**, 1374-1382 (2013).
6. Mareda, J. & Matile, S. Anion-pi Slides for Transmembrane Transport. *Chem-Eur J* **15**, 28-37 (2009).
7. Gokel, G.W. & Negin, S. Synthetic Ion Channels: From Pores to Biological Applications. *Accounts Chem Res* **46**, 2824-2833 (2013).
8. Li, X., Shen, B., Yao, X.Q. & Yang, D. Synthetic Chloride Channel Regulates Cell Membrane Potentials and Voltage-Gated Calcium Channels. *J Am Chem Soc* **131**, 13676-13680 (2009).
9. Valkenier, H. & Davis, A.P. Making a Match for Valinomycin: Steroidal Scaffolds in the Design of Electroneutral, Electrogenic Anion Carriers. *Accounts Chem Res* **46**, 2898-2909 (2013).
10. Cooper, J.A., Street, S.T.G. & Davis, A.P. A Flexible Solution to Anion Transport: Powerful Anionophores Based on a Cyclohexane Scaffold. *Angew Chem Int Edit* **53**, 5609-5613 (2014).
11. Jentzsch, A.V., Hennig, A., Mareda, J. & Matile, S. Synthetic Ion Transporters that Work with Anion-pi Interactions, Halogen Bonds, and Anion-Macrodipole Interactions. *Accounts Chem Res* **46**, 2791-2800 (2013).
12. Gale, P.A., Perez-Tomas, R. & Quesada, R. Anion Transporters and Biological Systems. *Accounts Chem Res* **46**, 2801-2813 (2013).
13. Matile, S. & Fyles, T. Transport Across Membranes. *Accounts Chem Res* **46**, 2741-2742 (2013).
14. Matile, S. & Sakai, N. Analytical methods in supramolecular chemistry (Ed. C. A. Schalley). *Wiley-VCH, Weinheim*, pp. 711-742 (2012).
15. Stamou, D., Duschl, C., Delamarche, E. & Vogel, H. Self-assembled microarrays of attoliter molecular vessels. *Angew Chem Int Edit* **42**, 5580-5583 (2003).
16. Walde, P., Cosentino, K., Engel, H. & Stano, P. Giant Vesicles: Preparations and Applications. *Chembiochem* **11**, 848-865 (2010).
17. Shimanouchi, T. et al. Permeation of a beta-heptapeptide derivative across phospholipid bilayers. *Bba-Biomembranes* **1768**, 2726-2736 (2007).
18. Li, S., Hu, P.C. & Malmstadt, N. Confocal Imaging to Quantify Passive Transport across Biomimetic Lipid Membranes. *Anal Chem* **82**, 7766-7771 (2010).
19. Tamba, Y. & Yamazaki, M. Single giant unilamellar vesicle method reveals effect of antimicrobial peptide magainin 2 on membrane permeability. *Biochemistry-Us* **44**, 15823-15833 (2005).
20. Tamba, Y. & Yamazaki, M. Magainin 2-Induced Pore Formation in the Lipid Membranes Depends on Its Concentration in the Membrane Interface. *J Phys Chem B* **113**, 4846-4852 (2009).

21. Tamba, Y., Ariyama, H., Levadny, V. & Yamazaki, M. Kinetic Pathway of Antimicrobial Peptide Magainin 2-Induced Pore Formation in Lipid Membranes. *J Phys Chem B* **114**, 12018-12026 (2010).
22. Islam, M.Z., Ariyama, H., Alam, J.M. & Yamazaki, M. Entry of Cell-Penetrating Peptide Transportan 10 into a Single Vesicle by Translocating Across Lipid Membrane and Its Induced Pores. *Biochemistry-Us* **53**, 386-396 (2014).
23. Robinson, T., Kuhn, P., Eyer, K. & Dittrich, P.S. Microfluidic trapping of giant unilamellar vesicles to study transport through a membrane pore. *Biomicrofluidics* **7** (2013).
24. Alam, J.M., Kobayashi, T. & Yamazaki, M. The Single-Giant Unilamellar Vesicle Method Reveals Lysenin-Induced Pore Formation in Lipid Membranes Containing Sphingomyelin. *Biochemistry-Us* **51**, 5160-5172 (2012).
25. Dezi, M., Di Cicco, A., Bassereau, P. & Levy, D. Detergent-mediated incorporation of transmembrane proteins in giant unilamellar vesicles with controlled physiological contents. *P Natl Acad Sci USA* **110**, 7276-7281 (2013).
26. Valkenier, H. et al. Preorganized Bis-Thioureas as Powerful Anion Carriers: Chloride Transport by Single Molecules in Large Unilamellar Vesicles. *J Am Chem Soc* **136**, 12507-12512 (2014).
27. McNally, B.A., Koulov, A.V., Smith, B.D., Joos, J.B. & Davis, A.P. A fluorescent assay for chloride transport; identification of a synthetic anionophore with improved activity. *Chem Commun*, 1087-1089 (2005).
28. McNally, B.A. et al. Structure-Activity Relationships in Cholapod Anion Carriers: Enhanced Transmembrane Chloride Transport through Substituent Tuning. *Chem-Eur J* **14**, 9599-9606 (2008).
29. Busschaert, N. et al. Towards predictable transmembrane transport: QSAR analysis of anion binding and transport. *Chem Sci* **4**, 3036-3045 (2013).
30. Bahmanjah, S., Zhang, N. & Davis, J.T. Monoacylglycerols as transmembrane Cl- anion transporters. *Chem Commun* **48**, 4432-4434 (2012).
31. Dawson, R.E. et al. Experimental evidence for the functional relevance of anion-pi interactions. *Nat Chem* **2**, 533-538 (2010).
32. Hussain, S., Brotherhood, P.R., Judd, L.W. & Davis, A.P. Diaxial Diureido Decalins as Compact, Efficient, and Tunable Anion Transporters. *J Am Chem Soc* **133**, 1614-1617 (2011).
33. Mora, N.L. et al. Preparation of size tunable giant vesicles from cross-linked dextran(ethylene glycol) hydrogels. *Chem Commun* **50**, 1953-1955 (2014).
34. Chiba, M., Miyazaki, M. & Ishiwata, S. Quantitative Analysis of the Lamellarity of Giant Liposomes Prepared by the Inverted Emulsion Method. *Biophys J* **107**, 346-354 (2014).
35. Note that F0/F is the reciprocal of the quantity shown in Figures 3 and 4. The analysis employs F0/F because, according to the Stern-Vollmer equation, it is this value which is directly proportional to quencher concentration.
36. Haugland, R.P. Handbook of Fluorescent Probes and Research Chemicals. *Invitrogen (Molecular Probes), Eugene, OR* (2005).

37. Marsden, H.R., Elbers, N.A., Bomans, P.H.H., Sommerdijk, N.A.J.M. & Kros, A. A Reduced SNARE Model for Membrane Fusion. *Angew Chem Int Edit* **48**, 2330-2333 (2009).

38. Zope, H.R. et al. In Vitro and In Vivo Supramolecular Modification of Biomembranes Using a Lipidated Coiled-Coil Motif. *Angew Chem Int Edit* **52**, 14247-14251 (2013).

39. Olsen, B.N., Schlesinger, P.H. & Baker, N.A. Perturbations of Membrane Structure by Cholesterol and Cholesterol Derivatives Are Determined by Sterol Orientation. *J Am Chem Soc* **131**, 4854-4865 (2009).

40. Ambroggio, E.E., Separovic, F., Bowie, J.H., Fidelio, G.D. & Bagatolli, L.A. Direct visualization of membrane leakage induced by the antibiotic peptides: Maculatin, citropin, and aurein. *Biophys J* **89**, 1874-1881 (2005).

Annex
Chapter V

Full datasets behind the average curves presented in Figure 3 of the main paper

Cross-sections of vesicles with rhodamine-labelled membranes in Figure 4a

Full datasets behind the average curves presented in Figure 3 of the main paper

No transporter

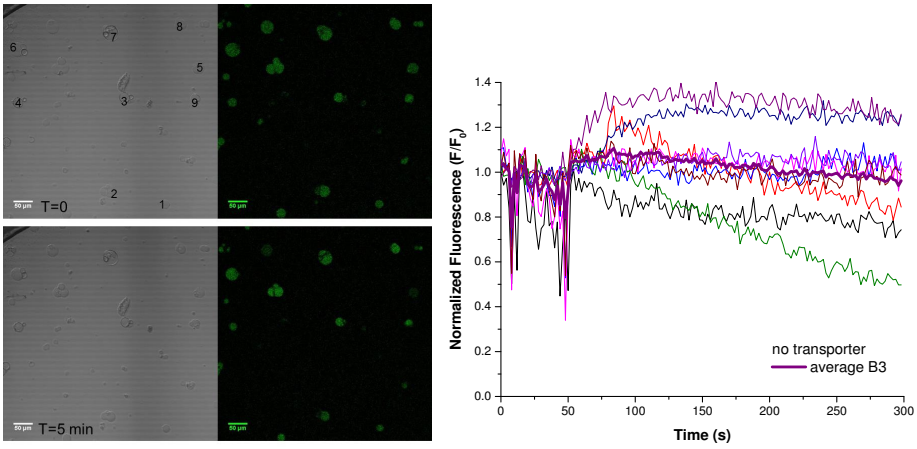

Figure A1. Bright-field and fluorescence microscopy images before (top) and after (bottom) addition of NaCl to GUVs without transporter (*experiment B3*). The normalized fluorescence intensity over time is given for the individual numbered GUVs and for the average of all numbered GUVs (fat purple line). The average diameter of the GUVs used in the average trace for 36 µm.

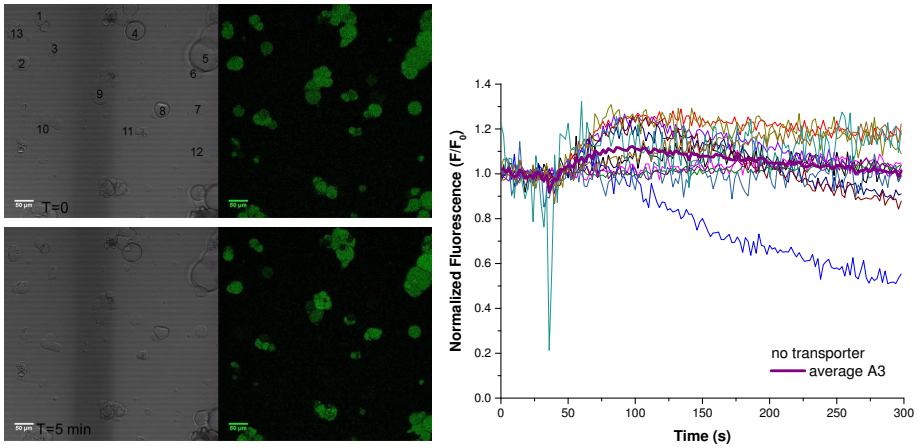

Figure A2. Bright-field and fluorescence microscopy images before (top) and after (bottom) addition of NaCl to GUVs without transporter (*experiment A3*). The normalized fluorescence intensity over time is given for the individual numbered GUVs and for the average of all numbered GUVs (fat purple line). The average diameter of the GUVs used in the average trace for 38 µm.

0.1% transporter

The decrease of fluorescence intensity before the addition of NaCl (sharp drops before t=0) in some traces is caused by the tip of the syringe used add the NaCl solution passing through the laser beam that is scanning the sample.

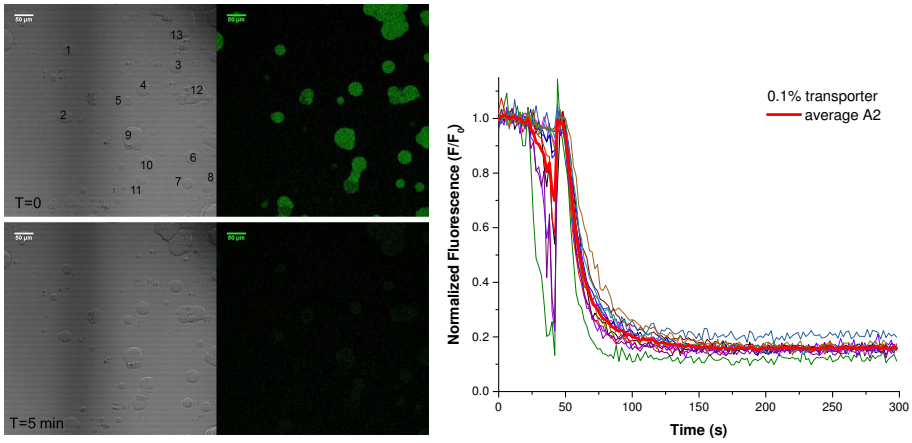

Figure A3. Bright-field and fluorescence microscopy images before (top) and after (bottom) addition of NaCl to GUVs containing 0.1% transporter (*experiment A2*). The normalized fluorescence intensity over time is given for the individual numbered GUVs and for the average of all numbered GUVs (fat red line). The average diameter of the GUVs used in the average trace for 36 µm.

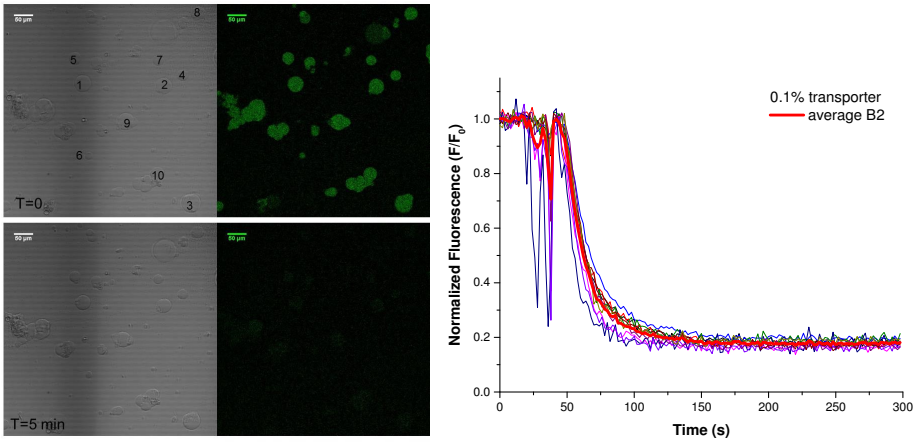

Figure A4. Bright-field and fluorescence microscopy images before (top) and after (bottom) addition of NaCl to GUVs containing 0.1% transporter (experiment B2). The normalized fluorescence intensity over time is given for the individual numbered GUVs and for the average of all numbered GUVs (fat red line). The average diameter of the GUVs used for the average trace is 36 µm.

0.04% transporter

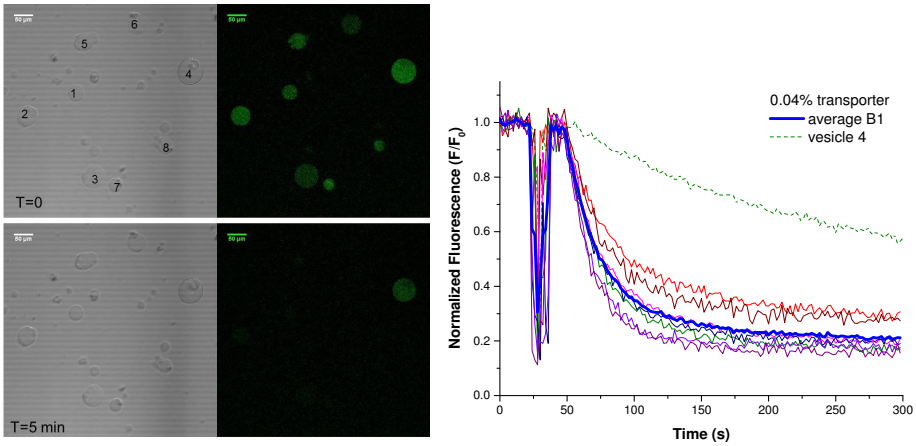

Figure A5. Bright-field and fluorescence microscopy images before (top) and after (bottom) addition of NaCl to GUVs containing 0.04% transporter (*experiment B1*). The normalized fluorescence intensity over time is given for the individual numbered GUVs and for the average of all numbered GUVs (fat blue line; excluded is vesicle 4, corresponding to green dashed line). The average diameter of the GUVs used for the average trace is 46 µm.

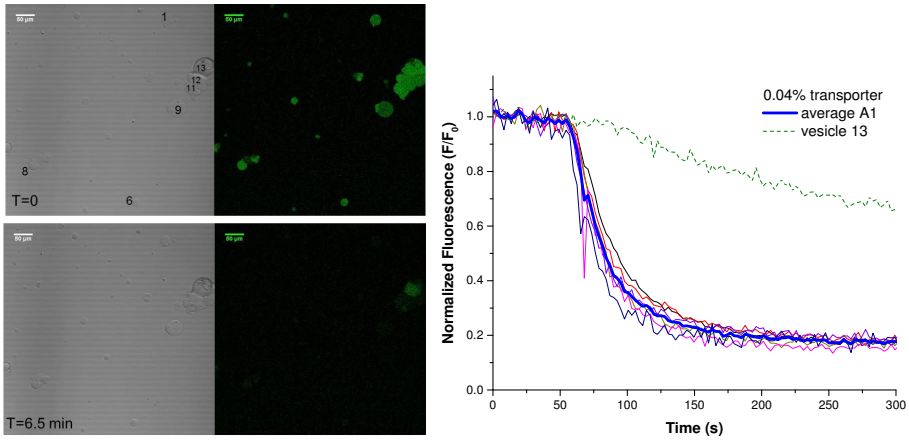

Figure A6. Bright-field and fluorescence microscopy images before (top) and after (bottom) addition of NaCl to GUVs containing 0.04% transporter (*experiment A1*). The normalized fluorescence intensity over time is given for the individual numbered GUVs and for the average of all numbered GUVs (fat blue line; excluded is vesicle 13, corresponding to green dashed line). The average diameter of the GUVs used for the average trace is 34 µm.

0.01% transporter

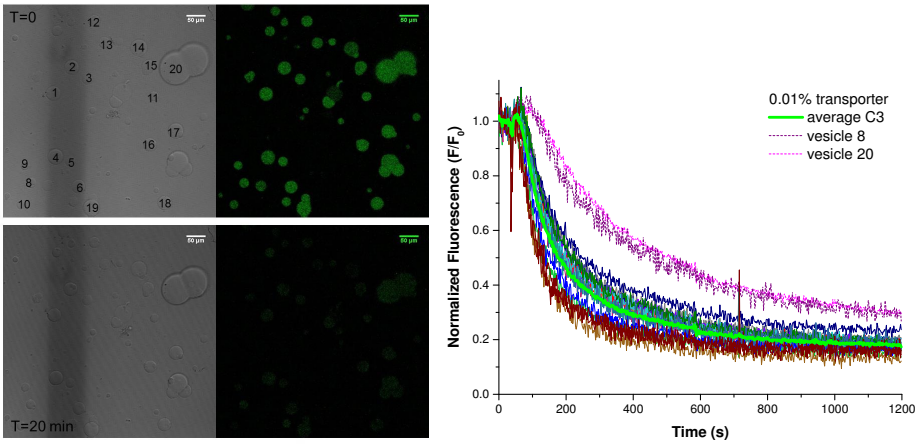

Figure A7. Bright-field and fluorescence microscopy images before (top) and after (bottom) addition of NaCl to GUVs containing 0.01% transporter (*experiment C3*). The normalized fluorescence intensity over time is given for the individual numbered GUVs and for the average of all numbered GUVs (fat light green line; excluded are vesicles 8 and 20). The average diameter of the GUVs used in the average trace for 34 µm.

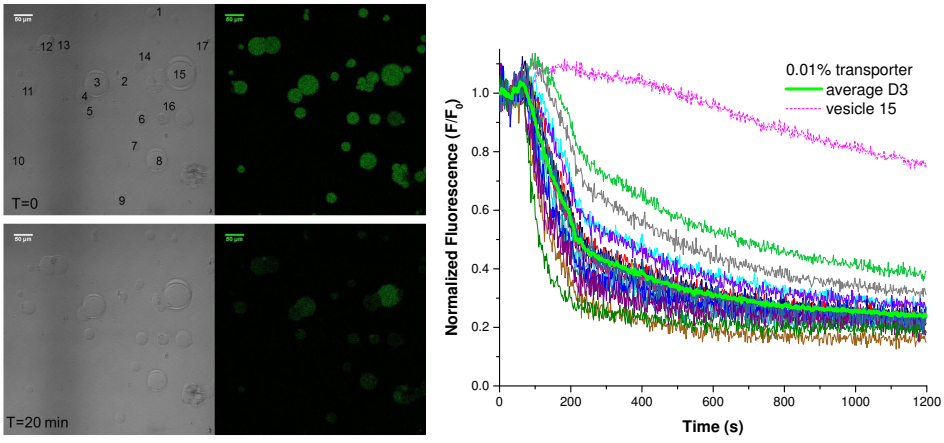

Figure A8. Bright-field and fluorescence microscopy images before (top) and after (bottom) addition of NaCl to GUVs containing 0.01% transporter (*experiment D3*). The normalized fluorescence intensity over time is given for the individual numbered GUVs and for the average of all numbered GUVs (fat light green line; excluded is vesicle 15). The average diameter of the GUVs used in the average trace for 34 µm.

0.01% transporter

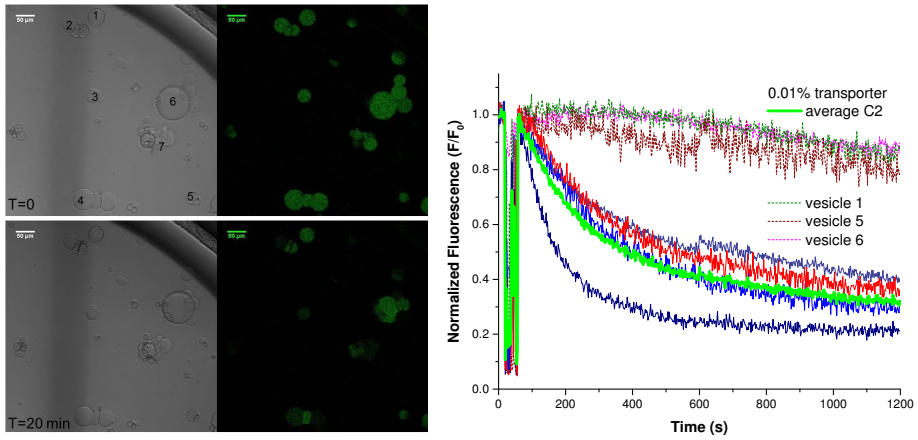

Figure A9. Bright-field and fluorescence microscopy images before (top) and after (bottom) addition of NaCl to GUVs containing 0.01% transporter (*experiment C2*). The normalized fluorescence intensity over time is given for the individual numbered GUVs and for the average of all numbered GUVs (fat light green line; excluded are vesicles 1, 5, and 6). The average diameter of the GUVs used in the average trace for 43 µm.

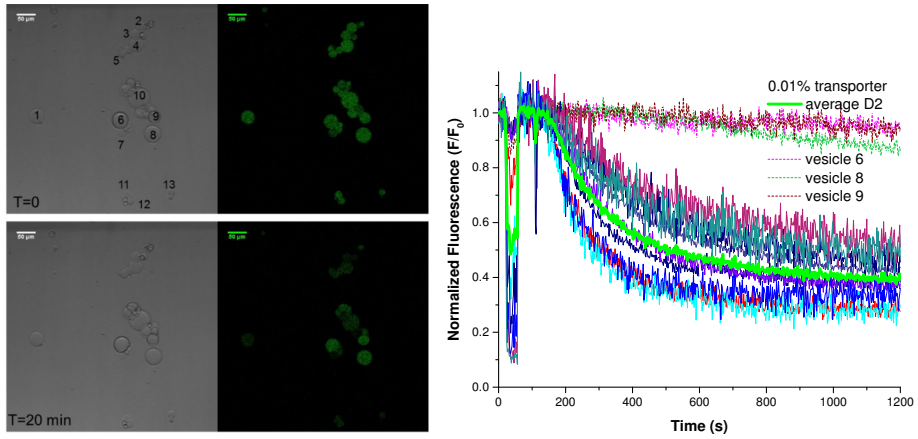

Figure A10. Bright-field and fluorescence microscopy images before (top) and after (bottom) addition of NaCl to GUVs containing 0.01% transporter (experiment D2). The normalized fluorescence intensity over time is given for the individual numbered GUVs and for the average of all numbered GUVs (fat light green line; excluded are vesicles 6, 8, and 9). The average diameter of the GUVs used in the average trace for 29 µm.

Test for photobleaching

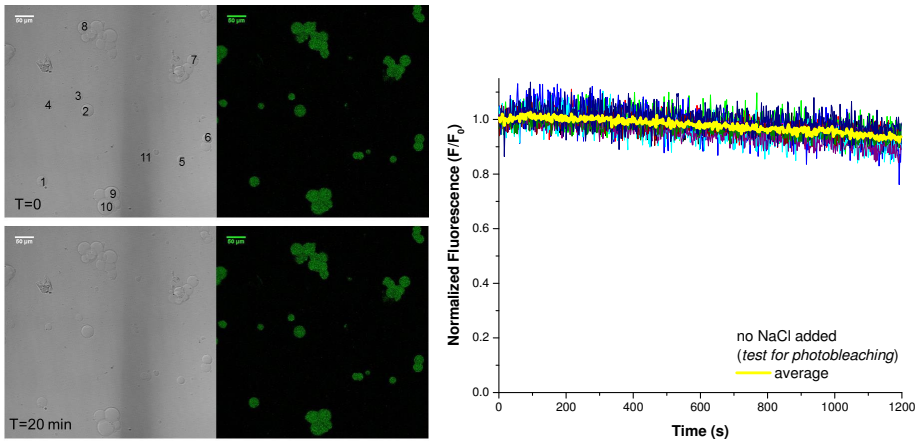

Figure A11. Bright-field and fluorescence microscopy images at the start and end of a 20 minute time lapse measurement to test for photobleaching (no NaCl added). The normalized fluorescence intensity over time is given for the individual numbered GUVs and for the average of all numbered GUVs (fat yellow line).

Cross-sections of vesicles with rhodamine-labelled membranes in Figure 4a.

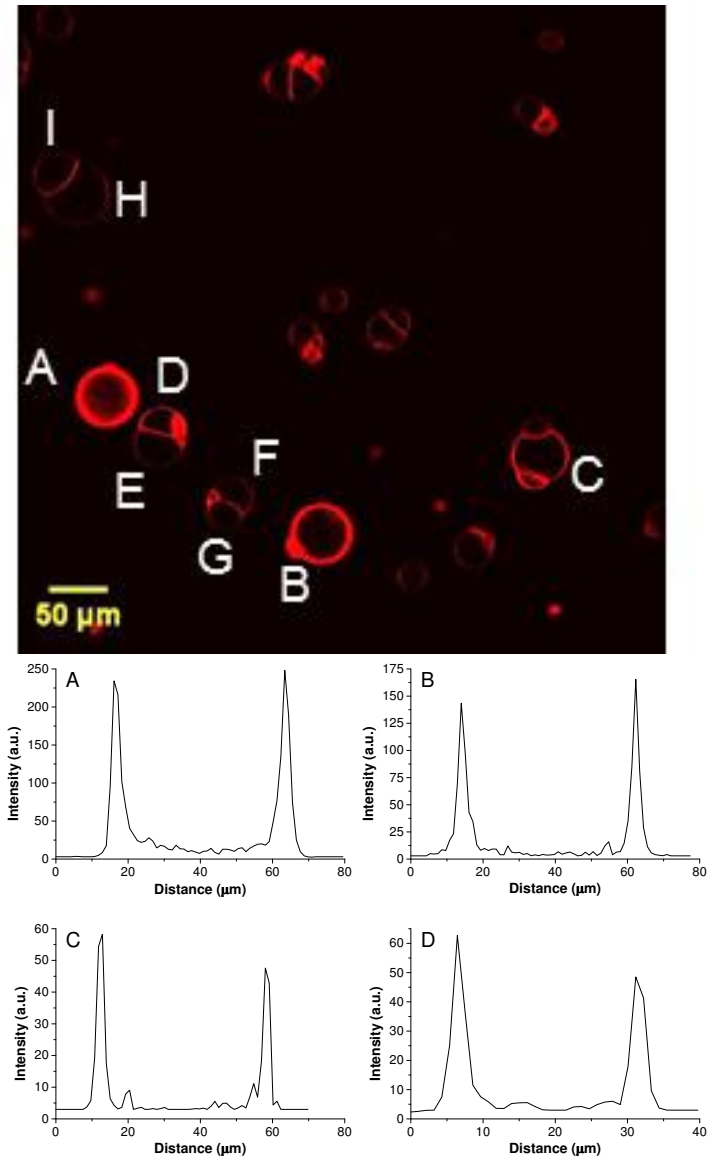

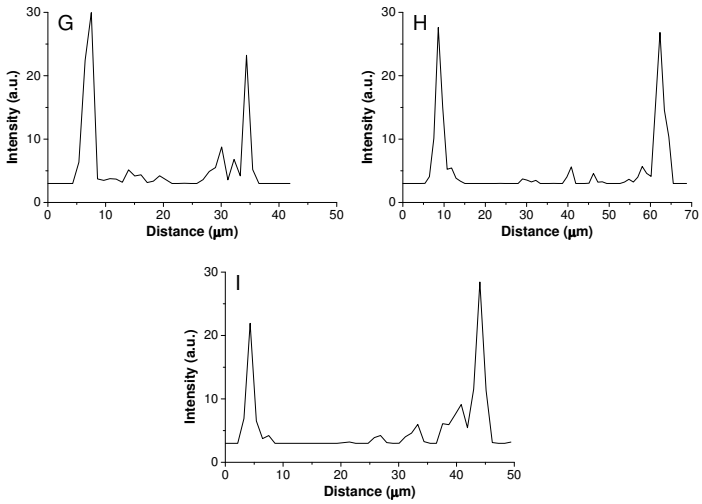

Figure A12. Fluorescence microscopy image of rhodamine labelled lipid **5** in the lipid bilayer membrane (top, copy of Figure 4a of the main paper). Intensity profiles of the cross-sections of the giant vesicles identified with a letter are given, showing intensities ~ 25 for vesicles E-G, ~ 50 for vesicles C and D, ~ 150 for B and ~ 250 for A. From the combination of these data and the transport curves in Figure 4c, we conclude that vesicles E-I are unilamellar and A-D are multilamellar.

Chapter VI

Targeted anion transporter delivery by coiled-coil driven membrane fusion

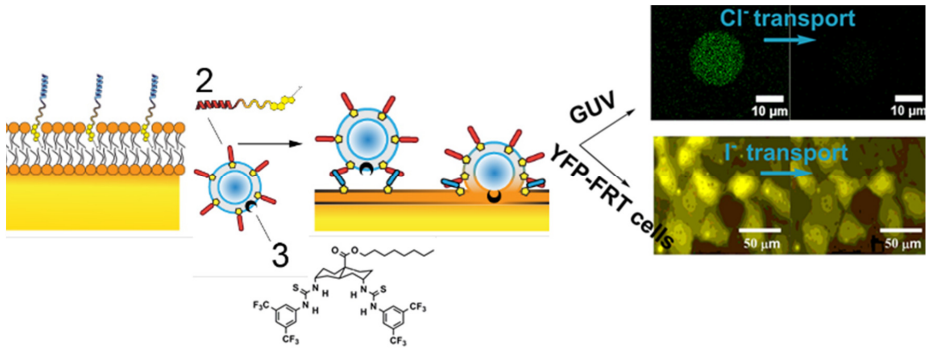

This work is published: Nestor Lopez Mora, Azadeh Bahreman, Hennie Valkenier, Hongyu Li, Thomas H. Sharp, David N. Sheppard, Anthony P. Davis, Alexander Kros. *Chem. Sci.*, **2016**, 7, 1768.

Abstract.

Synthetic anion transporters (anionophores) have potential as biomedical research tools and therapeutics. However, the efficient and specific delivery of these highly lipophilic molecules to a target cell membrane is non-trivial. Here, we investigate the delivery of a powerful anionophore to artificial and cell membranes using a coiled-coil-based delivery system inspired by SNARE membrane fusion proteins. Incorporation of complementary lipopeptides into the lipid membranes of liposomes and cell-sized giant unilamellar vesicles (GUVs) facilitated the delivery of a powerful anionophore into GUVs, where its anion transport activity was monitored in real time by fluorescence microscopy. Similar results were achieved using live cells engineered to express a halide-sensitive fluorophore. We conclude that coiled-coil driven membrane fusion is a highly efficient system to deliver anionophores to target cell membranes.

Introduction

There is urgent interest in Drug Delivery Systems (DDSs), such as cell penetrating peptides or liposomes, which are non-invasive and cause no damage to cellular membranes.[1] Liposomes of less than 1 μm in diameter have been used as models for studying biological and biophysical membrane properties, as well as DDSs, due to their biocompatibility and low toxicity. Delivery of molecules into the cytoplasm of cells can be achieved by functionalizing liposomes with positively charged lipids, polymers, antibodies or cell penetrating peptides.[2, 3] Whilst the encapsulation of water-soluble drugs into liposomes is one of the most used tools for drug delivery, the incorporation of lipophilic drugs into the phospholipid bilayer of liposomes has been less exploited.[4] Alternative approaches to delivering drugs with low water-solubility include the use of solubilizing agents or vehicles, such as micelle forming amphiphiles,[5, 6] cyclodextrins[7] or cucurbiturils,[8] although these are not targeted and tend to have limited stability.

One class of lipophilic compounds that could benefit from novel DDSs are transmembrane anion transporters (anionophores).[9] These molecules have potential as tools for biomedical research, and might also replace the function of anion channels which are defective or deficient in genetic diseases.[10-13] There is particular interest in bypassing the cystic fibrosis transmembrane conductance regulator (CFTR) whose dysfunction causes *cystic fibrosis*.[14-16] Anionophores require sufficient lipophilicity to partition exclusively into the membrane and to carry anions such as chloride across the apolar membrane interior.[17] They therefore tend to be water-insoluble, with low intrinsic deliverabilities using conventional DDS.[18, 19]

Inspired by the specific molecular recognition of native SNARE proteins,[20, 21] we have developed a DDS employing a synthetic model system to induce targeted membrane fusion.[22, 23] Our membrane fusion system consists of the use of two complementary peptide amphiphiles located in different membranes.[24] The formation of a dimeric coiled-coil by these peptides brings the two opposing membranes into close proximity, thereby inducing efficient membrane fusion.[25] In previous work, we successfully used this coiled-coil motif to modify surfaces of cancer cells and one-day-old zebra fish embryos *in vivo*.[26, 27]

Herein, we report the use of this DDS as a highly specific recognition system for delivering a lipophilic anion transporter to both giant unilamellar vesicles (GUVs) and the plasma membrane of cells. The pair of complementary lipopeptides employed in this study is presented in **Scheme 1**. This synthetic model system is constructed from two complementary amphiphilic coiled-coil peptides K_4 [$(KIAALKE)_4$] (**1**) and E_4 [$(EIAALEK)_4$] (**2**) coupled to a cholesterol anchor through a flexible polyethylene glycol linker. The heterodimeric coiled coil acts as a molecular zipper by the binding of two α-helical peptide strands, while the cholesterol anchor allows the insertion of the peptides into the lipid membrane of vesicles or cells.

The anionophore bis-(thioureido)decalin (**3**) has remarkable ability to transport anions across lipid bilayers, promoting rapid chloride-nitrate exchange even when operating as single molecules.[28] Recently, we evaluated the activity of **3** in individual GUVs by its direct incorporation into the lipid mixture *prior* to GUV formation. The average initial rate of chloride transport per molecule was determined by analyzing the quenching of the halide-sensitive fluorophore lucigenin encapsulated in the GUVs.[29] Transporter **3** showed exceptional chloride/nitrate exchange activity (820 ± 260 Cl^-/s) when incorporated *a priori* into the lipid membrane of liposomes or GUVs at different concentrations. However, the high lipophilicity of **3** limits its deliverability. Not only is it poorly delivered when added in methanol, but the use of simple vesicles as delivery vehicles is also ineffective (**Figure 4** in the *Experimental Section*).

The poor deliverability of **3** and similar anionophores is a critical barrier to future applications. When rates of anion transport were studied in cells, the best performance was obtained by an anionophore with excellent deliverability, but modest intrinsic activity (two orders of magnitude lower than **3** in liposomes).[19] Thus, solving the deliverability problem of **3** has great potential for applications in biophysics and perhaps therapeutics. Here we present a facile method to deliver the highly lipophilic transporter **3** pre-incorporated in liposomes by simple incubation with GUVs and cells.

Figure 1 outlines the protocol for delivering transporter **3** to the lipid membrane of cell-sized GUVs using our synthetic membrane fusion system. The experimental design comprises three main components: (i) GUVs functionalized with lipopeptide **1** as the

target membrane and biophysical cell model; (ii) the halide sensitive fluorophore lucigenin encapsulated in the GUVs as a sensing dye and (iii) the DDS which uses liposomes decorated with lipopeptide **2**, and with transporter **3** incorporated *a priori* into the lipid membrane. Following targeting and incorporation of anionophore **3** into the lipid membrane of GUVs by membrane fusion, the quenching of lucigenin fluorescence by chloride is used to measure the chloride transport activity.

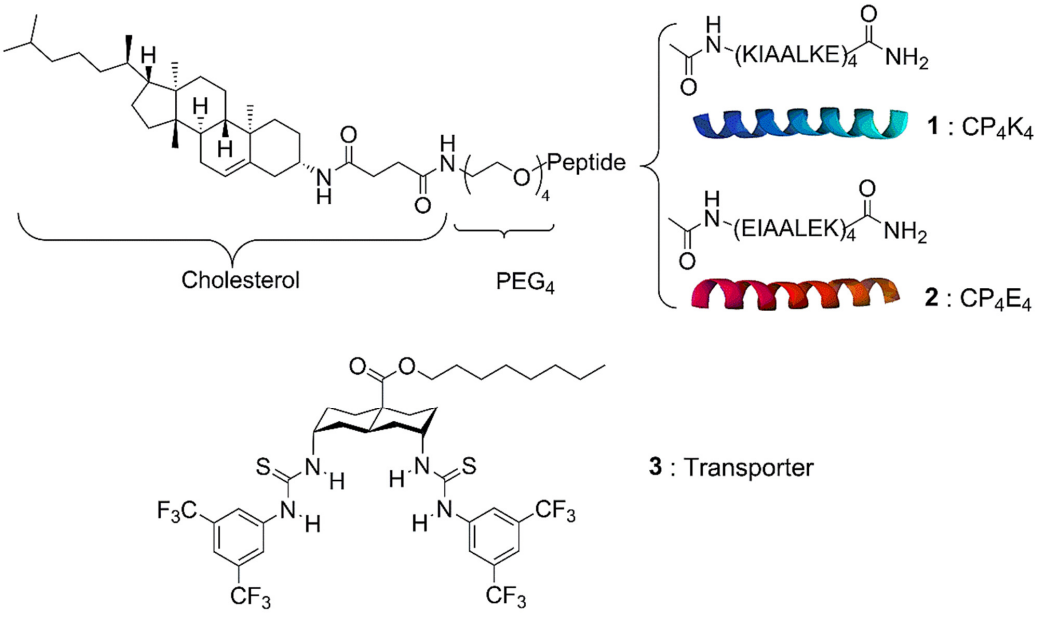

Scheme 1. Chemical structures of the synthetic membrane fusion model: lipopeptide CP_4K_4 (**1**), lipopeptide CP_4E_4 (**2**) and the anionophore bis-(thioureido)decalin (**3**).

Results and discussion

Liposomes were formed from the lipid mixture 1-palmitoyl-2-oleoylphosphatidylcholine (POPC) and cholesterol in a 7:3 molar ratio by sonication method in the presence of 10 mol % transporter **3** and 1 mol % lipopeptide CP_4E_4 (see *Experimental Section* for details). The hybrid lipid film was hydrated in an aqueous solution of 225 mM $NaNO_3$, 10 mM TRIS and 200 mM glucose (pH = 7, adjusted with

H_2SO_4) and sonicated for 4 minutes at 50-55 °C. Liposome formation was confirmed by dynamic light scattering measurements (**Figure 5** and **6** in the *Experimental Section*) and the peptide functionalized liposomes were characterized by cryo-transmission electron microscopy (cryoTEM) in the absence and presence of transporter (**Figure 7** in the *ESI*). Electron microscopy showed that the lipid membrane of the CP_4E_4 functionalized liposomes was not altered by the incorporation of **3**.

In parallel, GUVs were grown by lipid film hydration (POPC and cholesterol, 7:3 molar ratio) on chemically crosslinked dextran (polyethylene glycol) hydrogel (DexPEG) substrates.[30] The hydration of the lipid film was performed with a solution of 225 mM $NaNO_3$, 10 mM TRIS, 200 mM sucrose and 0.8 mM lucigenin at room temperature. The DexPEG hydrogel allows both the efficient encapsulation of the lucigenin fluorophore and the growth of GUVs under the high ionic strength conditions which are required to perform chloride/nitrate exchange.

Lucigenin-loaded GUVs were subsequently functionalized with CP_4K_4 by incubation in a solution containing lipopeptide **1**. Even though it is possible to grow GUVs with lipopeptide **1** pre-incorporated directly into the lipid mixture, we chose to make plain GUVs and modify them *a posteriori* with lipopeptide **1** because our aim is to deliver the transporter to cellular membranes, which do not contain **1** as a specific recognition motif. As mentioned above, we showed previously that similar cholesterol modified lipopeptides can be inserted efficiently into liposomal membranes[31] and the plasma membrane of cancer cells[26] by simple incubation. In the present work, we followed the same procedure for the peptide functionalization of GUVs.

Briefly, after the formation of lucigenin loaded GUVs, 300 µL of the solution containing the GUVs was transferred to 700 µL of solution containing 225 mM $NaNO_3$, 10 mM TRIS, 200 mM glucose and 1 µM CP_4K_4 (**1**). GUVs were incubated for one hour at room temperature to allow the incorporation of molecule **1** into the membrane of GUVs. The higher density of the sucrose lucigenin solution encapsulated in GUVs compared to external glucose solution caused the GUVs to sink to the bottom of the micro centrifuge tube. Transfer of sedimented GUVs to fresh external solution in further steps also enabled the removal of the excess of non-encapsulated lucigenin fluorophore.

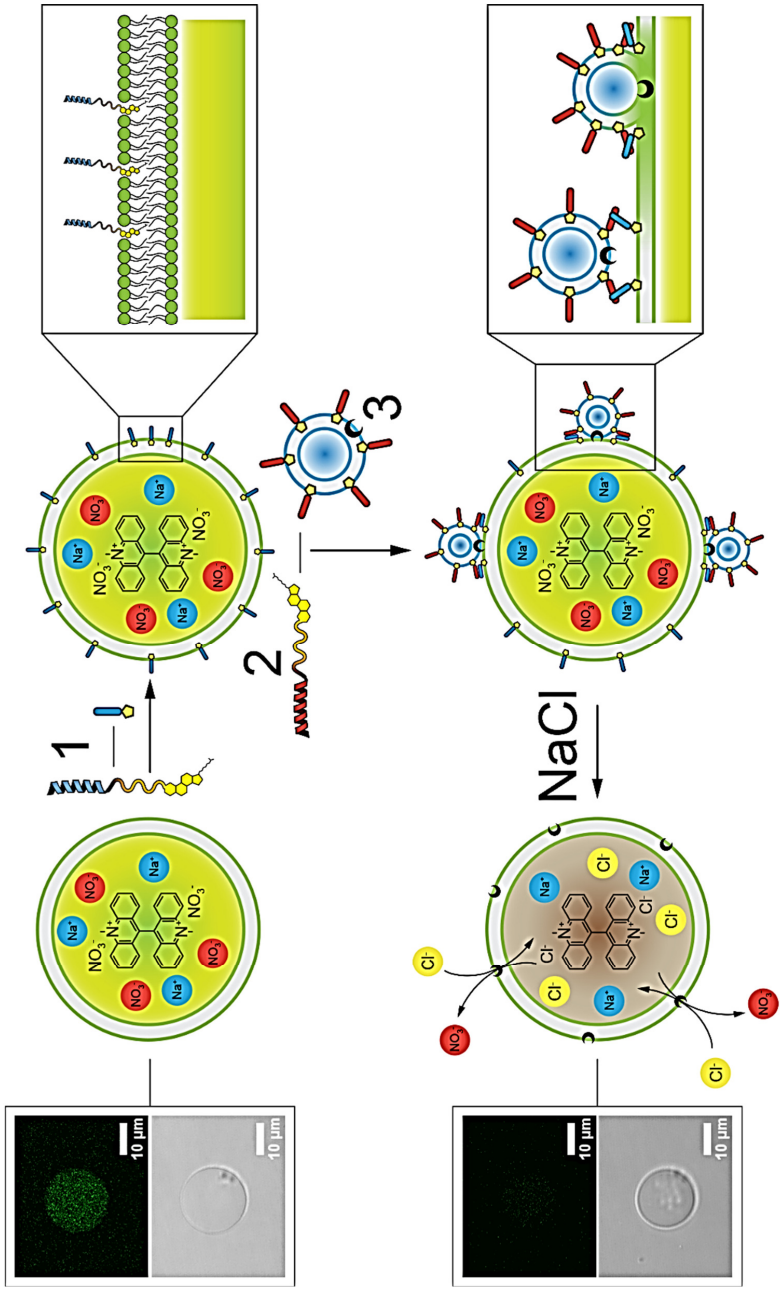

Figure 1. Schematic of the targeted delivery of lipophilic transporter **3** by membrane fusion. GUVs (70% POPC and 30% cholesterol) encapsulating 0.8 mM lucigenin fluorophore are incubated with lipopeptide **1** to functionalize the lipid membrane of the GUV. Subsequent formation of a dimeric coiled-coil allows the fusion of liposomes containing 10 mol % transporter **3** and the complementary lipopeptide **2**, resulting in targeted delivery of **3** to the membrane of the GUV. Finally, upon the addition of NaCl to the exterior solution, transporter **3** exchanges external chloride for internal nitrate, resulting in the quenching of the encapsulated lucigenin fluorophore.

Liposome-GUV membrane fusion was initiated by treating peptide **1**-functionalized GUVs (~20 μm diameter) containing the chloride-sensitive lucigenin fluorophore with peptide **2**-decorated liposomes (~150 nm diameter) containing **3** pre-incorporated in the lipid membrane (**Figure 1**). Briefly, CP_4K_4 membrane-functionalized GUVs (200 μL) and CP_4E_4 membrane-functionalized liposomes (100 μL) were combined in 700 μL of 225 mM $NaNO_3$, 10 mM TRIS and 200 mM glucose solution. After gentle mixing for 15 minutes using a rotary shaker, the mixture was incubated for 105 minutes more at room temperature to allow fusion of liposomes with GUVs and concomitant delivery of transporter **3** to the lipid bilayer of GUVs. Finally, 200 μL of the sedimented sucrose-containing GUVs were taken from the bottom of the micro centrifuge tube and transferred to a chamber on the stage of a confocal microscope with 100 μL of 225 mM $NaNO_3$, 10 mM TRIS and 200 mM glucose. The integrity of GUVs following membrane fusion was verified by confocal fluorescence (excitation at 488 nm) and bright field imaging.

To test for delivery of transporter **3** to the GUV membranes, the chloride-permeability of the GUVs was assayed through lucigenin fluorescence. NaCl (25 μL, 1 M solution) was added with a microsyringe to the microscope chamber containing the GUVs, and the lucigenin emission intensity was observed to decay markedly over a period of ~3 minutes (**Figure 2**, blue triangles). The quenching of lucigenin fluorescence after delivery of transporter **3** (76% after 3 minutes) was significantly stronger than the effect of photobleaching (9% after 3 minutes; **Figure 2**, black squares). This result agrees well with previous experiments where transporter **3** was pre-incorporated into the lipid bilayer of GUVs for direct visualization of chloride transport into GUVs.[29] Thus, membrane fusion efficiently delivered transporter **3** to the membrane of peptide-functionalized GUVs.

As a control, plain GUVs without CP_4K_4 were mixed with CP_4E_4-functionalized liposomes containing 10 mol % of transporter **3**. After the addition of the NaCl solution, the lucigenin emission intensity inside the GUVs did not decrease (**Figure 2**, red circles), proving that transporter **3** was not delivered to the GUV membrane. Instead, there was a small increase in the fluorescence intensity. We attribute this increase to the difference in osmotic pressure between the inside and the outside of the GUVs following NaCl addition. This results in a decrease in the diameter of the GUVs (as detected by

bright field microscopy) and hence, an increase in lucigenin concentration. We conclude that omission of the lipopeptide CP_4K_4 from the membrane of GUVs inhibits the delivery of transporter **3** to GUVs. Thus, membrane fusion induced by the lipopeptides **1** and **2** is required for the targeted delivery of transporter **3** to the membrane of GUVs.

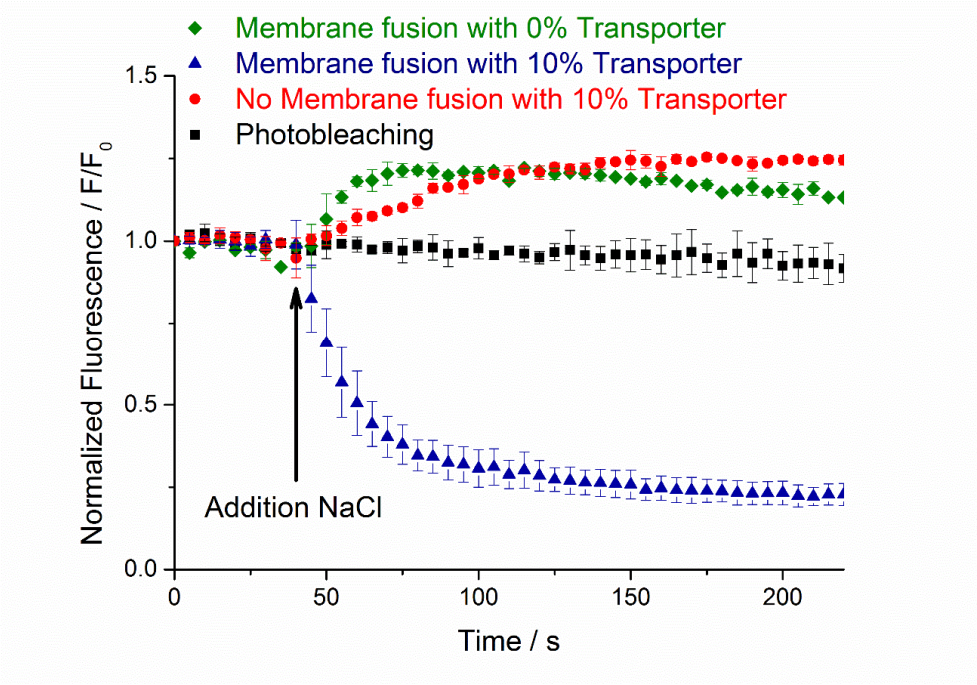

Figure 2. Averaged normalized lucigenin emission intensity after the addition of NaCl (t = 40 s) to: CP_4K_4-functionalized GUVs treated with CP_4E_4 liposomes containing the transporter **3** (blue triangles); plain GUVs treated with CP_4E_4 liposomes containing the transporter **3** (red circles); CP_4K_4-functionalized GUVs treated with CP_4E_4 liposomes without transporter **3** (green diamonds). The background photobleaching of CP_4K_4-decorated GUVs (no NaCl added) is shown as black squares. The normalized fluorescence traces plotted are the averages of three independent membrane fusion experiments on three different individual GUVs. Data are means ± SEM. For individual experiments, see **Figures A1 – A4**, *Annex Chapter VI*. The arrow indicates the addition of NaCl after 40 seconds of time lapse imaging.

In a second control experiment, we omitted transporter **3** from the CP_4E_4 liposomes. After membrane fusion, we added the NaCl solution and monitored the lucigenin emission intensity. Again the fluorescence of GUVs increased (**Figure 2**, green diamonds), presumably due to GUV shrinkage. This result suggests that the fusion of peptide-decorated liposomes and GUVs neither makes the lipid membrane permeable to chloride ions nor induces leakage of the encapsulated lucigenin fluorophore from GUVs. We conclude that coiled-coil driven membrane fusion is a specific and highly efficient system to deliver anionophores to GUVs.

To determine whether the lipopeptides **1** and **2** can also be used to deliver the lipophilic transporter **3** to live cells, we used cells engineered to express a halide-sensitive fluorophore. We selected for this study Fischer Rat Thyroid (FRT) cells expressing the halide-sensitive fluorophore yellow fluorescent protein (YFP) variant H148Q/I152L, which is highly sensitive for iodide vs. chloride (hereafter termed YFP-FRT cells);[32, 33] FRT cells are a model system used to investigate epithelial ion transport.[34] We demonstrated recently that YFP-FRT cells can be used to study chloride/iodide exchange by anionophores, by monitoring iodide-induced fluorescence quenching.[19] Herein, we use our membrane fusion system for the targeted delivery of transporter **3** to the plasma membrane of YFP-FRT cells. Using the same protocol as that presented in **Figure 1** to deliver **3** to GUVs, the plasma membrane of YFP-FRT cells was functionalized with CP_4K_4 by incubating the cells for 2 hours at 37 °C with the CP_4K_4 lipopeptide **1** in phosphate-buffered saline (PBS), followed by the addition and incubation with CP_4E_4 liposomes containing 10 mol % anion transporter **3** for 1 h at 37 °C. The YFP-FRT cells were then transferred to a perfusion chamber mounted on the stage of a fluorescence microscope and perfused with PBS.

After several minutes the PBS flow was changed to a PBS solution containing NaI (10 mM) for 5 minutes. This change of the external buffer led to a rapid and robust quenching of cell fluorescence (**Figure 8** in the *Experimental Section*). This decrease in cell fluorescence was almost completely reversed when NaI was washed from the extracellular solution with fresh PBS, indicating the efficient and reversible exchange of chloride and iodide by anionophore **3**. Repeating the exposure to NaI after an interval of 20 minutes elicited a further rapid quenching of cellular fluorescence followed by a recovery after washing NaI from the extracellular solution once more with PBS. We

performed two control experiments by treating the YFP-FRT cells with either plain POPC liposomes containing transporter **3**, the delivery method used in our previous work,[19] or with the targeted delivery system without **3** (**Figure 3**).

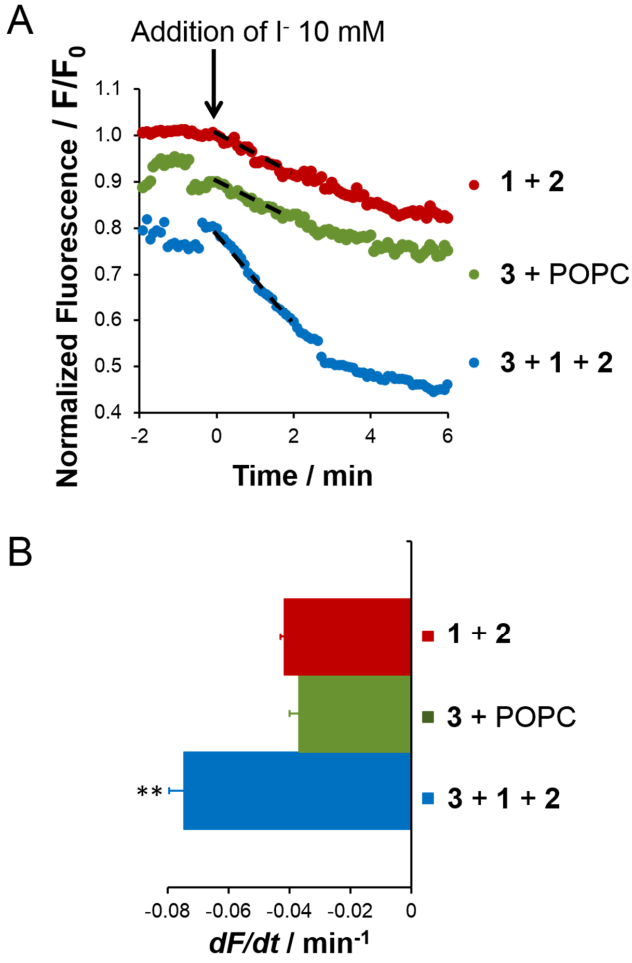

Figure 3. Targeted delivery of the anion transporter 3 to the plasma membrane of YFP-FRT cells by membrane fusion. A) Representative time courses of normalized cell fluorescence and B) Anion transport activity determined from the initial slope of the fluorescence decay for the indicated experimental conditions. Dashed lines in A indicate the fit of exponential functions to the first two minutes of the fluorescence decay following NaI (10 mM) addition. Data are means ± SEM (n = 25 – 45 cells from 5 independent experiments); **, $P < 0.01$ vs. lipopeptides **1** and **2**.

The magnitude of the fluorescence decay in both control experiments was significantly smaller than that elicited by the use of the membrane fusion lipopeptides **1** and **2** for the delivery of anionophore **3**. The result of the first control experiment is in agreement with the inability of **3** to be exchanged between membranes without membrane fusion (**Figure 4** in *Experimental Section*). The data are also consistent with the control experiments performed using liposomes and GUVs (**Figure 2**). Thus, the highly lipophilic anion transporter **3** can be successfully delivered to CP_4K_4-functionalized YFP-FRT cells via coiled–coil-driven membrane fusion, where it efficiently transports anions across the plasma membrane of YFP-FRT cells.

Conclusion

In conclusion, we demonstrate that the lipidated coiled-coil forming peptides **1** and **2** function as a highly specific molecular recognition system that facilitates membrane fusion. This synthetic model system can be applied as a fast and efficient tool in drug delivery studies. We use a supramolecular approach to solve the deliverability problem of a lipophilic anionophore, with powerful anion transport activity by leakage-free membrane fusion between cell-sized GUVs and liposomes. Similar results were observed using cells engineered to express a halide-sensitive fluorophore. We envisage the delivery of the fusogenic lipopeptides and anionophore by inhalation method, firstly by delivering peptide **1** and subsequently peptide **2** and anionophore **3**. This raises the hope that the system can be used to deliver anionophores to the apical membrane of airway epithelia, the key target tissue in *cystic fibrosis*. There is also potential for extending the method to deliver other poorly soluble molecules to biological membranes.

Experimental Section

Materials

Fmoc-protected amino acids were purchased from Novabiochem and Biosolve. Sieber amide resin was purchased from Agilent Technologies. Cholesterol, 1-palmitoyl-2-oleoyl-*sn*-glycero-3-phosphocholine (POPC), bovine serum albumin (BSA), biotin labeled bovine albumin (biotin-BSA), and streptavidin from streptomyces avidinii were purchased from Sigma Aldrich. 1,2-Dioleoyl-sn-glycero-3-phosphoethanolamine-N-(Biotinyl)(Sodium Salt) was purchased from Avanti Polar Lipids. 10,10'-dimethyl-9,9'-biacridinium nitrate (lucigenin) was purchased from Tokyo Chemical Industry UK Ltd. Chloroform was deacidified by passage through a column containing activated basic alumina before the preparation of the lipid solutions. The buffer solution for all GUV studies was prepared with $NaNO_3$ (225 mM) and TRIS (10 mM) in Millipore grade water and the pH was adjusted to 7 with sulfuric acid. The lucigenin (0.8 mM) and NaCl (1 M) solutions were prepared with the buffer solution. Lipid solutions of POPC and cholesterol (70 : 30 molar ratio, 1 and 14 mM) were prepared in deacidified chloroform.

The transporter octyl t-(2,7)-bis(3-(3,5-bis(trifluoromethyl)phenyl)thioureido)-t-8a-decahydronaphthalene-r-4a-carboxylate,[28] (**3**, 84 μM solution in methanol) was added to the lipid solution at 10 mol % (relative to total lipid). Experiments are performed at room temperature, unless stated otherwise.

Cells and cell culture.

Fischer Rat Thyroid (FRT) cells stably expressing the halide sensor YFP-H148Q/I152L (YFP-FRT cells)[32, 33, 35] were a generous gift of A. S. Verkman (University of California, San Francisco). YFP-FRT cells were cultured as described previously[34] with the exception that media contained 10% fetal bovine serum, 2 mM glutamine and the selection agent G418 (0.5 mg/mL). YFP-FRT cells were plated onto glass coverslips and used 4 – 5 days later.

The PBS buffer used for the experiments with YFP-FRT cells was composed of 137 mM NaCl, 2.7 mM KCl, 8.1 mM Na_2HPO_4, 1.5 mM KH_2PO_4, 1 mM $CaCl_2$ and 0.5 mM $MgCl_2$; pH 7.40.

General methods for liposomes and GUV studies

Synthesis of lipopeptides.

The spacer N_3-PEG_4-COOH, cholesteryl-4-amino-4-oxobutanoic acid, and the lipopeptides CP_4K_4 (**1**) and CP_4E_4 (**2**) were synthesized and utilized following procedures previously reported.[24, 27, 36] The peptide segments E: NH_2-$(EIAALEK)_4$-$CONH_2$ and K: NH_2-$(KIAALKE)_4$-$CONH_2$ were synthesized using standard Fmoc chemistry on a peptide synthesizer (CEM-Liberty 1), then the spacer N_3-PEG_4-COOH was coupled to the N-terminus of the peptide segment. The azide terminal group on the spacer was reduced to an amine to obtain an N-terminal free amine for coupling to cholesteryl-4-amino-4-oxobutanoic using 5 eq. of DIPEA and 4 eq. of PyBOP in DMF over 72 h. Finally, the lipopeptides were purified by RP-HPLC with a Gemini C4 column to yield a pure product (Yield: 20-25%) The identity and purity of the peptides and lipopeptides was determined by LC-MS.

Formation of GUVs.

Giant Unilamellar Vesicles (GUVs) were grown on Dex-PEG hydrogel (1:1 molar ratio) coated microscope glass slides as described previously.[30] A lipid solution (10 µL) with the lipid composition POPC and Cholesterol (70:30 molar ratio, 14 mM) and DOPE-Biotin (0.2 mol %) was deposited on a hydrogel coated glass slide, then the lipid solution was dried by evaporating the chloroform under a gentle stream of air and subsequently it was placed in a vacuum oven overnight. A liquid chamber was made by placing a 15 mm (OD) glass O-Ring on top of the hydrogel, sealed with high vacuum silicon grease. The lipid film was hydrated by adding 400 µL of an aqueous solution that contained lucigenin (0.8 mM), $NaNO_3$ (225 mM), TRIS (10 mM) and sucrose (200 mM) into each chamber and the GUVs were formed overnight at room temperature.

Decoration of GUVs with CPK.

GUVs were decorated with 1 mol % CP_4K_4 **1** (relative to lipids). A stock solution of CP_4K_4 **1** (15 µL, 50 µM in CH_3OH:$CHCl_3$ 1:1) was dried by evaporating the chloroform under a gentle stream of air. Subsequently the stock solution was placed in a vacuum oven overnight. The lipopeptide film was hydrated by adding 700 µL of buffer solution that contained $NaNO_3$ (225 mM), TRIS (10 mM) and glucose (200 mM), vortexed and transferred to a micro centrifuge tube. Subsequently, 300 µL of the solution with free floating GUVs was transferred into the

micro centrifuge tube containing the CP_4K_4 aqueous solution. The GUVs were incubated for 60 minutes in the lipopeptide solution and finally 300 µL of GUVs were transferred to 700 µL of buffer solution that contained $NaNO_3$ (225 mM), TRIS (10 mM) and glucose (200 mM).

Formation of Large Unilamellar Vesicles LUVs with CPE and transporter.

Peptide decorated LUVs were formed with 10 mol % transporter and 1 mol % CP_4E_4 **2** both relative to total lipids. Lipid solution (100 µL for experiments with GUVs or 500 µL for experiments with cells) with the lipids POPC and Cholesterol (70:30 molar ratio, 1 mM in $CHCl_3$) was mixed with CP_4E_4 stock solution (20 µL for GUVs or 100 µl for cells, 50 µM in CH_3OH:$CHCl_3$ 1:1) and transporter **3** (118 µL, 84 µM in methanol for GUVs or 267 µL, 187 µM in methanol for cells). Then, the lipid solution was dried by evaporating the chloroform under a gentle stream of air and subsequently, it was placed in a vacuum oven overnight. The lipid film was hydrated by adding 1 mL of buffer solution that contained $NaNO_3$ (225 mM), TRIS (10 mM) and glucose (200 mM) for experiments with GUVs or 2 mL of PBS for experiments with cells. Finally, the LUVs were formed by sonication at 50-55 °C for 4-5 minutes and the final size distribution was determined by DLS (Zetasizer Nano-S, Malvern) with sizes circa 100-180 nm.

Delivery of transporter to GUVs.

The transporter was delivered to the membrane of GUVs by targeted membrane fusion with peptide-decorated LUVs containing the transporter molecule. CP_4E_4 decorated LUVs (200 µL) and CP_4K_4 decorated GUVs (200 µL) were transferred into a micro centrifuge tube with the buffer solution (600 µL) containing $NaNO_3$ (225 mM), TRIS (10 mM) and glucose (200 mM), then the vesicles were mixed for 15 minutes using a tube rotator and incubated for 120 minutes.

Transport experiments in GUVs.

The visualization of GUVs after targeted membrane fusion was achieved with a microscopy chamber which was pre-treated first with an aqueous mixture of BSA (0.9 mg/mL) and biotin-BSA (0.1 mg/mL) for one hour and then with streptavidin for another hour. The solution with GUVs (200 µL) was transferred into the microscopy visualization chamber with the buffer solution (100 µL) containing $NaNO_3$ (225 mM), TRIS (10 mM) and glucose (200 mM). The GUVs were left to sediment for at least 30 minutes before imaging. During imaging of the GUVs in a time lapse experiment, 25 µL NaCl (1 M, in $NaNO_3$ and glucose solution) was

added to the well after 30-40 seconds with a microsyringe, giving a final NaCl concentration of ~80 mM.

Imaging of the GUVs and data analysis.

The imaging of GUVs was performed on a Leica TCS SPE confocal microscope system. Illumination was provided by a solid state laser using the 488 nm laser line (15% laser power) for irradiation of lucigenin. Fluorescence confocal microscopy was carried out using a 63× water objective. The analysis of the images was performed in ImageJ software,[37] by measuring the average intensity of an area corresponding to one GUV for the series of time lapsed microscopy image frames. These fluorescence intensity values (F) were normalized to the fluorescence intensity at the start of the time lapse (F_0).

Methods for cell studies

Decoration of YFP-FRT cells with CPK and delivery of the transporter.

Modification of YFP-FRT cell membranes was performed by two sequential incubations. 200 µL of the CP_4K_4 **1** stock solution (50 µM in CH_3OH:$CHCl_3$ 1:1) was dried by evaporating the solvent under a gentle stream of air and subsequently placed in high vacuum for 1 hour. The CP_4K_4 film was hydrated with 2 mL of PBS and sonicated for 1-2 minutes at 50 - 55 °C.

YFP-FRT cells plated on glass coverslips (confluency, 80%) were washed 3x with PBS and exposed to the CP_4K_4 solution (5 µM in PBS) for 2 hour at 37 °C. After this first treatment the cells were washed again with PBS and subsequently treated with a solution of liposomes (POPC/cholesterol/CP_4E_4 **2**/transporter **3**) in PBS (in which the total concentration of transporter **3** was 25 µM, see above for details) for 1 hour at 37 °C. For the first control experiment, cells were treated in an identical way, but transporter **3** was omitted from the POPC/cholesterol/CP_4E_4 liposomes. For the second control experiment liposomes were made using POPC with 10 mol % transporter **3**, analogous to our previously reported studies on the activity of anion transporters in cells, albeit the incubation period was longer (previous study, 10 minutes; current study, 1 hour).[18] For this second control experiment, the cells were not treated with CP_4K_4, but solely treated with the **3**/POPC liposomes in PBS (250 µM POPC, 25 µM **3**) for 1 hour at 37 °C.

On completion of the incubation periods, the YFP-FRT cells were transferred to a perfusion chamber mounted on the stage of a Leica DM IRB microscope for cell fluorescence measurements. Any anionophore not incorporated into YFP-FRT cell membranes was removed from the chamber by perfusion with PBS.

Transport studies with YFP-FRT cells.

Anionophore-mediated anion transport by YFP-FRT cells was quantified by measuring I^--induced quenching of YFP fluorescence.[19] In brief, a field of view with bright YFP-FRT cells was selected for fluorescence measurements and the cells were perfused with (i) PBS for 5 minutes, then (ii) PBS containing NaI (10 mM) (made by preparing PBS with 127 mM NaCl to maintain osmolarity) for 5 minutes and finally (iii) PBS for 20 – 30 minutes to remove thoroughly NaI from the perfusion chamber. In some experiments, if fluorescence had recovered sufficiently, anionophore-treated YFP-FRT cells were perfused a second time with PBS containing NaI (10 mM) for 5 minutes before cells were again washed with PBS. During all interventions, the rate of solution perfusion was 8 – 10 mL min^{-1}; temperature was 37 °C.

Fluorescence microscopy and data analysis.

For cell fluorescence measurements, we used the Volocity (Improvision) data acquisition and analysis system and a cooled CCD camera (Hamamatsu ORCA ER firewall) with the Leica DM IRB inverted fluorescence microscope equipped with an oil objective (x65, numerical aperture 1.32), excitation filter wheel and multiple band dichroic and emission filters (YFP: excitation, 500 ± 10 nm; emission, 545 ± 25 nm). Cell fluorescence data were sampled every 6 seconds.

Fluorescence data from 5 – 9 cells per coverslip were analysed with 4 coverslips tested per intervention. Cell fluorescence values (F) are expressed relative to the fluorescence value immediately before iodide (10 mM) addition to YFP-FRT cells (F_0). By fitting exponential functions to the first 2 minutes of the fluorescence decay following NaI (10 mM) addition, we determined the initial slope to quantify anion transport by compound **3**. Results are expressed as means ± SEM of N observations. To compare sets of data, we used Student's unpaired t-test. Differences were considered statistically significant when $P < 0.05$. All tests were performed using SigmaPlot 12 (Systat Software Inc., San Jose, CA, USA).

Liposome experiments showing the inability of transporter 3 to exchange between liposomes.

We tested the ability of transporter **3** to exchange between lipid bilayer membranes without the aid of membrane fusion using a fluorescence assay with liposomes. We mixed receiver liposomes which contain lucigenin, but no transporter and delivery liposomes with transporter **3** (but no lucigenin) and used fluorescence spectroscopy to test whether any transport of chloride into the receiver liposomes occurred.

Receiver liposomes.

POPC and cholesterol solutions in deacidified chloroform were combined in such a way that the resulting solution contained 7.0 µmol POPC and 3.0 µmol cholesterol. The chloroform was removed by a flow of N_2 and the resulting lipid film was dried for 1 h in vacuum. The lipid film was hydrated with 500 µL of an aqueous solution of 0.8 mM lucigenin and 225 mM $NaNO_3$, sonicated 30 s, and stirred for 1 h. The resulting mixture was frozen and thawed 10x and subsequently extruded 29x through a polycarbonate membrane (200 nm pore size). The external lucigenin was removed by size exclusion chromatography over a column of Sephadex G-50 eluted with an aqueous solution of 225 mM $NaNO_3$. The liposomes were collected and diluted with 225 mM $NaNO_3$ solution to 25 mL, to obtain a total lipid concentration of ~ 0.4 mM.

Delivery liposomes.

Solutions of POPC and cholesterol in deacidified chloroform and a solution of transporter **3** in methanol were combined to obtain a solution containing 1.4 µmol POPC, 0.6 µmol cholesterol, and 0.8 nmol **3**. The organic solvents were removed by a flow of N_2 and the resulting lipid film was dried for 1 h in vacuum. The lipid film was hydrated with 150 µL of an aqueous solution of 225 mM $NaNO_3$, sonicated for 30 s, and stirred for 1 h. The resulting mixture was frozen and thawed 10x, subsequently extruded 29x through a polycarbonate membrane (200 nm pore size), and diluted with 225 mM $NaNO_3$ solution to 5 mL (0.4 mM total lipid concentration, ratio **3**:lipid = 1:2500).

Transport experiments.

2.7 mL of receiver liposomes and 300 µL of delivery liposomes were combined in a cuvette and stirred at 25 °C. After a set amount of time (10 min, 1 h, 2 h or 3 h), 75 µL of a solution of

1.0 M NaCl (in 225 mM aqueous $NaNO_3$) was added while the fluorescence was monitored over time (using a PerkinElmer LS45 spectrometer, excitation at 450 nm, emission at 535 nm). The resulting fluorescence traces were normalized by dividing the fluorescence (F) by the fluorescence level just before the addition of NaCl (F_0).

Figure 4 shows that upon mixing of delivery and receiver liposomes and subsequent addition of NaCl, no quenching of fluorescence (and thus no transport of Cl^- into the receiver liposomes) takes place. The fluorescence curves obtained from this experiment are very similar to the blank curve from the receiver liposomes without added delivery liposomes. In contrast, when transporter **3** is preincorporated into the liposomes (which also contain lucigenin), fast quenching and thus rapid anion transport is observed.

If transporter **3** would have been able to exchange between liposomes, then the receiver liposomes with lucigenin (which make up 90% of the total of liposomes in the mixture) should have obtained transporter molecules, and these would have carried chloride into the liposomes to quench the fluorescence of lucigenin. If a full equilibrium situation would have been reached (with all transporter molecules spread evenly over all liposomes), the final transporter **3**:lipid ratio would have been 1:25,000 and the resulting fluorescence trace should have been identical to the experiment shown in **Figure 4** with the transporter preincorporated. The observation that no transport occurs between 10 minutes and 3 h after mixing receiver and delivery liposomes demonstrates that transporter **3** is not likely to be capable of exchanging between POPC/cholesterol (7:3 ratio) liposomes.

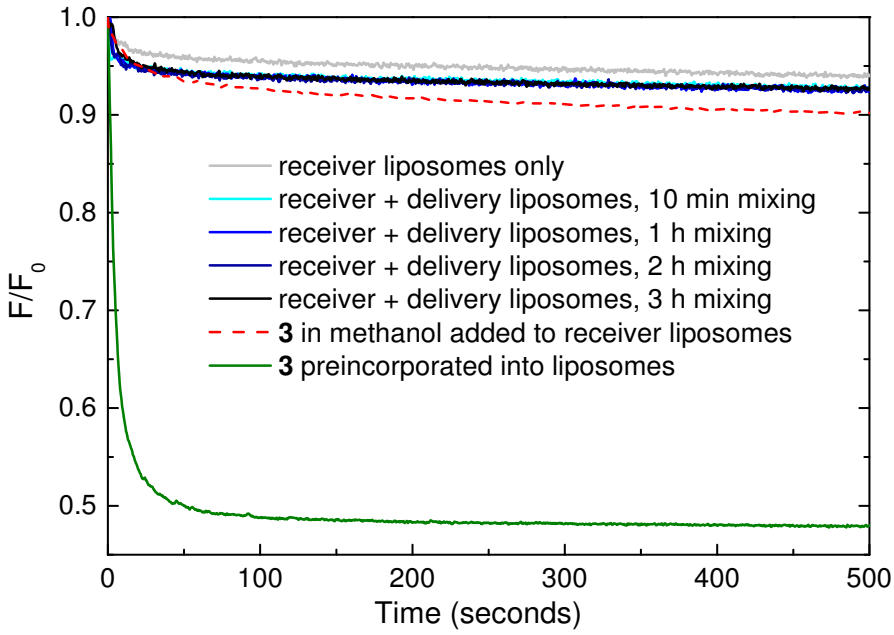

Figure 4. Normalized fluorescence curves of receiver liposomes (gray) and receiver liposomes mixed with delivery liposomes (different shades of blue for different mixing times) as a function of time after addition of NaCl. For comparison the fluorescence traces from liposomes with transporter **3** pre-incorporated (**3**:lipid = 1:25,000, green) and **3** added as solution in methanol (red dashed) are shown.

DLS of LUVs and CP4E4 peptide decorated LUVs with 10 mol % transporter.

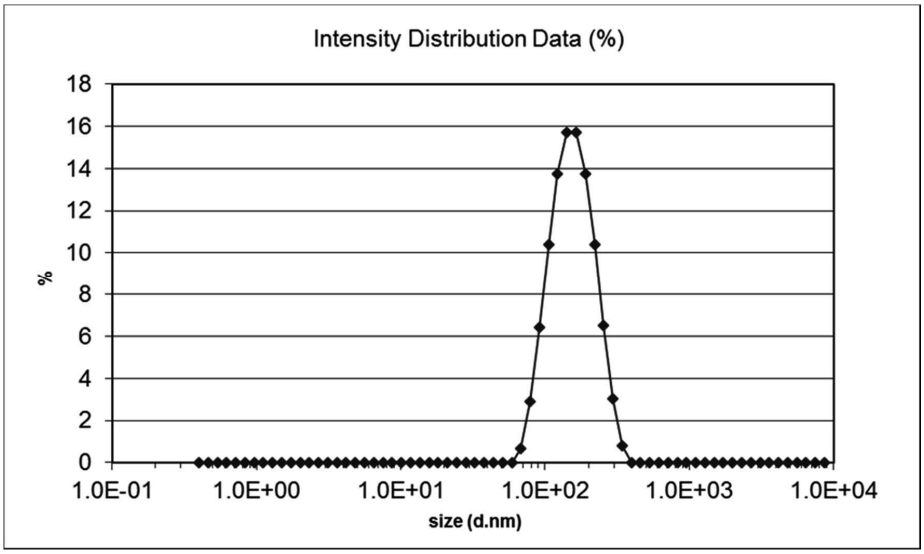

Figure 5. Dynamic Light Scattering of LUVs without CP_4E_4 and transporter **3**.

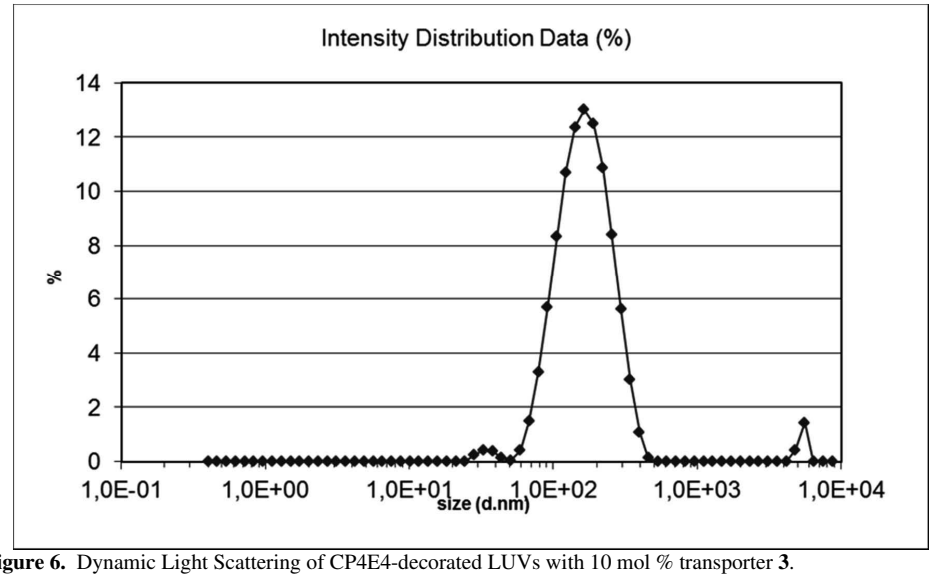

Figure 6. Dynamic Light Scattering of CP4E4-decorated LUVs with 10 mol % transporter **3**.

Cryo-TEM of peptide decorated LUVs containing 0 mol % and 10 mol % transporter.

Cryo-transmission electron microscopy.

Liposome samples were prepared as detailed in the section "Preparation and study of liposomes and GUVs" of the Supplementary Methods. A droplet of 5 µL CP_4E_4-decorated LUVs either with or without 10 mol % transporter **3** was applied to freshly glow-discharged lacey-carbon grids (Electron Microscopy Sciences) in a chamber with 95 % humidity at 21°C, blotted for 2 seconds and plunge-frozen in liquid ethane at -181 °C using a Leica EM GP (Leica Microsystems, Germany). Grids were mounted in a Gatan 626 cryo holder (Gatan, Pleasanton, USA) maintained at -178 °C with liquid nitrogen and imaged using a Tecnai 20 FEG (FEI Company) operated at 200 keV. Images were recorded at -1.5 µm underfocus with a Gatan Ultrascan 4000 camera (Gatan) using low-dose software at a nominal magnification of ×29k. Total dose was less than 10 electrons/Å2.

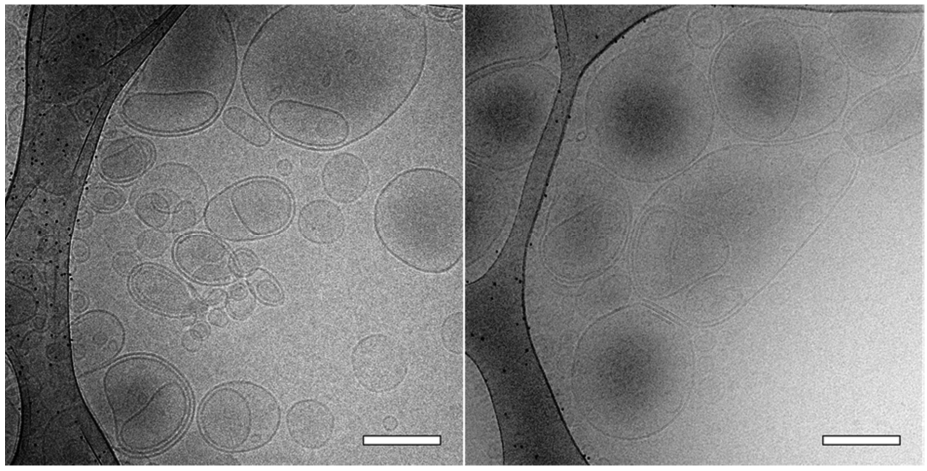

Figure 7. Representative cryo-transmission electron micrographs of CP_4E_4-decorated LUVs **A**) without transporter and **B**) with 10 mol % transporter **3**. The scale bars are 200 nm.

Time lapse and frames from an experiment showing anion transport in YPF-FRT cells upon targeted delivery of transporter 3.

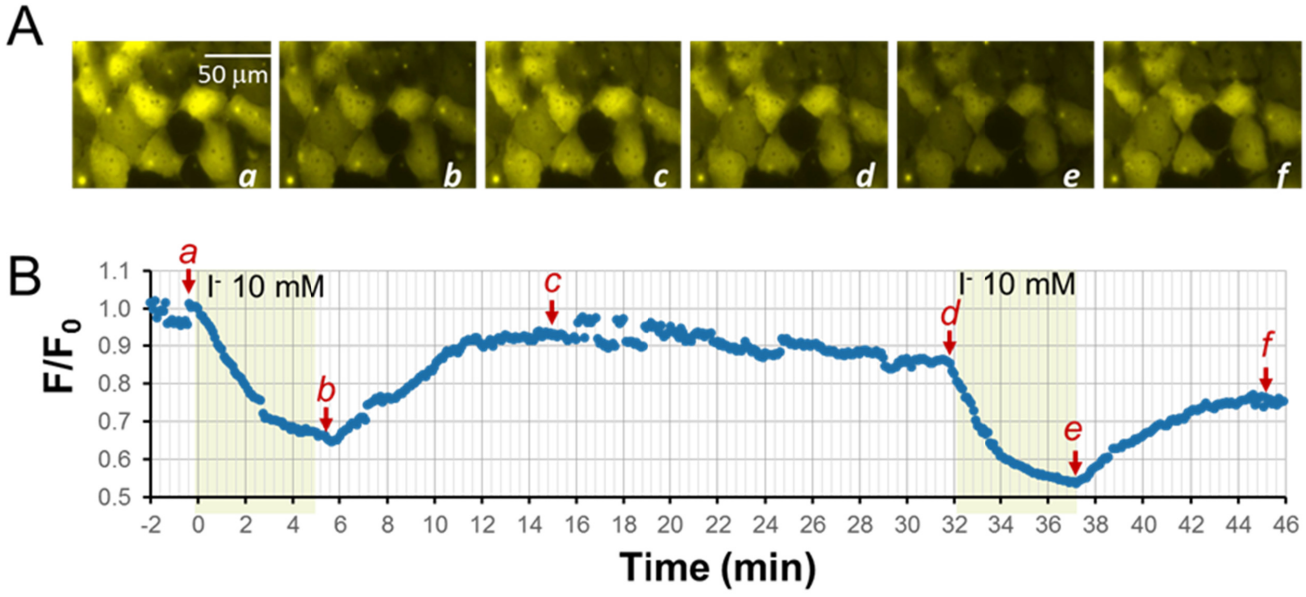

Figure 8. **A**) Images of YFP-FRT cells and **B**) Representative time courses of normalized cell fluorescence after delivery of transporter 3 to YFP-FRT cells using the lipopeptides 1 and 2. YFP-FRT cells were perfused with PBS for 5 minutes, then (a) PBS containing NaI (10 mM) for 5 minutes leading to a rapid and robust quenching of cell fluorescence. This decrease in cell fluorescence was almost completely reversed when NaI (10 mM) was washed with (b) PBS for 20 – 30 minutes to remove thoroughly NaI from the perfusion chamber. The images of cells in A were taken at the time points labeled a – f on the time course shown in B.

References

1. Gupta, B., Levchenko, T.S. & Torchilin, V.P. Intracellular delivery of large molecules and small particles by cell-penetrating proteins and peptides. *Adv Drug Deliver Rev* **57**, 637-651 (2005).
2. Lian, T. & Ho, R.J.Y. Trends and developments in liposome drug delivery systems. *J Pharm Sci* **90**, 667-680 (2001).
3. Gregoriadis, G. Engineering liposomes for drug delivery: Progress and problems. *Trends Biotechnol* **13**, 527-537 (1995).
4. Schwendener, R.A. Liposomes in biology and medicine. *Adv Exp Med Biol* **620**, 117-128 (2007).
5. Pattni, B.S., Chupin, V.V. & Torchilin, V.P. New Developments in Liposomal Drug Delivery. *Chem Rev* **115**, 10938-10966 (2015).
6. Torchilin, V.P. Micellar nanocarriers: Pharmaceutical perspectives. *Pharm Res* **24**, 1-16 (2007).
7. Brewster, M.E. & Loftsson, T. Cyclodextrins as pharmaccutical solubilizers. *Adv Drug Deliver Rev* **59**, 645-666 (2007).
8. Ma, D. et al. Acyclic cucurbit[n]uril molecular containers enhance the solubility and bioactivity of poorly soluble pharmaceuticals. *Nat Chem* **4**, 503-510 (2012).
9. Gale, P.A., Perez-Tomas, R. & Quesada, R. Anion Transporters and Biological Systems. *Accounts Chem Res* **46**, 2801-2813 (2013).
10. Davis, A.P., Sheppard, D.N. & Smith, B.D. Development of synthetic membrane transporters for anions. *Chem Soc Rev* **36**, 348-357 (2007).
11. Valkenier, H. & Davis, A.P. Making a Match for Valinomycin: Steroidal Scaffolds in the Design of Electroneutral, Electrogenic Anion Carriers. *Acc. Chem. Res.* **46**, 2898-2909 (2013).
12. Davis, J.T., Okunola, O. & Quesada, R. Recent advances in the transmembrane transport of anions. *Chem Soc Rev* **39**, 3843-3862 (2010).
13. Busschaert, N., Caltagirone, C., Van Rossom, W. & Gale, P.A. Applications of Supramolecular Anion Recognition. *Chem Rev* **115**, 8038-8155 (2015).
14. Stoltz, D.A., Meyerholz, D.K. & Welsh, M.J. Origins of Cystic Fibrosis Lung Disease. *New Engl J Med* **372**, 351-362 (2015).
15. Rommens, J.M. et al. Identification of the Cystic-Fibrosis Gene - Chromosome Walking and Jumping. *Science* **245**, 1059-1065 (1989).
16. Cutting, G.R. Cystic fibrosis genetics: from molecular understanding to clinical application. *Nat Rev Genet* **16**, 45-56 (2015).
17. Valkenier, H., Haynes, C.J.E., Herniman, J., Gale, P.A. & Davis, A.P. Lipophilic balance - a new design principle for transmembrane anion carriers. *Chem Sci* **5**, 1128-1134 (2014).
18. Haynes, C.J. et al. Acylthioureas as anion transporters: the effect of intramolecular hydrogen bonding. *Org Biomol Chem* **12**, 62-72 (2014).
19. Li, H. et al. Efficient, non-toxic anion transport by synthetic carriers in cells and epithelia. *Nat Chem* **8**, 24-32 (2016).
20. Rothman, J.E. The Principle of Membrane Fusion in the Cell (Nobel Lecture). *Angew Chem Int Edit* **53**, 12676-12694 (2014).

21. Sudhof, T.C. The Molecular Machinery of Neurotransmitter Release (Nobel Lecture). *Angew Chem Int Edit* **53**, 12696-12717 (2014).
22. Weber, T. et al. SNAREpins: Minimal machinery for membrane fusion. *Cell* **92**, 759-772 (1998).
23. Marsden, H.R. & Kros, A. Self-Assembly of Coiled Coils in Synthetic Biology: Inspiration and Progress. *Angew Chem Int Edit* **49**, 2988-3005 (2010).
24. Marsden, H.R., Elbers, N.A., Bomans, P.H.H., Sommerdijk, N.A.J.M. & Kros, A. A Reduced SNARE Model for Membrane Fusion. *Angew Chem Int Edit* **48**, 2330-2333 (2009).
25. Marsden, H.R., Korobko, A.V., Zheng, T.T., Voskuhl, J. & Kros, A. Controlled liposome fusion mediated by SNARE protein mimics. *Biomater Sci-Uk* **1**, 1046-1054 (2013).
26. Zope, H.R. et al. In Vitro and In Vivo Supramolecular Modification of Biomembranes Using a Lipidated Coiled-Coil Motif. *Angew Chem Int Edit* **52**, 14247-14251 (2013).
27. Voskuhl, J. et al. Immobilization of Liposomes and Vesicles on Patterned Surfaces by a Peptide Coiled-Coil Binding Motif. *Angew Chem Int Edit* **51**, 12616-12620 (2012).
28. Valkenier, H. et al. Preorganized Bis-Thioureas as Powerful Anion Carriers: Chloride Transport by Single Molecules in Large Unilamellar Vesicles. *J Am Chem Soc* **136**, 12507-12512 (2014).
29. Valkenier, H., Mora, N.L., Kros, A. & Davis, A.P. Visualization and Quantification of Transmembrane Ion Transport into Giant Unilamellar Vesicles. *Angew Chem Int Edit* **54**, 2137-2141 (2015).
30. Mora, N.L. et al. Preparation of size tunable giant vesicles from cross-linked dextran(ethylene glycol) hydrogels. *Chem Commun* **50**, 1953-1955 (2014).
31. Versluis, F. et al. In Situ Modification of Plain Liposomes with Lipidated Coiled Coil Forming Peptides Induces Membrane Fusion. *J Am Chem Soc* **135**, 8057-8062 (2013).
32. Verkman, A.S. & Galietta, L.J.V. Chloride channels as drug targets. *Nat Rev Drug Discov* **8**, 153-171 (2009).
33. Galietta, L.J.V., Haggie, P.M. & Verkman, A.S. Green fluorescent protein-based halide indicators with improved chloride and iodide affinities. *Febs Lett* **499**, 220-224 (2001).
34. Sheppard, D.N., Carson, M.R., Ostedgaard, L.S., Denning, G.M. & Welsh, M.J. Expression of Cystic-Fibrosis Transmembrane Conductance Regulator in a Model Epithelium. *Am J Physiol* **266**, L405-L413 (1994).
35. Galietta, L.V.J., Jayaraman, S. & Verkman, A.S. Cell-based assay for high-throughput quantitative screening of CFTR chloride transport agonists. *Am J Physiol-Cell Ph* **281**, C1734-C1742 (2001).
36. Versluis, F., Dominguez, J., Voskuhl, J. & Kros, A. Coiled-coil driven membrane fusion: zipper-like vs. non-zipper-like peptide orientation. *Faraday Discuss* **166**, 349-359 (2013).
37. Schneider, C.A., Rasband, W.S. & Eliceiri, K.W. NIH Image to ImageJ: 25 years of image analysis. *Nat Methods* **9**, 671-675 (2012).

Annex
Chapter VI

Datasets for the average curves presented in Figure 2 of the Chapter VI.

Photobleaching

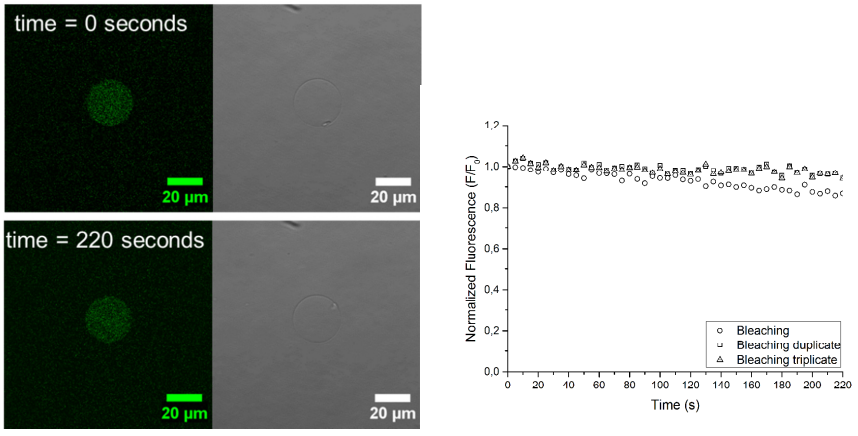

Figure A1. Fluorescence and bright-field microscopy images at the beginning and end of a 3 minute time lapse measurement to quantify the photobleaching of lucigenin dye during the experiment (no NaCl added). The normalized fluorescence intensity over time is given for individual GUVs from independent experiments.

CP_4E_4-decorated LUVs and CP_4K_4-decorated GUVs, 10 mol % transporter 3 is included in LUVs.

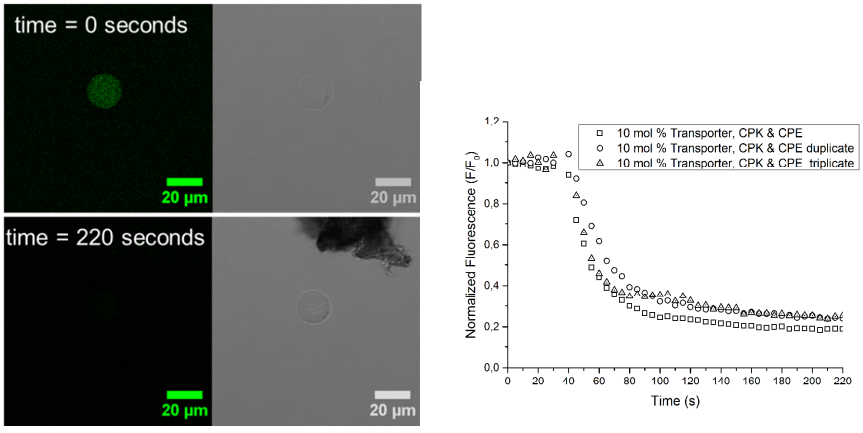

Figure A2. Fluorescence and bright-field microscopy images before (top) and after (bottom) addition of NaCl to GUVs previously incubated with LUVs (10 mol % transporter). The normalized fluorescence intensity over time is given for individual GUVs from independent experiments.

Control experiment: CP_4E_4-decorated LUVs and CP_4K_4-decorated GUVs, transporter 3 is excluded from LUVs.

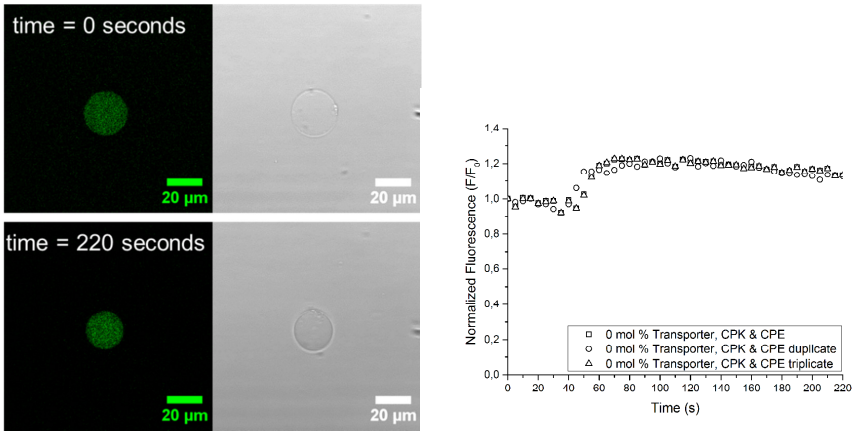

Figure A3. Fluorescence and bright-field microscopy images before (top) and after (bottom) addition of NaCl to GUVs previously incubated with LUVs (0 mol % transporter). The normalized fluorescence intensity over time is given for individual GUVs from independent experiments.

Control experiment: CP_4E_4-decorated LUVs and plain GUVs, CP_4K_4 is excluded from GUVs.

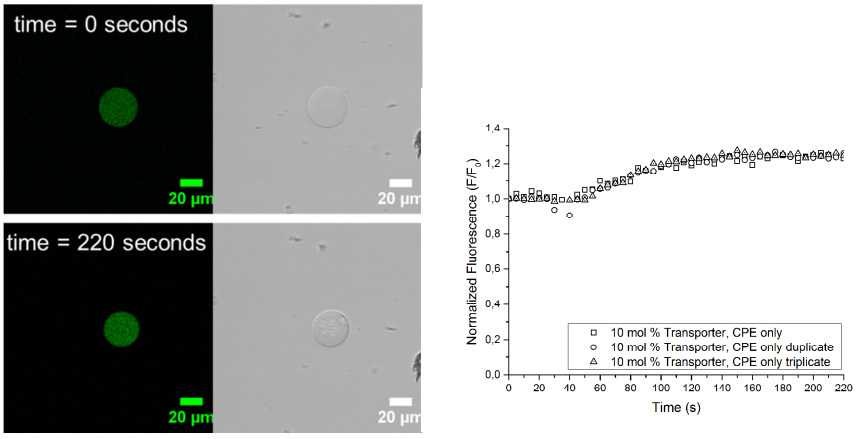

Figure A4. Fluorescence and bright-field microscopy images before (top) and after (bottom) addition of NaCl to GUVs previously incubated with LUVs (10 mol % transporter). CP4K4 is excluded from GUVs. The normalized fluorescence intensity over time is given for individual GUVs from independent experiments.

Chapter VII

Coiled coil driven membrane fusion on GUV–LUV: biophysical model evaluated at physiological ionic strength conditions

Manuscript in preparation: *Nestor Lopez Mora, Bart Jan van Kolck, Aimee Boyle, Anouk Rosen, Šárka Pokorná, Radek Šachl, Martin Hof and Alexander Kros.*

Introduction

Membrane fusion is a key process naturally occurring in cells. Firstly, vesicles dock at target membranes captured by proteins and tethering factors.[1, 2] Next, those two initially separated membranes come into molecular contact and they merge forming a continuous single membrane facilitating the transport of cargo between and within cells.[3] Highly specific biological processes such as neuronal exocytocis,[4, 5] fertilization,[6-8] and viral infection,[9, 10] are membrane fusion driven, thus understanding and mimicking the fusion of membranes is scientifically relevant. One of the most extensively studied biological systems is the synaptic vesicle fusion system, which is controlled by a coiled-coil interaction between three complementary proteins forming the SNARE (soluble *N*-ethylmaleimide sensitive factor attachment protein receptor) complex.[11, 12] This family of neuronal SNARE proteins involves the formation of a highly stable four-helix coiled-coil bundle which brings two opposing membranes into close proximity, followed by local disruption of the lipids and merging of the membranes.[3, 4] Moreover, it has been proposed that SNAREs, in combination with additional proteins, trigger fusion between synaptic vesicles and the plasma membrane.[13, 14] Because *in vivo* membrane fusion is a highly specific and controlled process, mimicking naturally occurring membrane fusion has resulted in the development of several artificial model systems that use a variety of molecules as the fusogens, such as double stranded DNA,[15, 16] covalent motifs,[17] hydrogen bonding motifs,[18] and coiled-coil peptides.[19, 20] In practice, these models have to fulfill fundamental requirements such as: specific molecular recognition to trigger the merging of membranes; leakage free content mixing; size increase in liposomal studies; and should be independent of curvature stress.[21, 22] However, all these requirements are often not achieved by all models systems.

We use two complementary peptide amphiphiles located in different membranes to mimic some of the aspects of SNARE driven membrane fusion.[21, 23, 24] The synthetic model is designed to fulfill all the functional aspects of native membrane fusion. Our model system is constructed from two complementary coiled-coil peptides K_4 [$(KIAALKE)_4$] and E_4 [$(EIAALEK)_4$] as recognition motifs coupled to a cholesterol anchor through a flexible polyethylene glycol linker (**Figure 1**). The formation of hetero dimeric coiled-coils by these peptides brings the two opposing membranes into close proximity, thereby inducing efficient leakage-free membrane fusion. The dimeric coiled coil acts as a molecular zipper by binding of two α-helical peptide strands, while the cholesterol anchor ensures the tight insertion of the peptides into synthetic

or cellular membranes. The efficiency of this system has been proven by performing lipid mixing and content mixing assays with liposomes, where efficient leakage-free fusion has been obtained.[21] Extension of these vesicle fusion assays has allowed for the study of the effect of altering the number of heptad repeats in the recognition motif ,[25] changing the lipid anchor,[26] and the examination of the response to temperature and pH in the membrane fusion process with our synthetic coiled-coil peptide system. In those previous studies Large Unilamellar Vesicles (LUVs), with sizes ranging between 100–200 nm, were used as a robust biophysical tool for understanding the fusion of membranes. Yet, LUV–LUV interaction exhibits an inherent high degree of membrane curvature and tension, which may have an effect in the energetics of the membrane fusion process. Moreover, the relative small size of LUVs does not allow the visualization of the budding and fusion steps in the membrane fusion process, restricting those studies to bulk measurements. In this study, we used time lapse fluorescence microscopy to monitor and provide additional insights of membrane fusion triggered by the synthetic coiled-coil peptide system at physiological ionic strength conditions. We used peptide-labeled Giant Unilamellar Vesicles (GUVs, sizes 10–20 μm), as a biophysical model of the plasma membrane of cells, and follow fusion upon the addition of LUVs bearing the complementary lipopeptide. We tested both the specific molecular recognition of the coiled-coil system by the mixing of the membranes and the mixing of the inner aqueous contents by content mixing assays in two-color fluorescence microscopy experiments (**Figure 1**).

Results and Discussion

GUVs with the lipid composition 50 mol% 1,2-dioleoyl-sn-glycero-3-phosphocholine (DOPC), 25 mol% 1,2-dioleoyl-sn-glycero-3-phosphoethanolamine (DOPE) and 25 mol% Cholesterol were prepared by hydration of hybrid lipid/DexPEG hydrogel films substrates.[27] The lipid mixture was supplemented with ATTO 488 DOPE (λ_{abs}=501 nm, λ_{fl}=523 nm) for fluorescence imaging in lipid mixing experiments. The use of DexPEG substrates allows the growth of GUVs in good yields, reaching physiological ionic strength conditions (see **Chapter I** and **Chapter II**), which are required for an efficient binding and formation of a dimeric coiled coil. The lipid film deposited on DexPEG substrates was hydrated with phosphate buffer solution (PBS), supplemented with $CaCl_2$ (1 mM), $MgCl_2$ (0.5 mM) and sucrose (200 mM) at room temperature. After GUV formation, the vesicles were transferred to a solution containing PBS supplemented with $CaCl_2$ (1 mM), $MgCl_2$ (0.5 mM), glucose (200 mM) and the

lipopeptide CP_4E_4 or CP_4K_4 (1 mol% with respect to the lipids). The lipopeptides are spontaneously inserted into the GUV membrane, via the cholesterol anchor (**Figure 1**), simulating the function of the transmembrane domain of SNARE proteins. Finally, peptide-labeled GUVs were transferred to a microscopy chamber where they were immobilized via streptavidin-biotin binding to the bottom of the chamber (see details in *Experimental Section*), and the integrity of GUVs was verified by fluorescence and optical microscopy (~20 µm diameter). In parallel, peptide-labeled LUVs (1 mM, ~120 nm diameter) were prepared by sonication with the same lipid composition used for GUVs, but doped with a different dye (ATTO 633 DOPE, λ_{abs}=629 nm, λ_{fl}=657 nm) in order to avoid signal overlapping of the fluorescence emission between GUVs and LUVs in the lipid mixing assay.

Next the lipid mixing assay was initiated by treating peptide labeled GUVs with 30 µL peptide labeled LUVs as represented in **Figure 1**. LUVs were directly added to a microscope chamber containing 300 µL of immobilized GUVs in PBS solution supplemented with $CaCl_2$ (1 mM), $MgCl_2$ (0.5 mM) and glucose (200 mM). The lipid mixing was detected in time by dual color fluorescence imaging of peptide-labeled GUVs doped with ATTO 488 DOPE and peptide-labeled LUVs doped with ATTO 633. The fluorescence signal was simultaneously monitored from GUVs at 500-550 nm and from LUVs at 650-700 nm in a Leica TCS SPE confocal microscope every minute for one hour. The arrival of LUVs to GUVs was observed 15–20 minutes after LUV addition to the GUVs solution. LUV docking on GUVs was detected after 25-30 minutes of liposome arrival to the GUVs and resulted in appearance of spotty places and non-homogeneously distributed fluorescence signal on edges of the GUVs. After 30 minutes, most of the GUVs showed homogeneously distributed fluorescence signal over the entire GUV. The fluorescence became even more intense and the bilayer more homogeneous after 60 min (**Figure 2**). The presence of intact GUVs was verified by observing fluorescence in the green channel.

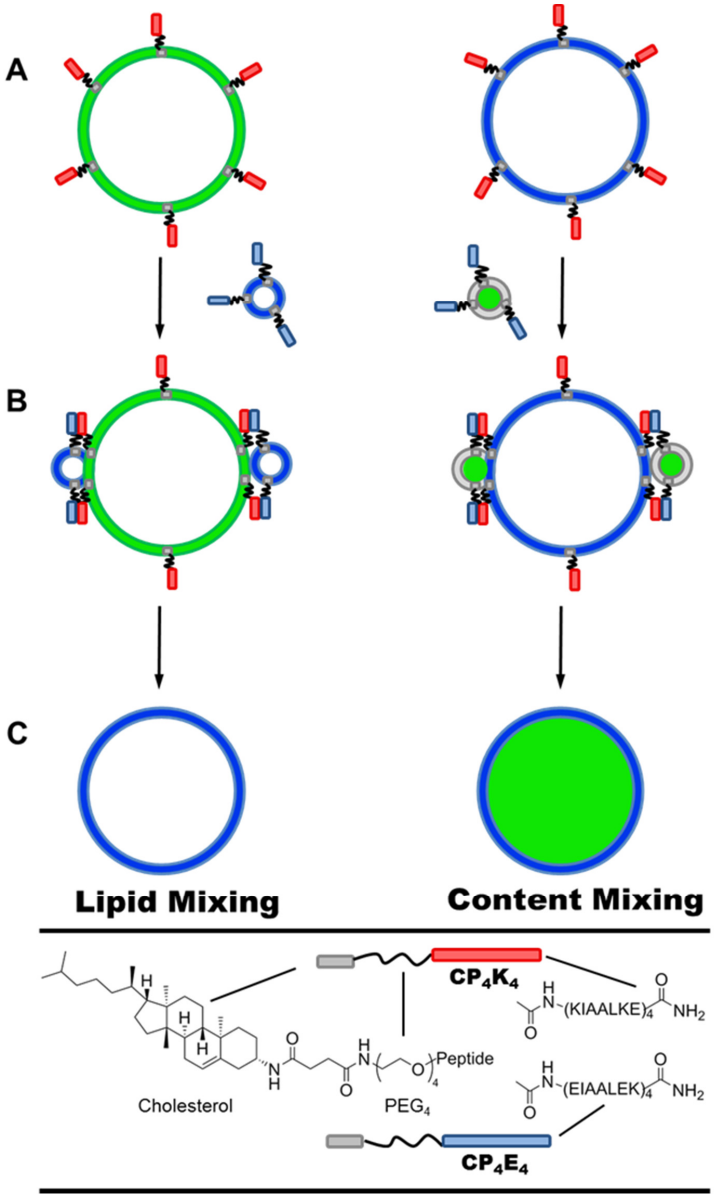

Figure 1. Schematic representation of coiled-coil peptide mediated membrane fusion between GUVs and LUVs. GUVs are labeled with lipopeptide CP_4K_4 (red) and LUVs with the lipopeptide CP_4E_4 (blue). The lipid mixing is showed in the left and in the right content mixing assay. **A**) Spontaneous incorporation of the lipidated peptide in the lipid membrane via cholesterol anchor results in the labeling of GUVs with either CP_4K_4 or CP_4E_4. **B**) Addition of CP_4E_4 labeled LUVs to CP_4K_4 labeled GUVs. The formation of a coiled-coil complex triggers the fusion of membranes. **C**) Transfer of the fluorescent lipid and mixing of inner aqueous contents in the GUV after membrane fusion with LUVs.

The mixing of non-exchangeable fluorescent lipids (ATTO 633 DOPE) in the target membrane of GUVs demonstrates the lipid mixing of membranes between LUVs and GUVs, independently of the selection of the peptide motif used in the target membrane of GUVs or LUVs, respectively. **Figure 2A** shows time lapse micrographs before the arrival (time=0 minutes) and after the arrival of CP_4E_4 peptide labeled LUVs to GUVs containing lipopeptide CP_4K_4 10, 30 and 60 minutes after the start of the experiment. Interchanging the lipopeptides, i.e. labeling GUVs with CP_4E_4 and LUVs with CP_4K_4, is presented in the **Figure 2B**. Whereas the GUVs showed docking 10 minutes after CP_4K_4 lipopeptide insertion into the target membrane, switching the lipopeptide to CP_4E_4 showed earlier docking and full lipid mixing already after 10 minutes. This result suggests that the interaction of CP_4K_4 labeled LUVs is stronger than CP_4E_4 labeled LUVs. Similar experimental conditions were used for mixing non-labeled GUVs and non-labeled LUVs (**Figure 2C**). Some docking of LUVs was observed in the target membrane after one hour, promoted by the negative curvature of the membrane due to the presence of DOPE in the lipid composition of both GUVs and LUVs.

As an additional control experiment, the lipopeptide was omitted from the target membrane of GUVs and the experiment was performed by mixing CP_4E_4 peptide labeled LUVs (**Figure A1**, in *Annex Chapter VII*). Fluorescence imaging showed that CP_4E_4 labeled LUVs have minimal interaction with the non-labeled target membrane, similar to the lipid mixing assay in the absence of both lipopeptides. Moreover, we performed the lipid mixing assay keeping the lipopeptide CP_4K_4 in the membrane of GUVs and mixing with non-labeled LUVs (**Figure A1**, in *Annex Chapter VII*). The fluorescence imaging showed that plain LUVs strongly interact with the CP_4K_4 labeled target membrane of GUVs, transferring the fluorescent lipid (ATTO 633 DOPE) to the membrane of GUVs in approximately 30 minutes. The same peptide-membrane interaction is expected by switching peptide CP_4K_4 to LUVs and targeting to non-labeled GUVs. Those control experiments reveal that peptide K_4 has interaction with the membrane of both GUVs and LUVs. This interaction has been recently reported in lipid monolayer studies combined with surface sensitive infrared reflection absorption spectroscopy (IRRAS).[28] In those studies, a snorkel mechanism is proposed to enhance the hydrophobic interactions between the amphiphatic helix and the lipid monolayer.

In summary, the use of the complementary coiled-coil membrane fusion system produces efficient lipid mixing between GUVs and LUVs, similar to lipid mixing detected in GUV-LUV studies where efficient lipid mixing was observed only in the presence of the SM protein Munc18-1 when t-SNARE complexes were reconstituted in the membrane of LUVs and

GUVs.[2] Moreover, the imaging of lipid in GUVs is in line with the lipid mixing results reported in LUV-LUV studies, where lipid mixing was assayed by fluorescence spectroscopy.[23, 25]

In addition to lipid mixing, the coiled-coil system was evaluated for content mixing between LUVs and GUVs (**Figure 1**, right). GUVs were prepared as described above for lipid mixing experiments, but now the lipid membrane of GUVs was doped with ATTO 633 DOPE (λ_{abs}=629 nm, λ_{fl}=657 nm). A concentrated solution of carboxyfluorescein (50 mM, pH=7) was encapsulated within LUVs by freeze-thawing, followed by extrusion, and the non-encapsulated carboxyfluorescein was removed by size exclusion chromatography.[29] The resulting LUVs were labeled with lipopeptides via incubation. Because the LUV solution was diluted by a factor of two after size exclusion, 60 µL of liposomes were added to the microscopy chamber to keep similar experimental conditions with respect to the lipid mixing assay. GUVs were imaged for 60 minutes, taking an image every 60 seconds, by dual fluorescence imaging. The fluorescence signal was simultaneously monitored for GUVs (633 nm laser line, filter detection 650-700 nm) and LUVs (488 nm laser line, filter detection 500-550 nm). All the experiments were performed in duplicate, imaging as many GUVs as possible for each experiment. Detailed analysis for each experiment is presented in traces of normalized fluorescence versus time (**Figures A2-A15** in *Annex Chapter VII*). The size of individual GUVs was measured directly from the micrographs before and after the membrane fusion assay and no change in the diameter of GUVs was observed during the time course of the experiments.

The content mixing experiment between CP_4K_4 labeled GUVs and CP_4E_4 labeled LUVs is presented in **Figure 3A**. A considerable background increase was detected immediately after the addition of carboxyfluorescein loaded LUVs. This background increase might be attributed to free carboxyfluorescein from the permeable membrane of highly loaded LUVs (50 mM).[30] Docking of LUVs to the target membrane of GUVs was observed after 10 minutes, even when the lipid membrane of LUVs was not supplemented with a fluorescent lipid for this assay. This result suggests that after the merging of LUVs with the target membrane, a fraction of inner carboxyfluorescein from LUVs is distributed along the lipid bilayer, depicting the boundaries of the GUVs (**Figure 3A**). This docking is in good agreement with the lipid mixing results obtained for this experiment. Inner content mixing was observed after 30 minutes of the addition of LUVs in some of the GUVs with small sizes (5-10 µm) and after 60 minutes in bigger GUVs (>15 µm); however the inner content mixing was not observed in all the GUVs.

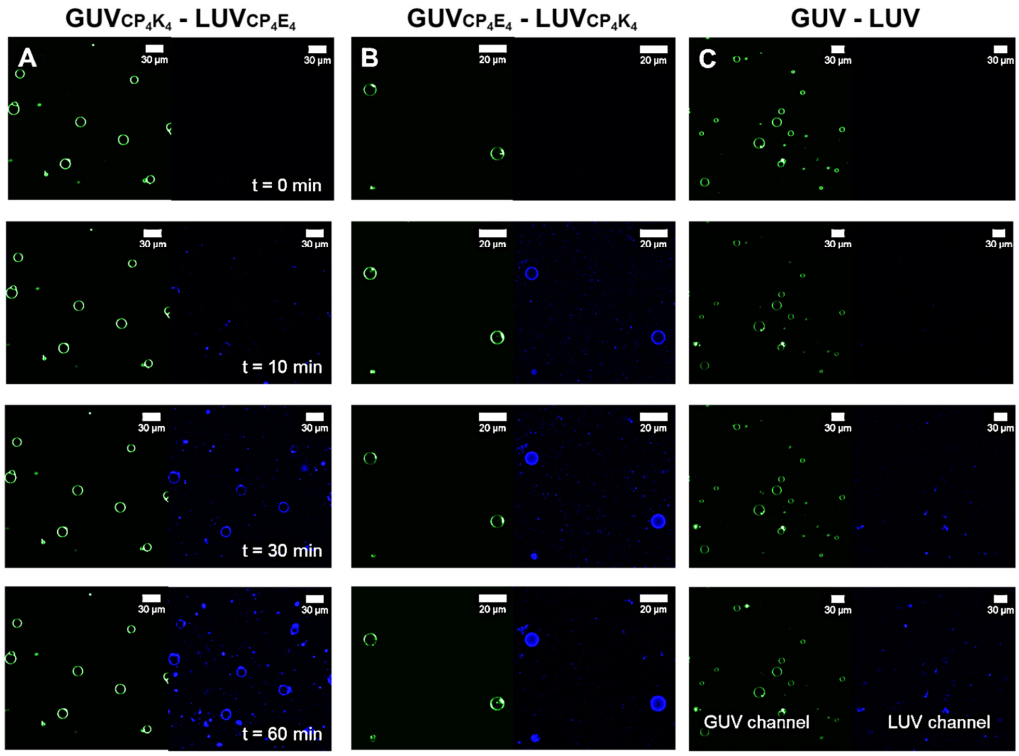

Figure 2. Time lapse micrographs of the lipid mixing assay between peptide labeled GUVs and peptide labeled LUVs before (time=0) and after (time=10, 30 and 60 minutes) appearance of LUVs in the confocal volume. The GUVs are excited at 488 nm and the emission of fluorescence is detected between 500-550 nm (green color), while LUVs are excited at 633 nm and the emission is detected between 650-700 nm (blue color). **A**) Lipid mixing assay between CP_4K_4 labeled GUVs and CP_4E_4 labeled LUVs, **B**) Lipid mixing assay between CP_4E_4 labeled GUVs and CP_4K_4 labeled LUVs and **C**) Lipid mixing assay between non-labeled GUVs and non-labeled LUVs. Imaging was performed every minute during one hour using a Leica TCS SPE microscope.

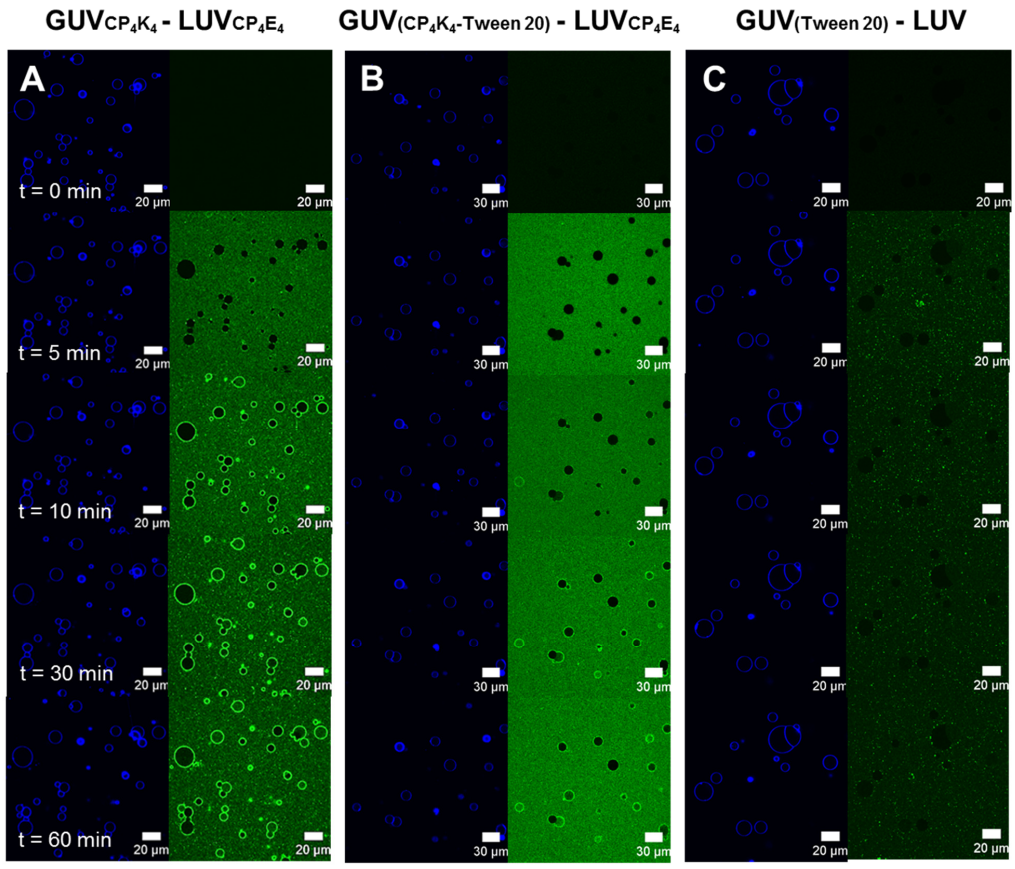

Figure 3. Time lapse micrographs of the content mixing assay between peptide-labeled GUVs and peptide-labeled LUVs before (time=0) and after (time=5, 10, 30 and 60 minutes) appearance of LUVs in the confocal volume. The GUVs are excited at 633 nm and the emission of fluorescence is detected between 650-700 nm (blue color), while LUVs are excited at 488 nm and the emission is detected between 500-550 nm (green color). **A**) Content mixing assay between CP_4K_4 labeled GUVs and CP_4E_4 labeled LUVs, **B**) Content mixing assay between, CP_4K_4-Tween 20 labeled GUVs and CP_4E_4 labeled LUVs and **C**) Lipid mixing assay between Tween 20-GUVs and non-labeled LUVs. Imaging was monitored every minute during one hour using a Leica TCS SPE microscope.

Analysis of individual GUVs after the membrane fusion showed that GUVs without content mixing exhibit large clustering of LUVs on the target membrane (*vide infra*). Our hypothesis is that CP_4K_4 creates clusters in the target membrane upon the insertion of the lipopeptide, decreasing the fusion efficiency of the peptide coiled-coil system. Polyoxyethylene (20) sorbitan monolaurate (Tween 20) is a non-ionic surfactant which has been proposed as a potential stabilizing agent for drug delivery systems because of its low toxicity,[31] and used in

this work to decrease the clustering of CP_4K_4 improving its incorporation into the lipid membrane of GUVs. Mixtures of CP_4K_4-Tween 20 at two different concentrations of the non-ionic surfactant (0.4 and 1 mol% respect to CP_4K_4) were tested for its ability to reduce CP_4K_4 clustering in the lipid membrane of GUVs. Fluorescence microscopy images are presented in **Figure 3B** for the experiment with the mixture containing 1 mol% of Tween 20, which presented better performance in comparison to 0.4 mol% in the mixture with lipopeptide (**Figures A4-5** vs **Figures A6-7** in *Annex Chapter VII*). Clustering of LUVs detected with the mixture CP_4K_4-Tween 20 was less after 10 minutes in comparison to the experiment in the absence of Tween 20. After 60 minutes of imaging most of the small GUVs presented the mixing of inner contents while bigger vesicles showed less or no fluorescence, in good agreement with the experiment without Tween 20; however we observed higher quantity of GUVs with content mixing. We evaluated the effect of Tween 20 in the content mixing assay by incubating GUVs only with Tween 20 and performing the assay with carboxyfluorescein loaded LUVs in the absence of the coiled-coil peptide (**Figure 3C**). After 60 minutes there was no transfer of inner content detected in the interior of GUVs, showing that the addition of Tween 20 does not promote content mixing between GUV and LUVs.

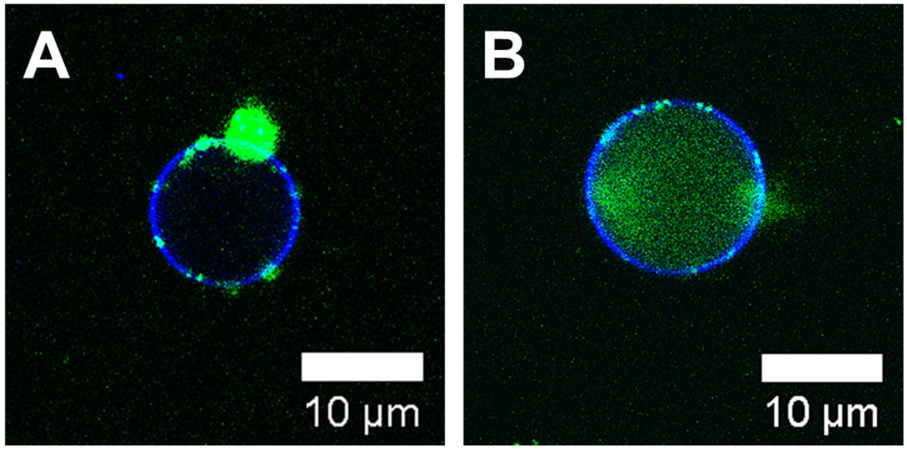

Figure 4. Overlay of fluorescence confocal microscopy images for 488 and 633 nm channels. **A**) Content mixing assay after one hour of incubation of CP_4K_4 peptide-labeled GUVs and CP_4E_4 peptide-labeled LUVs. The micrograph shows a single GUV (blue) without content mixing and large clustering of liposomes (green). **B**) Content mixing assay after one hour of incubation of CP_4K_4-Tween 20 peptide labeled GUVs and CP_4E_4 peptide labeled LUVs. The micrograph shows a single GUV (blue) with content mixing.

Furthermore, content mixing experiments without time lapse imaging between CP_4K_4 labeled GUVs and CP_4E_4 labeled LUVs in the presence and absence of the non-ionic surfactant Tween 20 were performed in microcentrifuge tubes to improve the mixing of GUVs and LUVs. After 60 minutes incubation, the GUVs were transferred from the tube to a microscope chamber containing fresh PBS solution supplemented with $CaCl_2$ (1 mM), $MgCl_2$ (0.5 mM) and glucose (200 mM) for dual fluorescence imaging. This experiment allowed the removal of the background signal associated to carboxyfluorescein leakage from LUVs during the time lapse imaging and the imaging of single GUVs at higher magnification. The micrograph for a single CP_4K_4 labeled GUV after membrane fusion is presented in **Figure 4A** (no content mixing observed) and the micrograph of a single CP_4K_4-Tween 20 labeled GUV is presented in **Figure 4B** (content mixing observed). This result confirms that mixing CP_4K_4 and Tween 20 makes the insertion of the lipopeptide into the target membrane presumable more homogeneous, producing a positive effect in the GUVs undergoing membrane fusion.

The clustering of CPK in GUVs was further studied by dual color fluorescence correlation spectroscopy (FCS). $CP_{12}K_4$, which is an analogue of CP_4K_4, but has a longer linker between the peptide strand and cholesterol anchor, was fluorescently labeled with ATTO 488 dye via maleimide-thiol chemistry. The diffusion coefficient of $CP_{12}K_4$ in a free standing lipid bilayer was determined as a function of the amount of a lipopeptide added to the GUVs (**Figure 5**, red bars), and compared with the mobility of the lipid tracer 1,1'-Dioctadecyl-3,3,3',3'-Tetramethylindodicarbocyanine Perchlorate (DiD) (**Figure 5**, pattern red bars) in the same GUV. The diffusion coefficient of $CP_{12}K_4$ drops from 9 $\mu m^2/s$ to 6 $\mu m^2/s$ when the amount of $CP_{12}K_4$ added to the GUVs reaches 1 mol%. This concentration corresponds to the concentration used in all lipid and content mixing experiments. The drop in the $CP_{12}K_4$ diffusion coefficient is greater than that observed for DiD. Such behavior supports the hypothesis that $CP_{12}K_4$ aggregates in/on the lipid bilayer. In contrast, the diffusion coefficient of both $CP_{12}E_4$ (**Figure 5**, blue bars) and DiD (**Figure 5**, blue patterned bars) keeps constant while $CP_{12}E_4$ is added to the GUVs, indicating no clustering and homogeneous incorporation of the lipopeptide. These results are in line with the lipid and content mixing assays, which showed interaction of CPK with the bilayer but no interaction of CPE.[28]

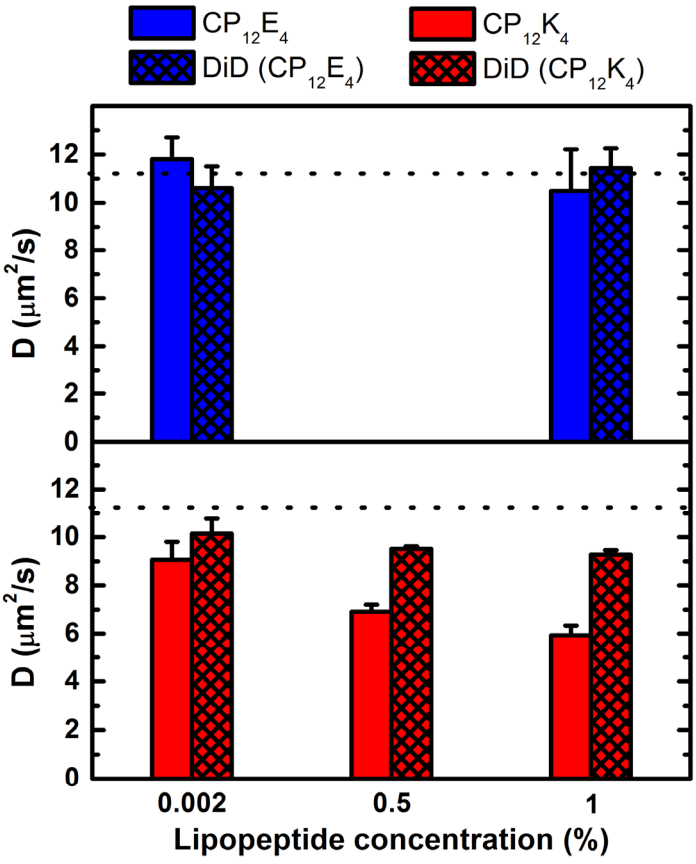

Figure 5. Diffusion coefficient of $CP_{12}E_4$ (blue, no pattern) and $CP_{12}K_4$ (red, no pattern) and membrane marker DiD (pattern) in the presence of lipopeptides for GUVs composed of DOPC/DOPE/Cholesterol (50/25/25). The black dotted line shows the reference value of the diffusion coefficient of DiD in GUVs with above mentioned lipid composition, but without any lipopeptide. Fluorescent lipopeptides labeled with Atto 488 were mixed with unlabeled lipopeptides to lipid ratio 1/50 000.

The effect of Tween 20 on the incorporation of $CP_{12}K_4$ into the lipid membrane is presented in **Figure 6,** as a function of the concentration of $CP_{12}K_4$. It has already been mentioned in the previous paragraph that diffusion of $CP_{12}K_4$ is slowed down significantly at 1 mol% lipopeptide concentration in the GUVs membrane. Using a mixture of $CP_{12}K_4$ and Tween 20 for the labeling of GUVs leads to slightly slower diffusion of both $CP_{12}K_4$ and DiD in comparison to the experiment in the absence of Tween 20. This finding might support the hypothesis that

Tween 20 improves the incorporation of CP_4K_4 into the GUVs. This effect may be more evident for the lipopeptide CP_4K_4, which is more hydrophobic due to a shorter PEG linker.

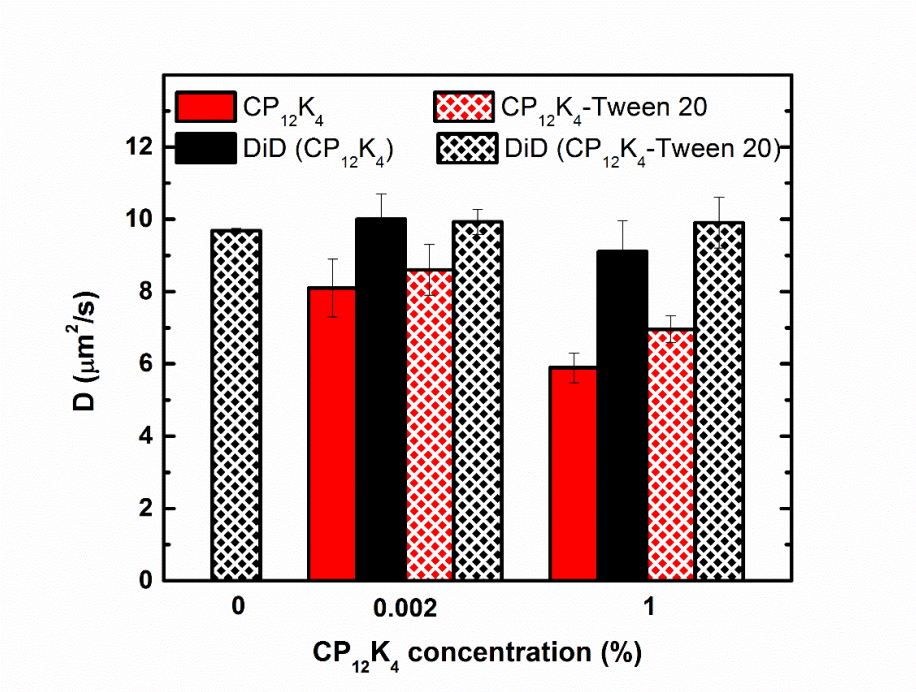

Figure 6. Diffusion coefficient of $CP_{12}K_4$ (red, no pattern), $CP_{12}K_4$-Tween 20 (red, pattern) and membrane marker DiD (black) in GUVs composed of DOPC/DOPE/Cholesterol (50/25/25). Tween 20 concentration is 0.01% of total lipid (Tween 20 1 mol% of 1 mol% $CP_{12}K_4$) in all $CP_{12}K_4$-Tween 20 samples.

In addition, several control experiments were performed to validate coiled-coil driven membrane fusion in the presence of Tween 20 (**Figures A8-13** in *Annex Chapter VII*). i) Removing CP_4K_4 from LUVs produced similar results to the experiment between non-labeled GUVs and non-labeled LUVs with minimal docking and no transfer of the aqueous content from LUVs to GUVs. On the other hand, docking of non-labeled LUVs on the target membrane of CP_4K_4-Tween 20 labeled GUVs was visible, which is in good agreement with the lipid mixing experiment. However, visual content mixing was not obvious due to a high background fluorescence originating from the liposomes. Development of fluorescence in time showed a

similar profile inside and outside GUVs (**Figures A10-11** in *Annex Chapter VII*). ii) GUVs previously incubated only with Tween 20, were transferred to a microscope chamber, followed by addition of carboxyfluorescein. The final concentration of carboxyfluorescein in the chamber was adjusted to 1 µM, which gives similar background fluorescence to the background detected in the membrane fusion experiments. Quantification of fluorescence inside individual GUVs showed that there was no leakage of carboxyfluorescein to the interior of the GUVs 60 minutes after the experiment was started (**Figures A14-15** in *Annex Chapter VII*). This result confirms that Tween 20 does not alter the GUV membrane properties. On the other hand, the strong interaction of CP_4K_4 with lipid bilayer may cause destabilization of the target lipid membrane. Those finding suggest that CP_4E_4 and CP_4K_4 are necessary for efficient content mixing and the mixture CP_4K_4-Tween 20 leads to an increase of GUVs with observable content mixing events. Therefore surfactant-lipopeptides interactions should be considered in further studies for understanding these interactions.

Conclusion

In conclusion we successfully visualized coiled-coil driven membrane fusion under physiological conditions. The use of GUVs as a target membrane allowed the visualization of the first steps of liposome docking and membrane fusion by dual color fluorescence microscopy. Time lapse imaging resulted in additional clues to the mechanism of membrane fusion, enabling optimization of the fusion efficiency under conditions that can be applied in the future to obtain fusion between liposomes and cells. Aggregation of CPK lipopeptides was observed in the membrane of GUVs, thereby decreasing the efficiency of membrane fusion. The use of Tween 20 as a co-surfactant solubilizing CPK improved the incorporation of the lipopeptide in the GUV membrane without affecting the properties of the membrane and improving the efficiency of the coiled-coil mediated membrane fusion between LUVs and GUVs. These results raise the hope that the coiled-coil membrane fusion system can be applied as a fast and efficient drug delivery system to cells *in vitro* and *in vivo*.

Experimental Section

Chemicals.

1,2-dioleoyl-sn-glycero-3-phosphocholine (DOPC), 1,2-dioleoyl-sn-glycero-3-phosphoethanolamine (DOPE), 1,2-dioleoyl-*sn*-glycero-3-phosphoethanolamine-*N*-(biotinyl) (sodium salt) (DOPE-Biotin), were purchased from Avanti Polar Lipids. Cholesterol (CH), Bovine Serum Albumin (BSA), biotin-labeled bovine albumin (Biotin-BSA), Streptavidin from Streptomyces avidinii, Poly(ethylene glycol) sorbitan monolaurate (Tween 20), Calcium chloride anhydrous ($CaCl_2$), Magnesium chloride hexahydrate ($MgCl_2 \cdot 6\ H_2O$), 5(6)-carboxyfluorescein, Sodium hydroxide (NaOH), sucrose and glucose were purchased from Sigma-Aldrich. 1,2-dioleoyl-*sn*-glycero-3-phosphoethanolamine-ATTO 488 (ATTO 488 DOPE), 1,2-dioleoyl-*sn*-glycero-3-phosphoethanolamine-ATTO 633 (ATTO 633 DOPE), ATTO 488 maleimide and ATTO 655 maleimide were purchased from ATTO-TEC GmbH. Fmoc-protected amino acids were purchased from Novabiochem and Biosolve. Sieber amide resin was purchased from Agilent Technology. Phosphate Buffered Saline (PBS, pH 7.4) was supplemented with $CaCl_2$ (1 mM) and $MgCl_2$ (0.5 mM) for all GUV studies. Lipid stock solutions of DOPC:DOPE:CH (50:25:25 molar ratio, 1 and 14 mM) were prepared in chloroform.

General methods for liposomes and GUV studies

Synthesis of lipopeptides CP_4K_4 and CP_4E_4.

The spacer N_3-PEG_4-COOH, cholesteryl-4-amino-4-oxobutanoic acid, and the lipopeptides CP_4K_4 and CP_4E_4 were synthesized and utilized following procedures previously reported.[21, 26, 32] The peptide segments E_4: NH_2-$(EIAALEK)_4$-$CONH_2$ and K_4: NH_2-$(KIAALKE)_4$-$CONH_2$ were synthesized using standard Fmoc chemistry on a peptide synthesizer (CEM-Liberty 1) and the spacer N_3-PEG_4-COOH was coupled to the N-terminus of the peptide segments. Next, the azide terminal group (N_3) on the spacer (PEG_4) was reduced to obtain an N-terminal free amine using 8 eq. of $P(CH_3)_3$ (1 M in toluene) in dioxane/H_2O (4:1 mixture). In the final step cholesteryl-4-amino-4-oxobutanoic acid (cholesterol anchor) was coupled to the terminal free amine in the PEG_4 spacer using 5 eq. of DIPEA and 4 eq. of PyBOP in DMF:DCM (2:1 mixture) over 72 h. Finally, the lipopeptides were purified by RP-HPLC with a Gemini C4 column to yield the pure product (Yield: 20-25%). CP_4K_4: LC-MS m/z Calcd. [1867.8

M+2H]$^{2+}$, found 1868.2. Calcd. [1245.6 M+3H]$^{3+}$, found 1246.2. Calcd. [934.4 M+4H]$^{4+}$, found 934.5). CP_4E_4: LC-MS m/z Calcd. [1869.5 M+2H]$^{2+}$, found 1869.9. Calcd. [1246.7 M+3H]$^{3+}$, found 1247.1. Calcd. [935.2 M+4H]$^{4+}$, found 935.5.

Synthesis of lipopeptides $CP_{12}K_4$ and $CP_{12}E_4$.

The peptide segments E_4: NH_2-(EIAALEK)$_4$-GC-$CONH_2$ and K_4: NH_2-(KIAALKE)$_4$-GC-$CONH_2$ were synthesized using standard Fmoc chemistry on a peptide synthesizer (CEM-Liberty 1). After synthesis, the resin was washed with DMF and Fmoc-PEG_{12}-COOH (1.1 equivalents) was coupled to the N-terminus of the peptides using 3 equivalents of HCTU and 4 equivalents of DIPEA. The reaction was left to proceed overnight. The resin was then washed with DMF, before the N-terminus was Fmoc deprotected using a 20% piperidine in DMF solution. Deprotection was achieved by incubating the resin with the piperidine/DMF solution for 10 minutes. This process was repeated 3 times, after which the resin was washed with DMF. Cholesteryl hemisuccinate was coupled using the same methodology as for the PEG coupling, (3 equivalents of HCTU and 4 equivalents of DIPEA, overnight reaction). The resin was washed with DMF, followed by DCM, before the product was cleaved from the resin using a mixture of TFA:TIPS:EDT (95:2.5 :2.5). The cleavage solution was left for one hour before the peptide was precipitated in ice-cold diethyl ether. The peptide was collected by centrifugation before being dissolved in water and freeze dried. Finally, the lipopeptides were purified by RP-HPLC with a Gemini C4 column to yield a pure product (Yield: 20-25%). $CP_{12}K_4$: MALDI-TOF m/z Calcd. [4260 M+H]$^+$, found 4260. $CP_{12}E_4$: MALDI-TOF m/z Calcd. [4264 M+H]$^+$, found 4270.

Fluorescent lipopeptides $CP_{12}K_4$-Atto488 and $CP_{12}E_4$-Atto488.

Lipopeptides were fluorescently labeled with ATTO 488 dye via maleimide-thiol reaction. Cysteine N-terminated lipopeptides (1 mg) were dissolved in 1 mL DCM and 1.3 fold molar excess of ATTO maleimide dye solution (1 mg/mL) was added to the reaction vessel. The reaction mixture was stirred for 1 hour protected from the light. Then the solvent was evaporated in vacuum and the lipopeptides were purified by RP-HPLC with a Gemini C4 column. $CP_{12}K_4$-Atto488: MALDI-TOF m/z Calcd. [4970 M+H]$^+$, found 4970. $CP_{12}E_4$-Atto488: MALDI-TOF m/z Calcd. [4975 M+H]$^+$, found 4986.

Formation of GUVs.

Giant Unilamellar Vesicles (GUVs) were grown on Dex-PEG hydrogel (1:1 molar ratio) coated microscope glass slide substrates as described previously.[27] Lipid solution (10 µL) with the lipid composition DOPC:DOPE:CH (2:1:1 molar ratio, 14 mM), DOPE-Biotin (0.2 mol% relative to [lipids]) and ATTO 488 DOPE (0.1 mol% relative to [lipid]) for lipid mixing experiments or ATTO 633 DOPE (0.1 mol% relative to [lipid]) for content mixing experiments was deposited on a hydrogel coated glass slide. Next the chloroform was evaporated under a gentle stream of N_2 and placed in a vacuum oven overnight at 40 °C. A liquid chamber was made by placing a glass O-Ring (diameter = 15 mm and height = 3 mm, Agar Scientific) on top of the hydrogel and sealed with high vacuum silicon grease. The lipid film was hydrated by adding 400 µL of PBS supplemented with $CaCl_2$ (1 mM), $MgCl_2$ (0.5 mM) and sucrose (200 mM) into each chamber and the GUVs were formed overnight at room temperature.

Labeling of GUVs with lipopeptides CP_4K_4 and CP_4E_4.

GUVs were labeled with 1 mol% CP_4K_4 or CP_4E_4 (relative to [lipid]). A stock solution of CP_4K_4 or CP_4E_4 (15 µL, 50 µM in CH_3OH:$CHCl_3$ 1:1) was dried by evaporating the solvent under a gentle stream of N_2 and placed in a vacuum oven overnight at 40 °C. The lipopeptide film was hydrated by adding 700 µL of PBS supplemented with $CaCl_2$ (1 mM), $MgCl_2$ (0.5 mM) and glucose (200 mM), vortexed and transferred to a micro centrifuge tube. Subsequently 300 µL of the solution with free floating GUVs was transferred into the micro centrifuge tube containing the CP_4K_4 aqueous solution. The GUVs were incubated during 60 minutes in the lipopeptide solution and finally 300 µL of GUVs were transferred to a microscopy chamber for experiments.

Labeling of GUVs with lipopeptide CP_4K_4 and Tween 20.

GUVs were labeled with a mixture of CP_4K_4 (1 mol% relative to [lipid]) and depending on the experiment, 0.4 or 1 mol% of Tween-20 with respect to CP_4K_4. A stock solution of CP_4K_4 (15 µL, 50 µM in CH_3OH:$CHCl_3$ 1:1) and Tween 20 (5.6 µL or 14 µL, 0.001 mM in CH_3OH) were mixed and dried by evaporating the solvent under a gentle stream of N_2. Next, the lipid film was placed in a vacuum oven overnight. The CP_4K_4-Tween 20 film was hydrated by adding 700 µL of PBS supplemented with $CaCl_2$ (1 mM), $MgCl_2$ (0.5 mM) and glucose (200 mM), vortexed and transferred to a micro centrifuge tube. Next 300 µL of a free floating GUVs solution was transferred into the micro centrifuge tube containing the mixture CP_4K_4-Tween

20 mixture. The GUVs were incubated during 60 minutes in this solution and finally 300 µL of GUVs were transferred to a microscopy chamber for experiments.

Formation of liposomes with lipopeptides CP_4K_4 or CP_4E_4 for lipid mixing experiments.

Peptide labeled Large Unilamellar Vesicles (LUVs) were formed with 1 mol% CP_4K_4 or CP_4E_4 (relative to total [lipid]). For this a lipid solution (1 mL) with the lipid composition DOPC:DOPE:CH (2:1:1 molar ratio, 1 mM), ATTO 633 DOPE (0.5 mol% relative to [lipid]) and lipopeptides CP_4K_4 or CP_4E_4 stock solution (50 µM in CH_3OH:$CHCl_3$ 1:1). The lipid solution was dried by evaporation of the organic solvents under a gentle stream of N_2 and placed in a vacuum oven overnight at 40 °C. The lipid film was hydrated by addition of 1 mL of PBS supplemented with $CaCl_2$ (1 mM), $MgCl_2$ (0.5 mM) and sucrose (200 mM) for lipid mixing experiments with GUVs. Finally, the LUVs were formed by sonication at room temperature for 2-4 minutes with an average diameter of 120 nm determined by dynamic light scattering (Zetasizer Nano-S, Malvern).

Formation of carboxyfluorescein loaded liposomes with lipopeptides CP_4K_4 or CP_4E_4 for content mixing experiments.

Large Unilamellar Vesicles (LUVs) were labeled with 1 mol% CP_4K_4 or CP_4E_4 (relative to total [lipid]). A lipid solution (1mL) with the lipid composition DOPC:DOPE:CH (2:1:1 molar ratio, 1 mM) and ATTO 633 DOPE (0.5 mol% relative to [lipid]). The lipid solution was dried by evaporation of the organic solvents under a gentle stream of N_2 and placed in a vacuum oven overnight at 40 °C. The lipid film was hydrated by the addition of 1 mL of carboxyfluorescein (50 µM) in PBS solution supplemented with $CaCl_2$ (1 mM), $MgCl_2$ (0.5 mM) and sucrose (200 mM). The LUVs were formed by extrusion (0.4 µm polycarbonate membrane) with 17 passes in a mini extruder with 250 µL syringes. Free carboxyfluorescein was separated from the liposome-encapsulated carboxyfluorescein by size exclusion using a Sephadex column (2.5 mL) eluting with PBS solution supplemented with $CaCl_2$ (1 mM), $MgCl_2$ (0.5 mM) and glucose (200 mM). Liposome formation was verified by dynamic light scattering. Next the LUVs were labeled with 1 mol% CP_4K_4 or CP_4E_4 (relative to [lipid]). A stock solution of CP_4K_4 or CP_4E_4 (200 µL, 50 µM in CH3OH:CHCl3 1:1) was dried by the evaporation of the organic solvent under a gentle stream of N_2 and placed in a vacuum oven overnight at 40 °C. The lipopeptide film was hydrated by the addition of 200 µL of PBS supplemented with $CaCl_2$ (1 mM), $MgCl_2$ (0.5 mM) and glucose (200 mM). Subsequently, the

solution of LUVs (~ 2.5 mL) was transferred into the micro centrifuge tube containing the CP_4K_4 or CP_4E_4 aqueous solution and vortexed. The LUVs were incubated for 60 minutes in the lipopeptide solution and used immediately in content mixing experiments with GUVs.

Lipid and content mixing assays LUVs - GUVs.

The visualization of GUVs after lipopeptide labeling was achieved with a microscopy chamber (µ-Slide 8 well, Ibidi) which was pre-treated firstly with an aqueous mixture of BSA (0.9 mg/mL) and biotin-BSA (0.1 mg/mL) for 30 minutes, with streptavidin (0.1 mg/mL) for another 30 minutes and finally rinsed with water. Next 100 µL of PBS solution supplemented with $CaCl_2$ (1 mM), $MgCl_2$ (0.5 mM) and glucose (200 mM) and 200 µL of the solution with peptide labeled GUVs were transferred into the microscopy visualization chamber. The GUVs were left to sediment for at least 30 minutes before imaging. During imaging of the GUVs in a time lapse experiment, either 30 µL of peptide labeled LUVs for lipid mixing experiment or 60 µL of peptide labeled LUVs loaded with carboxyfluorescein for content mixing experiments were added to the microscopy well and the imaging was performed during 120 minutes after the arrival of LUVs to the bottom of the microscopy chamber.

Imaging of the GUVs and data analysis.

Imaging of GUVs was performed on a Leica TCS SPE confocal microscope system. Illumination was provided by a solid state laser using 488 nm laser line (15% laser power) for irradiation of carboxyfluorescein and ATTO 488 DOPE, detection 500-550 nm and 635 nm laser line (15% laser power) for irradiation of ATTO 633 DOPE, detection 650-700 nm. Fluorescence confocal microscopy was carried out using either 40× air or 63× water objectives. The analysis of the images was performed in ImageJ software,[33] by measuring the average intensity of an area corresponding to one GUV for the series of time lapse microscopy image frames.

Z-Scan Fluorescent Correlation Spectroscopy (z-scan FCS).

FCS measurements were performed on an inverted home-built confocal microscope (IX71 Olympus, Hamburg, Germany). The excitation was achieved by two pulsed diode lasers at 470 nm (LDH-P-C-470) and 635 nm (LDH-D-C-635) produced by PicoQuant, Germany. The laser light (approx. 10 µW intensity in front of the objective) was pulsed alternatively in order to avoid artefacts caused by signal bleed-through. The emitted light was detected by two single

photon avalanche diodes using 515/50 and 697/58 band pass filters (Chroma Rockingham, VT). Z-scan measurements were performed on the top of a selected vesicle. The membrane was vertically scanned in 15 steps spaced 200nm apart from each other. A measurement at each point took 60s.

References

1. Waters, M.G. & Hughson, F.M. Membrane tethering and fusion in the secretory and endocytic pathways. *Traffic* **1**, 588-597 (2000).
2. Tareste, D., Shen, J., Melia, T.J. & Rothman, J.E. SNAREpin/Munc18 promotes adhesion and fusion of large vesicles to giant membranes. *P Natl Acad Sci USA* **105**, 2380-2385 (2008).
3. Rothman, J.E. The Principle of Membrane Fusion in the Cell (Nobel Lecture). *Angew Chem Int Edit* **53**, 12676-12694 (2014).
4. Sudhof, T.C. The Molecular Machinery of Neurotransmitter Release (Nobel Lecture). *Angew Chem Int Edit* **53**, 12696-12717 (2014).
5. Jahn, R., Lang, T. & Sudhof, T.C. Membrane fusion. *Cell* **112**, 519-533 (2003).
6. Wassarman, P. & Litscher, E. in Cell Fusion, Vol. 475. (ed. E. Chen) 99-113 (Humana Press, 2008).
7. Wassarman, P.M. Sperm protein finds its mate. *Nature* **508**, 466-467 (2014).
8. Schultz, R. & Williams, C. Developmental biology - Sperm-egg fusion unscrambled. *Nature* **434**, 152-153 (2005).
9. Harrison, S.C. Viral membrane fusion. *Nat Struct Mol Biol* **15**, 690-698 (2008).
10. Apellaniz, B., Huarte, N., Largo, E. & Nieva, J.L. The three lives of viral fusion peptides. *Chem Phys Lipids* **181**, 40-55 (2014).
11. Jahn, R. & Fasshauer, D. Molecular machines governing exocytosis of synaptic vesicles. *Nature* **490**, 201-207 (2012).
12. Sudhof, T.C. & Rothman, J.E. Membrane Fusion: Grappling with SNARE and SM Proteins. *Science* **323**, 474-477 (2009).
13. Rizo, J. & Sudhof, T.C. SNAREs and Munc18 in synaptic vesicle fusion. *Nat Rev Neurosci* **3**, 641-653 (2002).
14. Toonen, R.F. & Verhage, M. Munc18-1 in secretion: lonely Munc joins SNARE team and takes control. *Trends in neurosciences* **30**, 564-572 (2007).
15. Stengel, G., Zahn, R. & Hook, F. DNA-induced programmable fusion of phospholipid vesicles. *J Am Chem Soc* **129**, 9584-9585 (2007).
16. Chan, Y.H.M., van Lengerich, B. & Boxer, S.G. Effects of linker sequences on vesicle fusion mediated by lipid-anchored DNA oligonucleotides. *P Natl Acad Sci USA* **106**, 979-984 (2009).
17. Kashiwada, A., Tsuboi, M. & Matsuda, K. Target-selective vesicle fusion induced by molecular recognition on lipid bilayers. *Chem Commun*, 695-697 (2009).
18. Ma, M., Paredes, A. & Bong, D. Intra- and intermembrane pairwise molecular recognition between synthetic hydrogen-bonding phospholipids. *J Am Chem Soc* **130**, 14456-14458 (2008).
19. Meyenberg, K., Lygina, A.S., van den Bogaart, G., Jahn, R. & Diederichsen, U. SNARE derived peptide mimic inducing membrane fusion. *Chem Commun (Camb)* **47**, 9405-9407 (2011).
20. Gong, Y., Luo, Y. & Bong, D. Membrane activation: selective vesicle fusion via small molecule recognition. *J Am Chem Soc* **128**, 14430-14431 (2006).
21. Marsden, H.R., Elbers, N.A., Bomans, P.H.H., Sommerdijk, N.A.J.M. & Kros, A. A Reduced SNARE Model for Membrane Fusion. *Angew Chem Int Edit* **48**, 2330-2333 (2009).

22. Kumar, P., Guha, S. & Diederichsen, U. SNARE protein analog-mediated membrane fusion. *J Pept Sci* **21**, 621-629 (2015).
23. Marsden, H.R., Korobko, A.V., Zheng, T.T., Voskuhl, J. & Kros, A. Controlled liposome fusion mediated by SNARE protein mimics. *Biomater Sci-Uk* **1**, 1046-1054 (2013).
24. Marsden, H.R. & Kros, A. Self-Assembly of Coiled Coils in Synthetic Biology: Inspiration and Progress. *Angew Chem Int Edit* **49**, 2988-3005 (2010).
25. Zheng, T.T. et al. Controlling the rate of coiled coil driven membrane fusion. *Chem Commun* **49**, 3649-3651 (2013).
26. Versluis, F. et al. In Situ Modification of Plain Liposomes with Lipidated Coiled Coil Forming Peptides Induces Membrane Fusion. *Journal of the American Chemical Society* **135**, 8057-8062 (2013).
27. Mora, N.L. et al. Preparation of size tunable giant vesicles from cross-linked dextran(ethylene glycol) hydrogels. *Chem Commun* **50**, 1953-1955 (2014).
28. Rabe, M., Schwieger, C., Zope, H.R., Versluis, F. & Kros, A. Membrane Interactions of Fusogenic Coiled-Coil Peptides: Implications for Lipopeptide Mediated Vesicle Fusion. *Langmuir* **30**, 7724-7735 (2014).
29. Torchilin, V. & Weissig, V. Liposomes: A Practical Approach. *Oxford University Press* (2003).
30. Castanho, M.A.R.B. Membrane-active Peptides: Methods and Results on Structure and Function. *International University Line.* Chapter 8, pp 184 (2009).
31. Weiszhar, Z. et al. Complement activation by polyethoxylated pharmaceutical surfactants: Cremophor-EL, Tween-80 and Tween-20. *European journal of pharmaceutical sciences : official journal of the European Federation for Pharmaceutical Sciences* **45**, 492-498 (2012).
32. Voskuhl, J. et al. Immobilization of Liposomes and Vesicles on Patterned Surfaces by a Peptide Coiled-Coil Binding Motif. *Angew Chem Int Edit* **51**, 12616-12620 (2012).
33. Schneider, C.A., Rasband, W.S. & Eliceiri, K.W. NIH Image to ImageJ: 25 years of image analysis. *Nat Methods* **9**, 671-675 (2012).

Annex

Chapter VII

Full Data sets of lipid and content mixing assays.

Time lapse lipid mixing control experiments between GUVs and liposomes.

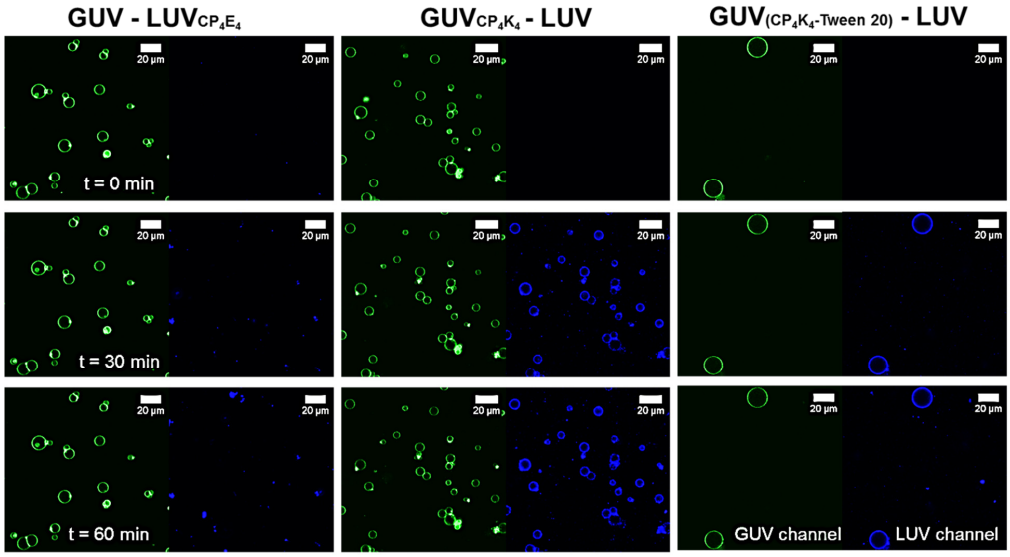

Figure A1. Time lapse micrographs of the lipid mixing control assay between GUVs and LUVs before (time=0) and after (time=30 and 60 minutes) appearance of LUVs in the confocal volume. The GUVs are excited at 488 nm and the emission of fluorescence is detected between 500-550 nm (green color), while LUVs are excited at 633 nm and the emission is detected between 650-700 nm (blue color). A) Lipid mixing assay between GUVs and CP_4E_4 labeled LUVs, B) Lipid mixing assay between CP_4K_4 labeled GUVs and non-labeled LUVs and C) Lipid mixing assay between CP_4K_4-Tween 20 labeled GUVs and CP_4E_4 labeled LUVs. Imaging was performed every minute during one hour using a Leica TCS SPE microscope.

Datasets for the time lapse content mixing experiments between GUVs and liposomes.

Content mixing between CP_4K_4 labeled GUVs and CP_4E_4 labeled LUVs loaded with carboxyfluorescein.

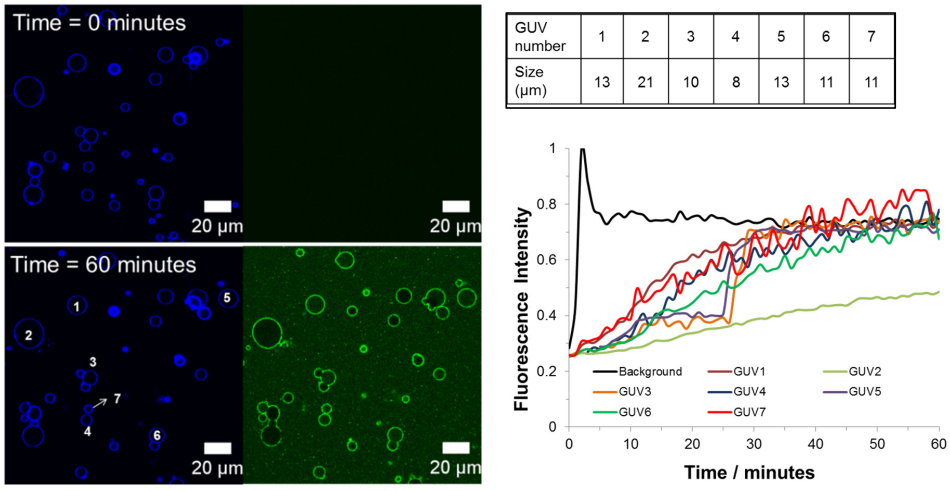

GUV number	1	2	3	4	5	6	7
Size (µm)	13	21	10	8	13	11	11

Figure A2. Fluorescence micrographs before (top) and after (bottom) addition of carboxyfluorescein loaded CP_4E_4 liposomes to CP_4K_4 GUVs. GUVs lipid membranes are supplemented with ATTO 633 DOPE (blue) and LUVs are loaded with carboxyfluorescein (green). In the right, normalized fluorescence intensity profiles over time for individual numbered GUVs and average background and in the upper panel the average diameter over time for GUVs.

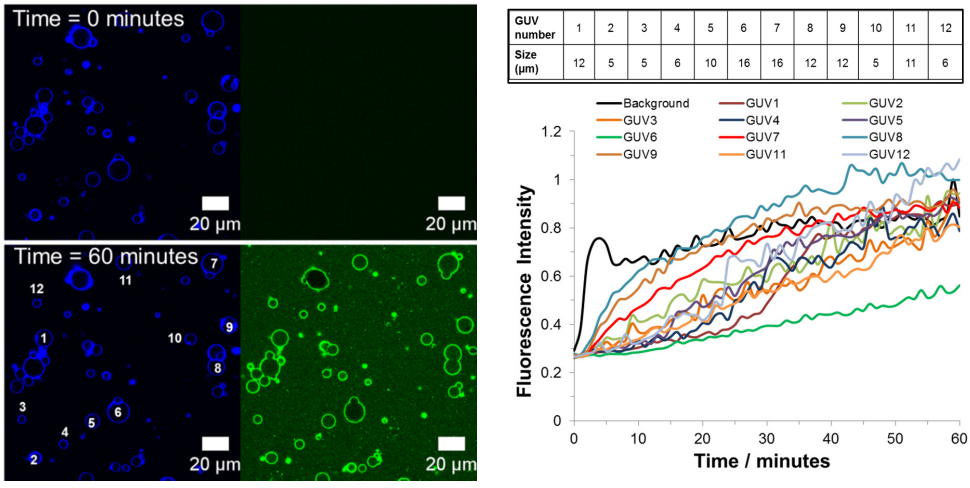

GUV number	1	2	3	4	5	6	7	8	9	10	11	12
Size (µm)	12	5	5	6	10	16	16	12	12	5	11	6

Figure A3. Fluorescence micrographs before (top) and after (bottom) addition of carboxyfluorescein loaded CP_4E_4 liposomes to CP_4K_4 GUVs. GUVs lipid membranes are supplemented with ATTO 633 DOPE (blue) and LUVs are loaded with carboxyfluorescein (green). In the right, normalized fluorescence intensity profiles over time for individual numbered GUVs and average background and in the upper panel the average diameter over time for GUVs.

Content mixing between 0.4 mol% Tween 20-CP_4K_4 labeled GUVs and CP_4E_4 labeled LUVs loaded with carboxyfluorescein.

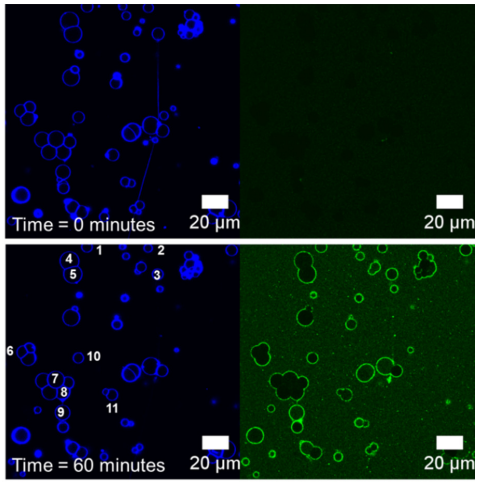

GUV number	1	2	3	4	5	6	7	8	9	10	11
Size (µm)	8	7	8	14	13	9	12	10	11	8	9

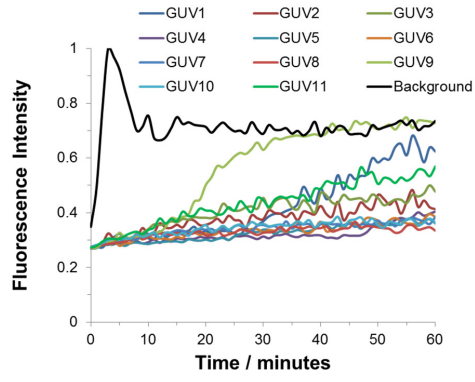

Figure A4. Fluorescence micrographs before (top) and after (bottom) addition of carboxyfluorescein loaded CP_4E_4 liposomes to CP_4K_4 GUVs. GUVs lipid membranes are supplemented with ATTO 633 DOPE (blue) and LUVs are loaded with carboxyfluorescein (green). In the right, normalized fluorescence intensity profiles over time for individual numbered GUVs and average background and in the upper panel the average diameter over time for GUVs.

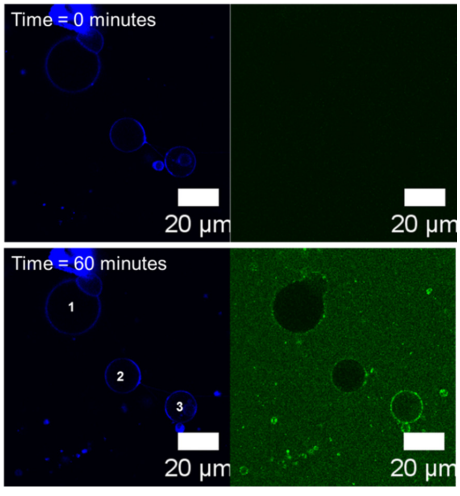

GUV number	1	2	3
Size (µm)	26	17	15

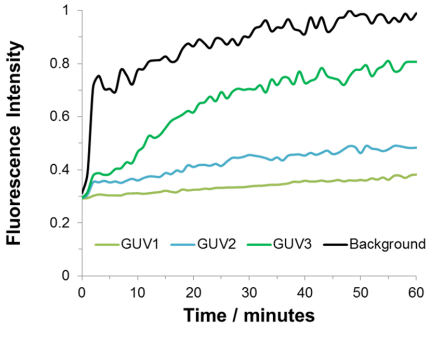

Figure A5. Fluorescence micrographs before (top) and after (bottom) addition of carboxyfluorescein loaded CP_4E_4 liposomes to CP_4K_4 GUVs. GUVs lipid membranes are supplemented with ATTO 633 DOPE (blue) and LUVs are loaded with carboxyfluorescein (green). In the right, normalized fluorescence intensity profiles over time for individual numbered GUVs and average background and in the upper panel the average diameter over time for GUVs.

Content mixing between 1 mol% Tween 20-CP_4K_4 labeled GUVs and CP_4E_4 labeled LUVs loaded with carboxyfluorescein.

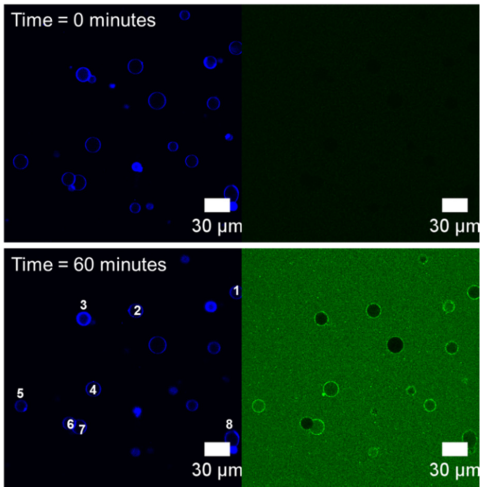

GUV number	1	2	3	4	5	6	7	8
Size (µm)	16	17	16	17	16	15	17	16

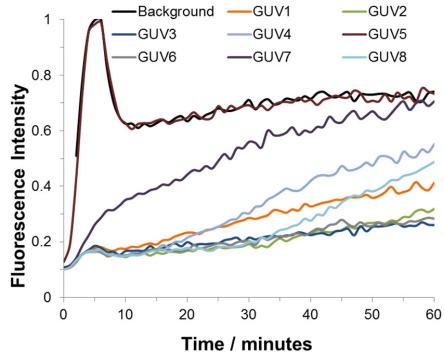

Figure A6. Fluorescence micrographs before (top) and after (bottom) addition of carboxyfluorescein loaded CP_4E_4 liposomes to CP_4K_4 GUVs. GUVs lipid membranes are supplemented with ATTO 633 DOPE (blue) and LUVs are loaded with carboxyfluorescein (green). In the right, normalized fluorescence intensity profiles over time for individual numbered GUVs and average background and in the upper panel the average diameter over time for GUVs.

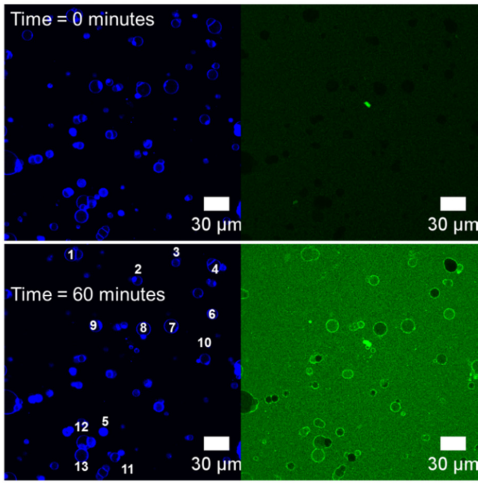

GUV number	1	2	3	4	5	6	7	8	9	10	11	12	13
Size (µm)	15	13	10	15	10	12	16	16	15	11	11	16	15

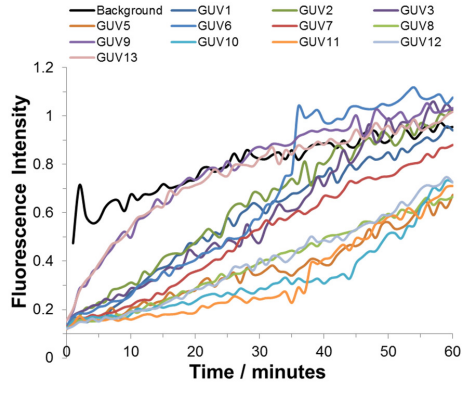

Figure A7. Fluorescence micrographs before (top) and after (bottom) addition of carboxyfluorescein loaded CP_4E_4 liposomes to CP_4K_4 GUVs. GUVs lipid membranes are supplemented with ATTO 633 DOPE (blue) and LUVs are loaded with carboxyfluorescein (green). In the right, normalized fluorescence intensity profiles over time for individual numbered GUVs and average background and in the upper panel the average diameter over time for GUVs.

Datasets for the time lapse control experiments between 1 mol% Tween GUVs and LUVs.

Control experiment between 1 mol% Tween GUVs and LUVs loaded with carboxyfluorescein.

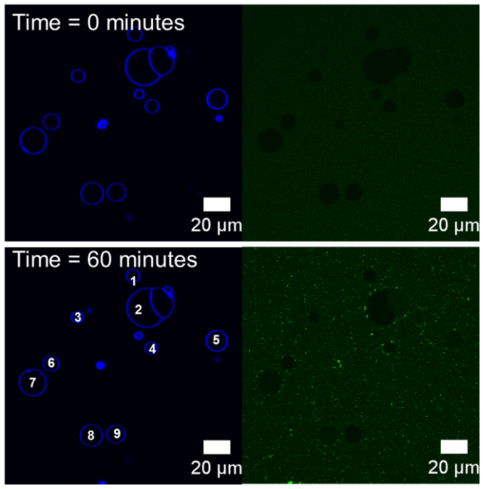

GUV number	1	2	3	4	5	6	7	8	9
Size (µm)	10	28	9	9	15	12	19	16	13

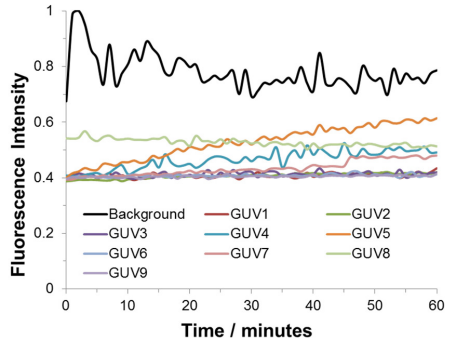

Figure A8. Fluorescence micrographs before (top) and after (bottom) addition of carboxyfluorescein loaded CP_4E_4 liposomes to CP_4K_4 GUVs. GUVs lipid membranes are supplemented with ATTO 633 DOPE (blue) and LUVs are loaded with carboxyfluorescein (green). In the right, normalized fluorescence intensity profiles over time for individual numbered GUVs and average background and in the upper panel the average diameter over time for GUVs.

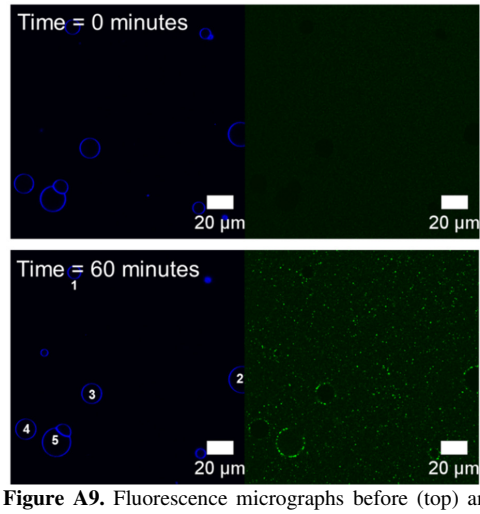

GUV number	1	2	3	4	5
Size (µm)	11	18	15	15	18

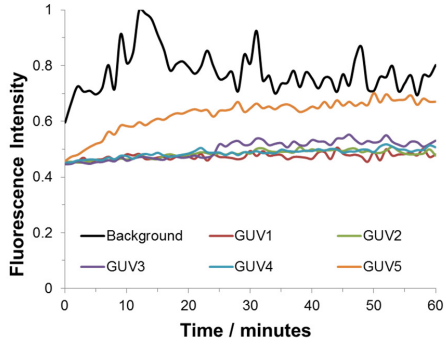

Figure A9. Fluorescence micrographs before (top) and after (bottom) addition of carboxyfluorescein loaded CP_4E_4 liposomes to CP_4K_4 GUVs. GUVs lipid membranes are supplemented with ATTO 633 DOPE (blue) and LUVs are loaded with carboxyfluorescein (green). In the right, normalized fluorescence intensity profiles over time for individual numbered GUVs and average background and in the upper panel the average diameter over time for GUVs.

Control experiment between 1 mol% Tween-CP_4K_4 labeled GUVs and LUVs loaded with carboxyfluorescein.

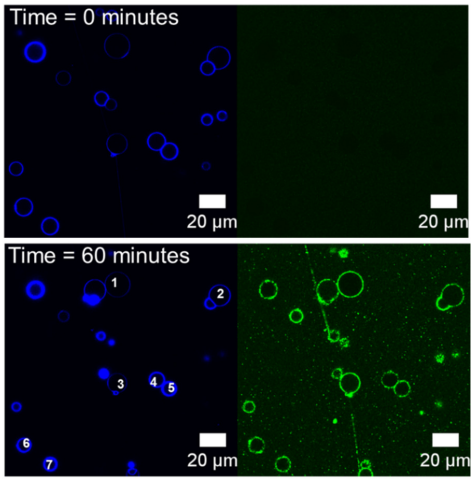

GUV number	1	2	3	4	5	6	7
Size (µm)	19	16	15	12	11	12	11

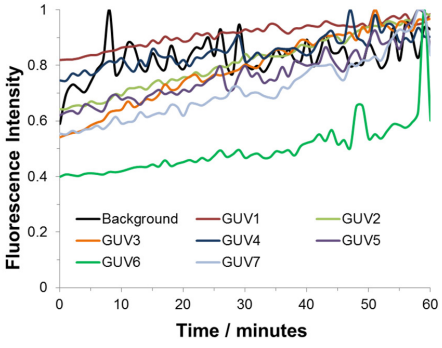

Figure A10. Fluorescence micrographs before (top) and after (bottom) addition of carboxyfluorescein loaded CP_4E_4 liposomes to CP_4K_4 GUVs. GUVs lipid membranes are supplemented with ATTO 633 DOPE (blue) and LUVs are loaded with carboxyfluorescein (green). In the right, normalized fluorescence intensity profiles over time for individual numbered GUVs and average background and in the upper panel the average diameter over time for GUVs.

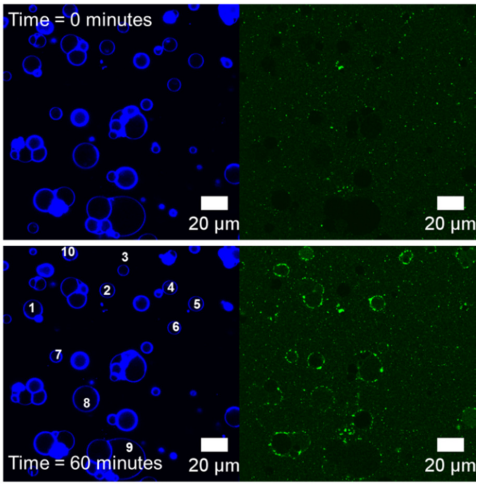

GUV number	1	2	3	4	5	6	7	8	9	10
Size (µm)	13	11	8	11	11	9	9	18	31	10

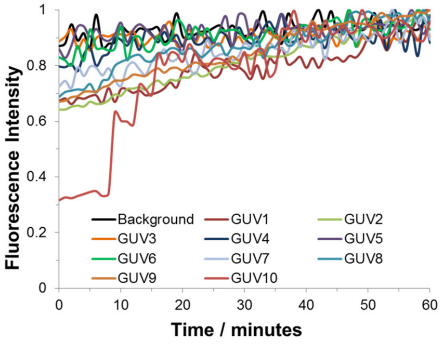

Figure A11. Fluorescence micrographs before (top) and after (bottom) addition of carboxyfluorescein loaded CP_4E_4 liposomes to CP_4K_4 GUVs. GUVs lipid membranes are supplemented with ATTO 633 DOPE (blue) and LUVs are loaded with carboxyfluorescein (green). In the right, normalized fluorescence intensity profiles over time for individual numbered GUVs and average background and in the upper panel the average diameter over time for GUVs.

Control experiment between 1 mol% Tween GUVs and CP_4E_4 LUVs loaded with carboxyfluorescein.

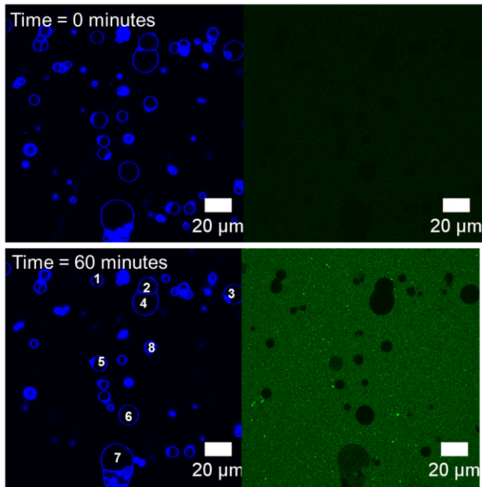

GUV number	1	2	3	4	5	6	7	8
Size (µm)	9	13	14	19	11	14	24	9

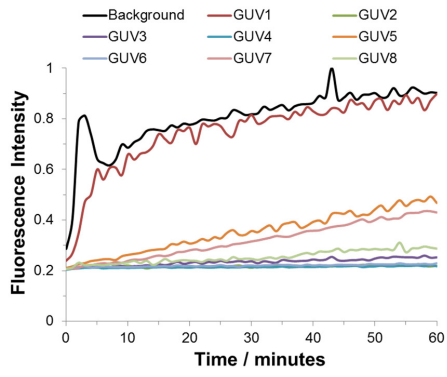

Figure A12. Fluorescence micrographs before (top) and after (bottom) addition of carboxyfluorescein loaded CP_4E_4 liposomes to CP_4K_4 GUVs. GUVs lipid membranes are supplemented with ATTO 633 DOPE (blue) and LUVs are loaded with carboxyfluorescein (green). In the right, normalized fluorescence intensity profiles over time for individual numbered GUVs and average background and in the upper panel the average diameter over time for GUVs.

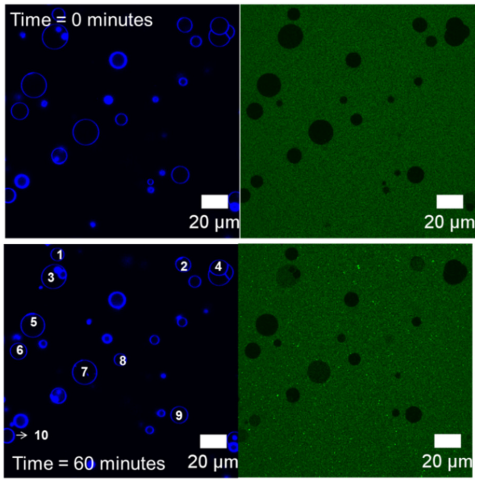

GUV number	1	2	3	4	5	6	7	8	9	10
Size (µm)	10	10	18	14	18	12	19	9	13	11

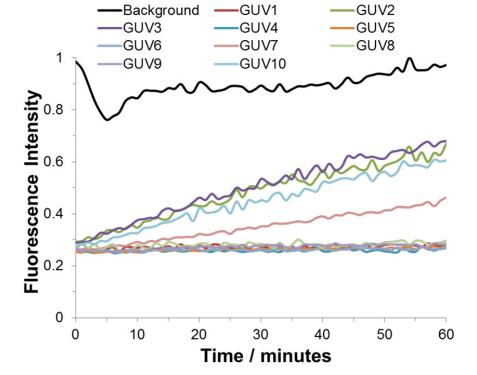

Figure A13. Fluorescence micrographs before (top) and after (bottom) addition of carboxyfluorescein loaded CP_4E_4 liposomes to CP_4K_4 GUVs. GUVs lipid membranes are supplemented with ATTO 633 DOPE (blue) and LUVs are loaded with carboxyfluorescein (green). In the right, normalized fluorescence intensity profiles over time for individual numbered GUVs and average background and in the upper panel the average diameter over time for GUVs.

Datasets for the time lapse leakage of carboxyfluorescein into 1 mol% CP_4K_4-Tween 20 labeled GUVs and LUVs.

Leakage of 1 µM carboxyfluorescein into 1 mol% Tween-CP_4K_4 labeled GUVs.

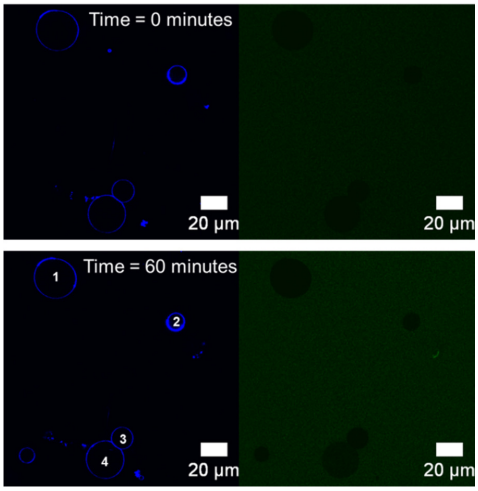

GUV number	1	2	3	4
Size (µm)	31	13	17	28

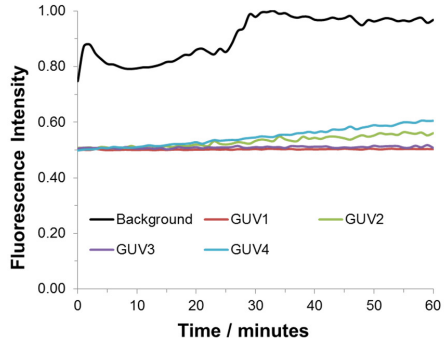

Figure A14. Fluorescence micrographs before (top) and after (bottom) addition of carboxyfluorescein loaded CP_4E_4 liposomes to CP_4K_4 GUVs. GUVs lipid membranes are supplemented with ATTO 633 DOPE (blue) and LUVs are loaded with carboxyfluorescein (green). In the right, normalized fluorescence intensity profiles over time for individual numbered GUVs and average background and in the upper panel the average diameter over time for GUVs.

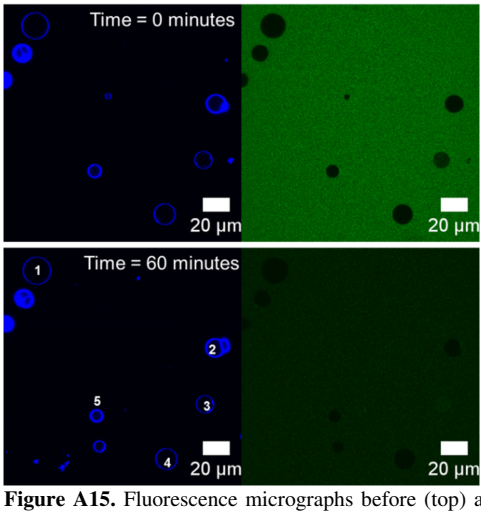

GUV number	1	2	3	4	5
Size (µm)	20	13	13	16	9

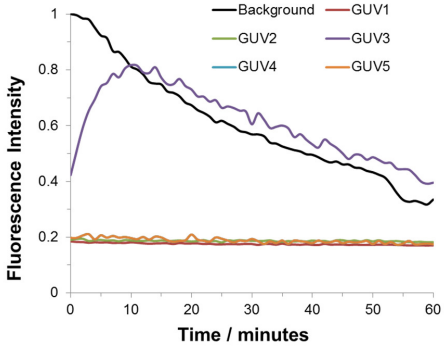

Figure A15. Fluorescence micrographs before (top) and after (bottom) addition of carboxyfluorescein loaded CP_4E_4 liposomes to CP_4K_4 GUVs. GUVs lipid membranes are supplemented with ATTO 633 DOPE (blue) and LUVs are loaded with carboxyfluorescein (green). In the right, normalized fluorescence intensity profiles over time for individual numbered GUVs and average background and in the upper panel the average diameter over time for GUVs.

Chapter VIII

Summary and Outlook

Summary

In this thesis Giant Unilamellar Vesicles (GUVs) were used as a minimal model system of the cellular membrane. GUVs are spherical assemblies of natural or synthetic lipids composed of a single lipid bilayer which separates the aqueous interior compartment from the exterior.[1, 2] The main advantage of this membrane model is that GUVs can be readily observed by optical microscopy. The giant size (5-100 μm) allows to image morphological changes in the lipid bilayer of GUVs.[3] This minimal model of the plasma cellular membrane has been broadly used for studying mechanical properties of membranes,[4] lipid organization,[5] interactions with proteins[6] and peptides[7] and more recently as a tool for creating a minimal cell in a bottom-up approach.[8, 9] Several protocols have been proposed to form GUVs, being the most common electroformation[10] and gentle hydration methods[11] for the formation of GUVs at low salt concentrations. However, the study of biological interactions requires the use of biologically relevant salt concentrations. To tackle this drawback from traditional preparation methods, alternative protocols such as water in oil emulsion,[12, 13] solvent exchange and gel films[14, 15] have been proposed. However, traces of impurities coming from the preparation method have been detected in the lipid bilayer as it has been deeply discussed in this work (**Chapter I** and **II**).

This thesis presents a new method, based on a chemically crosslinked hydrogel as a substrate for the growth of GUVs at relevant biological salt conditions without the transfer of impurities coming from the substrate (**Chapter I**). We studied the physical chemical properties of this hydrogel network and we characterized the final GUVs in terms of yield and size (**Chapter II**). Moreover the GUVs were used as a biophysical platform for membrane studies at high salt concentrations (**Chapters III** and **IV**). Finally, the application of GUVs as a cell mimicking platform for studying drug delivery (**Chapter V**) and membrane fusion processes (**Chapters VI** and **VII**) were investigated.

This work covers some biophysical aspects and applications of the GUV model applied at relevant salt concentrations and also shows that there is room for other studies. In the final chapter (**Chapter VIII**) preliminary results were obtained for filling gaps in the understanding of the GUV model and future research lines are proposed.

Outlook

Hydrogel substrates for GUV formation

The use of DexPEG hydrogel substrates for facilitating the growth of GUVs at high ionic strength conditions is presented and validated for several lipid compositions in **Chapter II**; however the preparation of those substrates is time consuming and requires a basic training in chemistry to perform the esterification of Dextran and maleimide (Dex-Mal), purification of the product and preparation of hydrogel functionalized glass substrates (DexPEG). In **Chapter III** an attempt to form a polyethylene glycol (PEG) hydrogel film by dissolving the commercially available 4 arms PEG thiol and mixing with catalytic quantities of H_2O_2 did not produce a suitable hydrogel film for the formation of GUVs. Moreover, thermal characterization (DSC) of the hybrid PEG hydrogel and DOPE lipid showed a strong interaction between lipids and PEG scaffold, while the interaction between lipids and DexPEG scaffold was weaker. Thus the use of other polysaccharides besides Dextran in the formation of hydrogel films is a subject of deeper research.

The high swelling efficiency of the DexPEG hydrogel films promotes the formation of GUVs at relevant salt conditions (**Chapter III**). In addition to DexPEG hydrogels, photocrosslinked Dextran-methacrylate hydrogels might be another option to produce Dextran-based hydrogel films for the vesicle growth.[16] The Dextran backbone and the high swelling ratios of Dextran-methacrylate hydrogels might produce similar results to those in DexPEG hydrogels. However, the ability of those hydrogels in the production of GUVs has not been tested as yet. The formation of inhomogeneities in the hydrogel structure due to unreacted methacrylate groups might be a possible drawback of Dextran-methacrylate hydrogels if the UV irradiation is variable trough the thickness of the hydrogel during photocrosslinking. The formation of inhomogeneities might affect directly the control of the size distribution in the final GUV population.

Encapsulation of bio-molecules

The formation of size controlled GUVs and efficient encapsulation of biologically active compounds has only been achieved successfully by microfluidic jetting until now.[17] In this thesis, DexPEG hydrogels were used in GUV formation and efficient encapsulation of small water soluble molecules such as lucigenin (**Chapter V** and **VI**) and carboxyfluorescein (**Chapter VII**). Furthermore, fluorescently labelled DNA was encapsulated into GUVs by

hydration of the hybrid DexPEG-lipid film with a solution (100 mM NaCl, 10 mM TES, 1 mM EDTA, 1 mM $CaCl_2$) containing fluorescently labelled DNA (5 µM). Bright field and fluorescence microscopy of DNA loaded GUVs are presented in **Figure 1**. It has been shown that DNA loaded GUVs represent a minimal model for studying the self-replication of DNA and the self-reproduction of the lipid compartment.[18] Thus, the use of DexPEG hydrogel substrates for the encapsulation of biomolecular cargo inside lipid compartments might have biotechnological applications and could be potentially a tool in synthetic biology for the creation of minimal cell models.[9]

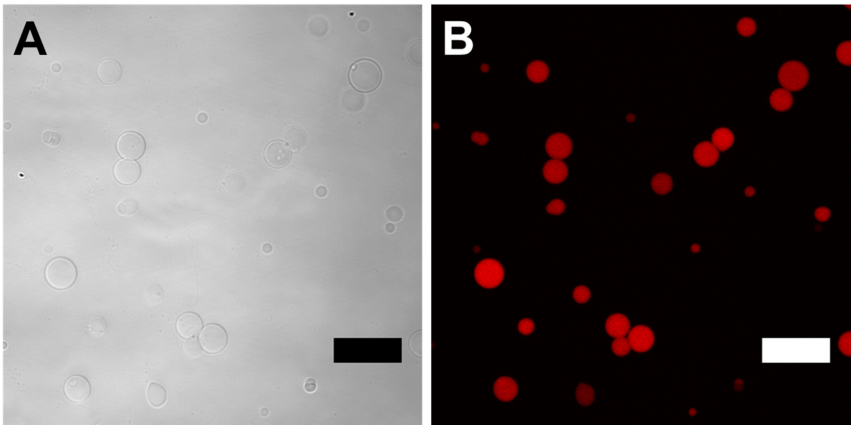

Figure 1. Encapsulation of biomolecular cargo into GUVs with the lipid composition DOPC:DOPE:Cholesterol (2:1:1). **A**) Bright Field microscopy and **B**) Fluorescence microscopy. The scale bar is 30 µm.

Compartmentalization in GUVs

One of the advantages of GUVs over liposomes is that they can be visualized, because of their "giant size", by optical microscopy. If those GUVs can be compartmentalized, they become a model system that can be studied as an individual entity. Thus, more insights of the cellular structure and function can be researched with the direct visualization of individual compartmentalized GUVs as a cellular synthetic model. The formation of compartmentalized GUVs is challenging so far and attempts for encapsulating particles inside GUVs have been done with the use of sophisticated equipment.[17] Here, the use of the DexPEG scaffold allowed the encapsulation of polystyrene-poly(ethylene oxide) (PS300-PEG44-OMe) polymersomes[19,20] (diameter=500 nm) in the lumen of GUVs. Polymersomes were embedded

into the hydrogel scaffold, firstly mixing Dextran precursor and polymersomes dispersion and finally by the addition of the PEG cross-linker to form the hydrogel (**Figure 2A**). The rehydration of hybrid DexPEG-lipids films with the polymersomes dispersion does not encapsulate the polymersomes into GUVs. This might be due to the growth mechanism of GUVs on the DexPEG scaffold (**Chapter III**). It might be possible that polymersomes are encapsulated when GUVs take on the honeycomb DexPEG network during swelling.

Fluorescence imaging of polymersome-loaded GUVs is presented in **Figure 2B**. The encapsulation of the polymersomes was observed by fluorescence microscopy in all GUVs. Inspection of individual GUVs showed few GUVs with a high concentration of polymersomes (super-filled GUVs). This is in contrast with the inner concentration of most of the GUVs and the external solution. This deviation from the average concentration was recently observed in liposome studies. In those studies proteins and dextrans were encapsulated into liposomes and a small fraction of liposomes were found super-filled of cargo.[21] Understanding the origin of super-filled GUVs, might give new clues about the origin of primitive cells. Herein, we propose the use of the DexPEG-polymersomes hybrid scaffold to study the formation of super-filled GUVs. Our hypothesis is that electrostatic interactions might play an important role in the formation of super-filled GUVs. Therefore GUVs with different lipid composition and colloidal particles with different charges and sizes should be considered in the formation of super-filled GUVs on DexPEG hydrogels.

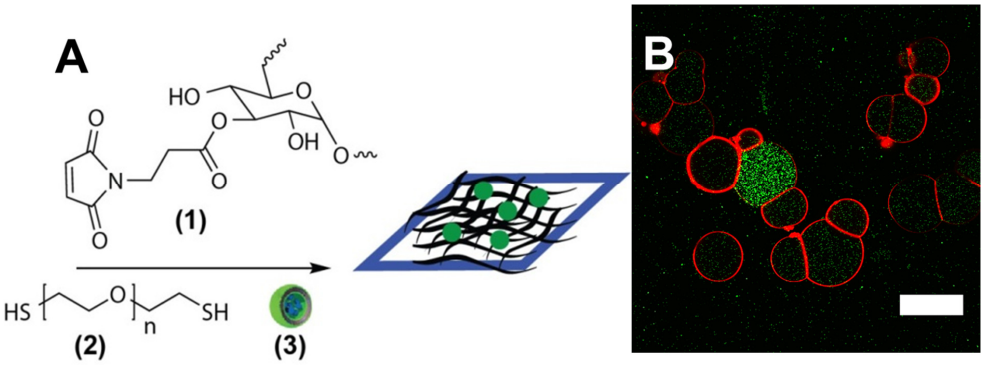

Figure 2. A) Preparation of the hybrid-DexPEG substrate for polymersomes encapsulation in GUVs. (**1**) Dex-Mal backbone, (**2**) PEG dithiol crosslinker and (**3**) Polymersomes. **B**) Encapsulation of polymersomes in conventional GUVs and in the center of the micrograph a polymersomes-super-filled GUV. The scale bar is 100 µm.

Membrane fusion and GUVs as bioreactors

The use of GUVs and LUVs in membrane fusion studies allowed the imaging of docking, mixing of membranes and mixing of inner contents (**Chapter VII**). However, a severe limitation of the content mixing assay is the huge dilution factor (10^6) once the cargo of the LUVs is released into GUVs. The use of an enzymatic reaction, where small quantities of substrate loaded in the inner volume of LUVs are delivered by membrane fusion to GUVs might improve the assay. The system proposed by Kahya et. al.,[22] consisting of β-Galactosidase entrapped into LUVs and fluorescein conjugated Galactopyranoside in GUVs might tackle the dilution drawback of our content mixing assay between GUVs and LUVs triggered by membrane fusion.

Compartmentalization creates separation of biomolecules and processes between different compartments of the cell. Compartmentalized GUVs containing enzymatic polymersomes nanoreactors in the lumen of GUVs resemble the structure of the cell and its organelles.[20] This "minimal cell" model might be used to simulate some of the cellular reaction pathways that take place in multiple and successive compartments of eukaryotic cells. Cascade reactions are a good example of reactions that can be performed in polymersomes-loaded GUVs. The **Figure 3** shows a schematic representation of a cascade reaction between LUVs containing NAD^+ and compartmentalized GUVs with polymersomes containing G6P and Resorufin (nanoreactors). The substrate NAD^+ is delivered to GUVs by membrane fusion between LUVs and the lipid membrane of GUVs. Once the substrate is delivered to the lumen of the GUV, it diffuses to the interior of the nanoreactors triggering an enzymatic reaction which is detected by the fluorescence of Resorufin in polymersomes. The importance of this model relies in the effort to provide insight over evolutionary molecules and processes in the origin of life.[23, 24]

In conclusion, these preliminary results demonstrate that DexPEG hydrogels are flexible scaffolds for preparing and encapsulating of a broad range of cargo in GUVs. The design of DexPEG hydrogels represents an advantage over other methods for preparing GUVs with several lipid compositions, defined size distribution and high ionic strength conditions. In addition to the use of GUVs as a membrane model, the encapsulation of biomolecular cargo and/or polymersomes makes GUVs a good candidate for the construction of more complex lipid-based systems. We envisage the application of the DexPEG method as a novel tool in the construction of "minimal cellular" models for studying origin and evolution of cellular life with

potential applications in synthetic biology and biotechnology. Furthermore, the incorporation of the membrane fusion system in the construction of synthetic cells increases the applicability of GUVs in the study of cellular functions and drug delivery.

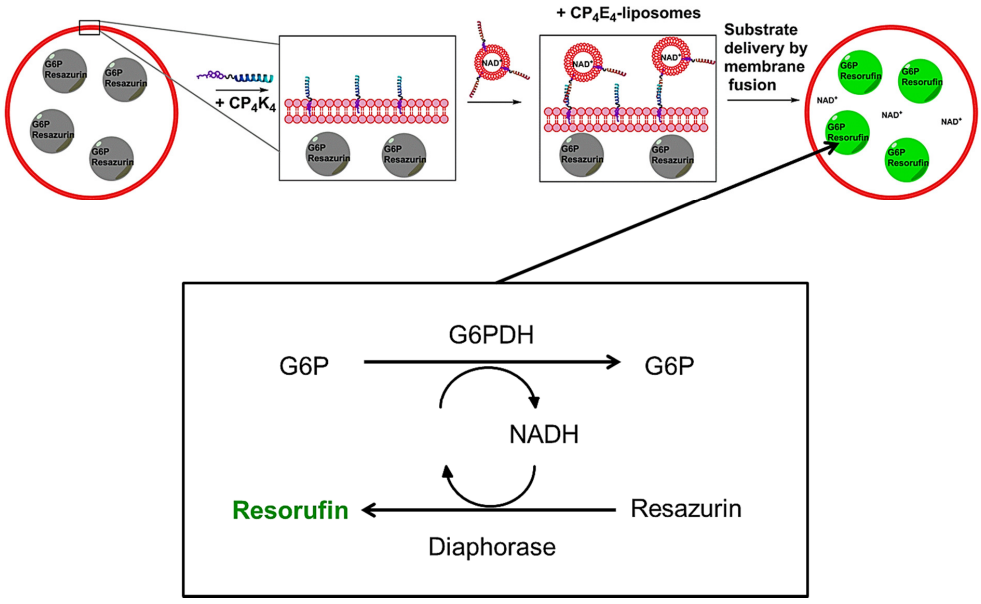

Figure 3. Schematic representation of membrane fusion between compartmentalized GUVs and LUVs. The release of NAD^+ by membrane fusion triggers the fluorescence of Resorufin in the interior of GUVs that can be detected by fluorescence microscopy.

Samenvatting

In dit proefschrift zijn Giant Unilamellar Vesicles (GUVs; reusachtige enkelwandige blaasjes) gebruikt als minimaal modelsysteem voor het membraan van een cel. GUVs zijn bolvormige structuren van natuurlijke of synthetische lipiden waarin de lipiden een enkele lipidendubbellaag vormen die het waterige binnenvolume van het buitenvolume scheidt.[1, 2] Het belangrijkste voordeel van dit membraanmodel is dat GUVs eenvoudig waargenomen kunnen worden met een optische microscoop. Door de reusachtige afmeting (5-100 μm) zijn morphologische veranderingen in de lipidendubbelaag van de GUVs zichtbaar.[3] Het GUV model wordt veel gebruikt voor het bestuderen van de mechanische eigenschappen van membranen,[4] lipidenorganisatie,[5] interactie met eiwitten,[6] en peptide,[7] en recentelijk ook voor het creëeren van een eenvoudige cel in een "bottom-up" aanpak.[8, 9] Verschillende protocollen voor het vormen van GUVs zijn voorgesteld en hiervan worden electroformatie[10] en langzame hydratie methodes[11] het meest toegepast. Deze methodes werken alleen bij lage zoutconcentraties, maar de studie van biologische intereacties vereist hogere zoutconcentraties, gelijk aan het niveau in levende biologische systemen. Om dit nadeel van de traditionele methoden te omzeilen zijn alternatieve protocollen ontwikkeld die gebruik maken van bijvoorbeeld water in-olie-emulsies,[12,13] oplosmiddeluitwisseling en dunne hydrogelfilms.[14, 15] Bij gebruik van deze methodes zijn echter sporen van onzuiverheden waargenomen in de lipidendubbellaag waardoor de (bio)fysische eigenschappen veranderen, zoals uitvoerig besproken in dit werk (**Hoofdstuk I** en **II**).

Dit proefschrift presenteert een nieuwe methode met een chemisch gecrosslinkte hydrogel als substraat voor de groei van GUVs in relevante biologische zoutconcentraties, zonder overdracht van onzuiverheden uit het substraat (**Hoofdstuk I**). De chemisch-fysische eigenschappen van de hydrogelnetwerken werden bestudeerd en de gevormde GUVs gekarakteriseerd in termen van opbrengst en grootte (**Hoofdstuk II**). Deze GUVs zijn vervolgens gebruikt als platform voor biofysische membraanstudies bij hoge zoutconcentraties (**Hoofdstukken III** en **IV**) en als een modelsysteem voor cellen om medicijnafgifte (**Hoofdstuk V**) en membraanfusieprocessen (**Hoofdstukken VI en VII**) te bestuderen. Dit werk gaat over de biofysische aspecten en toepassingen van het GUV model bij relevante zoutconcentraties, maar het toont ook aan dat er ruimte is voor andere studies. In het laatste hoofdstuk (**Hoofdstuk VIII**) worden de voorlopige resultaten betreffende het invullen van lacunes in de kennis van GUVs als model systeem gepresenteerd. Ook worden toekomstige onderzoekslijnen voorgesteld.

References

1. Menger, F.M. & Keiper, J.S. Chemistry and physics of plant vesicles as biomembrane models. *Curr Opin Chem Biol* **2**, 726-732 (1998).
2. Walde, P., Cosentino, K., Engel, H. & Stano, P. Giant Vesicles: Preparations and Applications. *Chembiochem* **11**, 848-865 (2010).
3. Morales-Penningston, N.F. et al. GUV preparation and imaging: Minimizing artifacts. *Biochimica Et Biophysica Acta-Biomembranes* **1798**, 1324-1332 (2010).
4. Bassereau, P., Sorre, B. & Levy, A. Bending lipid membranes: Experiments after W. Helfrich's model. *Adv Colloid Interfac* **208**, 47-57 (2014).
5. Lipowsky, R. The morphology of lipid membranes. *Current opinion in structural biology* **5**, 531-540 (1995).
6. Kahya, N. Protein-protein and protein-lipid interactions in domain-assembly: Lessons from giant unilamellar vesicles. *Bba-Biomembranes* **1798**, 1392-1398 (2010).
7. Koller, D. & Lohner, K. The role of spontaneous lipid curvature in the interaction of interfacially active peptides with membranes. *Bba-Biomembranes* **1838**, 2250-2259 (2014).
8. Carrara, P., Stano, P. & Luisi, P.L. Giant Vesicles "Colonies": A Model for Primitive Cell Communities. *Chembiochem* **13**, 1497-1502 (2012).
9. Luisi, P.L. & Stano, P. Synthetic Biology Minimal Cell Mimicry. *Nat Chem* **3**, 755-756 (2011).
10. Angelova, M.I. & Dimitrov, D.S. Liposome Electroformation. *Faraday Discuss.* **81**, 303-+ (1986).
11. Reeves, J.P. & Dowben, R.M. Formation and properties of thin-walled phospholipid vesicles. *Journal of Cellular Physiology* **73**, 49-60 (1969).
12. Pautot, S., Frisken, B.J. & Weitz, D.A. Production of unilamellar vesicles using an inverted emulsion. *Langmuir* **19**, 2870-2879 (2003).
13. Hansen, J.S. et al. Formation of Giant Protein Vesicles by a Lipid Cosolvent Method. *ChemBioChem* **12**, 2856-2862.
14. Horger, K.S., Estes, D.J., Capone, R. & Mayer, M. Films of Agarose Enable Rapid Formation of Giant Liposomes in Solutions of Physiologic Ionic Strength. *Journal of the American Chemical Society* **131**, 1810-1819 (2009).
15. Weinberger, A. et al. Gel-Assisted Formation of Giant Unilamellar Vesicles. *Biophysical Journal* **105**, 154-164 (2013).
16. Kim, S.H. & Chu, C.C. Synthesis and characterization of dextran-methacrylate hydrogels and structural study by SEM. *Journal of biomedical materials research* **49**, 517-527 (2000).
17. Stachowiak, J.C. et al. Unilamellar vesicle formation and encapsulation by microfluidic jetting. *Proc Natl Acad Sci U S A* **105**, 4697-4702 (2008).
18. Kurihara, K. et al. Self-reproduction of supramolecular giant vesicles combined with the amplification of encapsulated DNA. *Nat Chem* **3**, 775-781 (2011).
19. Kim, K.T., Meeuwissen, S.A., Nolte, R.J. & van Hest, J.C. Smart nanocontainers and nanoreactors. *Nanoscale* **2**, 844-858 (2010).

20. Peters, R.J. et al. Cascade reactions in multicompartmentalized polymersomes. *Angewandte Chemie* **53**, 146-150 (2014).
21. D'Aguanno, E. et al. Physical Routes to Primitive Cells: An Experimental Model Based on the Spontaneous Entrapment of Enzymes inside Micrometer-Sized Liposomes. *Life (Basel)* **5**, 969-996 (2015).
22. Kahya, N., Pecheur, E.I., de Boeij, W.P., Wiersma, D.A. & Hoekstra, D. Reconstitution of membrane proteins into giant unilamellar vesicles via peptide-induced fusion. *Biophys J* **81**, 1464-1474 (2001).
23. Szostak, J.W., Bartel, D.P. & Luisi, P.L. Synthesizing life. *Nature* **409**, 387-390 (2001).
24. Rasmussen, S. et al. Evolution. Transitions from nonliving to living matter. *Science* **303**, 963-965 (2004).

CURRICULUM VITAE

Nestor Fabian Lopez Mora was born on the 20th January 1978 in Mexico City, Mexico. After finishing high school studies, he started a Bachelors degree in Chemical Engineering at the Chemical Sciences School at La Salle University, Mexico City (1998 -2002). He obtained his Bachelor (B. Sc.) diploma in 2003 with the thesis "Conformational study of ethoxyl group in 1,4 diazanes and 1,4 diazenes". In 2003 he began a Masters degree in Chemical Sciences with specialization in Organic Chemistry at the National Autonomous University of Mexico (UNAM) in Mexico City. In 2005 he obtained a Master in Science (M. Sc.) diploma with the thesis "Secondary Orbital Interactions (SOI) in Diels-Alder Cycloadditions". In 2005, interested in applied sciences, he began to work in the Physical Chemistry department of the Polymer Research Centre (COMEX Group) as a Research Assistant, in Mexico City. In 2009, Nestor joined the Synthesis Department of the Polymer Research Centre, remaining until December 2010.

In January 2011, with a scholarship (181940) from the Mexican Council for Science and Technology (CONACyT) for foreign studies, Nestor started his PhD research in the Supramolecular and Biomaterials Chemistry group (SBC) of Dr. Alexander Kros at Leiden University, Leiden, The Netherlands. During his PhD he studied the production and applications of giant unilamellar vesicles (GUVs) as a biomembrane model for studying membrane fusion and drug delivery (2011 – 2015).

From 2015 to date, Nestor works as Research Associate in the Chemistry department of Kings College London (KCL), London, United Kingdom. His current research, carried out in Professor Paula Booth's group, concerns the study of protein - membrane interactions.

List of Publications

- **Lopez Mora**, **N**.; Bahreman, A.; Valkenier, H.; Li, H.; Sharp, T. H.; Sheppard, D. N.; Davis, A. P.; Kros, A. *Chemical Science* **2016**, 7, 1768.

- Valkenier, H.; **Lopez Mora**, **N**.; Kros, A.; Davis, A. P. *Angewandte Chemie* **2015**, 54, 2137.

- Askes, S. H.; **Lopez Mora**, **N**.; Harkes, R.; Koning, R. I.; Koster, B.; Schmidt, T.; Kros, A.; Bonnet, S. *Chemical Communications* **2015**, 51, 9137.

- **Lopez Mora**, **N**.; Hansen, J. S.; Gao, Y.; Ronald, A. A.; Kieltyka, R.; Malmstadt, N.; Kros, A. *Chemical Communications* **2014**, 50, 1953.

- Cuevas, G.; Martinez-Mayorga, K.; del Carmen Fernandez-Alonso, M.; Jimenez-Barbero, J.; Perrin, C. L.; Juaristi, E.; **Lopez Mora**, **N**. *Angewandte Chemie* **2005**, 44, 2360.